Understanding the mechanism of cardiac gene remodelling via PPAR-α signalling in cardiac hypertrophy

THESIS SUBMITTED FOR THE DEGREE OF DOCTOR OF PHILOSOPHY (SCIENCE)
to

JADAVPUR UNIVERSITY 2022

By

RITU KUMARI

CELL BIOLOGY & PHYSIOLOGY DIVISION

CSIR- INDIAN INSTITUTE OF CHEMICAL BIOLOGY
4, RAJA S. C. MULLICK ROAD, KOLKATA 700032, INDIA

CERTIFICATE FROM THE SUPERVISOR

This is to certify that the thesis entitled 'Understanding the mechanism of cardiac gene remodelling via PPAR-α signalling in cardiac hypertrophy' submitted by Smt. **Ritu Kumari**, who got her name registered on **26.09.2018** for the award of Ph.D. (Science) degree of Jadavpur University, is absolutely based upon her own work under the supervision of **Dr. Arun Bandyopadhyay** and that neither this thesis nor any part of it has been submitted for either any degree/diploma or any other academic award anywhere before.

27/5/2022

(Signature of the Supervisor(s) date with official seal)

Dedicated to my family

Acknowledgement

Table of Contents:

Abbreviations

ACAA1A-acetyl-CoenzymeA acyltransferase 1

ACAA2-Acetyl-CoA Acyltransferase 2

ACOX 1-Peroxisomal acyl-coenzyme A oxidase 1

CPT 2-Carnitine PalmitoylTransferase 2

FABP4-Fatty acid binding Protein 4

FABP4-Fatty Acid Binding Protein 7

FIS1-Mitochondrial Fission 1 Protein

HSD17B12-17-beta hydroxysteroid dehydrogenase-12

ISO-Isoproterenol

MCAT-medium-chain acyl-CoA dehydrogenase

OPA1-Dominant Optic Atrophy 1

PPAR-α-peroxisome proliferator-activated receptor-α

PTEN-3′-lipid phosphatase, phosphatase and tensin homolog on chromosome ten

WT-Wild-Type

ATP-Adenosine triphosphate

PIP 2-phosphatidylinositol (4, 5)-bisphosphate

PIP 3-phosphatidylinositol (3, 4, 5)-trisphosphate

DBC1-Deleted in Breast Cancer 1

MDM2-Mouse double minute 2 homolog

GAPDH-Glyceraldehyde-3-phosphate dehydrogenase

LC3A/B-Autophagy marker Light Chain 3

ABSTRACT

Understanding the mechanism of cardiac gene remodelling via PPAR α signalling in cardiac hypertrophy

Cardiac hypertrophy is a compensatory response to pressure-overload induced heart and is characterised by an increase in cardiomyocyte size. Prolonged hypertrophy becomes maladaptive and triggers significant pathological changes at both cellular and molecular levels. Cardiac hypertrophy is accompanied by down regulation of PPAR α that result in metabolic reprogramming. PPAR α is critical for mitochondrial biogenesis and fatty acid oxidation and reduction in fatty acid β oxidation further leads to cardiac dysfunction. Down regulation of PPARα therefore worsens the hypertrophic state. Yet, the role of PPAR α in adaptive phase of stress-induced cardiomyocytes is mostly unknown. To understand the role of PPAR α signalling in cardiac remodelling during cardiac hypertrophy, PPAR α $^{-/-}$ mice was used. PPAR α $^{-/-}$ mice exhibited significantly compromised hemodynamics as observed via echocardiography but an unexpected down regulation of apoptotic markers. Critical apoptotic marker like PTEN was also noticeably reduced along with several other apoptotic markers like p53, cCaspase9. This reduction in apoptotic markers was accompanied by an upsurge in autophagy markers. The autophagy markers like Atg3, Atg5, Atg7, Beclin1 and LC3 A/B were up regulated in PPAR α $^{-/-}$ mice. Significant increase in autophagosomes in Neonatal Rat Ventricular Myocytes (NRVMs) further confirmed this increase in autophagy. The data therefore revealed the role of PPARα signalling in this cardiac remodelling where an adaptive switch towards autophagy is observed in stress-induced cardiomyocytes in the absence of PPAR α. To further investigate this phenomenon, differential expression of miRNA in PPAR α $^{-/-}$ mice was studied. Role of miRNA has been majorly explored in cardiac hypertrophy but the biological relevance of the differentially expressed miRNA with the PPAR α signalling in hypertrophied condition is yet to be explored. Analysis of miRNA profile revealed differential expression of specific miRNAs like mmu-miR-3102-5p; mmu-miR-30a-5p; mmu-miR-30c-5p; mmu-miR-466i-5p that are involved in negative regulation of intrinsic apoptotic signalling pathway. Therefore the data revealed that the altered expression of miRNAs in the absence of PPAR α resulted in inhibition of apoptosis suggesting a critical role of this transcription factor in regulating the adaptive switch. Overall this study highlights the significance of PPAR α in regulating the cardiac remodelling in hypertrophy.

REVIEW
OF
LITERATURE

Review of Literature

Heart performs the herculean task of maintaining the consistent perfusion of all the peripheral organs thereby contributing to their proper functioning (*Nakamura and Sadoshima,2018*). To achieve this task, heart continuously pumps nutrient and oxygen-rich blood throughout the body. This requires significant expenditure of energy that is met primarily by the beta-oxidation of long chain fatty acids (*Dyck and Lopaschuk,2002; Lopaschuk et al. 2010*).

In response to the increased hemodynamic preload or afterload, heart responds by initially undergoing enlargement of individual cardiomyocytes, a condition called hypertrophy to enhance the contractility and decrease the left ventricular wall stress (*Schiattarella et al. 2015*). Cardiac hypertrophy can be either physiological or pathological (*Shimizu and Minamino, 2016*).
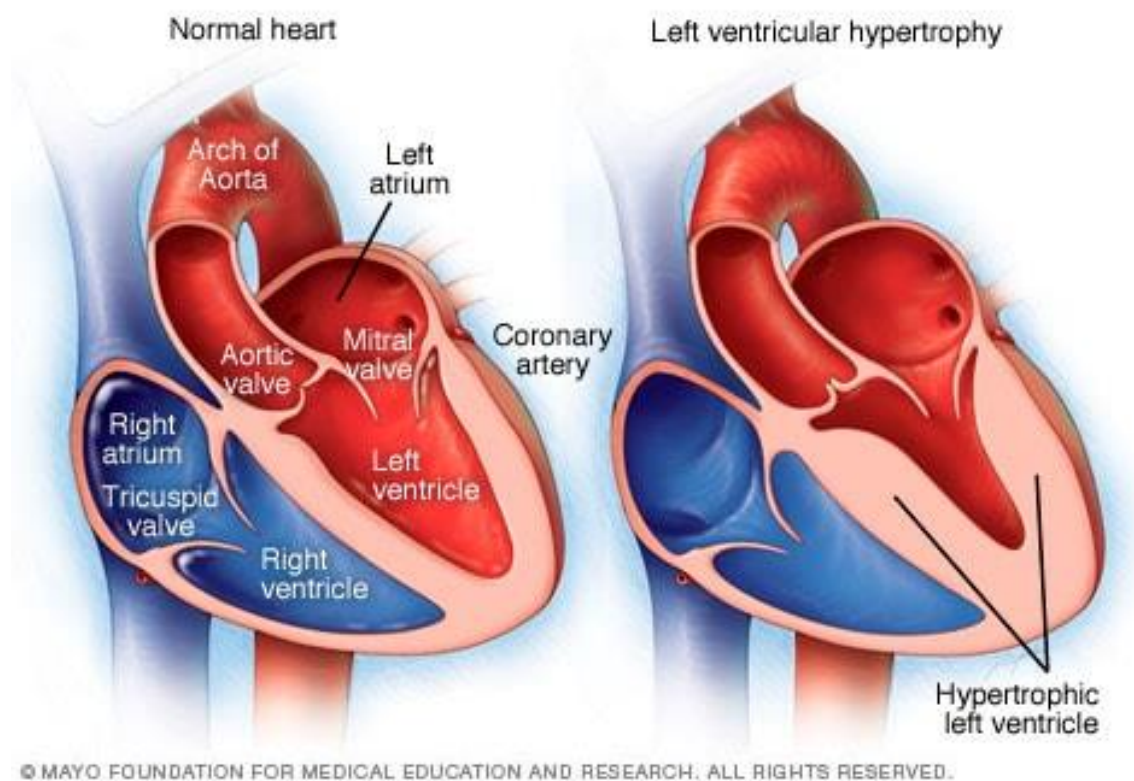
Fig.1. Left ventricular Hypertrophy: Images showing normal heart (Right) compared to Hypertrophied heart(Left).Hypertrophic left ventricle (Left) resulting from the thickening of the left ventricle wall **(Images Adapted from Mayoclinic.org)**

Physiological hypertrophy is mostly an outcome of pregnancy or endurance training like swimming or running, and is marked by a mild (10-20%) increase in ventricular volume that is associated with well-coordinated increase in wall thickness (*Strom et al. 2005*). Individual cardiomyocytes in case of physiological hypertrophy increase in both length and width

(*Nakamura and Sadoshima,2018*). After the stimulus sets off, the physiological hypertrophy is reversed and heart and the individual cardiomyocytes returns back to its previous original dimensions (*Nakamura and Sadoshima,2018*). On the contrary, Pathological hypertrophy is mostly associated with myocardial infarction, metabolic syndrome and valvular disease and is marked by a decrease in ventricular dimension along with enhanced wall thickness (concentric hypertrophy) (*Mohammed et al.2015*). Individual cardiomyocytes increase in width more than length. Although pathological hypertrophy is primarily induced as a compensatory response but eventually progresses to irreversible contractile dysfunction and heart failure, identified by ventricular chamber dilation and individual cardiomyocytes lengthening Additionally, foetal gene expression Atrial Natriuretic peptide (ANP), Brain Natriuretic peptide (BNP), cardiac muscle β-isoform (MYHCβ) remains unchanged or is decreased in case of physiological hypertrophy unlike pathological hypertrophy (*Nakamura and Sadoshima,2018*).

Pathological hypertrophy is mostly accompanied with fibrosis as well as collagen I deposition, followed by cardiomyocyte death whereas Physiological hypertrophy mostly stimulates signalling pathways involved in cell proliferation, cell growth, survival as well as angiogenesis (*Mohammed et al.2015*). Pathological hypertrophy is a maladaptive decompensation that is triggered due to cell death, altered Calcium handling proteins, metabolic dysfunction, reactivation of foetal genes, metabolic reprogramming, impaired protein and mitochondrial quality control and insufficient angiogenesis (*Strom et al. 2005; Zhang et al. 2013; Liew et al.2017*). Thereby, signalling pathways mostly triggered by pathological stimuli promotes maladaptive cardiac remodelling as well as dysfunction. Conversely, Physiological hypertrophy triggers pathways that antagonize pathological cardiac remodelling and dysfunction (*Nakamura and Sadoshima,2018*).

Cardiac hypertrophy attributes to significant metabolic remodelling (*Doenst et al. 2013*). Cardiac metabolism is differentially regulated in physiological and pathological hypertrophy and alterations in cardiac metabolism precedes development of cardiac hypertrophy (*Opie 1968; Opie 1969*). Impaired adaptation of cardiac energy metabolism as a result of the hypertrophic response aggravates pathological hypertrophy and triggers cardiomyocyte death (*Wisneski et al. 1990*). In Adult normal heart, 50-70% of ATP is obtained from Fatty acid β-oxidation (*Bing et al. 1954; Neely and Morgan, 1974; Lopaschuk et al. 1994*). The enzymes that regulate Fatty acid β-oxidation are under direct control of transcriptional regulation, thereby alterations in Fatty acid β-oxidation are associated with changes in the expression of Fatty acid β-oxidation enzymes (*Desvergne et al. 2006; Lopaschuk et al. 2007*). These transcriptional modulations, to a larger extent, are mediated via PPAR α and PGC 1 α (*Finck and Kelly, 2002; Huss and Kelly, 2004; Finck and Kelly, 2007;Madrazo and Kelly, 2008*). Impaired Fatty acid metabolism may directly induce cardiac hypertrophy and cardiac dysfunction via pathological signalling mechanisms (*Cheng et al.2004*). During prenatal development, Glucose is the major source of energy used by proliferating cardiomyocytes. During perinatal stage, cardiomyocytes switch their energy source preference from carbohydrates to Fatty acids that results in concomitant increase in oxidative capacity to support persistent contractility of the heart (*Neubauer 2007*). Cardiac remodelling of ATP production is observed during the development of pathological hypertrophy leading to reduced Fatty acid

β-oxidation and enhanced glycolysis thereby reverting back foetal-stage energy production (*Lai et al. 2014*). This metabolic reprogramming is accompanied by downregulation of enzymes mediating mitochondrial energy transduction during initial stages of cardiac hypertrophy (*Aubert et al. 2013*). Persistent decrease in Fatty acid oxidation is observed during maladaptive hypertrophy in response to pressure-overload (*Doenst et al. 2010*).Conversely, Fatty acid oxidation is enhanced during physiological hypertrophy that is accompanied with upregulation of fatty acid oxidation enzymes(*Riehle et al. 2014;Burelle et al. 2004*).As per many reports, utilization of glucose as well as other substrates such as lactate, ketone bodies and BCAAs might not sufficiently compensate for the impaired Fatty acid oxidation, resulting in deficiency of cardiac energy and development of heart failure (*Bing et al. 1954; Neely and Morgan, 1974*).Thus previous report suggests metabolic remodelling might lead to pathological hypertrophy.
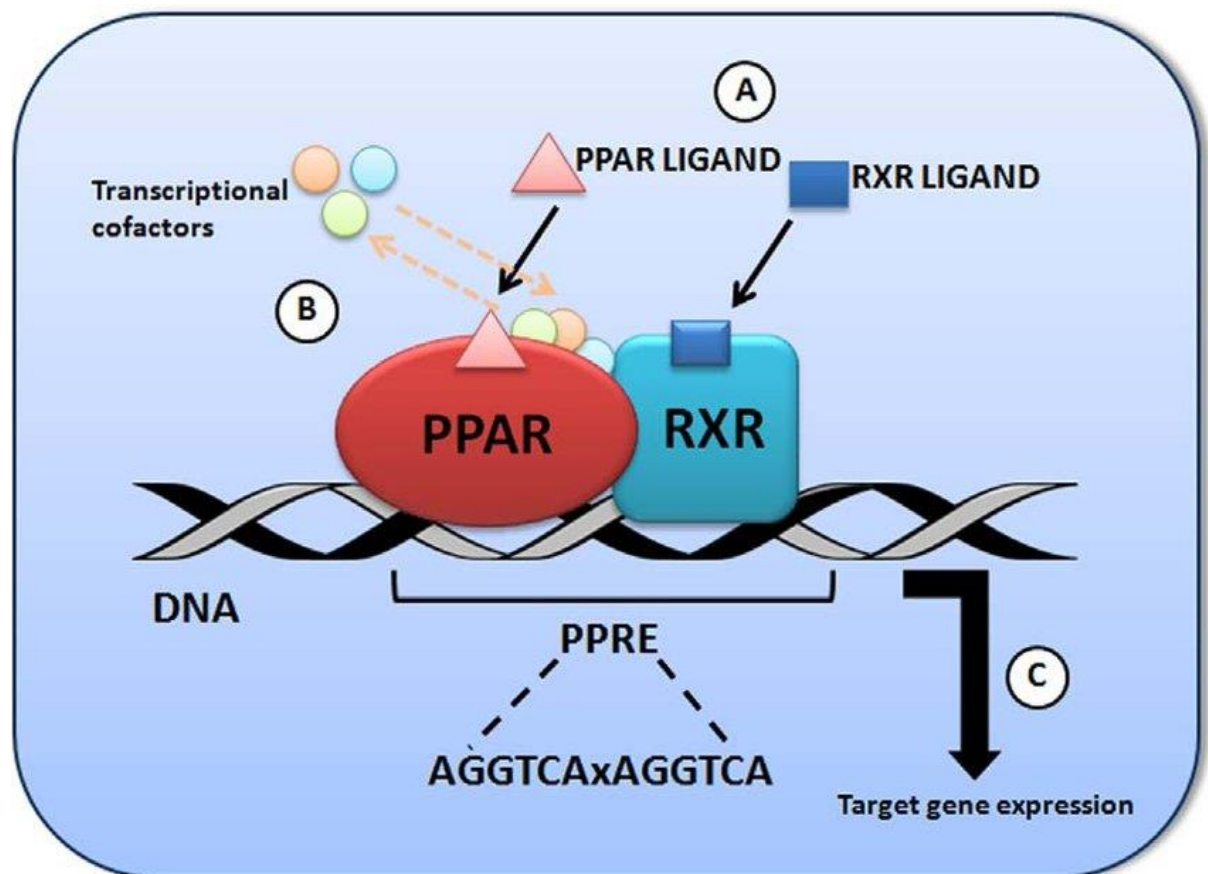
Fig.2. PPAR α transcriptional activation via ligands: PPAR α transcriptional activation in the cell nucleus. (A) Binding of PPAR/RXR ligands; (B) Changes in the associated transcriptional cofactors; (C) Activation of the transcriptional complex **(Rigano et al. 2017).**

The nuclear receptor markedly responsible for regulating Fatty acid metabolism and abundantly expressed in heart is peroxisome proliferator-activated receptor-α (PPAR-α) (*Burkart et al. 2007*).Exercise induced physiological hypertrophy results in up regulation of PPARα in the heart, whereas it is downregulated in pathological hypertrophy (*Barger et al. 2000*).PPAR α

belongs to the ligand-activated nuclear receptor superfamily that forms a heterodimer with retinoid X receptor and binds to the PPRE elements located on the promoter region of its target genes. Target genes of PPARα mostly include genes involved in fatty acid uptake(FAT/CD36,FATP1), Fatty acid binding(FABP) and Fatty acid beta-oxidation (very-long chain acyl CoA dehydrogenase, long chain acyl CoA dehydrogenase, acetyl-Co A Acyl transferase 2,Acetyl Co A Carboxylase) (*Yang and Li, 2007; Huss and Kelly, 2004;Rakhshandehroo et al. 2010*).Previous studies have shown the significant increase in Fatty acid utilization , Fatty acid oxidation as well as lipid overload due to overexpression of PPAR α in the heart(*Chiu et al. 2002*; *Finck et al. 2002;Yagyu et al. 2003; Chiu et al. 2005*).On the contrary, deletion of PPAR α results in downregulation of Fatty acid β-oxidation genes and concordant increase in glucose oxidation(*Watanabe et al. 2000;Campbell et al. 2002;Son et al. 2007*). Epigenetic remodelling of cardiac genes regulated via PPAR α is very well known that is reprogrammed in response to pathological stress(*Warren et al. 2017; Kanherkar et al. 2014*) .Many reports have mentioned recruitment of Sirt 1 via PPARα to the specific promoter region of its target genes during pressure overload-induced heart failure (*Oka et al. 2015*).Recruitment of Sirt1 results in transcriptional repression of target genes of PPAR α indicating the potential role of PPAR α in Epigenetic remodellling. Downregulation of a subset of PPAR α target genes that are involved in the TCA cycle and Electron Transport chain exacerbates the impaired mitochondrial bioenergetics in the pressure-overload induced heart that leads to redox imbalance and stimulates negative feedback loop (*Warren et al. 2017*). Fenofibrate is a well-known PPAR α agonist that is an activator of PPAR α and is known to attenuate cardiac hypertrophy via multiple signalling pathways (*Irukyama-Tomobe 2004; Li et al. 2007*).Many reports have shown the role of fenofibrate in preventing the progression towards heart failure by reducing myocardial fibrosis and inflammation (*Ogata et al. 2004*). Bezafibrate, another well reported PPAR α agonist has been used to treat hyperlipidemia but its role in cardiac hypertrophy is yet to be explored (*Barbosa-Da-Silva et al. 2015*).

Apoptosis has emerged as an important factor contributing to myocardial remodelling as it leads to loss of cardiomyocytes in response to pressure-overload (*van Empel et al. 2005*). As per reports, growth signals persist chronically in cardiomyocytes whereas pressure-overload resulting in hypertrophy causes loss of these survival signals resulting in a contradictory genetic demand that eventually triggers apoptotic response (*Saraste et al. 1999;Kang and Izumo, 2000*).
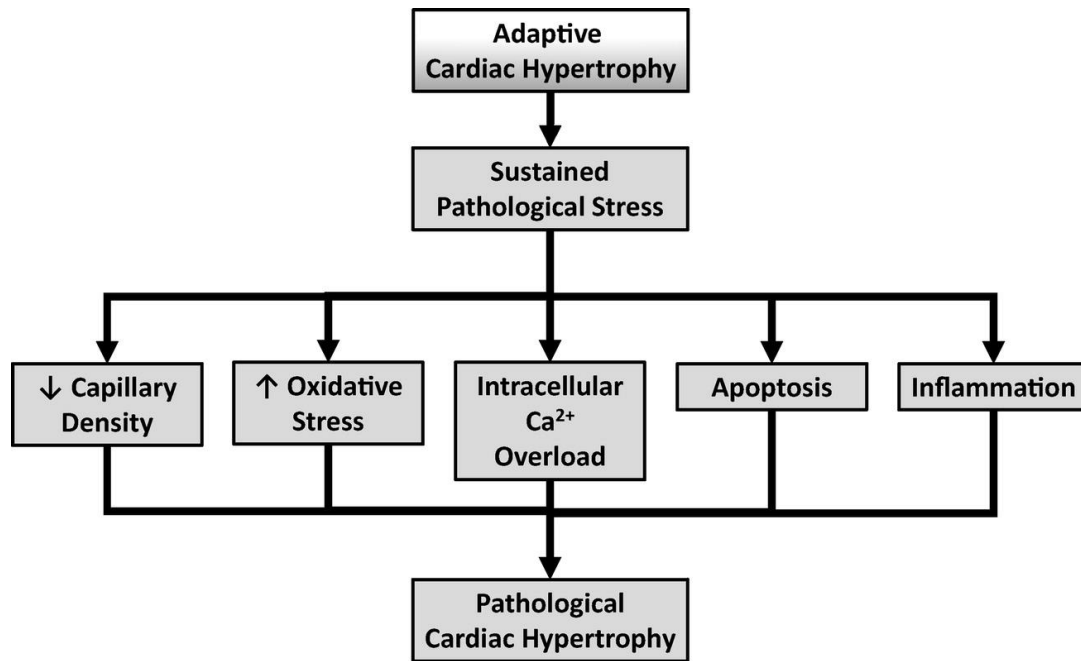
Fig.3.Proposed mechanism for the development of pathological cardiac hypertrophy: Involvement of apoptosis in the development of pathological cardiac hypertrophy resulting from sustained pathological stress **(Oldfield et al. 2020)**

Cellular response to various signalling pathways is tightly regulated to maintain cardiac homeostasis that helps in preventing pathological cardiac hypertrophy.

miRNAs belong to a widespread class of small non-coding RNAs that regulates gene expression through sequence complementarity to their targets (*Ladomery et al. 2011*). The first miRNA was discovered in the nematode *C. elegans* by the Ambros group in the year 1993 (*Lee et al. 1993*).Ambros and colleagues identified two genes, *lin-4* and *let-7*, which to their surprise did not encode proteins but small RNAs that were eventually called miRNAs.

Biogenesis of miRNA is a sequential process and majority of miRNAs follow the dominant canonical biogenesis pathway. In this canonical pathway, pri-miRNAs that are transcribed from their respective genes are processed into pre-miRNAs by the microprocessor complex that consists of an RNA binding protein DiGeorge Syndrome Critical Region 8 (DGCR8) and a ribonuclease III enzyme, Drosha (*Denli et al.2004*).Next; the DGCR8 recognizes a motif consisting of an N6-methyladenylated GGAC and several other motifs within the pri-miRNA(*Alarcon et al. 2015*).The ribonuclease III enzyme Drosha cleaves the pri-miRNA duplex at the base of the characteristic hairpin structure of pri-miRNA resulting in the formation of a 2 nt 3′ overhang on the pre-miRNA (*Alarcon et al. 2015; Han et al. 2004*).Pre-miRNAs that are generated are then exported to the cytoplasm
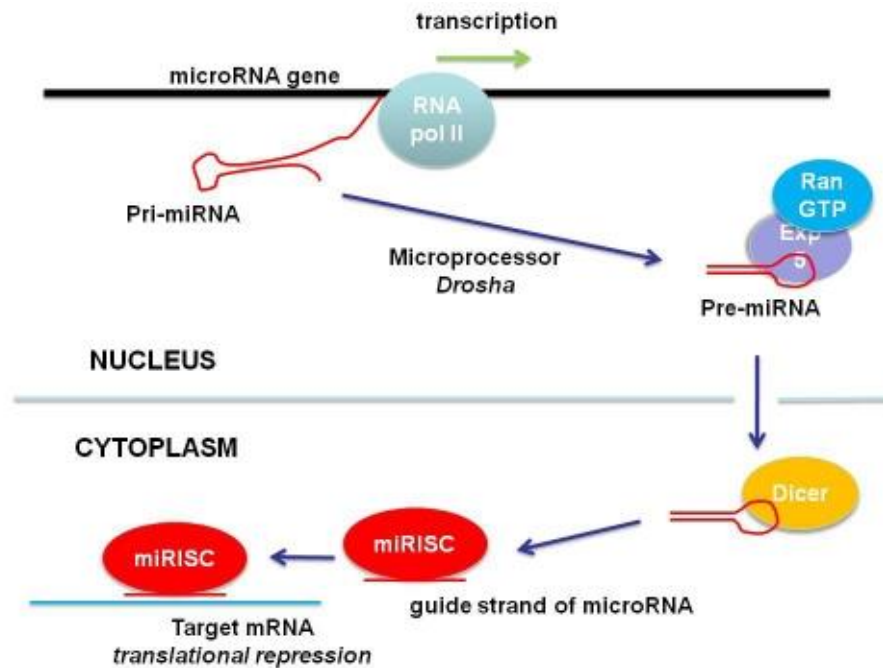
Fig.4.Biogenesis of miRNA: miRNA gene is transcribed by RNA polymerase II. The resultant primary transcript is termed pri-miRNA. The pri-miRNAs is trimmed into a 60-100 nucleotide pre-miRNA by Drosha in the nucleus.It is then exported by binding to Exportin 5 via RanGTP into the cytoplasm. In the cytoplasm the nuclease Dicer further trims the pre-miRNA into a mature 22 nucleotide miRNA which becomes incorporated into a miRISC complex that retains the "guide strand". Target mRNAs have multiple target sites for any given miRNA; and a given miRNA may target several mRNAs**.(Ladomery et al. 2011)**

by an exportin 5 (XPO5)/RanGTP complex and processed by the RNase III endonuclease Dicer (*Denli et al. 2004; Okada et al. 2009*). The terminal loop is processed and removed resulting in a mature miRNA duplex (*Zhang et al. 2004*). The directionality of the miRNA strand governs the naming of the mature miRNA form as the 5p strand arises from the 5′ end of the pre-miRNA hairpin whereas the 3p strand originates from the 3′ end. Both the strands that are derived from the mature miRNA duplex are loaded into the Argonaute (AGO) family of proteins in an ATP-dependent manner (*Yoda et al. 2010).*The selection of the 5p or 3p strand depends upon the thermodynamic stability at the 5′ ends of the miRNA duplex or a 5′ U at nucleotide position 1 (*Khvorova et al. 2003*). Normally, the strand with lower 5′ stability or lower 5′ uracil is preferably loaded into AGO, and is considered as the guide strand whereas unloaded strand is called the passenger strand, which gets unwound from the guide strand through various mechanisms on the basis of the degree of complementarity. The passenger strands containing no mismatches are cleaved by AGO2 and degraded by cellular machinery. Otherwise, miRNA duplexes with central mismatches or non-AGO2 loaded miRNA are passively unwound and degraded (*Ha and Kim, 2014; Wehbe et al. 2019*).

Previous reports on miRNA-3'untranslated region (UTR) interactions as well as gain/loss-of-function studies, have addressed various miRNAs that regulate the expression of genes related to cardiovascular disease (*Wongsurawat et al. 2018*).Different miRNAs have been implicated in myocardial infarction (*Wongsurawat et al. 2018*; *Derda et al. 2018*; *Wongsurawat et al. 2018*), valvular heart disease (*Chen et al. 2016*), cardiac arrhythmia (*Jin et al. 2018*) and genetically inherited cardiomyopathy (*Calore et al. 2019;Raso et al. 2019*).Additionally, few miRNAs have been reported to be associated with cardiac remodelling wherein miRNAs may act as positive or negative regulators of cardiac hypertrophy through targeting pro-hypertrophic signalling pathways (*Boon and Dimmeler, 2015;Creemers and Van Rooji, 2016;Wang et al. 2016;Wojciechowska et al. 2017;Li et al. 2018;Roncarati et al. 2014*)
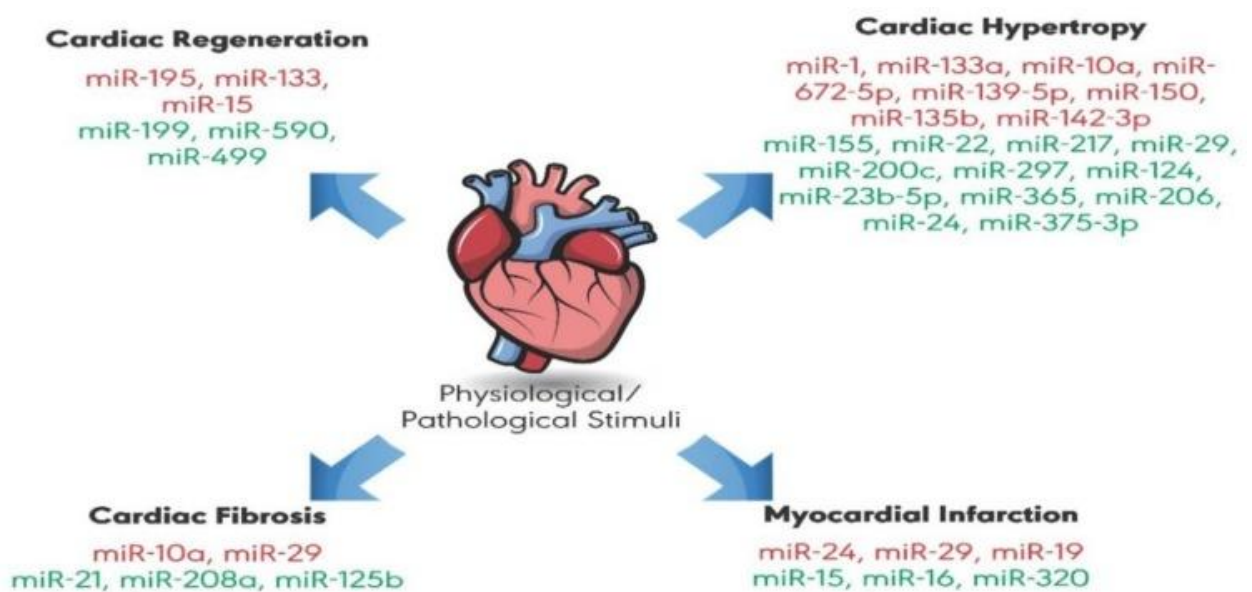
Fig.5. Role of miRNAs in physiological and pathological cardiac remodeling. Some miRNAs have a protective role against cardiovascular diseases, whereas others promote extensive cardiac remodeling, leading to disease. The red color indicates miRNAs that negatively regulate cardiac remodeling. The green color indicates miRNAs having a positive regulatory role.**(Wehbe et al. 2019).**

Dysregulation of miRNA has already been demonstrated in cardiac hypertrophy using high-throughput miRNA microarray analyses. Reports have stated dysregulated miRNAs affect various targets that are involved with different signalling networks (*Naga et al. 2009*).

Stress signals stimulate pathological response resulting in cardiac hypertrophy (*Ruwhof and van der Laarse, 2000*). Alteration of signalling pathway is observed as a response to the resultant hypertrophy. Recent reports have demonstrated that the miRNAs that are regulated by these signalling pathways are associated with cardiac hypertrophy
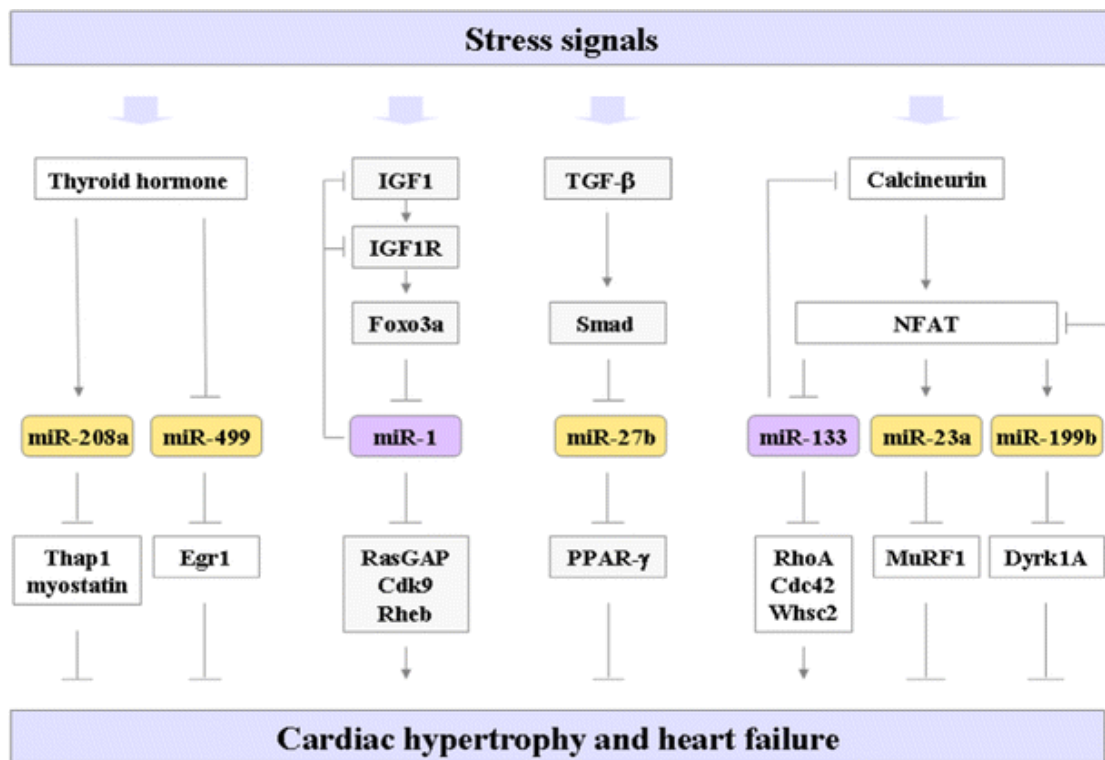
Fig.6. Cell-autonomous function of miRNAs in cardiac hypertrophy: Multiple signalling pathways and cascades control the hypertrophic response of cardiomyocytes in the heart in response to various stresses. **(Wang and Yang, 2012).**

Various signalling cascade that are associated with cardiac hypertrophy can modulate hypertrophic responses by regulating different miRNAs. The results suggest that cardiac miRNAs are integrated into complex regulatory networks, and dysregulation of miRNAs can affect multiple cellular processes in ways that are conducive to the establishment of cardiac diseases.

CHAPTER 1

Downregulation of PTEN promotes autophagy in cardiac hypertrophy in PPAR α$^{-/-}$ mice

Introduction

Cardiac hypertrophy is a compensatory response to overcome the increased demands of the pressure-overload induced heart (*Tardiff 2006*).However, prolonged hypertrophy switches to pathological condition and eventually leads to heart failure (*Kehat and Molkentin,2010*).Cardiac hypertrophy is accompanied by significant changes at both cellular and molecular levels, increase in cardiomyocyte size along with extensive collagen depostion leading to cardiac fibrosis(*Vega et al. 2017*).Reprogramming of foetal genes like ANP (Atrial Natriuretic Factor), BNP (Brain Natriuretic Factor) is observed along with reduction in fatty acid β-oxidation (*Aubert et al. 2013; Vega et al. 2017*). Since heart uses fatty acids as the preliminary source of energy, reduction in fatty acid β-oxidation mostly leads to cardiac dysfunction (*Aubert et al. 2013*). Previous reports have established the role of PPAR α signalling in the regulation of fatty acid β-oxidation (*Warren et al. 2017*).

According to previous reports, stimulation of β-adrenergic receptors leads to cardiac hypertophy and is accompanied by down regulation of PPAR α leading to metabolic reprogramming (*Warren et al. 2017*). Under normal condition, the heart utilises unsaturated fats as the preliminary metabolic fuel. However, in the absence of PPAR α activity, heart relies more on glycolysis and uses glucose as its preferential substrate (*Lionetti et al. 2011*). There is a growing consensus that the metabolic remodelling in failing hearts is accompanied by metabolic switch from Fatty acid oxidation towards glycolysis (*Lionetti et al. 2011*)As per previous studies, β adrenergic receptor agonist such as Isoproterenol (ISO)administered as well as high-cholesterol diet fed mice hearts have been associated with significant cardiomyocyte death that develops into heart failure (*Kang et al. 2009*).Hypercholesterolemia that is usually accompanied with atherosclerosis is also being associated with cardiac hypertrophy in growing reports but the data is sparse (*Muthuramu et al. 2019*).

Cardiomyocyte death in cardiac hypertrophy contributes to the development of heart failure and is a characteristic hallmark of various cardiovascular diseases.Multiple signalling molecules and pathways regulate cardiomyocyte apoptosis (*Chiong et al. 2011*). Previous studies have reported the abundant expression of 3′-lipid phosphatase, phosphatase and tensin homolog on chromosome ten (PTEN) in cardiomyocytes and its role in regulating cardiomyocyte death. Growing evidences have reported the critical role of (PTEN), in modulating cell survival/apoptosis, hypertrophy, metabolism and contractility.PTEN is a lipid phosphatase that dephosphorylates phosphatidylinositol (3, 4, 5)-trisphosphate (PIP3) to phosphatidylinositol (4, 5)-bisphosphate (PIP2) and negatively regulates PI3K/AKT signalling pathway (*Oudit et al. 2004*). Elevated Akt/PKB signalling has been reported to mediate physiological hypertrophy and attenuate pathological stress that prevents heart failure. eriaOn the contrary, Loss of PTEN has been associated with adaptive responses that inhibit the progression towards maladaptive cardiac remodelling and heart failure

Many reports have addressed the activation of apoptotic pathway mediated by stress especially under conditions where the cellular mechanism fails to cope up with the elevated energy requirements (*Xia et al. 2016*).However, studies have shown the induction of autophagy

pathway might help in sustaining the metabolic stress whilst defects in autophagy could promote cell death and inflammation (*Degenhardt et al. 2006*)

Autophagy is a very well-known dynamic self-degradative process that is quite essential in maintaining the cellular homeostasis. Previous reports have addressed the relationship between cardiac hypertrophy and autophagy *(Kaushik and Cuervo,2006; Liu et al. 2014)*.As per studies, autophagy contributes to the removal of damaged cellular components and thereby helps in the preservation of cell physiological function(*Bravo-San Pedro et al. 2007*).Impaired autophagy has been associated with exacerbation of cardiac hypertrophy(*Li et al. 2015*).

Previous literatures have already demonstrated the role of PPAR α signalling in the transcription of various genes associated with fatty acid β-oxidation as well as mitochondrial biogenesis and therefore play a pivotal role in the cardiac function, so the association of PPAR α with cardiac hypertrophy requires to be explored in details.

To understand the involvement of PPAR α in the adaptive mechanism of the cardiomyocytes under stress conditions, PPAR $\alpha^{-/-}$ mice was treated with or without isoproterenol, β adrenergic receptor agonist, which is known to induce hypertrophy in heart and subsequently proteomics analysis was conducted. Proteomics study revealed down regulation of PTEN which plays significant role in apoptosis via PPARα transcription factor. Interestingly, PTEN was found to be decreased in PPAR $\alpha^{-/-}$ mice that were treated with hypertrophic agent isoproterenol. Therefore, we unveiled how the absence of PPAR α impacts the apoptotic pathway in hypertrophied cardiomyocytes as an adaptive mechanism in the myocardium. The present chapter describes

1. Identification of proteins in hypertrophied heart by mass spectrometry

2. Understanding the physiological relevance of the differentially expressed proteins

3. Molecular mechanism of PPAR α signalling in the regulation of apoptosis in cardiac hypertrophy

Materials and Methods

Animal Studies

The protocol was approved by the Institutional Ethics Committee (Reference no. IICB/AEC/Meeting/Sep/2019/4) and the animals were handled in accordance with the Committee for the Purpose of Control and Supervision of Experiments on Animals (CPCSEA), Ministry of Social Justice, and Government of India (Registration no. 147/1999/CPCSEA). Male and female mPPAR $\alpha^{-/-}$ mice (F2 homozygotes; hybrids of Sv/129 3 C57BL/6N genetic background 3 months-old were obtained from The Jackson Laboratory (Bar Harbor, Maine, USA) and bred in the Central Animal Facility CSIR-IICB, Kolkata. C57BL/6 wild-type mice and PPAR$\alpha^{-/-}$ mice were intraperitoneally injected with 30 mg/kg/day dose of isoproterenol for 14-days. 3 months-old PPAR$\alpha^{-/-}$ mice were divided into two groups and were fed two types of diet, normal chow diet (kcal: protein = 25%; carbohydrate = 58%; fat =17%) and high cholesterol diet (HCD, Research Diets Inc., catalog no. D12336 with 1.25% cholesterol). Mice were maintained on 12-h dark /12-h light cycle and allowed to have easy access to food and water. The number of animals (n) was at least 6 for all the different experimental conditions. At the end of the experimental duration, the animals were anesthetized by an intraperitoneal injection of 100 mg/kg ketamine with 10 mg/kg xylazine hydrochloride and sacrificed via cervical dislocation. The heart was collected for histological and biochemical analysis.

Histological Staining

The heart tissues were fixed in 10% formalin, embedded in paraffin and then cut into 5µm thin sections using microtome. Haematoxylin and Eosin (H&E) staining and Masson Trichome staining were performed to observe increase in cardiomyocyte size (morphological changes) and collagen deposition, respectively. Stained slides were visualised using light microscope.

RNA extraction and reverse-transcription

RNA was isolated using Tri Reagent solution (Sigma) according to manufacturer protocol. RNA concentration and purity (A260/A280 N 1.9) was analyzed using Nanodrop 2000. Real-time PCR was performed using Luna® Universal One-Step RTqPCR Kit (NEB) with 300 ng of RNA per reaction in 96-well optical reaction plates in AB Real Time 7500 Fast system. RT-PCR primers were designed using Primer Bank. The primer sequences are provided in **Table 1.**

S.No.	GENE	FORWARD PRIMER	REVERSE PRIMER
1	GAPDH	TGGCCTTCCGTGTTCCTAC	GAGTTGCTGTTGAAGTCGCA
2	Acaa1a	TCTCCAGGACGTGAGGCTAAA	CGCTCAGAAATTGGGCGATG
3	HSD17B12	GGCTTCCTGTACTGGGTGG	CACGTTTTGCTAACTCTTCTGC
4	ACAA2	CTGCTACGAGGTGTGTTCATC	AGCTCTGCATGACATTGCCC
5	Acox1	TAACTTCCTCACTCGAAGCCA	AGTTCCATGACCCATCTCTGTC

| 6 | PRKAG2 | AATGAACACTTTCAAGAGACCCC | CCAACTTGGAACTTGTGGGAAT |
| 7 | Ep300 | TTCAGCCAAGCGGCCTAAA | CGCCACCATTGGTTAGTCCC |

Tissue Homogenization

Heart tissue was homogenized using Teflon Homogenizer in RIPA Buffer with protease inhibitor cocktail (ProteoGuard™ EDTA-Free Protease Inhibitor Cocktail, Clonetech) and centrifuged at 16,000g at 4 °C for 20 min.

Western Blot Analysis

Protein concentrations were determined using DC™ Protein Assay Kit (Bio-Rad). Equal amount (30ug) protein Samples were separated on 1.5 mm 10% sodiumdodecylsulfate polyacrylamide gels and transferred onto PVDF membranes (Merck-Millipore). Membranes were blocked with 5% skimmed milk or 5% BSA (HiMedia, #TC194) and probed using the following antibodies: Anti-Opa1 (ab42364), Anti-Annexin V (8555S), Anti-c-PARP (sc-56196), Anti-Caspase 9 (9508S), Anti-p53 (2524S), Anti-Mdm2 (sc-965), Anti-Dbc1 (5857S), Anti-mTOR(sc-517464), Anti-pAkt:ser-473(sc-293125), Anti-PTEN(sc-7974), Anti-Bcl-2(sc-7382), Anti-LC3 A/B(ab128025), Anti-p62(ab91526), Anti-Beclin1 (ab55878) , Anti-Atg3(3415T), Anti-Atg5(12994T), Anti-Atg7(8558T),Anti-Calpain (sc-271856), Anti-GAPDH (G8795) and anti-β-actin (Sigma A5441) overnight at 4 °C. The membranes were washed three times in TBS-T and incubated with alkaline phosphatase conjugated secondary antibodies (Sigma A5153 (Mouse) and Sigma A9919 (Rabbit)) for 2 h at room temperature. Membranes were washed three times with TBST and developed using NBT-BCIP (Fermentes R0841, R821) in alkaline phosphatase buffer. After development of colored product on the membranes, they were washed with water, dried and images acquired using a scanner. Images were quantified using Image J software using β-actin and GAPDH as loading control for mice samples.

Mass- Spectrometry

Heart tissue samples were homogenized using Rapigest SF Surfactant (Waters, #186001861), protein concentration was estimated and 100ug of protein was used for sample preparation. 100mM of freshly prepared 1, 4-dithiothreitol (DTT; Sigma #10197777001; final conc.10 mM) was added and incubated at 56 °C for 40 min. The tubes were cooled to room temperature and 200 mM of freshly prepared Iodoacetamide (IAA, Sigma #I6125; final conc. 20 mM) was added and incubated for 1hr at room temperature. Excess IAA was quenched by adding DTT and incubated at room temperature for 20 min. Digestion was performed at 37 °C overnight with mild agitation using 1μg Trypsin protease (Pierce Thermo, #90057). The reaction was stopped the next morning using 0.1% Formic Acid (Sigma, #5330020050) and incubated at room temperature for 20 min. The samples were frozen, lyophilized and reconstituted in 0.1% formic acid before mass spectrometry analysis.

Reconstituted samples were subjected to mass spectrometric analysis using Orbitrap mass spectrometer (LTQ-XL, ThermoFisher Scientific) after chromatographic separation and peptide fractionation through a C18 easy spray nano column (3μm, 100A) by nano LC (Easy-nLC1000). The injection volume was 2μl for each sample. Total gradient was set for 145 min with a spray rate of 300nl/min.

Scan range for Orbitrap was from 350-2000(m/z) with minimum 3 peaks and a resolution of 60000. Ionic fragmentation was done by collision induced dissociation (CID) method. Protein identification was performed by Thermo Proteome Discoverer version 1.4.0. MS/MS spectra were matched against MASCOT in assistance with Percolator. Static Modification was set for N-terminal acetylation and Carbamidomethylation of Cysteine.Dynamic modification was set for Methionine (oxidation) and minimum missed cleavage number was set at two. Swissprot was used as reference software for protein identification.

Biological triplicates of the eight groups were compared using label-free relative quantification proteomic software SIEVE (Thermofisher Scientific, Waltham, MA, version.2.1.377). SIEVE directly processed the raw files from Thermo experimental datasets. To identify the statistically significant differences between LC-MS experiment datasets, the software calculated the p-value for the expression ratio of each differential peak. Spectra belonging to the peaks that were found to have statistically significant differential expression were then searched against the protein database MASCOT for peptide and protein identifications. Heat map was generated using graph pad prism software for the dataset.

PANTHER software (http://www.pantherdb.org/) was used for analyzing the significant alterations in the expressions of proteins and genes obtained from Thermo Proteome Discoverer and to identify their percent enrichment in Biological Processes and Molecular Functions.

Cell culture and Treatment

H9C2(2-1) cardiomyocytes were acquired from the National Centre for Cell Science (Pune, India) and cultured in Dulbecco's modified Eagle medium (DMEM) with high glucose (4.5g/litre), sodium bicarbonate (3.7g/litre) and fetal bovine serum (FBS;10%) in an incubator maintained at 37°C, 5% CO_2 and 80% relative humidity (RH). Cells were serum starved for 18 to 24 h before experimentation. Hypertrophy was induced by treating serum-starved H9C2 (2-1) cells with 100µM Phenylephrine (PE; Sigma-Aldrich, USA) for 24h. PPAR α antagonist, GW 6471 (TOCRIS, 4618) dissolved in ethanol was used at a working concentration of 10uM to block the PPAR α signalling.

Autophagy Assay

H9C2 (2-1) cell line was seeded in a 6-well and divided into 6 groups. I-control, II-PE treated (treatment dose, 100 µM), III-serum starved, IV-GW6471 incubated (treatment dose, 10µM), V-PE+GW6471, VI-serum starved+GW6471. After 24 hr incubation, medium was removed 100 ul of autophagosome detection reagent working solution was added to each well as per manufacturer's instructions (Sigma-Aldrich, MAK138). After 15 minutes incubation at 37°C, 5% $CO_2$and 80% relative humidity (RH), each well was washed 3 times using PBS. Experiment was repeated along with two more groups I-cholesterol (50µM), II-cholesterol+GW6471 to resemble the in vivo high cholesterol diet induced cardiac hypertrophy. Cells were seeded in a 96-well and same protocol was followed except the reading was taken using a microplate reader (Varioskan, LUX) at 518nm.

Proteome Profiler™ Antibody Array

Proteome profiler Antibody assay was performed using Proteome Profiler™ Antibody Array kit (R&D SYSTEMS) with 400µg of protein per sample and the data obtained was quantified using Image J software.

Echocardiography

The animal cardiac function was measured using the small animal imaging system (Vevo LAZR-X 3100, FUJIFILM Visual Sonics). Animals were anesthetized with 4% isoflurane and maintained anesthesia with 1-2% isoflurane during the Imaging procedure. Post-anesthesia, the animal was placed over the animal imaging platform. Essential parameters like respiration rate, electrocardiogram (ECG), body temperature, and heart rate were recorded throughout the imaging. The MX400 ultrasound transducer was used with a mouse small cardiology application in parasternal long-axis view (PLAX). Cardiac functions like cardiac output, ejection fraction, and fractional shortening were calculated from brightness mode (B-mode), where the heart left ventricular region was focused in a two-dimensional manner. Whereas Left ventricular mass (LV mass),systolic volume, diastolic volume were measured for each animal from the Motion Mode (M-mode) image. The echocardiography images were captured from videotape, and data were collected with the help of digital image analysis cardiac package software (Vevo Lab 3.1.1).

Isolation and culture of neonatal rat ventricular myocytes.

Neonatal rat ventricular myocytes (NRVM) from 2-day-old Sprague-Dawley rat pups were isolated. Hearts were dissected and rinsed in Ads buffer (116.3 mMNaCl, 19.7 mM HEPES, 9.4 mMNaH2PO4, 5.5 mM glucose, 5.3 mMKCl, 0.83 mMMgSO4 [pH 7.4]). Atria were removed, and ventricles were minced and incubated at 37°C in a solution of enzymes containing 0.2% collagenase type II (381 U/mg) and pancreatin (0.6 mg/ml) in Ads buffer in the presence of 95% O_2 and 5% CO_2 for 4 successive digestions of 10 min each. The supernatant of the first tissue digestion was discarded. The supernatants obtained after each digestion were centrifuged for 5 min at 1,000 rpm. The cell pellets obtained in each round of digestion were resuspended in M199 growth medium (supplemented with 10% fetal bovine serum, and 100 U/ml penicillin-streptomycin, pH 7.2). The resuspended cells were pooled and passed through cell strainer ,preplated in T25 cm2 flask (BD), and incubated for 1 h in a CO_2 incubator for cardiomyocyte enrichment. The supernatants containing cardiomyocytes were collected by brief centrifugation and resuspended in growth medium. The cells were seeded onto collagen I-coated coverslips (Biocoat; BDLabware, Bedford, USA) in M199 medium supplemented with 10% FBS. Fresh media was replaced after 18 hrs of cell seeding and cultured for 2 days.

Immunofluorescence and Microscopy

Cells were fixed in 4% paraformaldehyde for 20 min washed in PBS and incubated for 5 min in 0.2% triton X-100 in PBS. Cells were blocked in 1% BSA for 30 min before incubating with anti alpha -sarcomeric antibody (Sigma Aldrich) for overnight. Cells were washed 2 times in PBS for 5 min each and incubated with anti-mouse Allexa flour 594 (molecular probes) for 1 hr washed 3X and mounted on slide and pictured.High resolution image were aquired on 63x oil immersion objective lensNA 1.4,on Zeiss LSM 980 confocal microscope and processed on ZEN Blue. All images were acquired under identical Laser power, detector gain, offset and pinhole apperture window.

Statistical analysis

Statistical analysis was performed using Graph-Pad Prism Software version 6. Unpaired, 2-tailed Student's t-test or two-way ANOVA followed by post-hoc Tukey's Test was used to calculate statistically significant differences between control and experimental groups. Data represents mean ± S.D. of 3 individual experiments. Difference between two groups were analyzed using Student's t-test (control and experimental group), along with that individual experimental groups were also compared using Unpaired, 2-tailed Student's t-test. $P < 0.05$ was set as the threshold for statistical significance between the control and various experimental groups.

RESULTS

1.1. Elevated Heart weight/Body weight (HW/BW) ratio and Heart weight/Tibia length ratio on ISO treatment in PPAR α[-/-]mice

ISO treatment in PPAR α[-/-]mice for 2weeks led to increase in Heart weight/Body weight ratio (Fig 1).Heart weight/Body weight ratio (HW/BW) was enhanced in ISO treated wild-type (WT) mice (4.00 ± 0.059 mg/g, $p > 0.0001$) when compared to untreated wild-type mice(3.44 ± 0.13 mg/g, $p > 0.0001$).Untreated PPAR α[-/-]mice even in the absence of ISO showed elevated HW/BW ratio (4.45 ± 0.29 mg/g) when compared to un-treated wild type mice as well as ISO treated wild type mice. However, only marginal increase in HW/BW ratio in ISO-treated PPAR α[-/-]mice (4.6 ± 0.29 mg/g, $p > 0.0001$)) was observed when compared to untreated PPAR α[-/-]mice
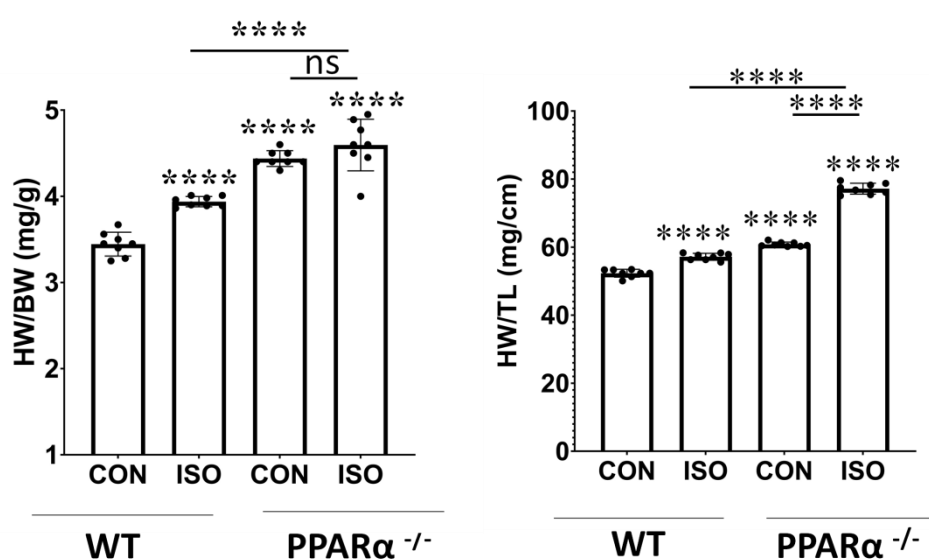
Fig.1. Development of cardiac hypertrophy: Heart weight to body weight ratio (HW/BW) and heart weight to tibia length ratio (HW/TL) in C57BL/6 wild-type mice and PPAR α[-/-]mice (N=8) treated with or without isoproterenol (IP) for 14 days. Data was analysed using two-way ANOVA with Tukey's post-hoc analysis. Difference between two groups was analysed using Student's t-test. (*$p < 0.05$, **$p < 0.01$, ***$p < 0.001$ vs. CON).

Heart weight/Tibia length (HW/TL) ratio resembled the same pattern as the HW/BW ratios in wild-type mice, where significant increase in HW/TL ratio was observed in ISO-treated wild-type as compared to the untreated wild-type mice. Similar results were observed when HW/TL ratio of PPAR α[-/-] mice was calculated, which was enhanced in comparison to the untreated wild type mice. On the contrary, HW/BW ratio and HW/TL ratio were significantly elevated in ISO-treated PPAR α[-/-] mice when compared to PPAR α[-/-] mice. Significant increase in HW/TL ratio was observed when comparison was made between ISO-treated wild type mice as well as ISO-treated PPAR α[-/-] mice, as the latter group was observed to have significantly increased HW/TL ratios when compared to former group.

1.2.Re-expression of foetal genes in response to ISO treatment

Atrial Natriuretic protein (ANP) and Brain Natriuretic protein (BNP) are known to be the markers of cardiac hypertrophy. Therefore, mRNA levels of both ANP and BNP were measured in the control as well as the experimental groups by RT-PCR. Data compared between wild-type mice as well as ISO treated wild-type mice revealed enhanced ANP and BNP mRNA levels in ISO-treated wild type mice as compared to wild-type mice (Fig2). Significant increase in the ANP and BNP mRNA levels were observed in PPAR $\alpha^{-/-}$ mice, even without ISO-treatment. Similar elevated levels of ANP and BNP mRNA were obtained for ISO-treated PPAR $\alpha^{-/-}$ mice, as no significant difference was observed between PPAR $\alpha^{-/-}$ mice as well as ISO-treated PPAR $\alpha^{-/-}$ mice.
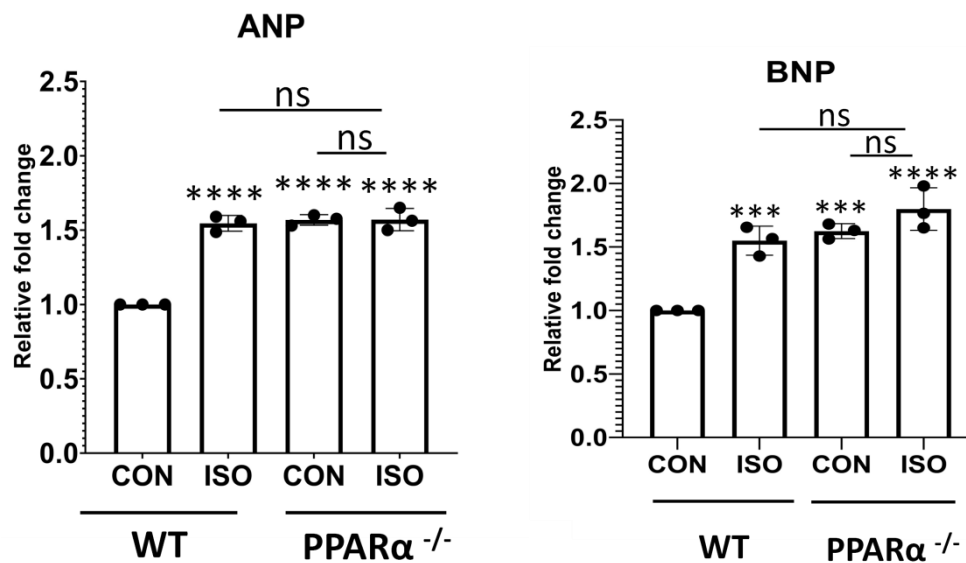
Fig.2.Elevation of foetal genes response to ISO treatment: Gene expression of cardiac stress markers ANP and BNP analysed by real time PCR to assess hypertrophy in C57BL/6 wild-type mice and PPAR $\alpha^{-/-}$mice. Data represent mean $\pm$ S.D. of 3 individual experiments. Data was analysed using two-way ANOVA with Tukey's post-hoc analysis. Difference between two groups was analysed using Student's t-test. (*$p<0.05$, **$p<0.01$, ***$p<0.001$ vs. CON).

No significant change was observed between the elevated ANP and BNP mRNA levels in ISO-treated wild-type mice as well as ISO-treated PPAR $\alpha^{-/-}$ mice. Enhanced levels of ANP and BNP mRNA in ISO-treated wild type mice, untreated PPAR $\alpha^{-/-}$ mice and ISO-treated PPAR $\alpha^{-/-}$ mice were observed when compared to untreated wild-type mice.

1.3.Estimation of cardiac Fibrosis

Myocardial fibrosis is one of the critical pathological changes associated with cardiac hypertrophy as cardiac stress triggers collagen accumulation. Histological evaluation reveals the changes triggered as a response to hypertrophic cardiomyopathy. Masson trichome staining was therefore used to assess cardiac fibrosis. Collagen deposition measured using Masson Trichome staining in control untreated wild-type group showed no accumulation of collagen in

the untreated wild type group, whereas in the ISO-treated wild-type mice collagen deposition was observed (Fig.3.).
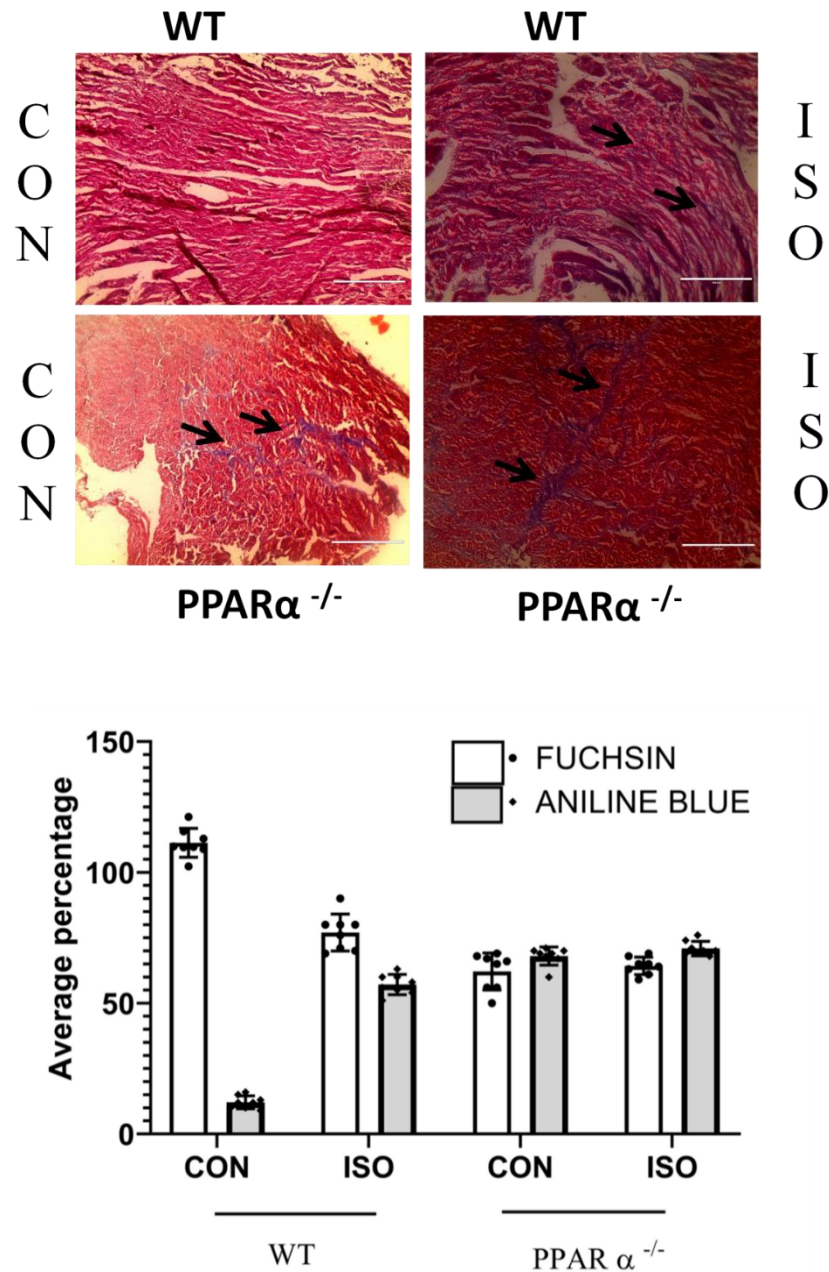
Fig.3. Collagen deposition in cardiac-hypertrophy induced wild-type and PPAR α⁻/⁻mice: Masson Trichome staining to detect collagen deposition; scale bar=200µm; (Blue=Fibrous collagen Red=myocytes, Black=Nuclei). Bar graph representing statistically significant difference in collagen deposition (Aniline Blue) between C57BL/6 and PPAR α⁻/⁻ mice treated with or without isoproterenol. Data represent mean ± S.D. of 8 individual experiments. One histological section per individual sample. Data was analysed using two-way ANOVA with

Tukey's post-hoc analysis. Difference between two groups was analysed using Student's t-test. (*p<0.05, **p<0.01, ***p<0.001 vs. CON).

Aniline Blue stained Fibrous deposition revealed collagen accumulation in ISO-treated wild type mice as indicated by the arrows. Significant increase in collagen deposition was observed in untreated PPAR α⁻/⁻ mice tissue as the Fuchsin stained cytoplasm of the cardiac muscle was distinctly decreased in comparison to the aniline blue stained collagen. ISO treated PPAR α⁻/⁻ mice tissue showed similarly enhanced collagen deposition as untreated PPAR α⁻/⁻ mice tissue. Untreated wild type mice group as well as PPAR α⁻/⁻ mice group exhibits increased fibrosis due to collagen deposition when compared to untreated wild type mice group.
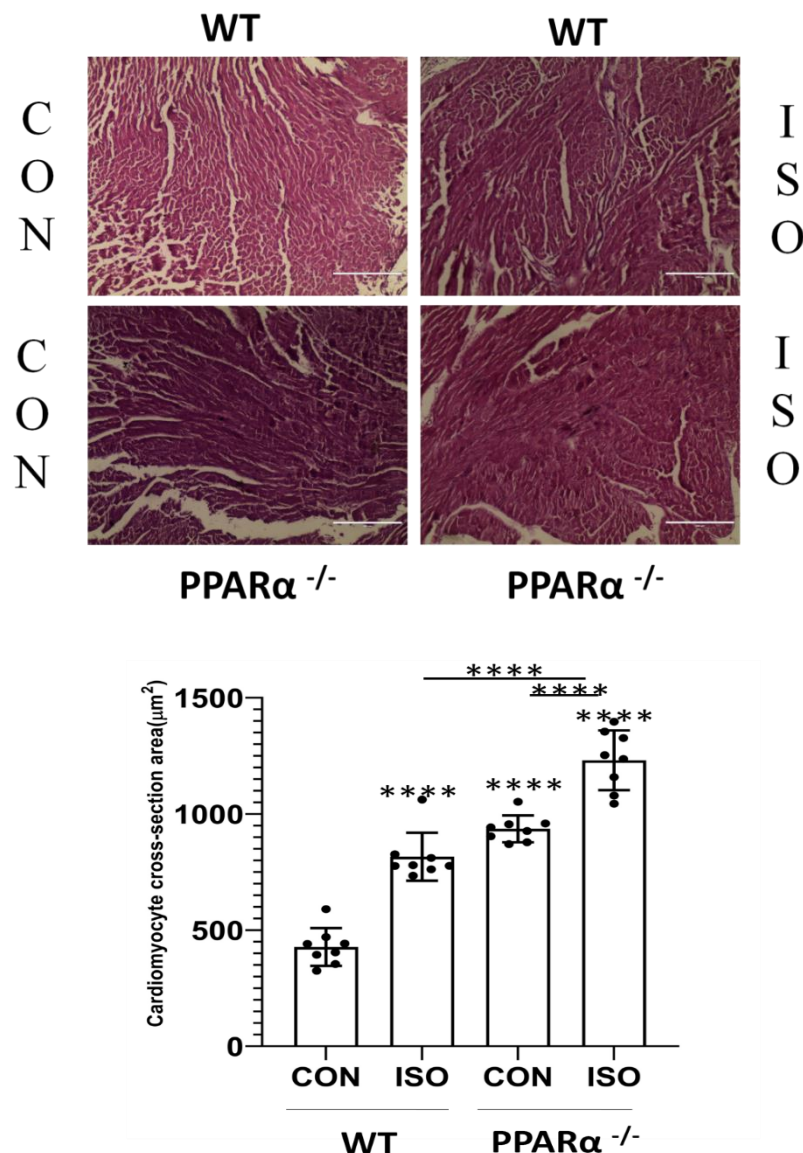
Fig.4. Increase in cardiomyocyte size in wild-type and PPAR α⁻/⁻ mice: Haematoxylin and Eosin (H & E) staining to detect morphological changes; scale bar=200µm Pink=Cytoplasmic protein, Blue/Purple=Nuclei and Bar Graph representing cardiomyocyte cross-section area

(μm^2). Data represent mean ± S.D. of 8 individual experiments. One histological section per individual sample.

1.4. Increase in Cardiomyocyte size

ISO-treated wild type mice exhibits increase in cardiomyocyte size as compared to wild –type control (Fig.4.).Similar increase in cardiomyocyte cross-section area was observed in untreated PPAR $\alpha^{-/-}$ mice. ISO-treated PPAR $\alpha^{-/-}$ mice exhibits increase in cardiomyocyte size resembling untreated PPAR $\alpha^{-/-}$ mice as compared to wild-type control.

1.5. Hemodynamics in Cardiac Hypertrophy

Cardiac function was assessed in wild-type control as well as PPAR $\alpha^{-/-}$ mice by echocardiography. Representative images in M-mode for wild-type control showed no such cardiac abnormalities as observed through the echocardiography (Fig.5.).
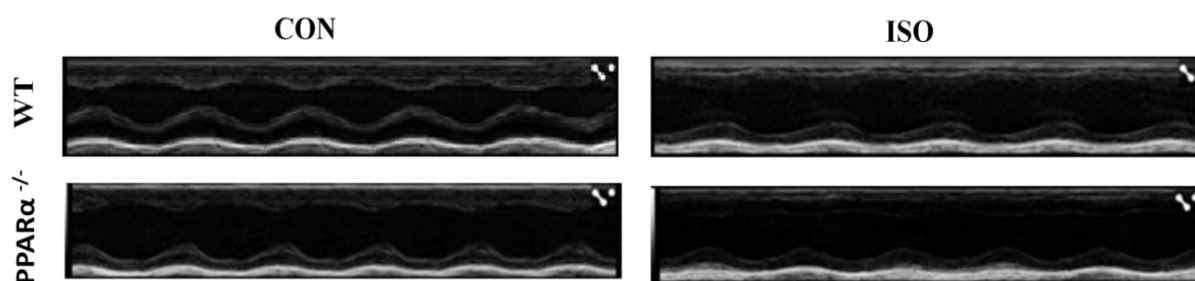
Fig.5.Echocardiography assessment of cardiac function in wild-type and PPAR $\alpha^{-/-}$mice: Representative Images from parasternal short axis view of the heart acquired in M-Mode.

Chronic administration of ISO in wild-type mice elicited severe cardiac abnormalities as observed via the representative images of mice heart in M-mode. Similar impact was observed on untreated PPAR $\alpha^{-/-}$ mice as well as ISO-treated PPAR $\alpha^{-/-}$ mice wherein, the cardiac abnormalities were strikingly noticeable.

EJECTION FRACTION

Ejection fraction calculations that is a measure of systolic dysfunction were obtained. Ejection Fraction for both the control as well as experimental groups revealed significant differences. ISO-treated wild-type mice exhibited significant decrease of 33.29% in Ejection fraction when compared to untreated wild-type control (Fig.6.). Similar significant decrease of 39.4% and 38.73% was observed for untreated PPAR $\alpha^{-/-}$ mice as well as ISO-treated PPAR $\alpha^{-/-}$ mice respectively when compared to untreated wild-type mice. No significant changes were discovered between ISO-treated wild –type mice as well as untreated PPAR $\alpha^{-/-}$ mice and ISO-treated PPAR $\alpha^{-/-}$ mice.

FRACTIONAL SHORTENING

Resembling Ejection Fraction, Fractional shortening is also a measure of the muscular contractility of heart. Fractional shortening was decreased noticeably by 46.7% in ISO-treated wild-type mice when compared to untreated wild-type control (Fig.6.).Untreated PPAR $\alpha^{-/-}$ mice exhibited around 53.5% of decrease in fractional shortening as compared to untreated wild-type control. ISO-treatment of PPAR $\alpha^{-/-}$ mice resulted in similar decrease in Fractional
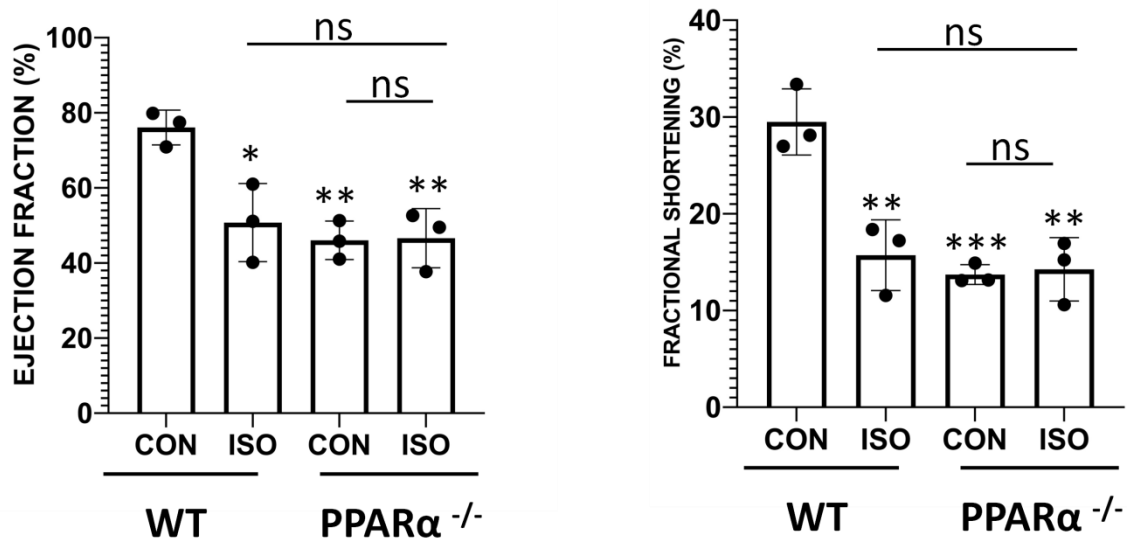
Fig.6. Cardiac function assessment *in vivo*: Bar graphs showing Ejection fraction and Fractional shortening. Data represent mean ± S.D. of 3 individual experiments. Data was analysed using two-way ANOVA with Tukey's post-hoc analysis. (*p<0.05, **p<0.01, ***p<0.001 vs. CON).

Shortening of around 51.67% in comparison to wild-type control. Comparison between ISO-treated wild-type mice as well as untreated PPAR $\alpha^{-/-}$ mice and ISO-treated PPAR $\alpha^{-/-}$ mice revealed no noticeable changes.

LV MASS

LV MASS that is estimated using Echocardiography reveals the weight of the left ventricle and represents the impact of blood pressure on the heart.LV MASS (mg) was markedly enhanced in ISO-treated wild type in comparison to the wild-type control (Fig 7.).Even more pronounced increase in LV MASS was observed for both untreated PPAR $\alpha^{-/-}$ mice as well as ISO-treated PPAR $\alpha^{-/-}$ mice. Significant increase in LV MASS was observed for ISO-treated PPAR $\alpha^{-/-}$ mice when compared to ISO-treated wild type, whereas no noticeable difference was found when comparison was made between PPAR $\alpha^{-/-}$ mice and ISO-treated PPAR $\alpha^{-/-}$ mice.

CARDIAC OUTPUT

Cardiac Output measures the amount of blood heart pumps every minute and thereby reveals the efficiency of the heart. ISO-treated wild-type mice and untreated PPAR $\alpha^{-/-}$ mice exhibited significant decrease of around 31% in cardiac output as compared to wild-type control (Fig.7.).Cardiac output of ISO-treated PPAR $\alpha^{-/-}$ mice revealed marked decrease of around 24.57% when compared to untreated wild-type control. No significant difference was observed in cardiac output between the ISO-treated wild-type mice and ISO- treated PPAR $\alpha^{-/-}$ mice. Similarly, no noticeable change was observed between PPAR $\alpha^{-/-}$ mice and ISO-treated PPAR $\alpha^{-/-}$ mice.
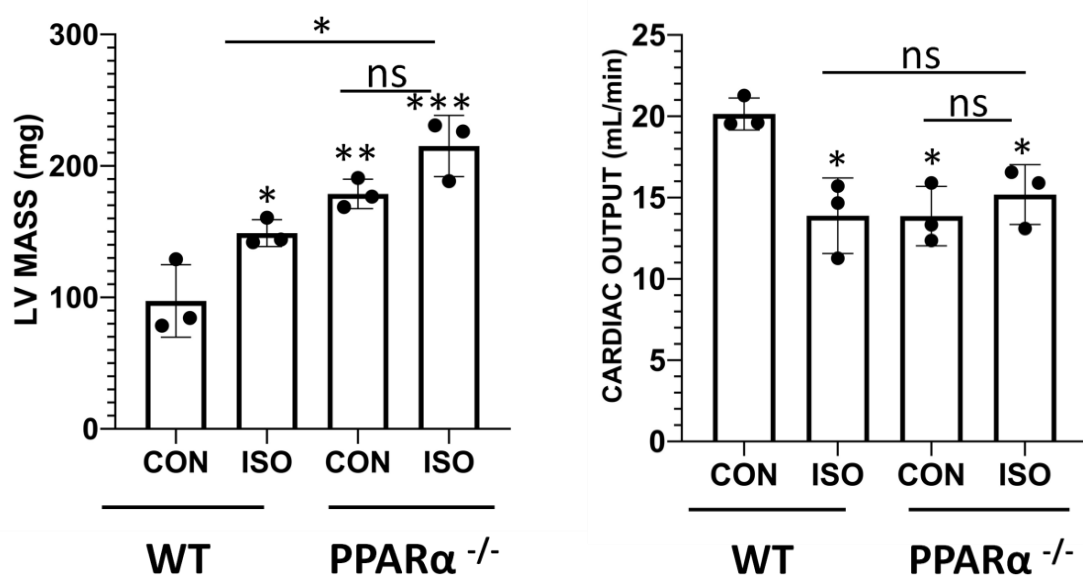
Fig.7. Cardiac function assessment *in vivo*: Bar graphs showing LV Mass and cardiac output. Data represent mean ± S.D. of 3 individual experiments. Data was analysed using two-way ANOVA with Tukey's post-hoc analysis. (*p<0.05, **p<0.01, ***p<0.001 vs. CON).

LV-VOLUME END-SYSTOLE

LV-VOLUME END-SYSTOLE refers to the volume of the blood remaining in the ventricle after the end of systole (contraction) and thereby is another measure of cardiac efficiency. End-systolic volume was markedly elevated in ISO-treated wild-type mice by around 65.24% when compared to untreated wild-type mice (Fig.8.). Untreated PPAR $\alpha^{-/-}$ mice and ISO-treated PPAR $\alpha^{-/-}$ mice exhibited significant increase of 105.5% and 121.5% in LV-Volume End-systole respectively. No remarkable changes were observed in LV-Volume End Systole of ISO-treated wild-type mice as well as ISO-treated PPAR $\alpha^{-/-}$ mice. Similarly, no noticeable difference was observed between untreated PPAR $\alpha^{-/-}$ mice and ISO-treated PPAR $\alpha^{-/-}$ mice.

LV VOLUME END DIASTOLE

LV VOLUME END-DIASTOLE refers to the volume of the heart remaining in the left ventricle before the beginning of diastole (contraction) and pertains to the cardiac efficiency. ISO-treated wild-type mice exhibited remarkably enhanced LV VOLUME END-DIASTOLE
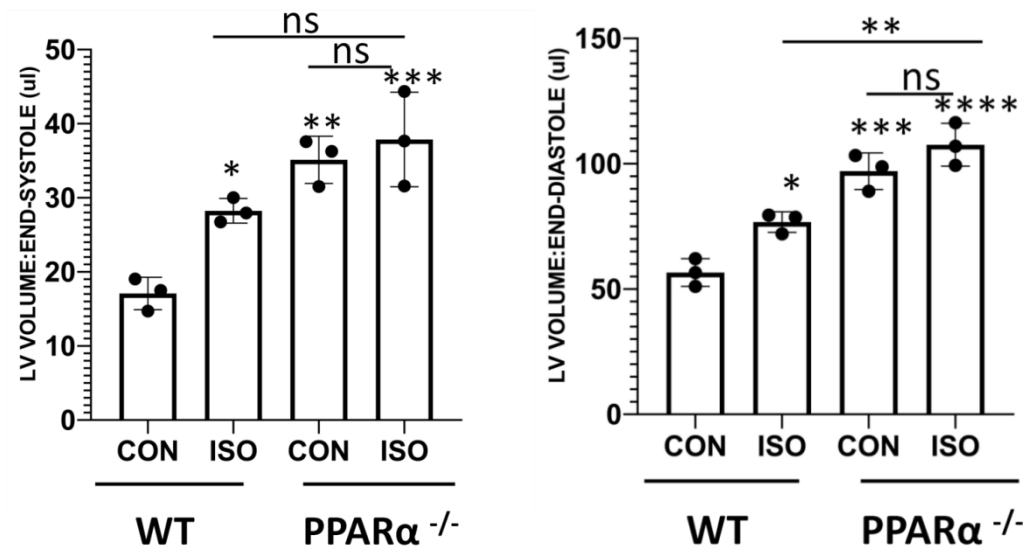
Fig.8. Cardiac function assessment *in vivo*: Bar graphs showing LV Volume: End Systole and LV Volume: End Diastole. Data represent mean ± S.D. of 3 individual experiments. Data was analysed using two-way ANOVA with Tukey's post-hoc analysis. (*$p<0.05$, **$p<0.01$, ***$p<0.001$ vs. CON).

By 34.86%, as compared to untreated wild-type control (Fig.8.).Noticeable increase in LV VOLUME END-DIASTOLE by 71.7% and 90.4% was observed for untreated PPAR $\alpha^{-/-}$ mice and ISO-treated PPAR $\alpha^{-/-}$ mice   respectively. Significant difference in LV VOLUME END-DIASTOLE was observed when comparison was made between ISO-treated wild-type mice and ISO-treated PPAR $\alpha^{-/-}$ mice, thereby revealing remarkable increase in LV VOLUME END-DIASTOLE of ISO-treated PPAR $\alpha^{-/-}$ mice as compared to ISO-treated wild-type mice. No significant change was observed in the LV VOLUME END-DIASTOLE of untreated PPAR $\alpha^{-/-}$ mice as well as ISO-treated PPAR $\alpha^{-/-}$ mice.

1.6. Differential protein expression revealed decrease in specific proteins

Specific proteins and pathways were explored via protein profiling using high resolution mass spectrometry in wild type and PPAR $\alpha^{-/-}$ mice heart tissue. Data obtained from high-resolution mass spectrometer was analysed using SIEVE that revealed significant decrease in proteins involved in Fatty acid β oxidation like Fatty Acid Binding Protein 4(FABP4), Fatty Acid Binding Protein 7 (FABP7), Carnitine PalmitoylTransferase 2 (CPT 2), Acetyl-CoA Acyltransferase 2 (ACAA2), Peroxisomal acyl-coenzyme A oxidase 1(ACOX1) and medium-

chain acyl-CoA dehydrogenase (MCAD) in ISO-treated PPAR $\alpha^{-/-}$ mice (Fig.9.).Mitochondrial proteins like Dominant Optic Atrophy 1 (OPA1) that is mitochondrial Dynamin GTPase and Mitochondrial Fission 1 Protein (FIS 1) were also reduced in ISO-treated PPAR $\alpha^{-/-}$ mice as compared to untreated wild-type control group. Surprisingly, Annexin V that is an apoptosis related protein was found to be significantly downregulated in ISO-treated PPAR $\alpha^{-/-}$ mice. Untreated PPAR $\alpha^{-/-}$ mice resembled the data obtained in ISO-treated PPAR $\alpha^{-/-}$ mice and exhibited similar decrease in the specific proteins.
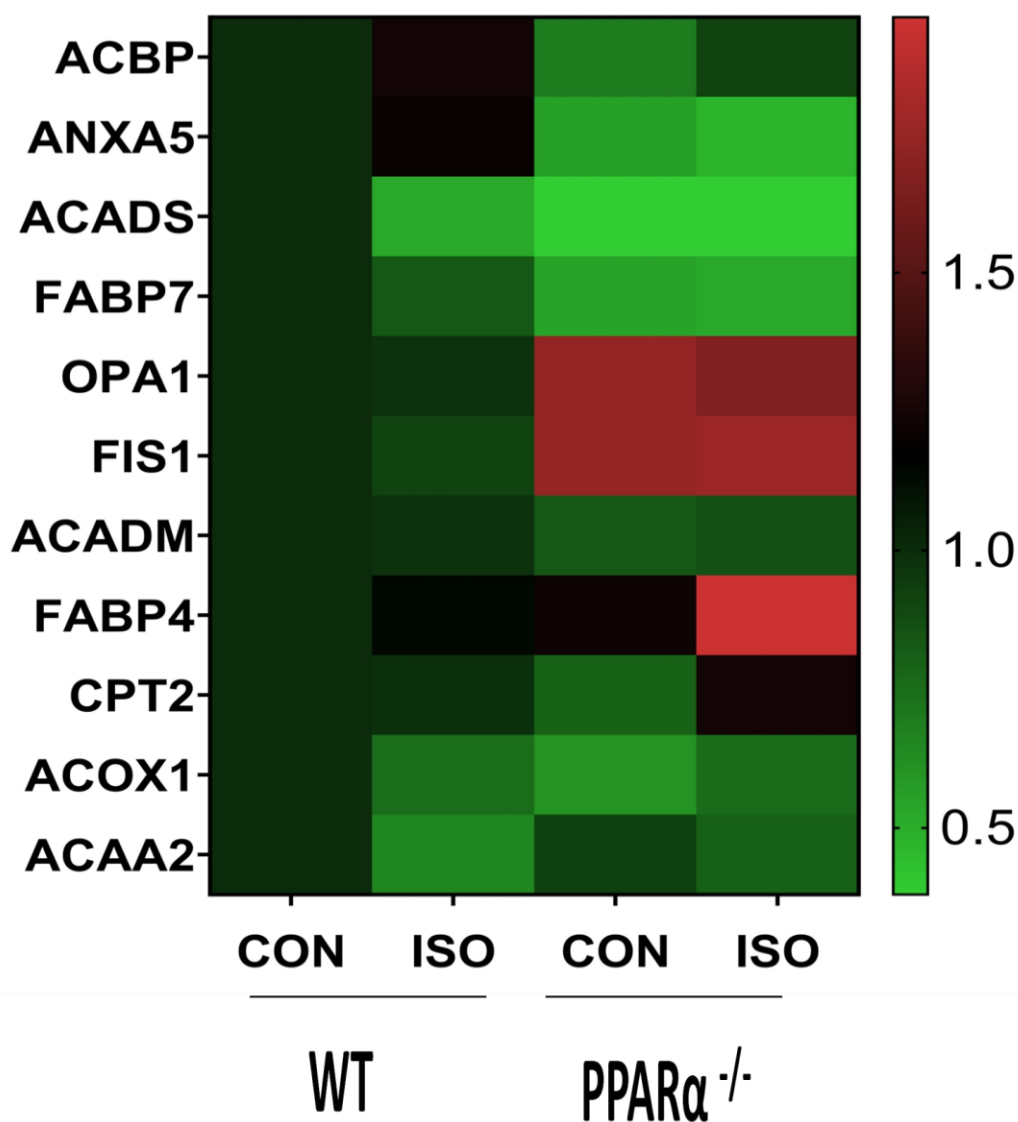
Fig.9. Identification of impaired signalling pathways in wild-type and PPAR $\alpha^{-/-}$ mice heart by Proteomic analysis: Cardiac tissue from wild-type and PPAR $\alpha^{-/-}$ mice were analysed by Orbitrap LC-MS (N=5) followed by relative quantification of differentially expressed protein by SIEVE

1.7. Proteomics Data analysis using PANTHER PATHWAY ANALYSIS TOOL

Proteomics Data analysed using PANTHER SOFTWARE revealed enrichment of p53 Pathway in ISO-treated wild-type mice when compared to untreated wild-type control (Fig.10.).Surprisingly, p53-pathway was significantly decreased in untreated PPAR $\alpha^{-/-}$ mice and ISO-treated PPAR $\alpha^{-/-}$ mice as compared to ISO-treated wild-type mice group.
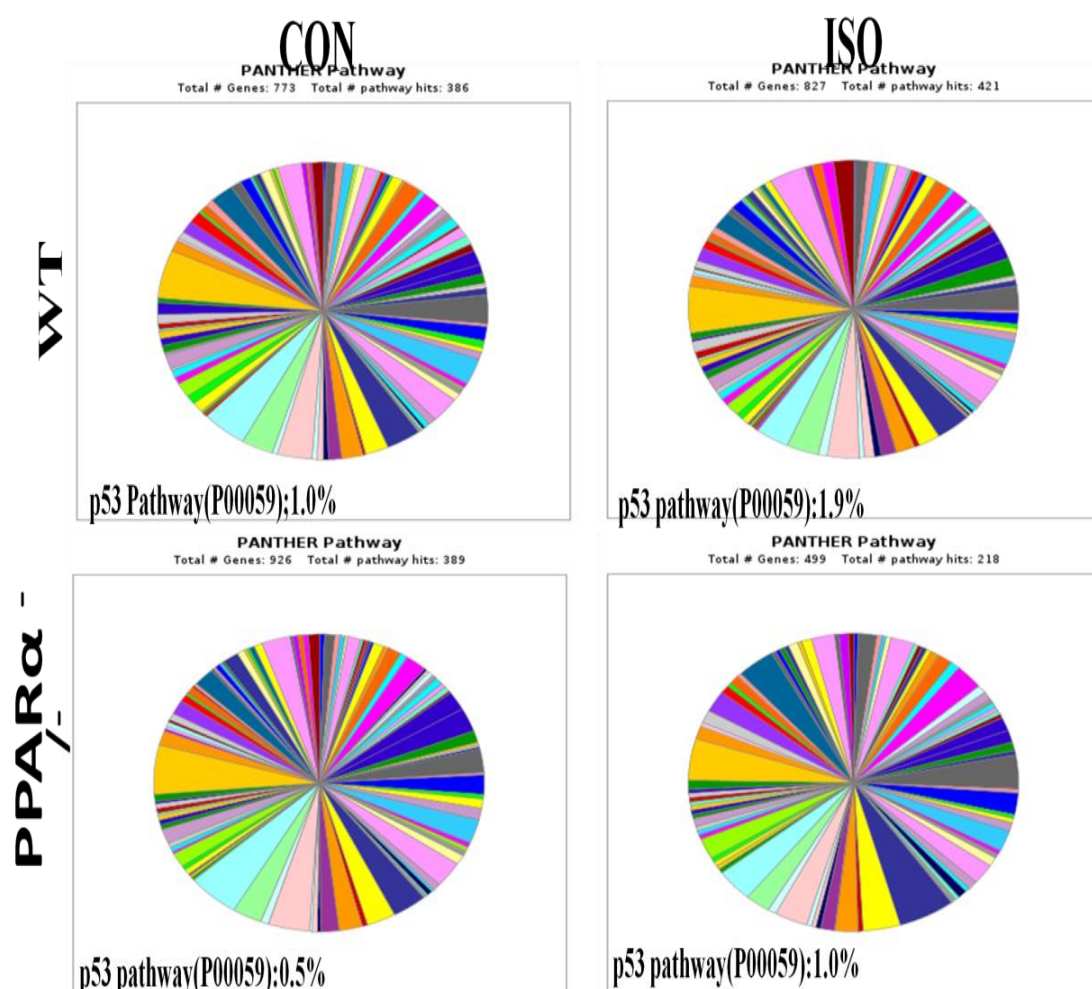
Fig.10. Panther classification of differentially enriched signalling pathways: Enrichment of specific pathways analysed using Panther classification.

1.8. VALIDATION OF CARDIAC GENES DOWN REGULATION USING RT-PCR

ISO-treated wild type mice exhibited reduction in ACOX1, Acyl CoA Oxidase 1, mRNA levels as compared to wild-type control (Fig.11).Untreated PPAR $\alpha^{-/-}$ mice revealed no significant change in ACOX1 as compared to wild-type control. On the contrary, ACOX1 levels were noticeably enhanced in ISO-treated PPAR $\alpha^{-/-}$ mice in comparison to wild-type control group. No significant change was observed when comparison was made between ISO-treated wild-

type control and ISO-treated PPAR $\alpha^{-/-}$ mice. Remarkable difference was observed between the ACOX1 mRNA levels of untreated PPAR $\alpha^{-/-}$ mice and ISO-treated PPAR $\alpha^{-/-}$ mice as untreated PPAR $\alpha^{-/-}$ mice group exhibited no noticeable difference from wild-type control group.

ISO-treated wild type mice and PPAR $\alpha^{-/-}$ mice group, both treated as well as untreated PPAR $\alpha^{-/-}$ mice group displayed remarkable elevated ACAA2, Acetyl-CoA Acyltransferase 2, mRNA levels in comparison to untreated wild-type control (Fig.11.).ISO- treated wild-type exhibited no significant difference in comparison to ISO-treated PPAR $\alpha^{-/-}$ mice, whereas ACAA2 mRNA levels were significantly increased in ISO-treated PPAR $\alpha^{-/-}$ mice when compared to untreated PPAR $\alpha^{-/-}$ mice.

Fig.11. Validation of proteomics data using RT-PCR: Expression of PPAR α target genes, such as ACOX1 and ACAA2 was examined. GAPDH was used as the loading control. Data represents mean ± S.D. of 3 separate experiments. Data was analysed using two-way ANOVA with Tukey's post-hoc analysis. Difference between two groups was analysed using Student's t-test. (*p<0.05, **p<0.01, ***p<0.001 vs. CON).

Significant downregulation of ACAA1A, acetyl-CoenzymeA acyltransferase 1, was observed in ISO- treated wild-type mice, untreated PPAR $\alpha^{-/-}$ mice and ISO-treated PPAR $\alpha^{-/-}$ mice on comparison with wild-type control group (Fig.12.).No remarkable change was observed between the experimental groups, ISO- treated wild-type mice and ISO-treated PPAR $\alpha^{-/-}$ mice. Similarly, untreated PPAR $\alpha^{-/-}$ mice exhibited no noticeable change in ACAA1A mRNA levels when compared to ISO-treated PPAR $\alpha^{-/-}$ mice.

Another Fatty acid β oxidation enzyme, HSD17B12, 17-beta hydroxysteroid dehydrogenase-12, was significantly downregulated in ISO- treated wild-type mice, untreated PPAR $\alpha^{-/-}$ mice and ISO-treated PPAR $\alpha^{-/-}$ mice when compared to untreated wild-type control (Fig.12).Both the experimental groups ISO- treated wild-type mice as well as ISO-treated PPAR $\alpha^{-/-}$ mice

exhibited similar downregulation with no remarkable change in HSD17B12 mRNA levels between the two groups. Untreated PPAR $\alpha^{-/-}$ mice resembled the experimental groups in the downregulation of HSD17B12, with no noticeable change in comparison to ISO-treated PPAR $\alpha^{-/-}$ mice.

Expression of Protein Kinase AMP-Activated Non-Catalytic Subunit Gamma 2(PRKAG 2), an enzyme independent of PPAR α regulation was examined in both the control as well as experimental groups (Fig.13.).Significant downregulation of PRKAG2 was observed in ISO-treated wild-type mice, whereas untreated PPAR $\alpha^{-/-}$ mice displayed no significant change when compared to wild-type control group. ISO- treated PPAR $\alpha^{-/-}$ mice resembled ISO- treated wild-type mice in the downregulation of PRKAG 2 in comparison to wild-type control, and no significant change was observed between the two experimental groups. Untreated PPAR $\alpha^{-/-}$ mice displayed significant difference when compared to ISO- treated PPAR $\alpha^{-/-}$ mice.

E1A Binding Protein P300 (EP300), another enzyme that is independent of PPAR α regulation was examined. ISO-treated wild-type mice exhibited significant decline in EP300 mRNA levels as compared to wild-type control (Fig.13.).On the contrary, untreated PPAR $\alpha^{-/-}$ mice revealed no such change in comparison to wild-type control. ISO-treated PPAR $\alpha^{-/-}$ mice resembled ISO-treated wild-type mice in down regulation of EP300, and the two experimental groups exhibited no noticeable change unlike untreated PPAR $\alpha^{-/-}$ mice that displayed similar expression pattern of EP300 as wild-type control group.
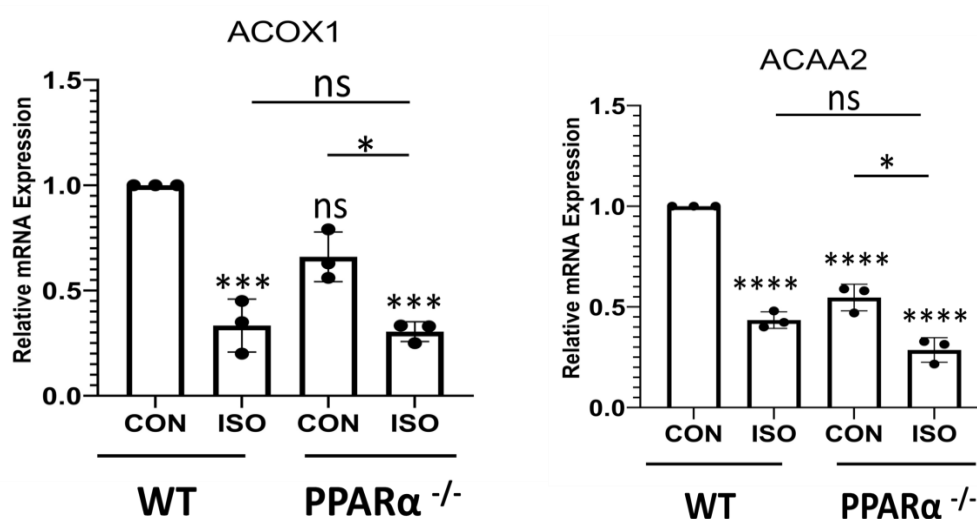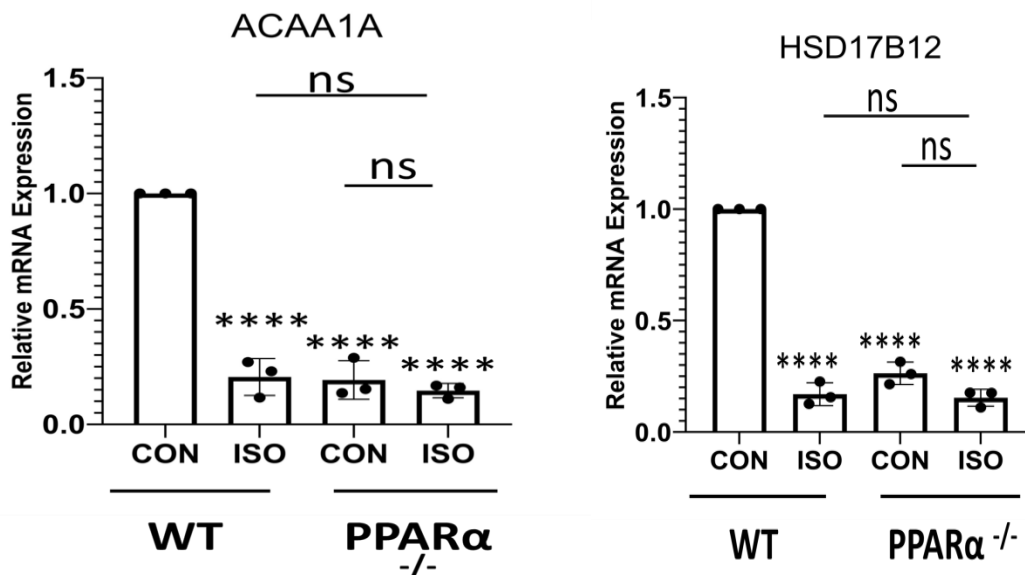

Fig.12. Validation of proteomics data using RT-PCR: Expression of PPAR α target genes, such as ACAA1A and HSD17B12 was examined. GAPDH was used as the loading control. Data represents mean $\pm$ S.D. of 3 separate experiments. Data was analysed using two-way ANOVA with Tukey's post-hoc analysis. Difference between two groups was analysed using Student's t-test. (*$p<0.05$, **$p<0.01$, ***$p<0.001$ vs. CON).
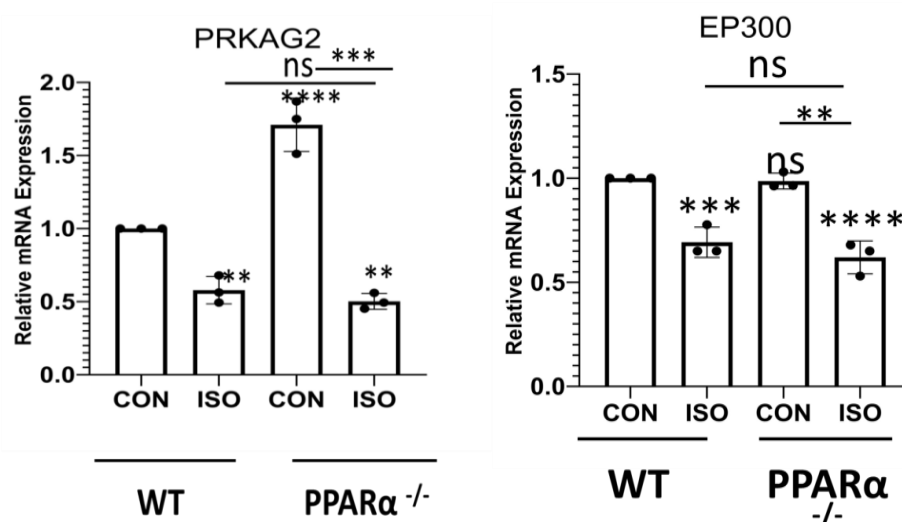
Fig.13. Validation of proteomics data using RT-PCR: Expression of PPAR α unregulated genes, such as PRKAG2 and EP300 was examined. GAPDH was used as the loading control. Data represents mean ± S.D. of 3 separate experiments. Data was analysed using two-way ANOVA with Tukey's post-hoc analysis. Difference between two groups was analysed using Student's t-test. (*$p<0.05$, **$p<0.01$, ***$p<0.001$ vs. CON).

1.9. VALIDATION OF DIFFERENTIAL EXPRESSION OF CARDIAC GENES BY IMMUNOBLOTTING

Expression of proteins like Dominant Optic Atrophy 1(OPA 1) and Annexin V was examined in both control as well as experimental groups using western blotting (Fig.14).Western Blotting data revealed downregulation of OPA1 in ISO-treated wild type mice group whereas untreated PPAR $\alpha^{-/-}$ mice exhibited no remarkable change as compared to wild-type control group. On the contrary to the untreated PPAR $\alpha^{-/-}$ mice, ISO-treated PPAR $\alpha^{-/-}$ mice exhibited noticeable down regulation of OPA 1 protein when compared to wild-type control group. Annexin V, an apoptosis related protein was significantly enhanced in ISO-treated wild-type mice group in comparison to wild-type control group. Surprisingly, both untreated PPAR $\alpha^{-/-}$ mice as well as ISO-treated PPAR $\alpha^{-/-}$ mice exhibited significant decline in Annexin V protein levels in comparison to wild-type control group.
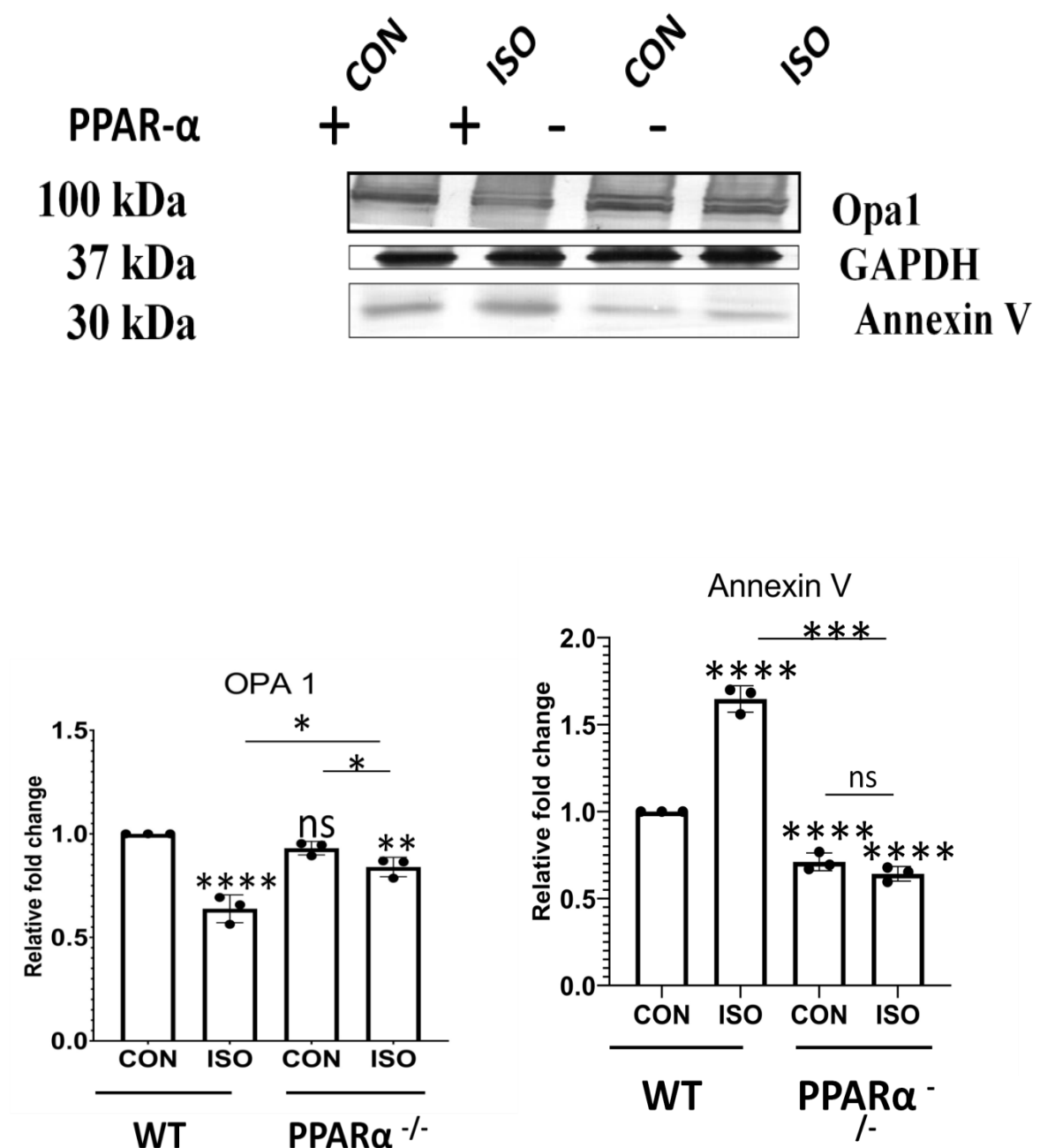
Fig.14. Validation of proteomics data by immunoblotting: The expression of Annexin V and OPA 1 was examined by immunoblotting which was quantitated by densitometric analysis. GAPDH was used as the loading control. Data represents mean ± S.D. of 3 separate experiments. Data was analysed using two-way ANOVA with Tukey's post-hoc analysis. Difference between two groups was analysed using Student's t-test. (*p<0.05, **p<0.01, ***p<0.001 vs. CON).
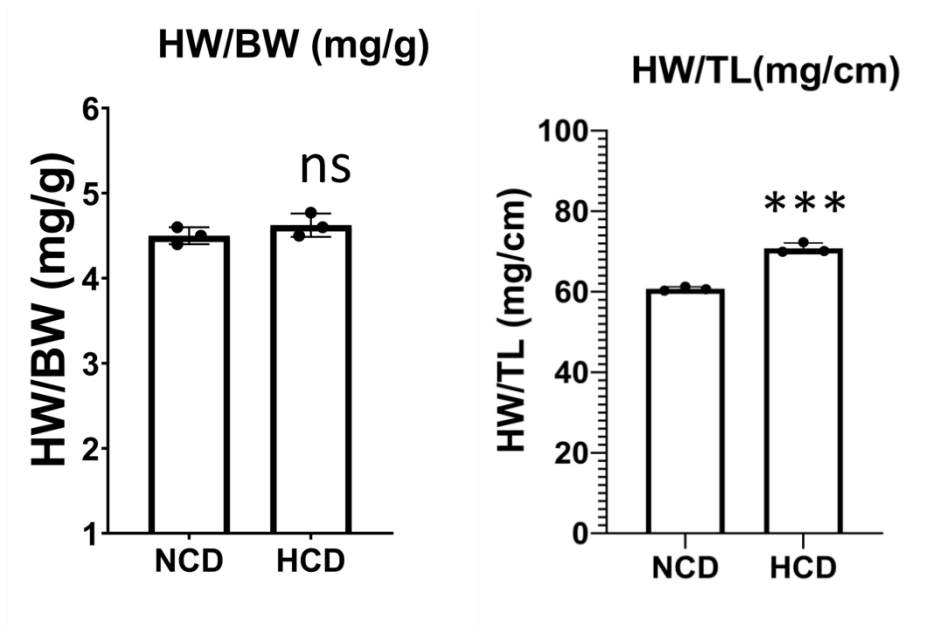
Fig.15. Development of cardiac hypertrophy in HCD-fed PPAR α$^{-/-}$mice: Heart weight to body weight ratio (HW/BW) and heart weight to tibia length ratio (HW/TL) in PPAR α$^{-/-}$mice fed with High-cholesterol diet (HCD) or without HCD (NCD). Data represent mean ± S.D. of 3 individual experiments Difference between two groups was analysed using Student's t-test. (*p<0.05, **p<0.01, ***p<0.001 vs. CON).

1.10. Heart weight/Body weight(HW/BW) ratio and Heart weight/Tibia length ratio in High-Cholesterol Diet fed PPAR α$^{-/-}$mice

To further explore this downregulation of Annexin V, an apoptosis related protein, another mouse model was used i.e., High-cholesterol Diet fed PPAR α$^{-/-}$mice model. Heat weight/Body weight ratio (HW/BW) in High-cholesterol Diet fed PPAR α$^{-/-}$mice exhibited no significant change in comparison to Normal chow Diet fed PPAR α$^{-/-}$mice (Fig.15.) .On the contrary, Heart weight/Tibia length (HW/TL) was markedly enhanced in High-cholesterol Diet fed PPAR α$^{-/-}$mice when compared to Normal chow Diet fed PPAR α$^{-/-}$mice(Fig.15.).

1.11. Re-expression of foetal gens in High-Cholesterol Diet fed PPAR α$^{-/-}$mice

Atrial Natriuretic protein (ANP) and Brain Natriuretic protein (BNP) mRNA levels were measured in the control as well as the experimental groups using RT-PCR (Fig.16.). Data compared between Normal chow Diet fed PPAR α$^{-/-}$mice and High-cholesterol Diet fed PPAR α$^{-/-}$mice revealed no significant change.

Fig.16.Elevation of foetal genes in response to HCD: Gene expression of cardiac stress markers ANP and BNP analysed by real time PCR to assess hypertrophy in HCD-fed PPAR $\alpha^{-/-}$mice. Data represent mean ± S.D. of 3 individual experiments Difference between two groups was analysed using Student's t-test. (*p<0.05, **p<0.01, ***p<0.001 vs. CON).

1.12. Extensive Collagen accumulation in High-Cholesterol Diet fed PPAR $\alpha^{-/-}$mice

Masson Trichome staining used to measure collagen accumulation in Normal chow Diet fed PPAR $\alpha^{-/-}$mice and High-cholesterol Diet fed PPAR $\alpha^{-/-}$mice revealed significant deposition of fibrous collagen, as indicated by Aniline Blue stained collagen against Fuchsin stained cytoplasmic background of the cardiac muscle (Fig.17.).

1.13. Cardiac hypertrophy in High-Cholesterol Diet fed PPAR $\alpha^{-/-}$mice

Cardiomyocyte size as calculated by the cardiomyocyte cross section area (μm^2) was significantly enhanced in High-Cholesterol Diet fed PPAR $\alpha^{-/-}$mice as compared to Normal chow Diet fed PPAR $\alpha^{-/-}$mice (Fig.18.).
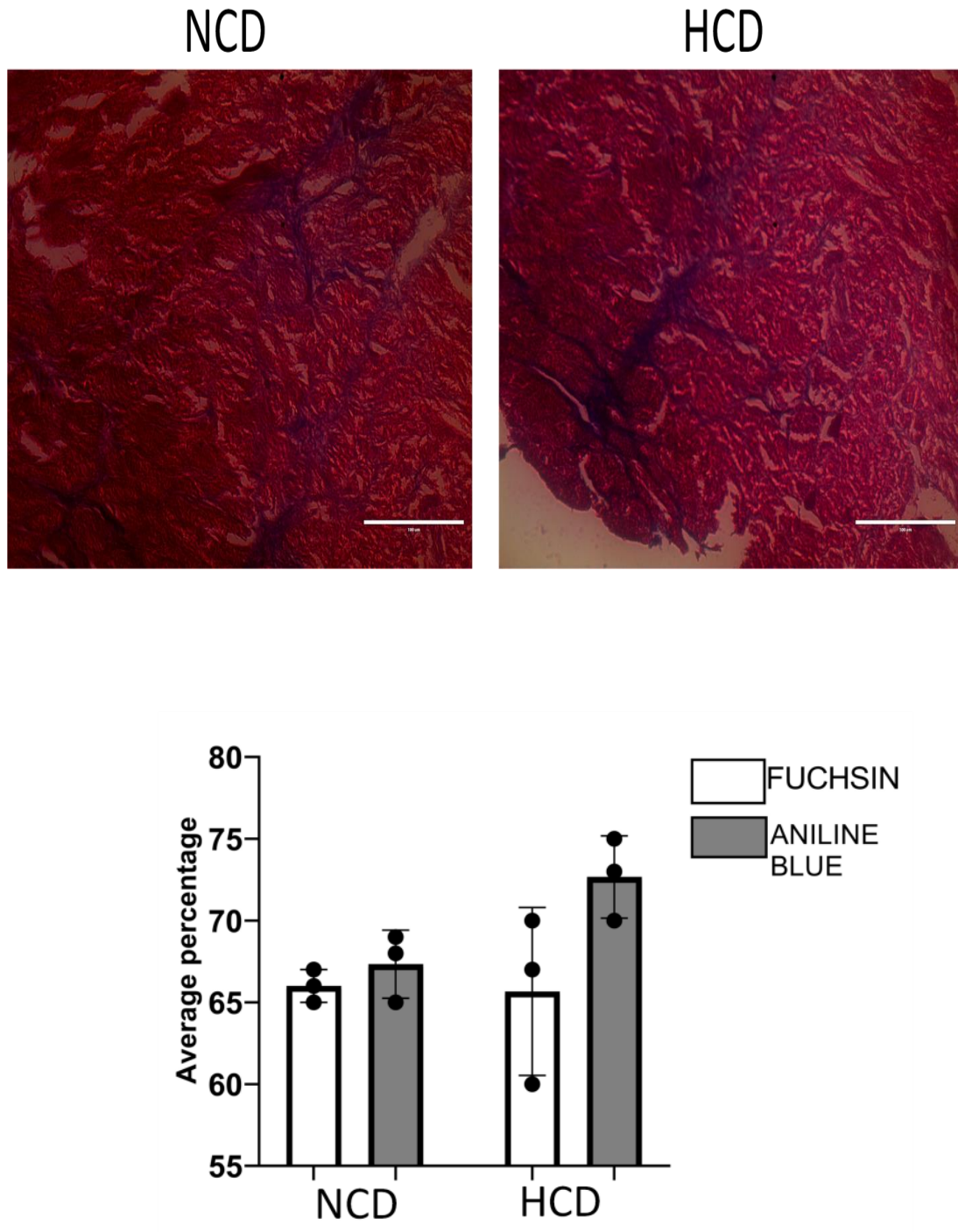
Fig.17. Collagen deposition in HCD-fed PPAR α$^{-/-}$mice: Masson Trichome staining to detect collagen deposition; scale bar=200µm; (Blue=Fibrous collagen Red=myocytes, Black=Nuclei). Data represent mean ± S.D. of 3 individual experiments. One individual section per individual sample. Bar graph representing statistically significant difference in collagen deposition (Aniline Blue) between NCD and HCD-fed mice. Difference between two groups was analysed using Student's t-test. (*p<0.05, **p<0.01, ***p<0.001 vs. CON).
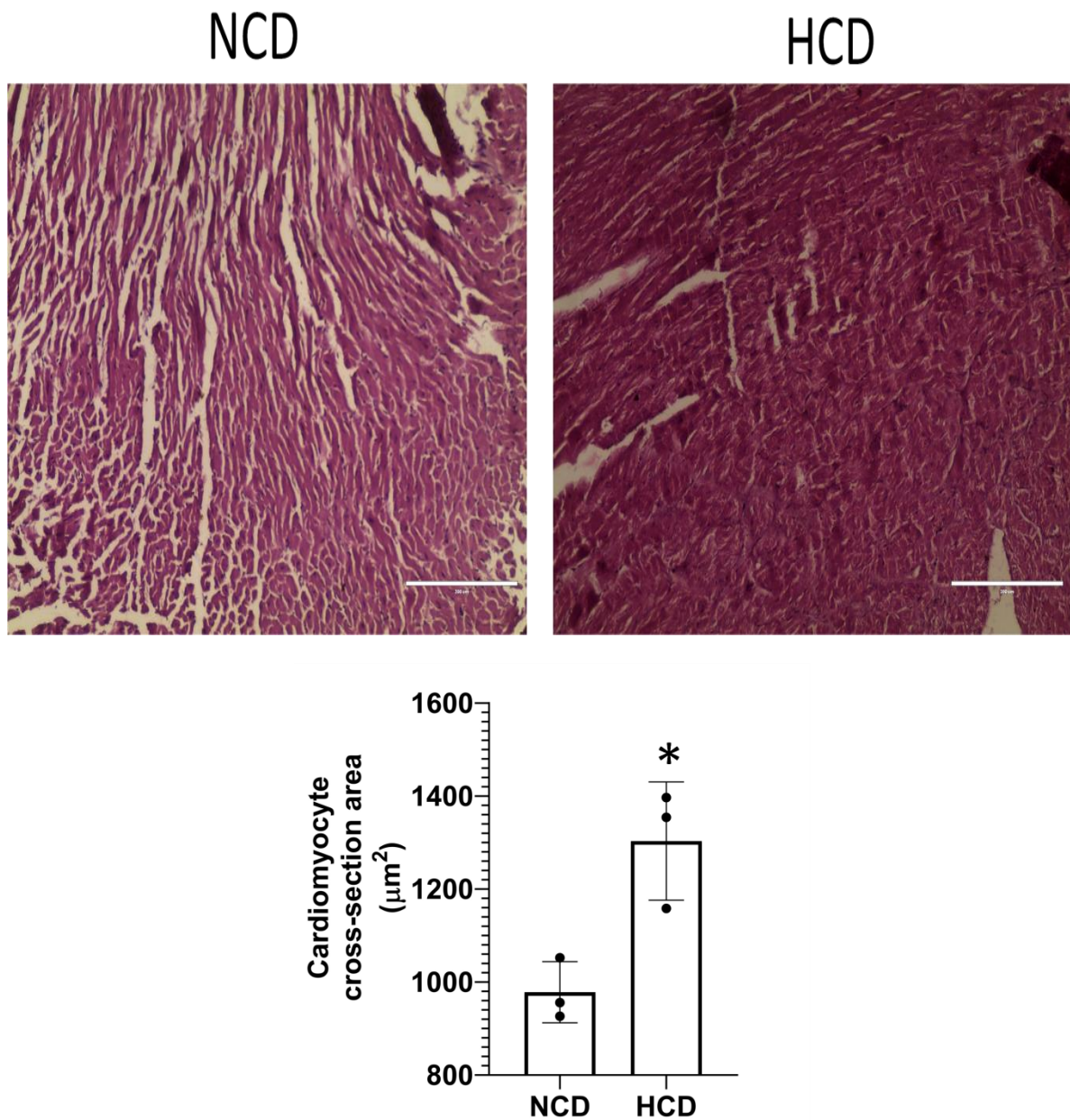
Fig.18. Increase in cardiomyocyte size in HCD-fed PPAR α$^{-/-}$mice: Haematoxylin and Eosin (H & E) staining to detect morphological changes; scale bar=200µm Pink=Cytoplasmic protein, Blue/Purple=Nuclei and Bar Graph representing cardiomyocyte cross-section area (µm^2). Data represent mean ± S.D. of 3 individual experiments. One histological section per individual sample.
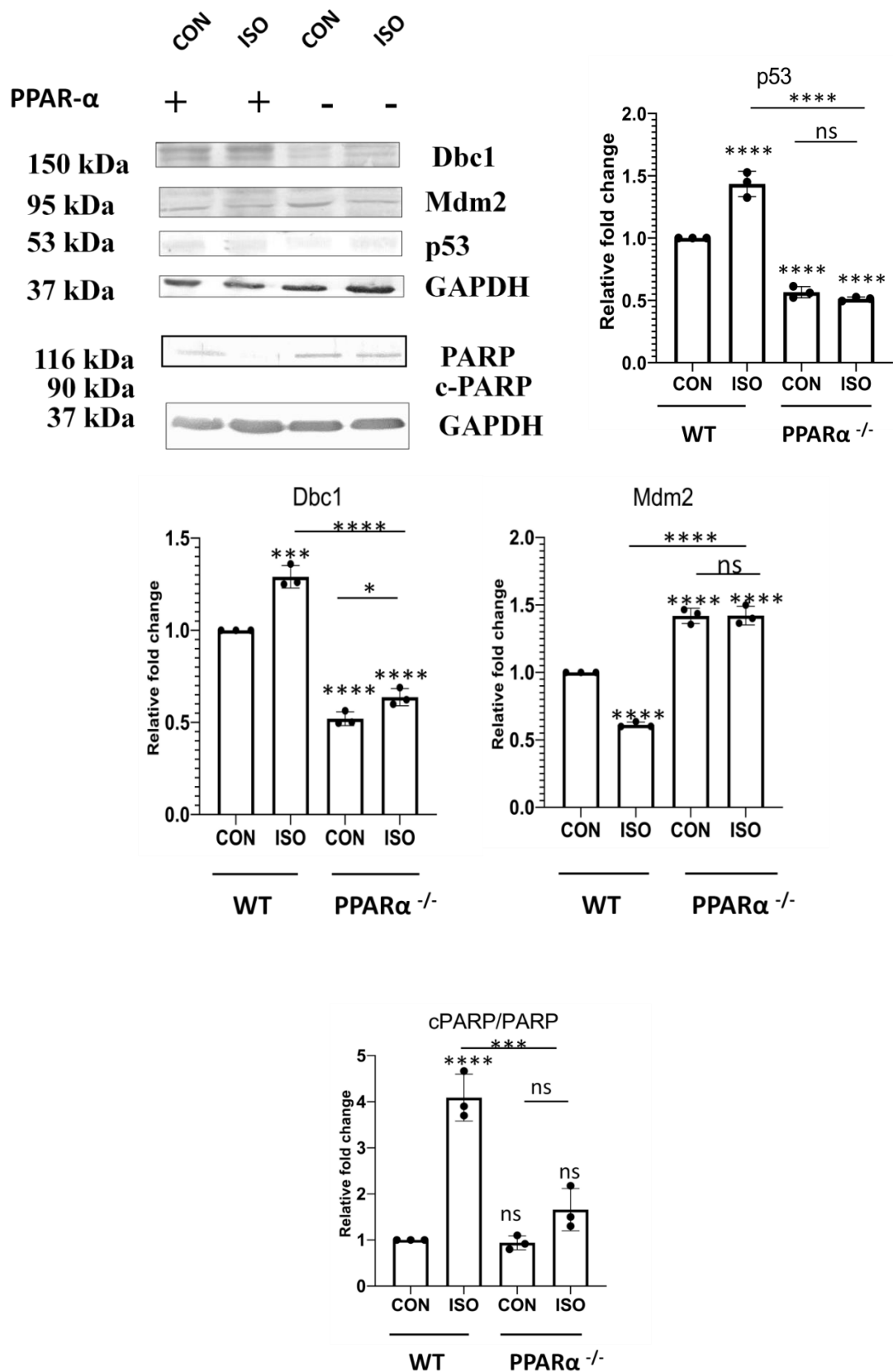
Fig.19. Attenuation of Apoptotic markers: Protein levels of apoptotic markers p53, Dbc1, Mdm2 and c-PARP in mice heart tissue compared via immunoblot. GAPDH was used as a loading control. Data represents mean ± S.D. of 3 individual experiments. Data was analysed

using two-way ANOVA with Tukey's post-hoc analysis. Difference between two groups was analysed using Student's t-test. (*p<0.05, **p<0.01, ***p<0.001 vs. CON).

1.14. Down regulation of apoptotic marker p53

Apoptotic marker p53 protein level was significantly enhanced in ISO-treated wild-type mice as compared to wild-type control (Fig.19.).On the contrary, p53 protein level was significantly declined in untreated PPAR $\alpha^{-/-}$ mice as well as ISO-treated PPAR $\alpha^{-/-}$ mice as compared to wild-type control group. ISO-treated PPAR $\alpha^{-/-}$ mice exhibited remarkable decrease in p53 protein level in comparison to ISO-treated wild-type mice.

1.15. Downregulation of Dbc1 along with concurrent increase in Mdm2

To further explore this downregulation of p53 in PPAR $\alpha^{-/-}$ mice, two critical regulators of p53, i.e., Deleted in Breast Cancer 1 (DBC1) and Mouse double minute 2 homolog (MDM2) were examined (Fig.19.).Protein level of DBC1 was noticeably enhanced in ISO-treated wild-type mice and resembled the same expression pattern as p53.Conversely, DBC1 was significantly downregulated in untreated PPAR $\alpha^{-/-}$ mice as well as ISO-treated PPAR $\alpha^{-/-}$ mice as compared to wild-type control and similarly resembled p53 in its expression pattern. On the contrary, protein expression of MDM2 was distinctly opposite to that of DBC1 and was significantly upregulated in PPAR $\alpha^{-/-}$ mice, both untreated as well as ISO-treated. ISO-treated wild-type mice exhibited significant downregulation of MDM2 when compared to wild-type control, untreated PPAR $\alpha^{-/-}$ mice and ISO-treated PPAR $\alpha^{-/-}$ mice.

1.16. Decrease in cPARP/ PARP protein ratio in ISO-treated PPAR $\alpha^{-/-}$ mice

 Another apoptotic marker cPARP/ PARP ratio was examined in both control as well as experimental groups (Fig.19.). Protein ratio of cPARP/ PARP was significantly elevated in ISO-treated wild-type when compared to wild-type control. Surprisingly, cPARP/PARP protein ratio was remarkably decreased in untreated PPAR $\alpha^{-/-}$ mice and ISO-treated PPAR $\alpha^{-/-}$ mice, thereby resembling p53 protein expression pattern.

1.17. Decrease in   c-Caspase 9/Procaspase 9 protein ratio in ISO-treated PPAR $\alpha^{-/-}$ mice

To further explore down regulation of apoptotic markers in ISO-treated PPAR $\alpha^{-/-}$ mice, another apoptotic marker, c-Caspase 9/Procaspase 9 protein ratio was analysed (Fig.20.). Data revealed significant decline in the c-Caspase 9/Procaspase 9 protein ratio in ISO-treated PPAR $\alpha^{-/-}$ mice whilst ISO-treated wild-type mice and untreated PPAR $\alpha^{-/-}$ mice exhibited no change in comparison to wild-type control group.
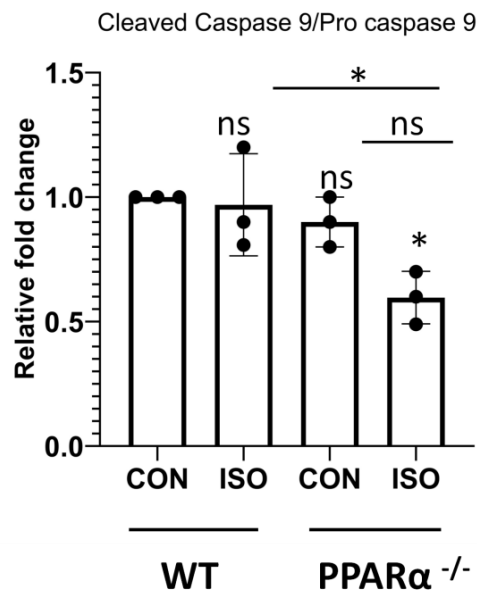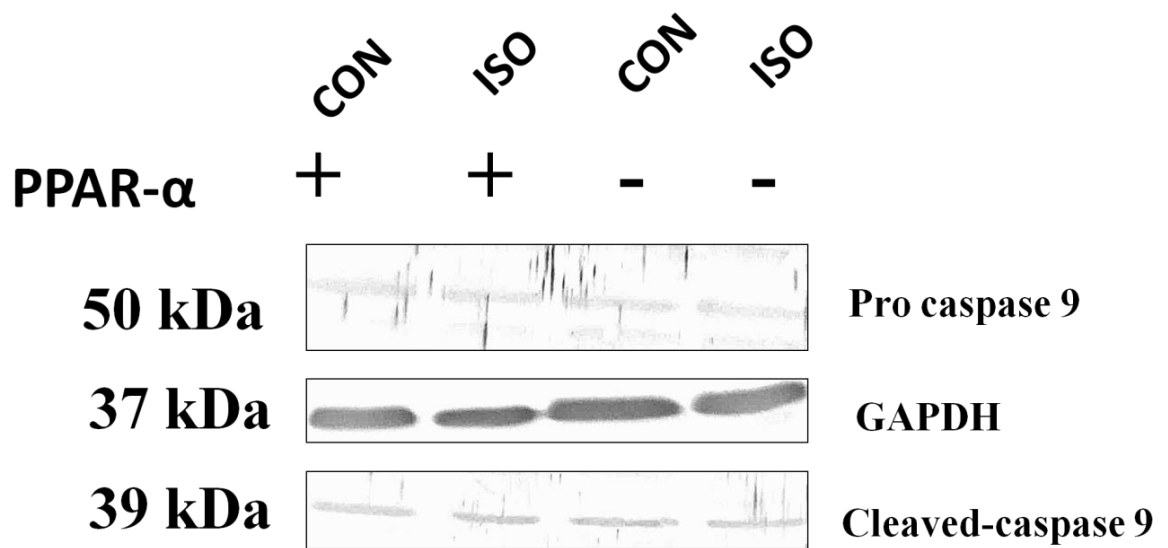
Fig.20. Attenuation of Apoptotic markers: Protein levels of apoptotic marker cCaspase 9 in mice heart tissue examined via immunoblot. GAPDH was used as a loading control. Data represents mean ± S.D. of 3 individual experiments. Data was analysed using two-way ANOVA with Tukey's post-hoc analysis. Difference between two groups was analysed using Student's t-test. (*$p < 0.05$, **$p < 0.01$, ***$p < 0.001$ vs. CON).
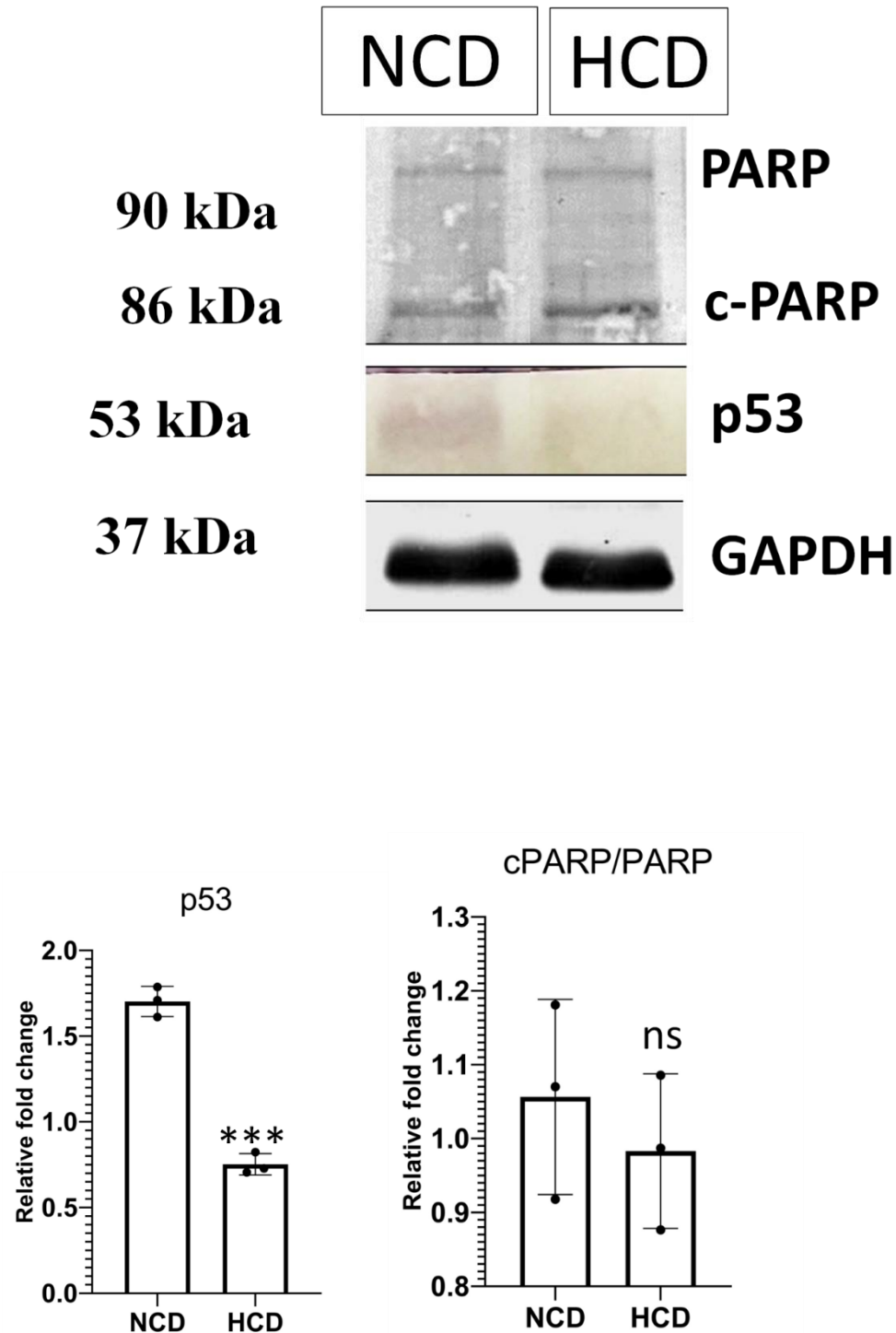
Fig.21. Attenuation of Apoptotic markers: Protein levels of apoptotic markers p53 and c-PARP in normal chow diet fed (NCD) PPAR α $^{-/-}$ mice as well as high cholesterol diet fed (HCD) PPAR α $^{-/-}$ mice compared using immunoblot. GAPDH was used as a loading control. Data represents mean ± S.D. of 3 individual experiments. Difference between two groups was analysed using Student's t-test. (*p<0.05, **p<0.01, ***p<0.001 vs. CON).

1.18. Downregulation of apoptotic markers in High-Cholesterol Diet fed PPAR α$^{-/-}$ mice

To further establish this phenomenon of downregulation of apoptosis in Cardiac hypertrophy in PPAR α$^{-/-}$ mice, apoptotic markers were also examined in High-Cholesterol Diet (HCD) fed PPAR α$^{-/-}$mice (Fig.21.).Protein level of p53 in HCD fed PPAR α$^{-/-}$mice resembled ISO-treated PPAR α$^{-/-}$ mice in expression pattern as p53 was remarkably downregulated in HCD-fed PPAR α$^{-/-}$ mice when compared to Normal chow Diet (NCD) fed PPAR α$^{-/-}$ mice. Another protein marker cPARP was analysed in both the control as well as experimental groups. Protein ratio of cPARP/ PARP showed no noticeable change between NCD fed PPAR α$^{-/-}$mice and HCD fed PPAR α$^{-/-}$ mice.

1.19. Down regulation of PTEN in ISO-treated PPAR α$^{-/-}$mice

Phosphatase and tensin homolog (PTEN), that is a major positive regulator of apoptosis was examined to further unleash the mechanism behind the remarkable downregulation of apoptotic markers in cardiac hypertrophy induced PPAR α$^{-/-}$mice. Protein level of PTEN was noticeably elevated in ISO-treated wild-type mice whereas downregulated in untreated PPAR α$^{-/-}$mice and ISO-treated PPAR α$^{-/-}$mice in comparison to wild-type control (Fig.22.).
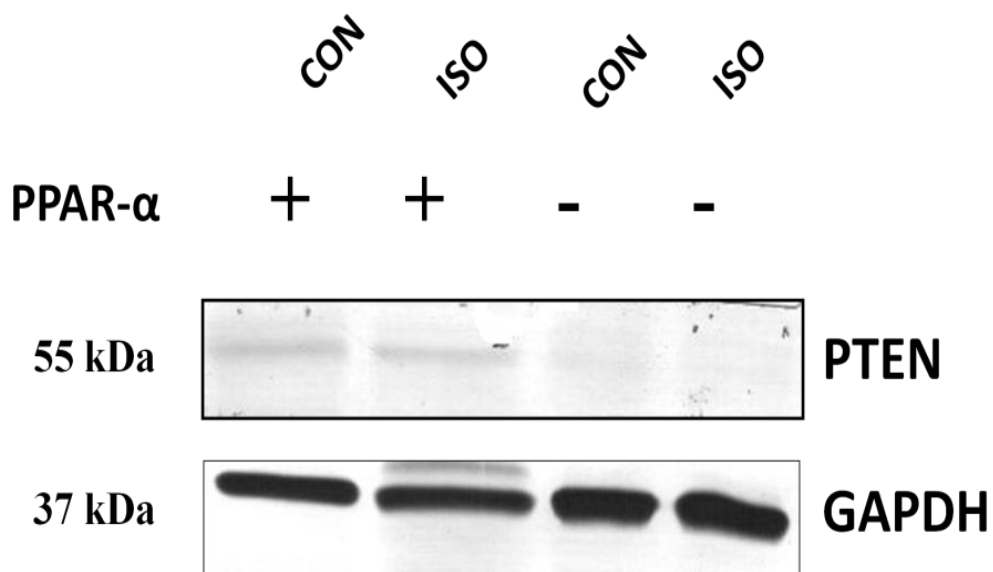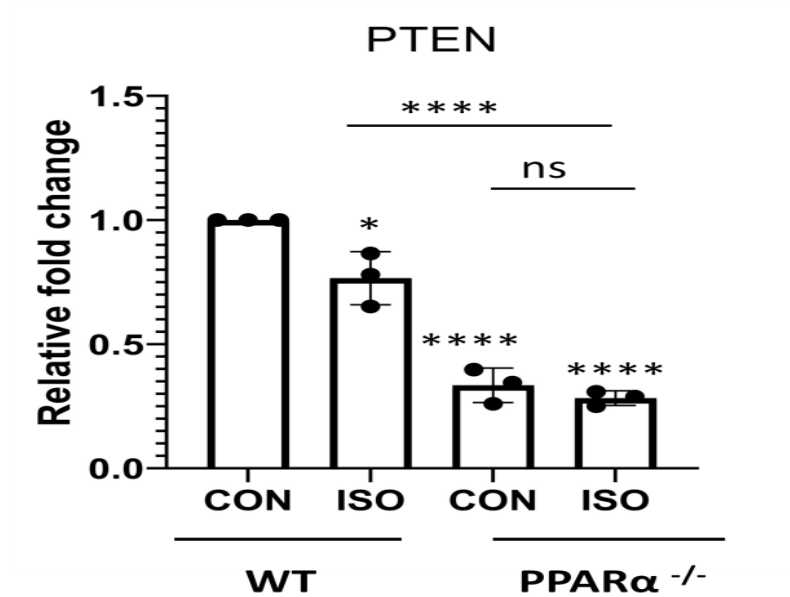
Fig.22. Modulation of PTEN in PPAR α⁻/⁻ mice: Protein level of PTEN in ISO-treated C57BL/6 wild-type mice and PPAR α⁻/⁻ mice was examined. GAPDH was used as a loading control. Data represent mean ± S.D. of 3 individual experiments. Data was analysed using two-way ANOVA with Tukey's post-hoc analysis. Difference between two groups unpaired Student's t-test. ($*p<0.05$, $**p<0.01$, $***p<0.001$ vs. CON).

1.20. Down regulation of PTEN in HCD fed PPAR α⁻/⁻ mice

PTEN was examined in both NCD fed PPAR α⁻/⁻ mice and HCD fed PPAR α⁻/⁻ mice (Fig.23.). Protein level of PTEN was remarkably enhanced in HCD fed PPAR α⁻/⁻ mice as compared to NCD fed PPAR α⁻/⁻ mice similar to the results obtained in ISO-treated PPAR α⁻/⁻ mice.
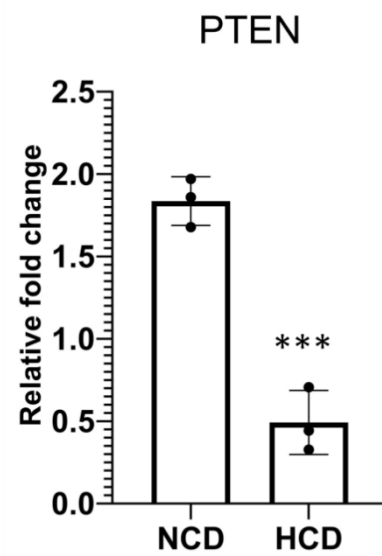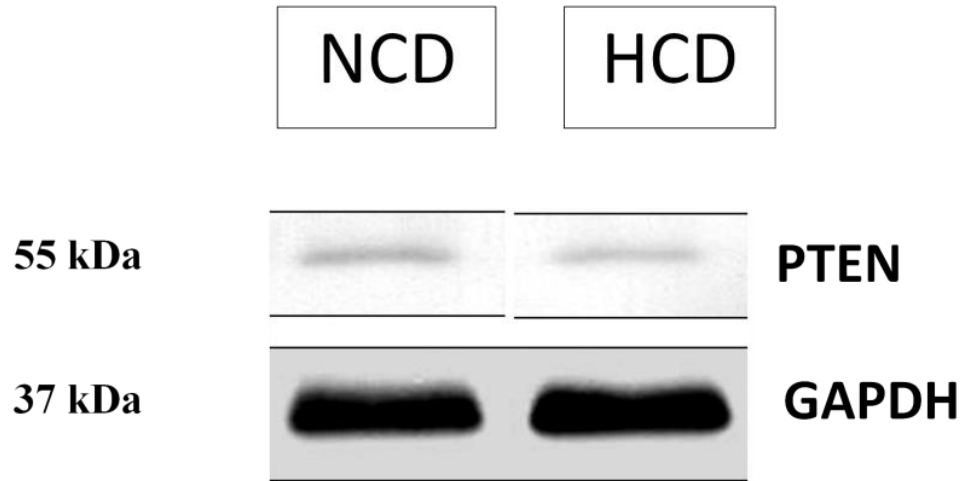
Fig.23. Modulation of PTEN in HCD-fed PPAR α⁻/⁻ mice: Protein level of PTEN in normal chow diet fed (NCD) PPAR α⁻/⁻ mice as well as high cholesterol diet fed (HCD) PPAR α⁻/⁻ mice compared using immunoblot. GAPDH was used as a loading control. Data represent mean ± S.D. of 3 individual experiments. Difference between two groups unpaired Student's t-test. (*p<0.05, **p<0.01, ***p<0.001 vs. CON).
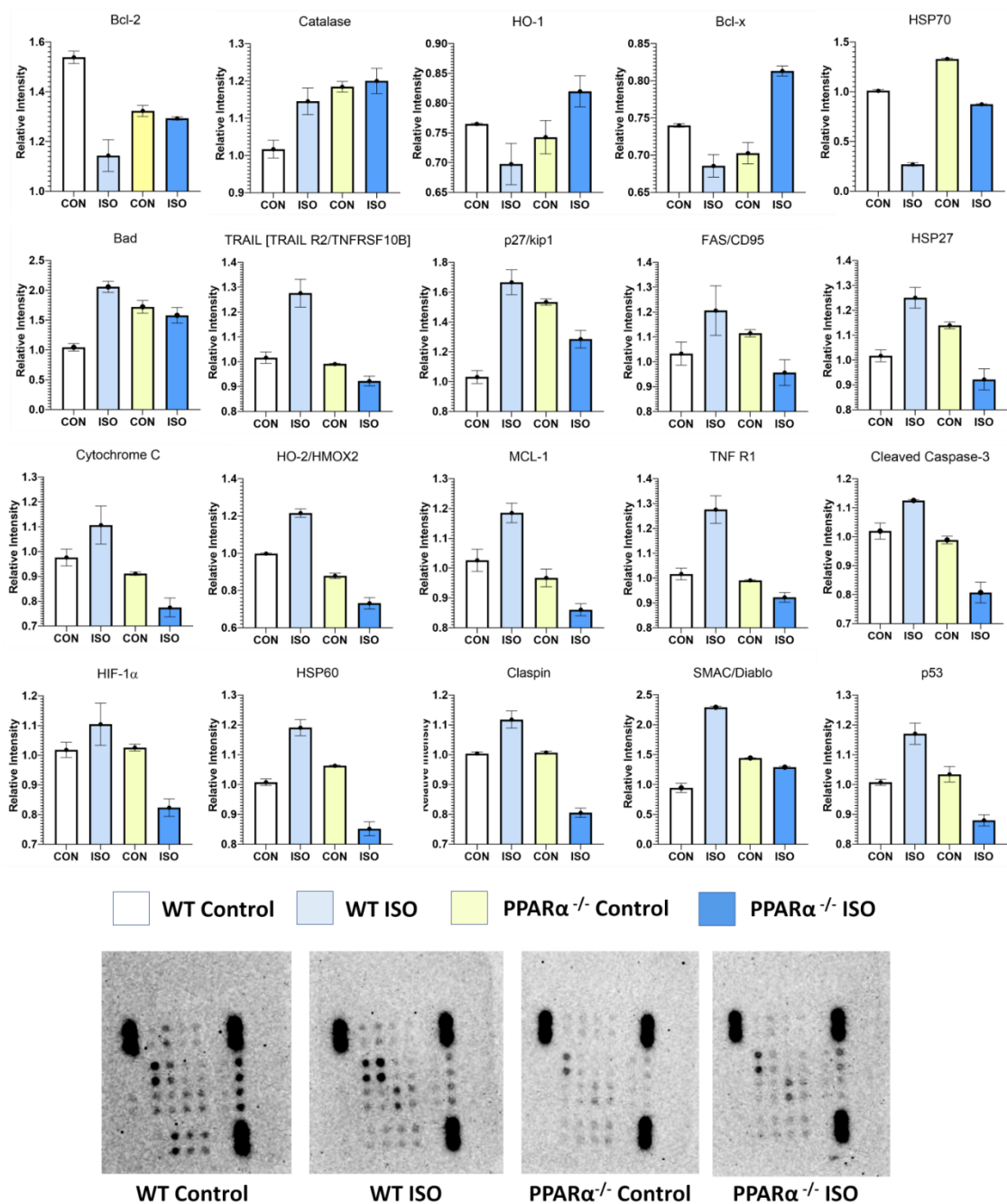
Fig.24. Altered expression of apoptotic markers in PPAR α⁻/⁻ mice using Proteome profiler Antibody assay

1.21. Downregulation of major apoptotic markers and increase in anti-apoptotic markers

Cardiac hypertrophy associated stress results in increase in apoptotic markers, therefore in context to the previous results, further major apoptotic markers were analysed (Fig.24.).Anti-apoptotic markers like Bcl-2, Bcl-x, Catalase, HO-1, HO-2, Hsp70, Hsp27 and Hsp60 were examined.Bcl-2 was significantly decreased in ISO-treated wild-type mice when compared to wild-type control, whereas untreated PPAR $\alpha^{-/-}$ mice and ISO-treated PPAR $\alpha^{-/-}$ mice exhibited noticeable upregulation of Bcl-2 in comparison to ISO-treated wild-type mice. Conversely, Catalase was comparatively enhanced in ISO-treated wild type mice but reduced in comparison to untreated PPAR $\alpha^{-/-}$ mice and ISO-treated PPAR $\alpha^{-/-}$ mice.HO-1 protein levels were remarkably lowered in ISO-treated wild-type mice but significantly elevated in untreated PPAR $\alpha^{-/-}$ mice and ISO-treated PPAR $\alpha^{-/-}$ mice. Although, untreated PPAR $\alpha^{-/-}$ mice exhibited significantly reduced HO-1 protein levels as compared to ISO-treated PPAR $\alpha^{-/-}$ mice. Bcl-x resembled HO-1 in expression pattern where in the protein levels of Bcl-x were significantly decreased in ISO-treated wild type mice compared to untreated PPAR $\alpha^{-/-}$ mice and ISO-treated PPAR $\alpha^{-/-}$ mice.Hsp-70,another anti-apoptotic protein was again remarkably reduced in ISO-treated wild-type mice in comparison untreated PPAR $\alpha^{-/-}$ mice and ISO-treated PPAR $\alpha^{-/-}$ mice. Among all the anti-apoptotic protein examined ,three anti-apoptotic proteins i.e. ,HO-2, Hsp27 and Hsp60 were downregulated in untreated PPAR $\alpha^{-/-}$ mice and ISO-treated PPAR $\alpha^{-/-}$ mice compared to ISO-treated wild-type mice suggesting compensatory role of Hsp70(Fig.24.) .

Pro-apoptotic proteins like Bad, Caspase 3, Claspin, Cytochrome C, FAS/CD95, Mcl-1, p53, p27/kip1, Smac/Diablo, TRAIL R2/TNFRSF10B, and TNFR1/TNFRSF1A were also examined. Pro-apoptotic protein like Bad was significantly enhanced in ISO-treated wild-type mice in comparison to untreated PPAR $\alpha^{-/-}$ mice and ISO-treated PPAR $\alpha^{-/-}$ mice wherein Bad protein levels were significantly reduced. Similar results were observed for TRAIL which was remarkably reduced in untreated PPAR $\alpha^{-/-}$ mice as well as ISO-treated PPAR $\alpha^{-/-}$ mice in comparison to the elevated level in ISO-treated wild-type mice.p27/kip1, another pro-apoptotic protein exhibited similar expression pattern and was noticeably decreased in PPAR $\alpha^{-/-}$ mice in both untreated as well as ISO-treated animals compared to the enhanced levels of p27 protein in ISO-treated wild-type mice. FAS/CD95 that initiates apoptotic pathway was also significantly decreased in untreated PPAR $\alpha^{-/-}$ mice as well as ISO-treated PPAR $\alpha^{-/-}$ mice resembling similar expression pattern as the previously examined pro-apoptotic proteins. Cytochrome c along with TNF R1 protein levels were similarly downregulated in PPAR $\alpha^{-/-}$ mice in both untreated as well as ISO-treated mice. ISO-treated wild-type mice exhibited enhanced protein levels of both Cytochrome C as well as TNF R1 when compared to wild-type control ,untreated PPAR $\alpha^{-/-}$ mice and ISO-treated PPAR $\alpha^{-/-}$ mice. Caspase 3 another critical apoptotic marker was examined and exhibited similar results whereas Caspase 3 protein was significantly reduced in the PPAR $\alpha^{-/-}$ mice group and elevated in ISO-treated wild-type mice group when compared to wild-type. Similarly, other apoptotic markers like Claspin, Mcl-1 and Smac/Diablo resembled similar expression pattern as previous apoptotic markers and were remarkably reduced in both untreated PPAR $\alpha^{-/-}$ mice and ISO-treated PPAR $\alpha^{-/-}$ mice. Conversely, Claspin, Mcl-1 and Smac/Diablo were distinctly enhanced in ISO-treated wild-

type mice. p53, in context to the previous results was also examined and exhibited similar pattern. p53 was significantly upregulated in ISO-treated wild-type mice when compared to wild-type control and downregulated in both untreated PPAR $\alpha^{-/-}$ mice as well as ISO-treated PPAR $\alpha^{-/-}$ mice (Fig.24.).

1.22. Upregulation of Autophagy markers in ISO-treated PPAR $\alpha^{-/-}$ mice

Autophagy markers were examined to understand this increase in apoptotic markers. Autophagy marker Light Chain 3 (LC3A/B) protein levels were significantly elevated in PPAR $\alpha^{-/-}$ mice as well as ISO-treated PPAR $\alpha^{-/-}$ mice in comparison to wild-type control, whereas ISO-treated wild-type mice showed no change when compared to wild-type control (Fig.25.).

However, protein levels of Beclin 1, another autophagy markers were significantly enhanced in ISO-treated PPAR $\alpha^{-/-}$ mice but showed no noticeable change in PPAR $\alpha^{-/-}$ mice as well as ISO-treated wild-type mice when compared to wild-type control.

1.23. Upregulation of Autophagy marker in HCD-fed PPAR $\alpha^{-/-}$ mice

Autophagy markers were also examined in NCD-fed as well as HCD-fed PPAR $\alpha^{-/-}$ mice. HCD-fed PPAR $\alpha^{-/-}$ mice exhibited remarkably enhanced levels of Beclin1 protein when compared to wild-type control (Fig.26.). Similar results were observed for LC 3 A/B protein, as the protein levels of LC3A/B were elevated in HCD-fed PPAR $\alpha^{-/-}$ mice as compared to wild-type control.
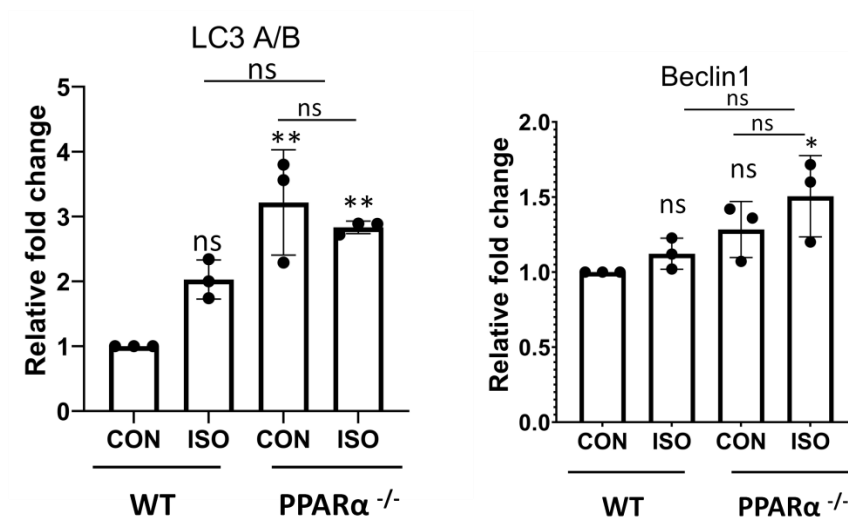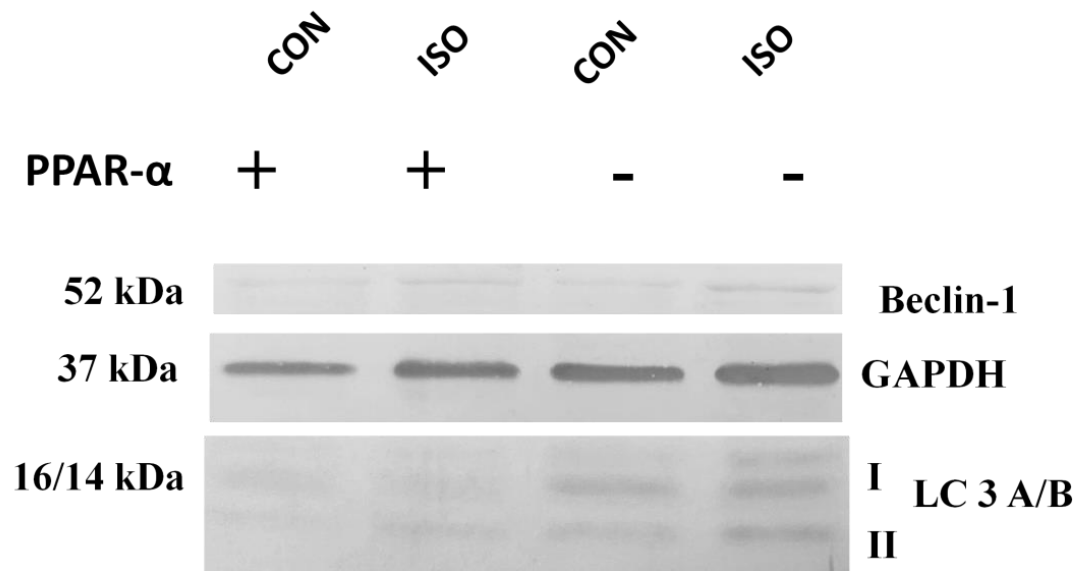
Fig.25. Upregulation of autophagy markers in ISO-treated PPAR α$^{-/-}$ mice: Autophagy markers Beclin-1 and LC3 A/B were examined using western blot. GAPDH was used as a loading control. Data represent mean ± S.D. of 3 individual experiments. Data was analysed using two-way ANOVA with Tukey's post-hoc analysis. Difference between two groups was analysed using Student's t-test. (*p<0.05, **p<0.01, ***p<0.001 vs. CON).
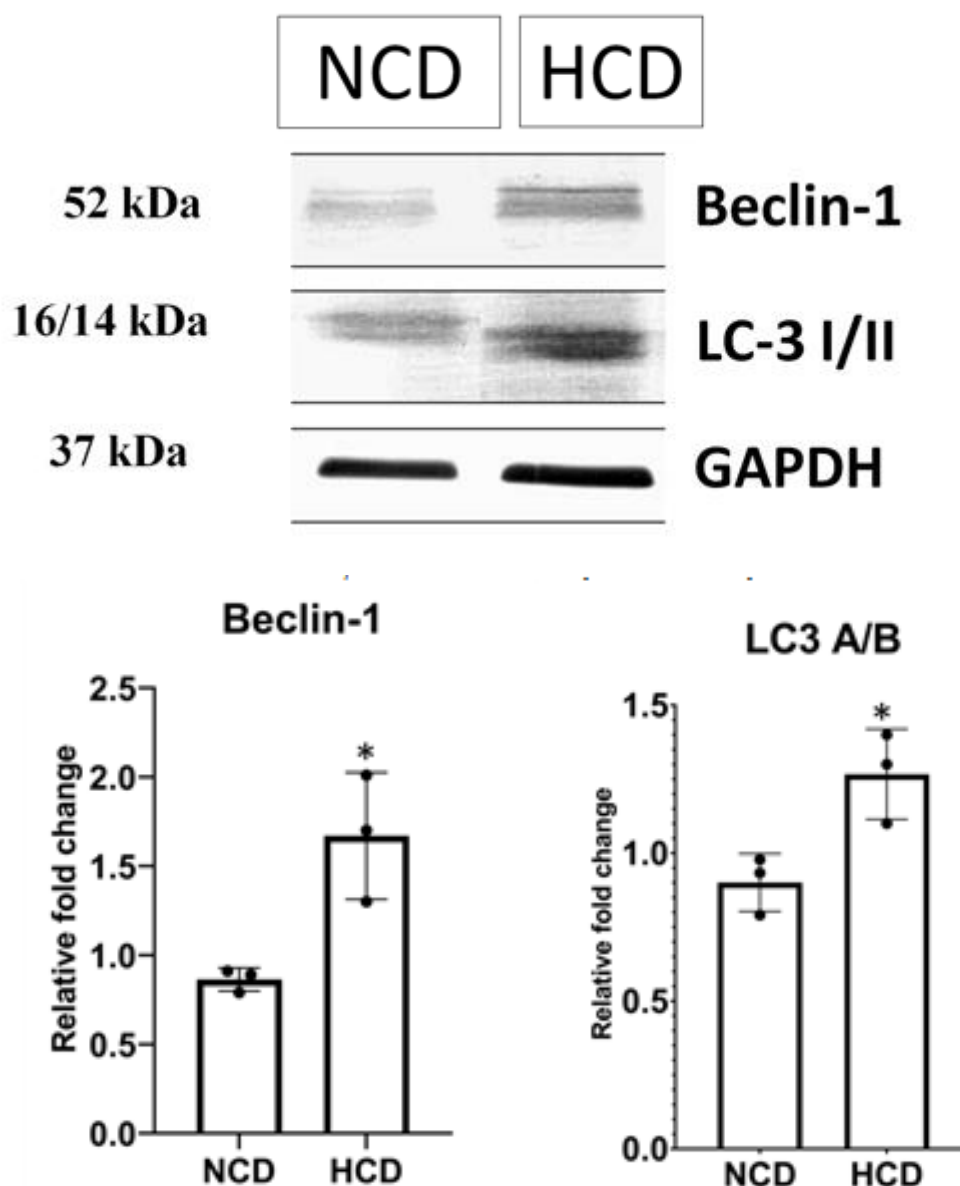
Fig.26. Upregulation of autophagy markers in HCD-fed PPAR α⁻/⁻ mice: Autophagy markers Beclin-1 and LC3 A/B were examined using western blot and densitometric analysis in normal chow diet fed (NCD) PPAR α⁻/⁻ mice as well as high cholesterol diet fed (HCD) PPAR α⁻/⁻ mice GAPDH was used as a loading control. Data represent mean ± S.D. of 3 individual experiments. Difference between two groups was analysed using Student's t-test. (*p<0.05, **p<0.01, ***p<0.001 vs. CON).
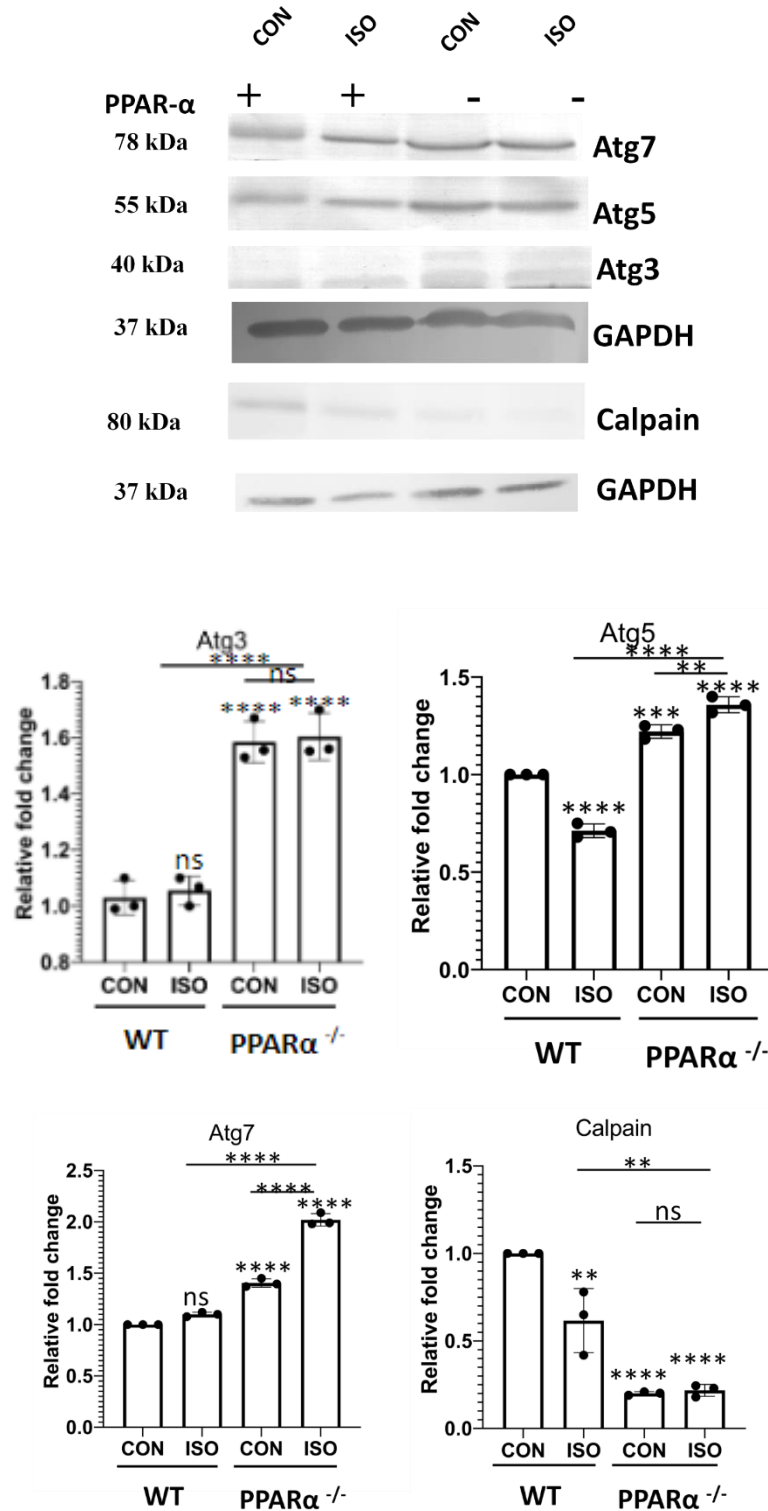
Fig.27. Downregulation of Calpain and upsurge of Atg genes in ISO-treated PPAR $\alpha^{-/-}$ mice: Atg 3, Atg 5 and Atg7 along with Calpain were examined using western blot and densitometric analysis). GAPDH was used as a loading control. Data represent mean ± S.D. of 3 individual experiments. Data was analysed using two-way ANOVA with Tukey's post-hoc analysis. Difference between two groups was analysed using Student's t-test. (*p<0.05, **p<0.01, ***p<0.001 vs. CON).

1.24. Upregulation of ATG3,5, and 7 along with downregulation of Calpain in ISO-treated PPAR $\alpha^{-/-}$ mice

To further analyse autophagy in the absence of apoptosis, other major autophagy markers were examined in both control as well as experimental groups (Fig.27.).Atg3 showed no change in ISO-treated wild-type mice but was significantly enhanced in both untreated PPAR $\alpha^{-/-}$ mice as well as ISO-treated PPAR $\alpha^{-/-}$ mice when compared to wild-type control. Similar results were observed for Atg5 as Atg5 was noticeably elevated in PPAR $\alpha^{-/-}$ mice ,both ISO-treated as well as untreated whereas significantly decreased in ISO-treated wild-type mice when compared to wild-type control.Similarly,Atg7, another autophagy marker was remarkably up regulated in ISO-treated PPAR $\alpha^{-/-}$ mice as well as untreated PPAR $\alpha^{-/-}$ mice when compared to wild-type control whereas ISO-treated wild-type mice showed no change in comparison to wild-type control.

Calpain, a protein that has been reported to be involved in inhibiting autophagy was examined to further understand this switch towards autophagy. Protein levels of Calpain was significantly decreased in case of ISO-treated wild-type when compared to wild-type control. Surprisingly, Calpain protein was remarkably downregulated in PPAR $\alpha^{-/-}$ mice both treated as well as untreated when compared to ISO-treated wild-type mice as well as untreated wild-type control (Fig.27.).

1.25. Upregulation of ATG3,5, and 7 along with downregulation of Calpain in HCD-fed PPAR $\alpha^{-/-}$ mice

Autophagy markers were also examined in NCD-fed PPAR $\alpha^{-/-}$ mice as well as HCD-fed PPAR $\alpha^{-/-}$ mice (Fig.28.).Similar to the previous results obtained for ISO-treated PPAR $\alpha^{-/-}$ mice Atg 3 was not significantly changed in HCD-fed PPAR $\alpha^{-/-}$ mice when compared to NCD-fed PPAR $\alpha^{-/-}$ mice. However, Atg5 was noticeably elevated in HCD-fed PPAR $\alpha^{-/-}$ mice in comparison to NCD-fed PPAR $\alpha^{-/-}$ mice. Similarly, Atg 7 was also upregulated in HCD-fed PPAR $\alpha^{-/-}$ mice compared to NCD –fed PPAR $\alpha^{-/-}$ mice.
Calpain was significantly downregulated in HCD-fed PPAR $\alpha^{-/-}$ mice in comparison to NCD-fed PPAR $\alpha^{-/-}$ mice, thereby resembling the same expression pattern as in ISO-treated PPAR $\alpha^{-/-}$ mice
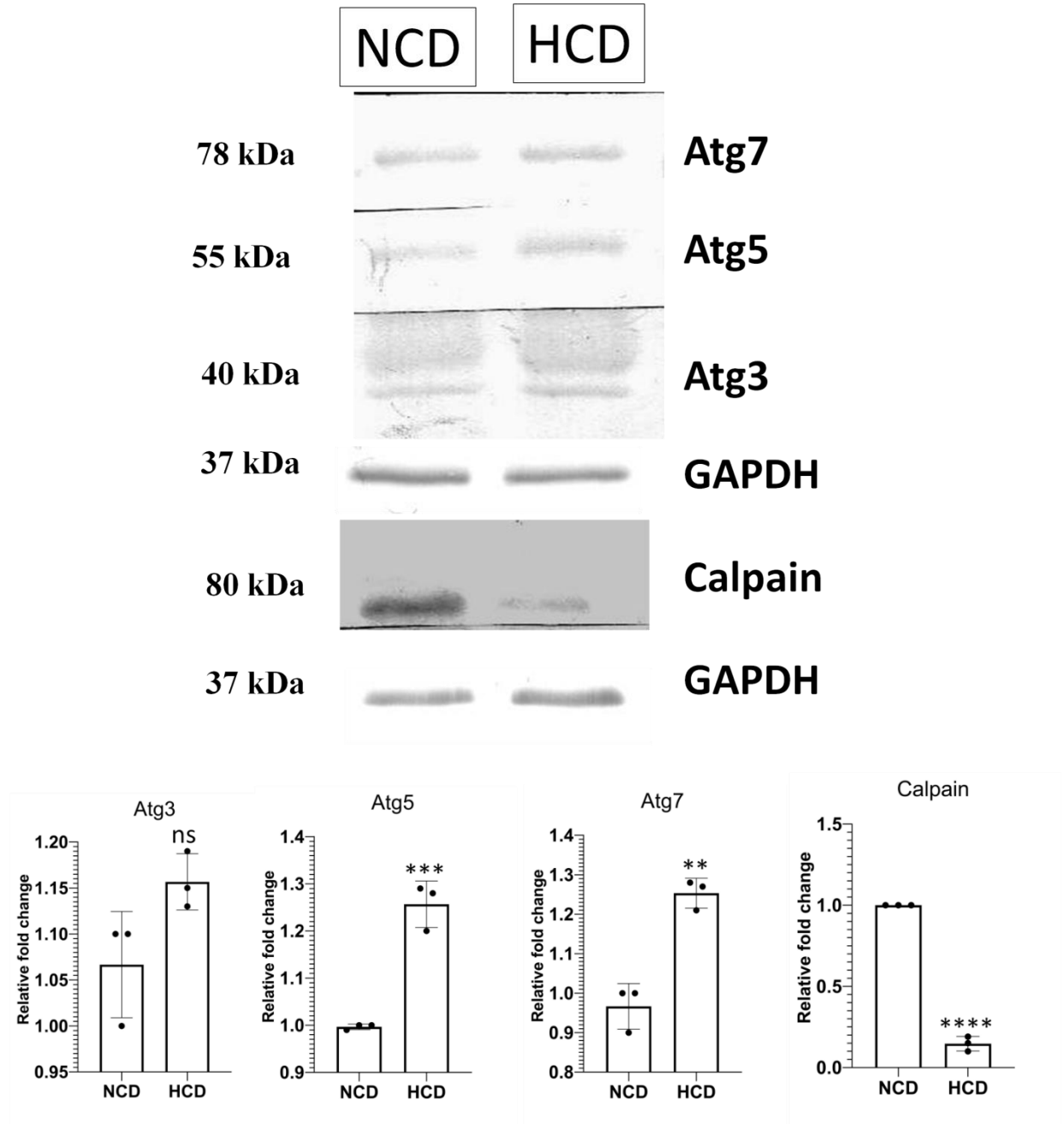
Fig.28. Downregulation of Calpain and upsurge of Atg genes in HCD-fed PPAR α$^{-/-}$ mice: Expression of Atg 3, Atg 5, Atg 7 and Calpain was analysed in normal chow diet fed (NCD) PPAR α$^{-/-}$ mice as well as high cholesterol diet fed (HCD) PPAR α$^{-/-}$ mice using immunoblot. GAPDH was used as a loading control. Data represent mean ± S.D. of 3 individual experiments. Difference between two groups was analysed using Student's t-test. (*p<0.05, **p<0.01, ***p<0.001 vs. CON).
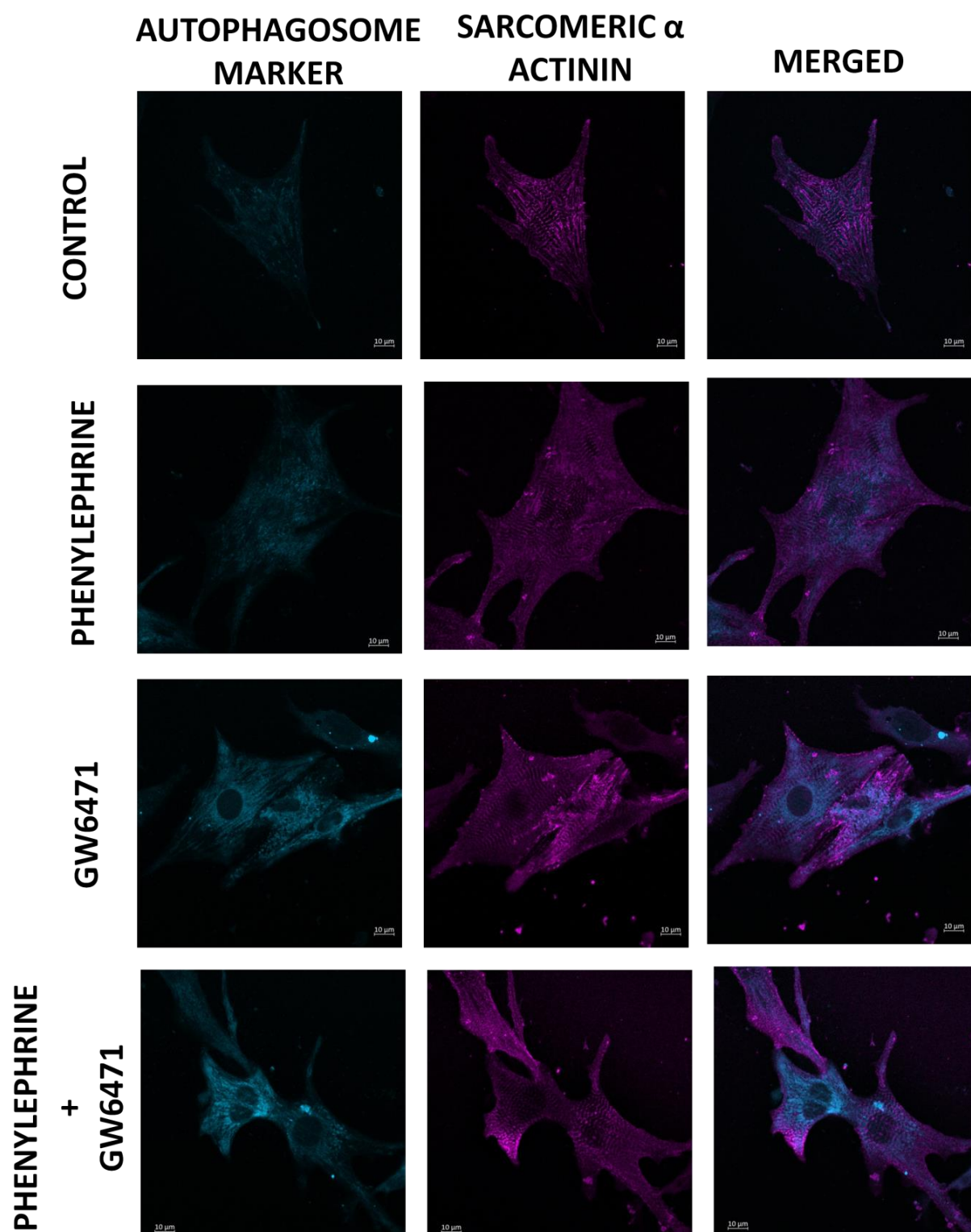
Fig.29. Enhanced Autophagy in Neonatal Rat Ventricular Myocytes (NRVMs): Representative Confocal images of Autophagy Assay in NRVM of different treatment groups; scale bar=10µm.

1.26. Induction of Autophagy in cardiomyocytes *in vitro*

As per previous observations, downregulation of apoptosis was accompanied with concurrent upregulation of autophagy in both the hypertrophy-induced mice models. So next we investigated the impact of the absence of PPAR α in hypertrophy-stimulated cardiomyocytes *in vitro* (Fig.29.).Neonatal rat ventricular myocytes (NRVM) were stimulated with phenylephrine (PE) for around 48 hr and PPAR α was functionally blocked using GW6471, PPAR α antagonist. NRVMs treated with PE alone, showed no significant increase in the autophagic vacuoles as was indicated by the number of bright blue dot stained autophagic vacuoles present (Fig.29.). Consistent with previous results, autophagy assay revealed remarkably increased autophagy in GW6471 incubated myocytes, even in the presence of PE when compared to control as was observed, with an enhanced number of bright blue dot stained autophagic vacuoles. Confocal microscopy revealed sarcomeric striation pattern through α-actinin staining (pink) along with the autophagic vacuoles and was distinctly visible.
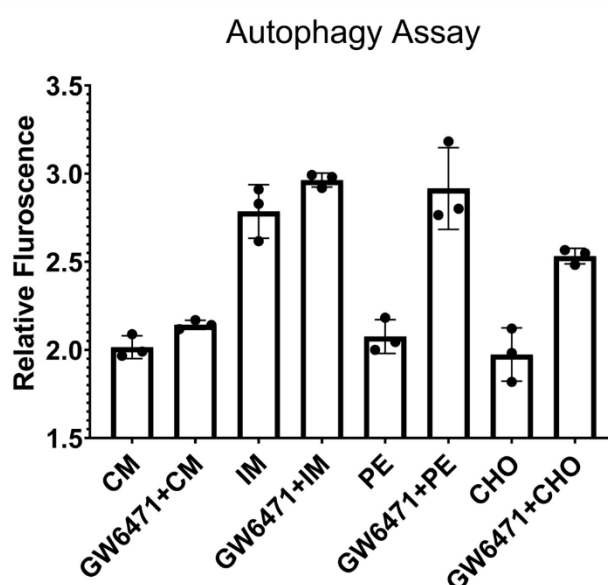
Fig.30.Enhanced autophagy in hypertrophy-induced and cholesterol-incubated cardiomyocytes: Bar Graph depicting the relative fluorescence in the indicated experiments in H9C2 cell line

1.27. Upregulation of Autophagy examined using relative fluorescence

Measurement of relative fluorescence for autophagy in H9C2 cardiomyocytes revealed enhanced autophagy in cardiomyocytes incubated with GW6471, which is a PPAR α antagonist resembling previous results (Fig.30.). Similarly, Cholesterol incubated cardiomyocytes in the presence of PPAR α antagonist, GW6471 exhibited increased autophagy in comparison to cardiomyocytes incubated with cholesterol alone.
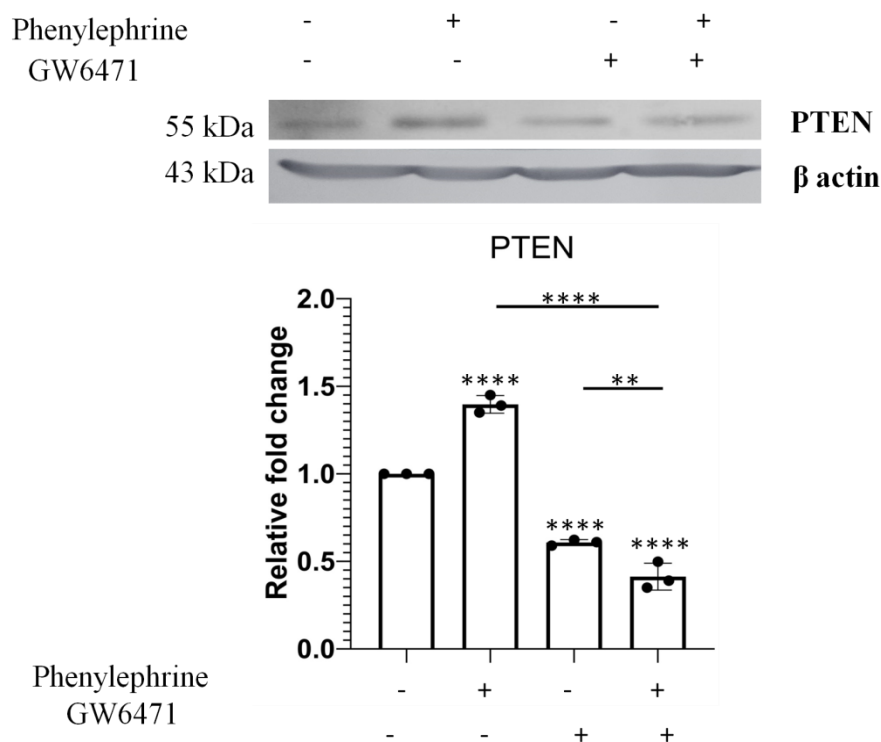
Fig.31.Decrease in PTEN protein level in H9C2 cell line: Western Blot analysis and the quantitative results of PTEN. Data represent mean ± S.D. of 3 individual experiments. β-actin was used as a loading control. Data was analysed using two-way ANOVA with Tukey's post-hoc analysis. Difference between two groups was analysed using Student's t-test. (*$p<0.05$, **$p<0.01$, ***$p<0.001$ vs. CON).

1.28. Downregulation of PTEN in H9c2 cell line

Cardiomyocytes (H9C2 cell line) incubated with GW6471 exhibited significant down regulation of PTEN as compared to cardiomyocytes treated solely with PE (Fig.31.). Cardiomyocytes subjected to PE along with GW6471 also exhibited noticeable down regulation of PTEN.

1.29. Down regulation of apoptotic marker c PARP and up regulation of Beclin1

Downregulation of apoptotic marker cPARP/PARP was observed in cardiomyocytes subjected to both PE and GW6471 (Fig.32.). Similar down regulation was observed in cardiomyocytes treated solely with GW6471.On the contrast, upregulation of autophagy marker Beclin1 was observed in cardiomyocytes treated with both PE and GW6471 when compared to cardiomyocytes treated with PE alone (Fig.32.).
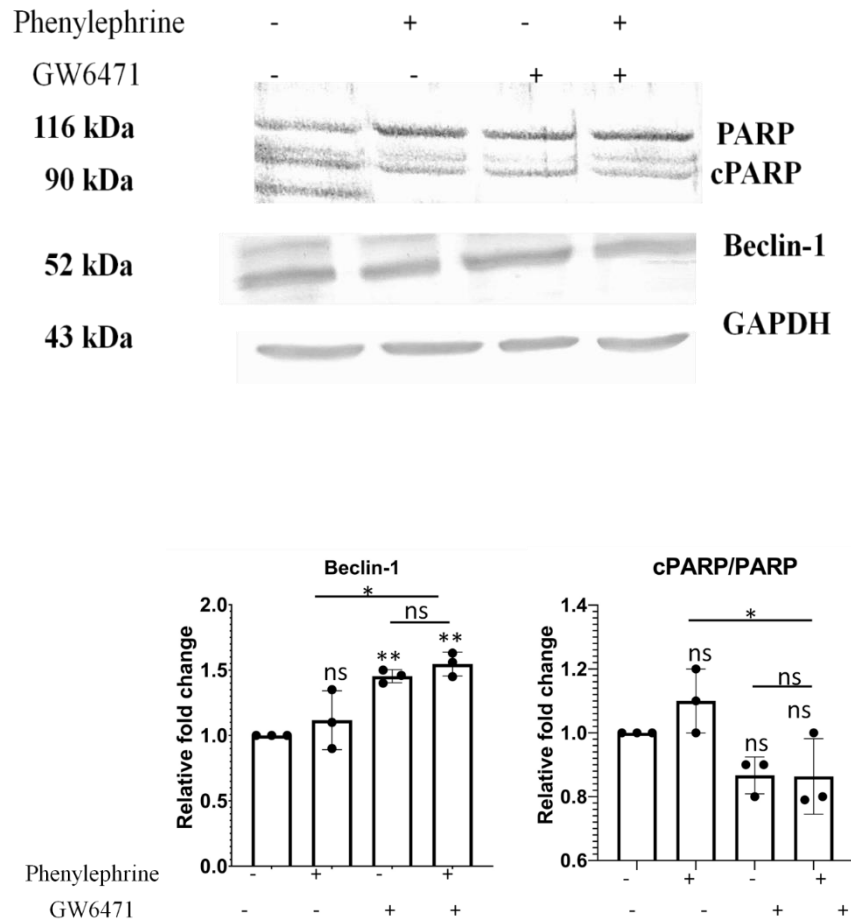
Fig.32. Modulation of apoptotic and autophagic markers in H9C2 cell line: Western Blot analysis and the quantitative results of Beclin 1 and cPARP. Data represent mean ± S.D. of 3 individual experiments. GAPDH was used as a loading control. Data was analysed using two-way ANOVA with Tukey's post-hoc analysis. Difference between two groups was analysed using Student's t-test. (*p<0.05, **p<0.01, ***p<0.001 vs. CON).
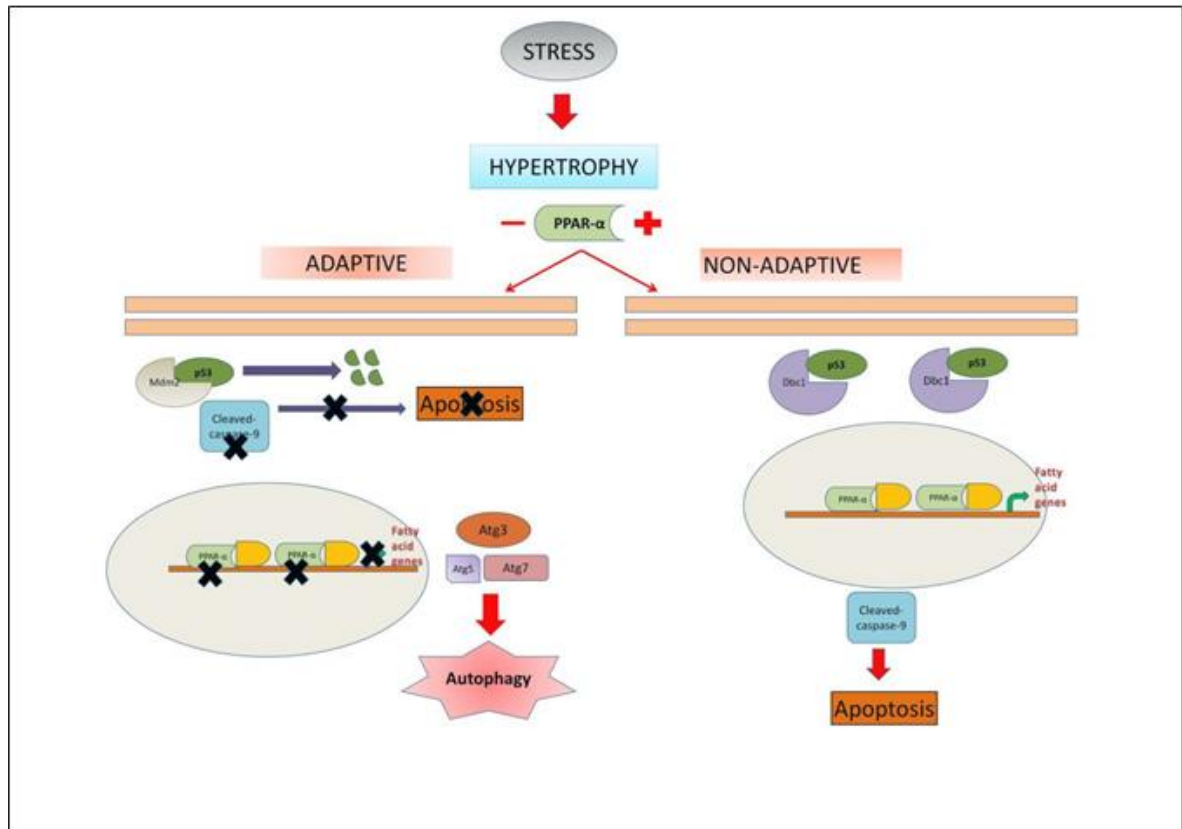
Fig.33. Schematic representation depicting the possible mechanism of cell fate regulation via PPAR α: In hypertrophic conditions, PPAR α is likely to promote apoptosis of the cardiomyocytes leading to dysfunctional state of the myocardium whereas in the absence of PPAR α, cardiomyocytes are driven toward autophagy which appears to be an adaptive phase.

Conclusion

Cardiac hypertrophy is an adaptive response to pressure-overload that leads to cardiac remodelling which ultimately becomes maladaptive. Pressure-overload induced cardiac hypertrophy is associated with downregulation of PPAR α signalling. Involvement of PPARα in regulating the adaptive phase of cardiac hypertrophy has not yet been explored in detail. Our study revealed the significance of PPAR α signalling in regulating apoptosis in response to cardiac hypertrophy. To understand the role of PPARα, cardiac hypertrophy was examined in PPAR α$^{-/-}$ mice. Increase in HW/BW ratio and HW/TL ratio was observed in both PPAR α$^{-/-}$ mice as well as ISO-treated PPAR α $^{-/-}$ mice along with extensive collagen accumulation. Reactivation of foetal genes along with alteration of majority of genes involved in Fatty acid β oxidation was observed. Cardiac function was severely impaired and PPAR α$^{-/-}$ mice exhibited significant cardiac dysfunction even in the absence of ISO-treatment thereby suggesting that loss of PPARα hampers normal cardiac activity. Proteomic analysis revealed around 1200 proteins that were significantly altered accompanied by downregulation of signalling pathways involved in Fatty acid β oxidation. Interestingly, apoptotic pathway was significantly downregulated in PPAR α$^{-/-}$ mice and ISO-treated PPAR α$^{-/-}$ mice that was further followed-up with analysis of apoptotic array. Another cardiac hypertrophy model, HCD diet fed PPAR α $^{-/-}$ mice revealed similar down regulation of apoptotic markers thus supporting the previous observation. Most of the pro-apoptotic markers were down regulated in PPAR α$^{-/-}$ mice and ISO-treated PPAR α$^{-/-}$ mice with a concurrent increase in anti-apoptotic markers in the same groups. On the contrary, ISO-treated wild-type mice revealed an upregulation of pro-apoptotic markers and a significant down regulation of anti-apoptotic markers. This data was further validated and downregulation of critical apoptotic marker like PTEN was observed suggesting prominent decline in apoptosis in PPAR α$^{-/-}$ mice. On the contrary, autophagy markers were significantly upregulated in both PPAR α$^{-/-}$ mice and ISO-treated PPAR α$^{-/-}$ mice indicating a shift towards a compensatory mechanism that could prevent cardiomyocyte death. Consistent with the previous results, autophagy assay performed in primary cell culture in the presence of PPAR α inhibitor GW6471 exhibited similar increase in autophagy. The data therefore suggests a signalling switch that triggers autophagy in the absence of PPAR α rather apoptosis, when induced with hypertrophic stimuli. This signalling switch could help the cardiomyocytes to maintain a sustainable state wherein cellular machinery bypasses cell death by adapting to an alternative coping mechanism. In conclusion, this study unveiled a novel mechanism of cardiomyocyte adaptation in the absence of PPAR α. Under normal conditions, PPAR α drives cardiomyocytes towards apoptosis whereas, in the absence of PPAR α, hypertrophic cardiomyocytes are driven towards autophagy which might help cardiomyocytes to sustain through the early adaptive phase of hypertrophy (Fig 33).

CHAPTER 2

Understanding the role of miRNA in transcriptional remodelling in cardiac hypertrophy

Introduction

The first miRNA was discovered in the year 1993 in the nematode Coenorhabditis elegans as the development regulator *lin-4*(*Horvitz and Sulston,1980*). Initially, it was believed to be a protein-coding gene but Ruvkun and Ambros made a major breakthrough in the field of RNA biology by identifying lin-4 as a 22-nucleotide regulatory RNA (*Lee et al. 1993; Wightman et al. 1993*)

More than 2000 miRNAs have been discovered as of now, and almost all the miRNAs undergo a canonical biogenesis pathway that include a series of steps converting primary miRNA transcript into active, ~22 nucleotide mature miRNA (*Hammond 2015*).In this canonical biogenesis pathway, pri-miRNA are transcribed from their respective genes and then processed into pre-miRNAs by the enzyme Drosha yielding the precursor miRNA (*Denli et al. 2004*).Pre-miRNAs are then exported to the cytoplasm by an exportin 5 (XPO5)/RanGTP complex and then cleaved by the RNase III endonuclease Dicer(*Okada et al. 2009*). After Dicer cleavage the mature miRNA is loaded into the effector complex RISC where it directs the translational repression of its mRNA targets (*Yoda et al. 2010*).

Biological importance of miRNAs was first discovered using mice models deficient in Dicer and DGCR8, an RNA binding protein DiGeorge Syndrome Critical Region 8 that plays key role in miRNA biogenesis. Mice models deficient for DGCR8 and Dicer exhibited impaired miRNA biogenesis resulting in developmental lethality (*Bernstein et al. 2003;Wang et al. 2007*).Roles of specific miRNAs have been addressed by miRNA knockout-mice models(*Park et al. 2010;Vidigal and Ventura, 2014*).miRNAs have been implicated in various disorders and are modulated as a remodelling response to stress(*van Rooji et al. 2006*).Previous studies have reported the alteration in miRNA expression during cardiovascular diseases(*Small et al. 2010*).The altered pattern of miRNA expression in hypertrophic mice heart indicates that a subset of miRNAs could serve as molecular signature of cardiac hypertrophy(*van Rooji et al. 2006*).Previous reports have addressed the involvement of miRNAs in the induction of foetal genes as miRNA expression also gets altered along with this canonical switch in gene expression that is observed during cardiac hypertrophy (*Rane et al. 2007*).One of the first characterized miRNA involved in the induction of hypertrophic growth was miRNA-195 and as per reports, overexpression of this miRNA is sufficient enough to induce cardiac hypertrophy(*van Rooji et al. 2006; Harris et al. 2006*).miRNA-195 has been reported to act as pro-hypertrophic factor and leads to cardiomyopathy as well as cardiac dysfunction.(*van Rooji et al. 2006; Harris et al. 2006*).

Previous studies have established the potential involvement of miRNAs in cardiac hypertrophy using microarray analysis (*Hill et al. 2000*).Distinct mice models of cardiac hypertrophy have been used to explore differentially expressed miRNAs that includes, mice models subjected to thoracic aortic banding as well as Tg mice models expressing activated calcineurin A (CnA) in the heart (*van Rooji et al. 2006*).As absence of PPARα has already been established to cause cardiac hypertrophy, miRNA microarray analysis was performed in PPARα-/- mice subjected to isoproterenol. PPAR α mediated regulation is very critical in

cardiac hypertrophy associated transcriptional alteration. Reactivation of foetal genes and down regulation of fatty acid β-oxidation are well reported in the absence of PPAR α thereby suggesting essential regulation of transcriptional machinery via PPAR α signalling pathway.

In the light of previous reports addressing the involvement of miRNA in regulating the response of heart towards cardiac stress and since PPAR α signalling pathway plays key role in transcriptional remodelling associated with hypertrophy, we elucidated differentially expressed miRNAs in PPAR $\alpha^{-/-}$ mice with or without Isoproterenol treatment. Here, we aim to compare the different miRNAs getting altered as a result of the absence of PPARα and whether the altered miRNAs overlap with the ones observed in PPAR α-/- mice in the presence of Isoproterenol treatment. Since miRNAs act as key regulators of cardiac growth as well as function, they tend to regulate multiple signalling pathways.

Therefore, in this chapter we elucidate the differential expression of miRNAs that drive the transcriptional and translational changes in gene expression. The following objectives were undertaken:

1. Identification of differentially expressed miRNA in PPAR $\alpha^{-/-}$ mice

2. Understanding the biological relevance of the differentially expressed miRNA with the PPAR α signalling in hypertrophied condition.

3. Molecular mechanism of the regulation of apoptosis by miRNA critical to PPAR α signalling.

Methods:

RNA Extraction

Total RNA from tissue samples was prepared using a *mir*Vana miRNA extraction Kit (Ambion, Austin, TX, USA) according to the manufacturer's instruction. Concentrations of RNA was measured with the Nanodrop-100 Spectrophotometer (Nanodrop Technologies,Wilmington, DE).

Microarray Labelling and Hybridization

miRNA microarrays were manufactured by Agilent Technologies (Santa Clara, CA, USA) and 100 ng of total RNA was labeled and hybridized using the mouse microRNA Microarray Kit protocol for use with Agilent microRNA microarrays Version 1.5 and Mouse microRNA Microarray Kit protocol for use with Agilent microRNA microarrays Version 1.0. Hybridization signals were detected with a DNA microarray scanner G2505B (Agilent Technologies) and the scanned images were analyzed using Agilent feature extraction software (v9.5.3.1). Data were analyzed using GeneSpring GX 7.3.1 software (Agilent Technologies) and normalized.

Validation of miRNA using MIRCURY CUSTOM PCR ARRAYS

Custom Panel designed for the samples were used according to the manufacturer's instructions (Qiagen, #339332). RT-PCR was performed using Applied Biosystems7500-Fast Real Time qPCR Machine.

RESULTS
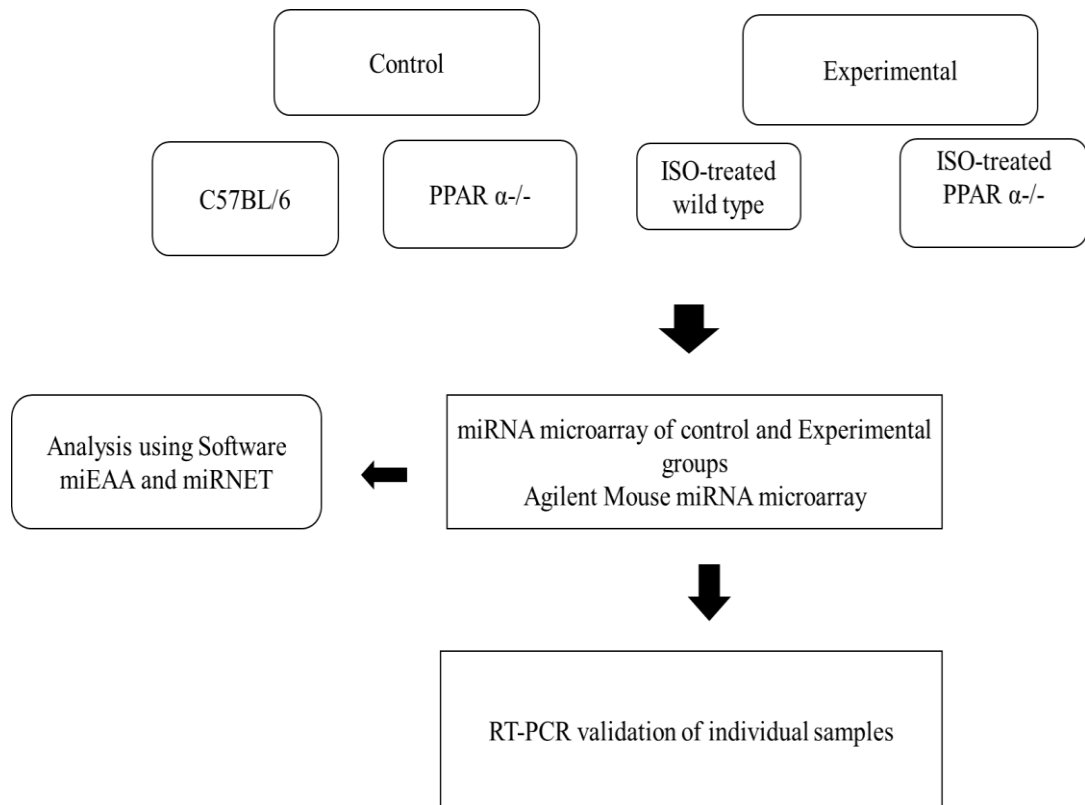
Fig.1. Flow chart showing the outline of Experimental design

Differentially Expressed miRNAs
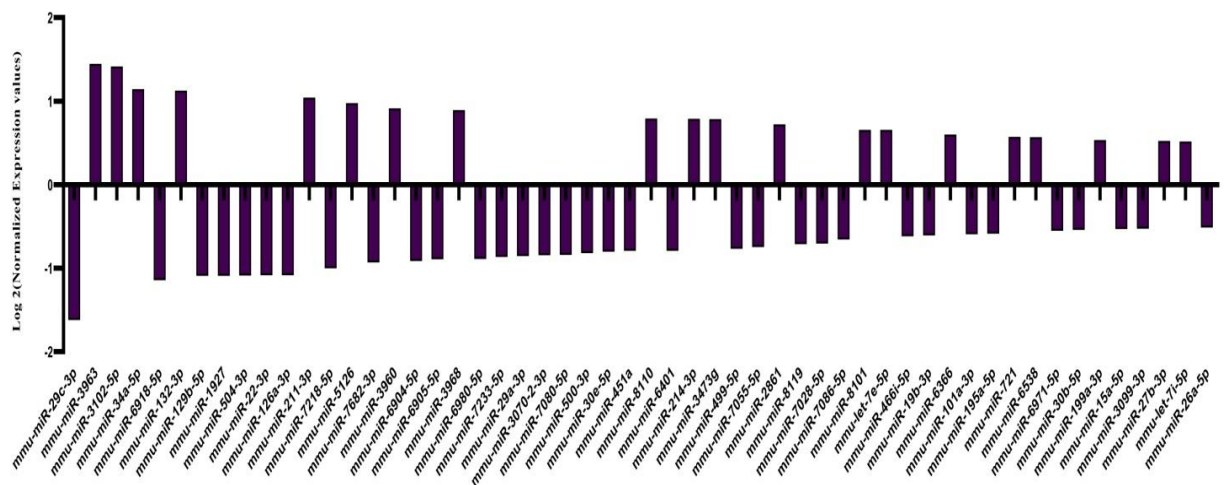
miRNA ID	Log FC
mmu-miR-29c-3p	-1.62034
mmu-miR-3963	1.444391
mmu-miR-3102-5p	1.413803
mmu-miR-34a-5p	1.141081
mmu-miR-6918-5p	-1.14108
mmu-miR-132-3p	1.122759
mmu-miR-129b-5p	-1.09032
mmu-miR-1927	-1.08929
mmu-miR-504-3p	-1.08494
mmu-miR-22-3p	-1.08344
mmu-miR-126a-3p	-1.08304
mmu-miR-211-3p	1.03918
mmu-miR-7218-5p	-0.9989
mmu-miR-5126	0.97353
mmu-miR-7682-3p	-0.92948
mmu-miR-3960	0.91181
mmu-miR-6904-5p	-0.91052
mmu-miR-6905-5p	-0.89258
mmu-miR-3968	0.891251
mmu-miR-6980-5p	-0.88739
mmu-miR-7233-5p	-0.86423
mmu-miR-29a-3p	-0.85447
mmu-miR-3070-2-3p	-0.84099
mmu-miR-7080-5p	-0.83859
mmu-miR-500-3p	-0.81948
mmu-miR-30e-5p	-0.79978
mmu-miR-451a	-0.79172
mmu-miR-8110	0.789007
mmu-miR-6401	-0.78888
mmu-miR-214-3p	0.78555
mmu-miR-3473g	0.78458
mmu-miR-499-5p	-0.76424
mmu-miR-7055-5p	-0.74373
mmu-miR-2861	0.720604
mmu-miR-8119	-0.71025
mmu-miR-7028-5p	-0.70191
mmu-miR-7086-5p	-0.6551
mmu-miR-8101	0.653809
mmu-let-7e-5p	0.653583
mmu-miR-466i-5p	-0.61492
mmu-miR-19b-3p	-0.60747
mmu-miR-6366	0.600303
mmu-miR-101a-3p	-0.59176
mmu-miR-195a-5p	-0.58554
mmu-miR-721	0.57072
mmu-miR-6538	0.568169

mmu-miR-6971-5p	-0.55028
mmu-miR-30b-5p	-0.53836
mmu-miR-199a-3p	0.534331
mmu-miR-15a-5p	-0.52786
mmu-miR-3099-3p	-0.52732
mmu-miR-27b-3p	0.52176
mmu-let-7i-5p	0.513987
mmu-miR-26a-5p	-0.51268

Fig.2. Differentially expressed miRNAs in untreated wild-type mice group vs ISO-treated wild-type control group
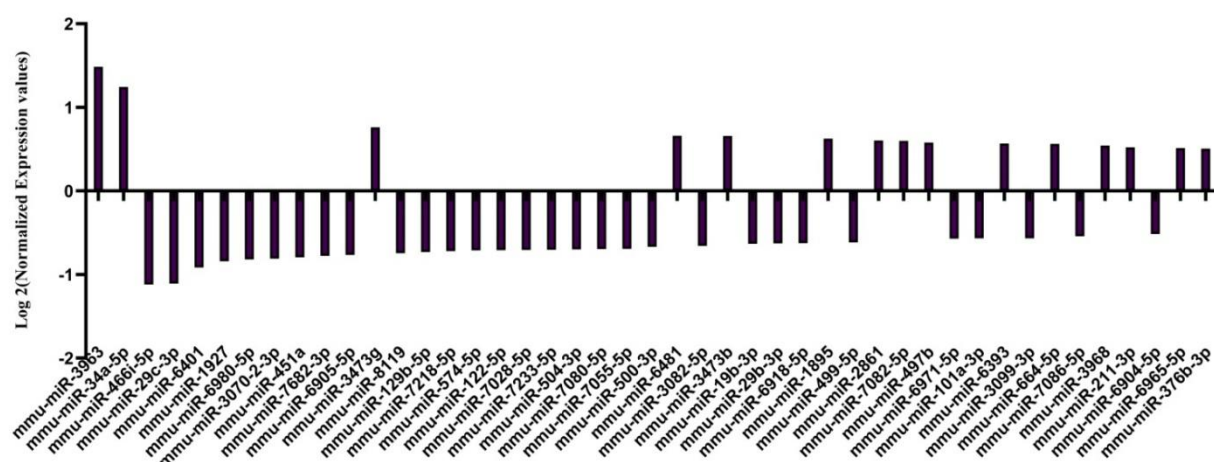
miRNA ID	Log FC
mmu-miR-3963	1.483749
mmu-miR-34a-5p	1.244586
mmu-miR-466i-5p	-1.11914
mmu-miR-29c-3p	-1.10769
mmu-miR-6401	-0.91706
mmu-miR-1927	-0.84106
mmu-miR-6980-5p	-0.81988
mmu-miR-3070-2-3p	-0.81009
mmu-miR-451a	-0.79388
mmu-miR-7682-3p	-0.777
mmu-miR-6905-5p	-0.76543
mmu-miR-3473g	0.761882
mmu-miR-8119	-0.74512
mmu-miR-129b-5p	-0.73065
mmu-miR-7218-5p	-0.72128
mmu-miR-574-5p	-0.71054
mmu-miR-122-5p	-0.70863
mmu-miR-7028-5p	-0.70662
mmu-miR-7233-5p	-0.70574
mmu-miR-504-3p	-0.69944
mmu-miR-7080-5p	-0.69673
mmu-miR-7055-5p	-0.69298
mmu-miR-500-3p	-0.66898
mmu-miR-6481	0.660494
mmu-miR-3082-5p	-0.65701
mmu-miR-3473b	0.656935
mmu-miR-19b-3p	-0.63357
mmu-miR-29b-3p	-0.62848
mmu-miR-6918-5p	-0.62517
mmu-miR-1895	0.624853

mmu-miR-499-5p	-0.61557
mmu-miR-2861	0.603286
mmu-miR-7082-5p	0.598042
mmu-miR-497b	0.577704
mmu-miR-6971-5p	-0.57191
mmu-miR-101a-3p	-0.56667
mmu-miR-6393	0.566487
mmu-miR-3099-3p	-0.56629
mmu-miR-664-5p	0.562536
mmu-miR-7086-5p	-0.54277
mmu-miR-3968	0.542484
mmu-miR-211-3p	0.522644
mmu-miR-6904-5p	-0.51569
mmu-miR-6965-5p	0.512752
mmu-miR-376b-3p	0.506903

Fig.3. Differentially expressed miRNAs in wild-type control vs untreated PPAR α⁻/⁻ mice
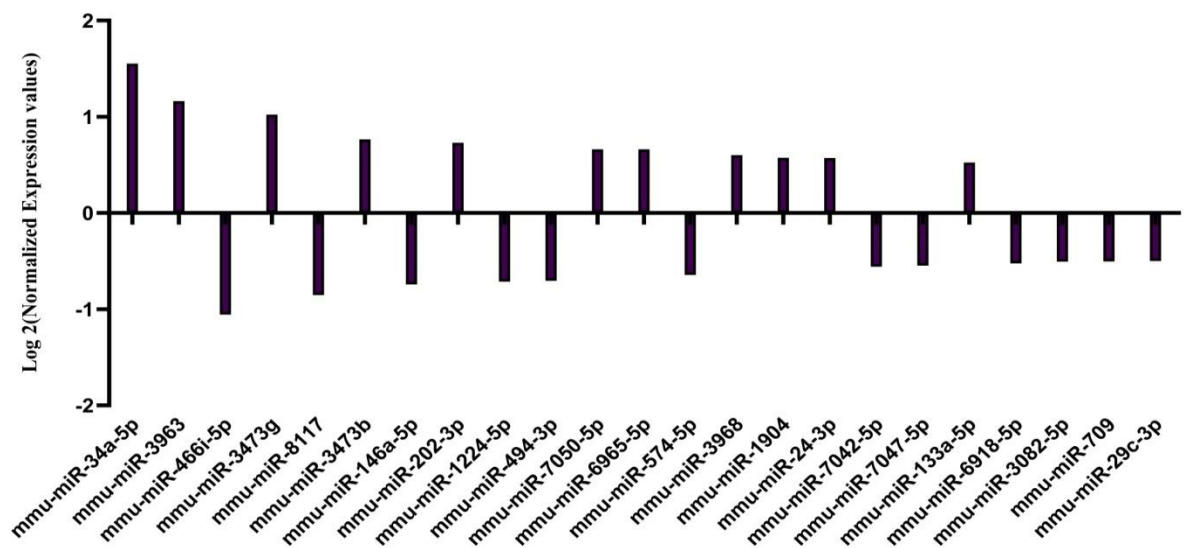
miRNA ID	Log FC
mmu-miR-34a-5p	1.553237
mmu-miR-3963	1.16318
mmu-miR-466i-5p	-1.05612
mmu-miR-3473g	1.023427
mmu-miR-8117	-0.85435
mmu-miR-3473b	0.764666
mmu-miR-146a-5p	-0.74386
mmu-miR-202-3p	0.729144
mmu-miR-1224-5p	-0.71277
mmu-miR-494-3p	-0.70374
mmu-miR-7050-5p	0.662691
mmu-miR-6965-5p	0.661179
mmu-miR-574-5p	-0.64468
mmu-miR-3968	0.600872
mmu-miR-1904	0.574271
mmu-miR-24-3p	0.571641
mmu-miR-7042-5p	-0.55883
mmu-miR-7047-5p	-0.54602
mmu-miR-133a-5p	0.524499
mmu-miR-6918-5p	-0.52341
mmu-miR-3082-5p	-0.50604
mmu-miR-709	-0.50432
mmu-miR-29c-3p	-0.5004

Fig.4. Differentially expressed miRNAs in wild-type control group vs ISO-treated PPAR α⁻/⁻ mice group
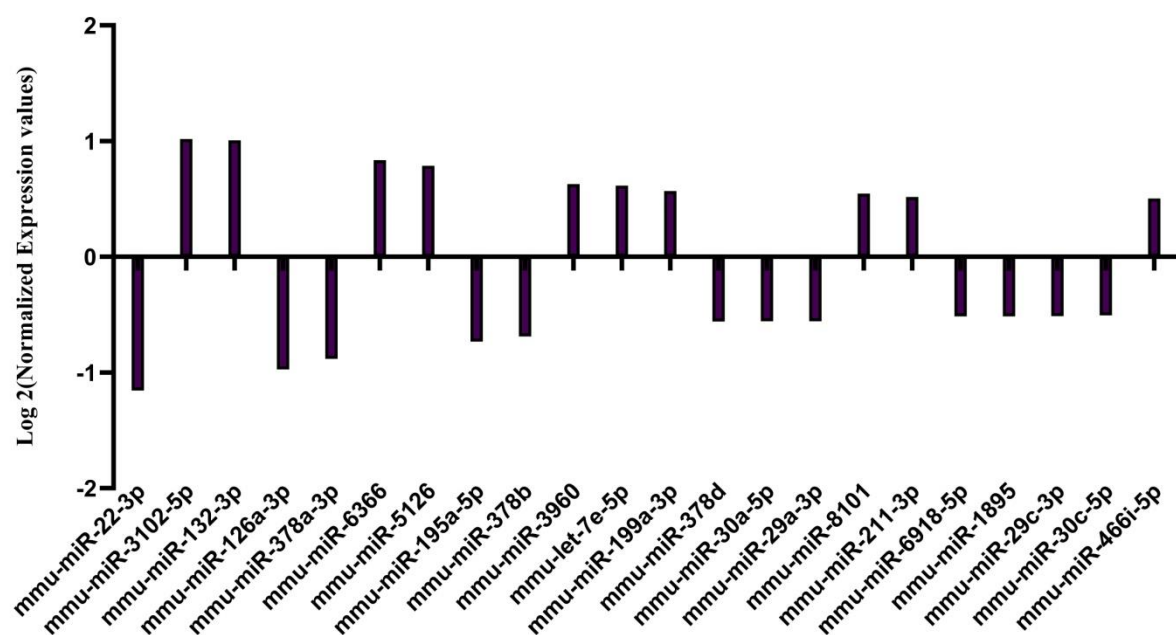
miRNA ID	Log FC
mmu-miR-22-3p	-1.15593
mmu-miR-3102-5p	1.016792
mmu-miR-132-3p	1.006908
mmu-miR-126a-3p	-0.97361
mmu-miR-378a-3p	-0.88163
mmu-miR-6366	0.83624
mmu-miR-5126	0.786542
mmu-miR-195a-5p	-0.73242
mmu-miR-378b	-0.6894
mmu-miR-3960	0.629218
mmu-let-7e-5p	0.615148
mmu-miR-199a-3p	0.568875
mmu-miR-378d	-0.5602
mmu-miR-30a-5p	-0.55708
mmu-miR-29a-3p	-0.55692
mmu-miR-8101	0.545983
mmu-miR-211-3p	0.516537
mmu-miR-6918-5p	-0.51592
mmu-miR-1895	-0.51575
mmu-miR-29c-3p	-0.51265
mmu-miR-30c-5p	-0.50626
mmu-miR-466i-5p	0.504217

Fig.5. Differentially expressed miRNAs in ISO-treated wild-type mice vs untreated PPAR $\alpha^{-/-}$ mice
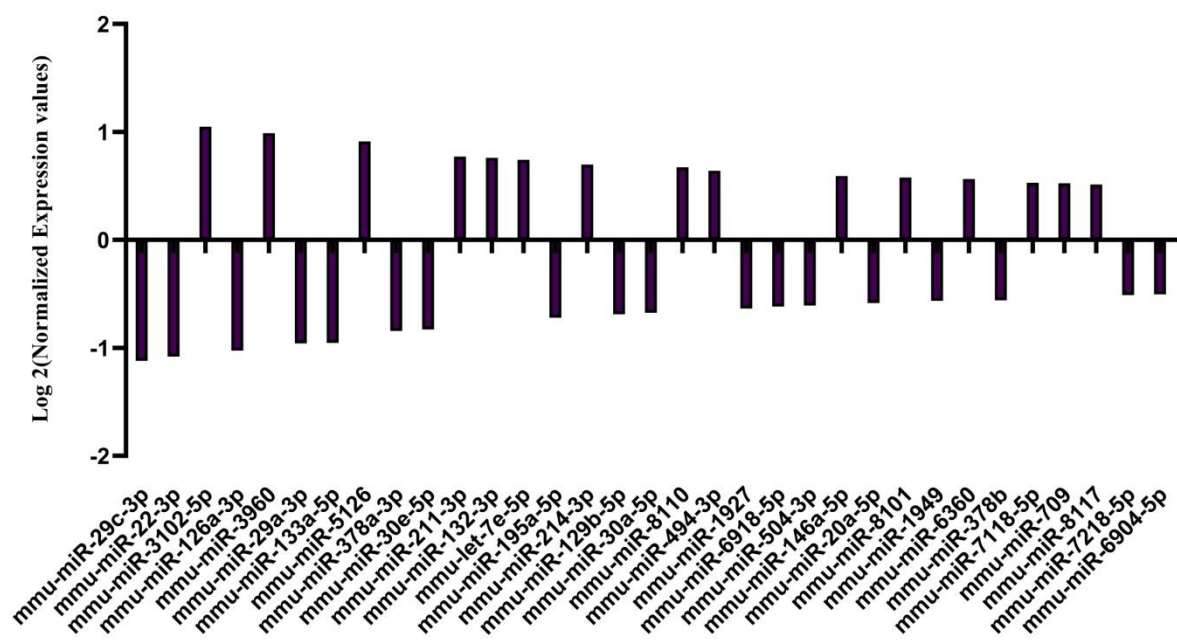
miRNA ID	LogFC
mmu-miR-29c-3p	-1.11994
mmu-miR-22-3p	-1.08087
mmu-miR-3102-5p	1.04929
mmu-miR-126a-3p	-1.02507
mmu-miR-3960	0.987457
mmu-miR-29a-3p	-0.95859
mmu-miR-133a-5p	-0.95412
mmu-miR-5126	0.912301
mmu-miR-378a-3p	-0.84372
mmu-miR-30e-5p	-0.82936
mmu-miR-211-3p	0.771782
mmu-miR-132-3p	0.759793
mmu-let-7e-5p	0.742663
mmu-miR-195a-5p	-0.72039
mmu-miR-214-3p	0.697023
mmu-miR-129b-5p	-0.68832
mmu-miR-30a-5p	-0.67556
mmu-miR-8110	0.673365
mmu-miR-494-3p	0.640188
mmu-miR-1927	-0.635
mmu-miR-6918-5p	-0.61767
mmu-miR-504-3p	-0.6086
mmu-miR-146a-5p	0.592636
mmu-miR-20a-5p	-0.58422
mmu-miR-8101	0.578414
mmu-miR-1949	-0.56479
mmu-miR-6360	0.563814
mmu-miR-378b	-0.55961
mmu-miR-7118-5p	0.529352
mmu-miR-709	0.524624
mmu-miR-8117	0.512603
mmu-miR-7218-5p	-0.51193
mmu-miR-6904-5p	-0.50298

Fig.6. Differentially expressed miRNAs in ISO-treated wild-type mice vs ISO-treated PPAR $\alpha^{-/-}$ mice
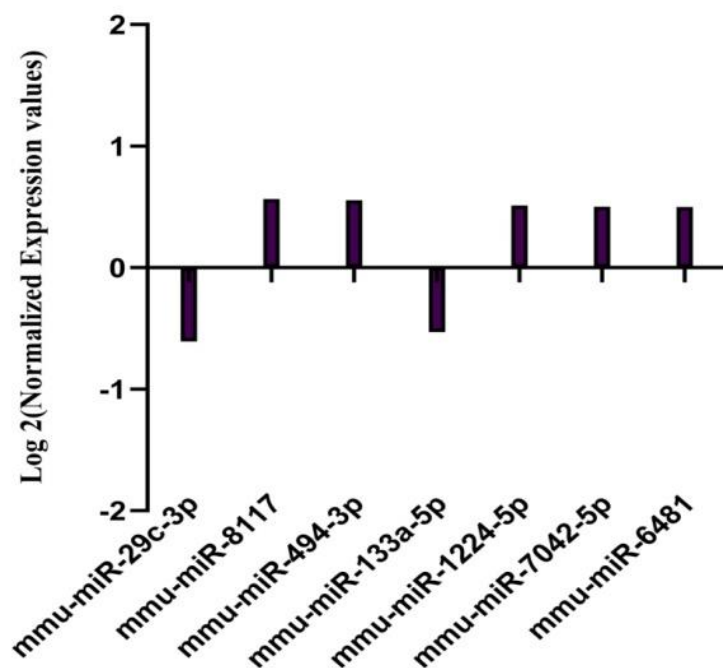
miRNA ID	Log FC
mmu-miR-29c-3p	-0.6073
mmu-miR-8117	0.565451
mmu-miR-494-3p	0.553838
mmu-miR-133a-5p	-0.53024
mmu-miR-1224-5p	0.512538
mmu-miR-7042-5p	0.503002
mmu-miR-6481	0.500472

Fig.7. Differentially expressed miRNAs in untreated PPAR $\alpha^{-/-}$ mice vs ISO-treated PPAR $\alpha^{-/-}$ mice

We employed miRNA Enrichment Analysis and Annotation Tool (miEAA) that facilitates the functional analysis of sets of miRNAs to analyse the control and experimental groups.
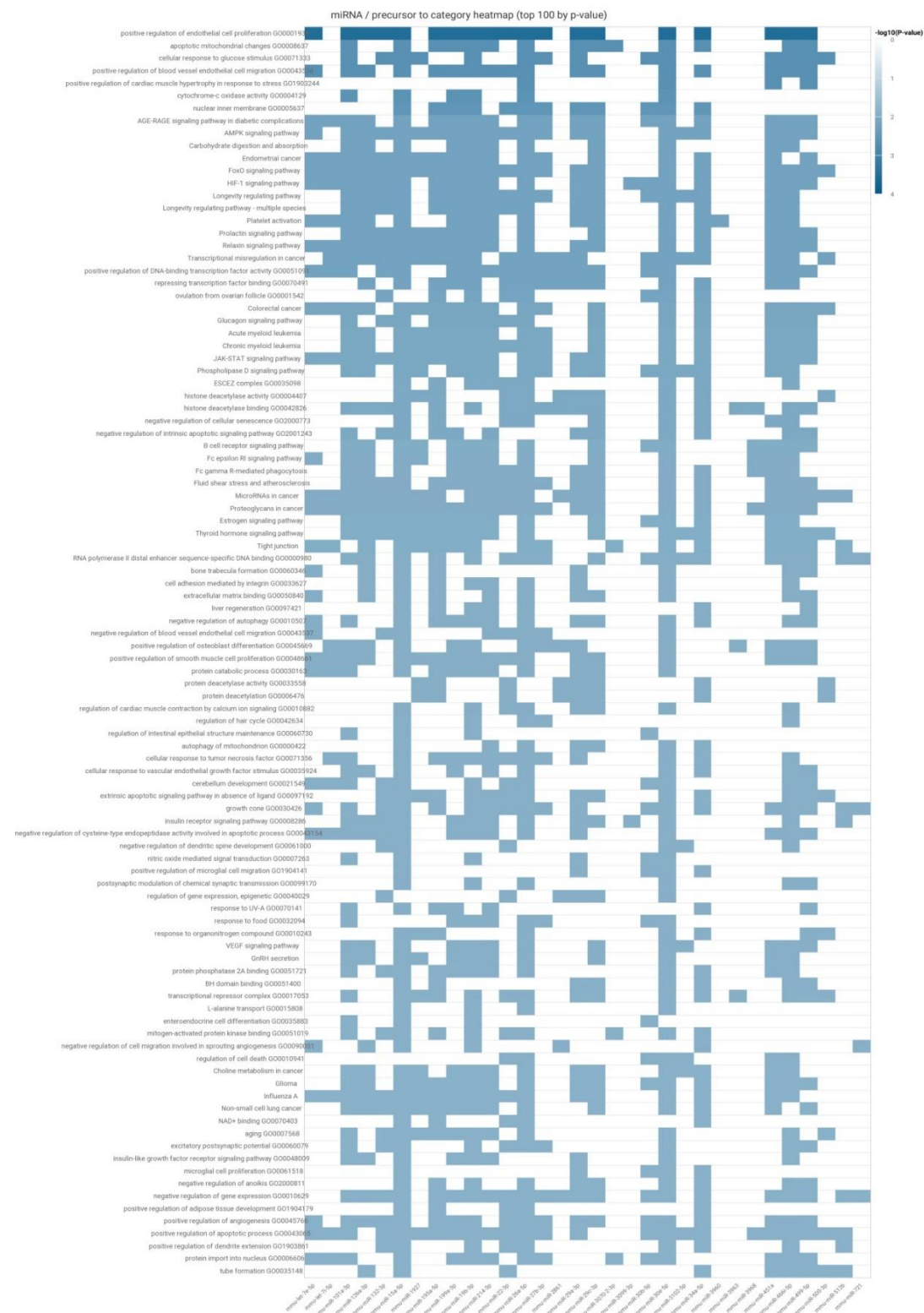
Fig.8 Heat map showing differential enrichment of pathways in ISO-treated wild-type mice vs wild-type control group

Table 1: Differential enrichment of signalling pathways in wild-type vs. ISO-treated wild-type control

Signalling Pathway	miRNA
positive regulation of endothelial cell proliferation	mmu-miR-29c-3p; mmu-miR-34a-5p; mmu-miR-132-3p; mmu-miR-22-3p; mmu-miR-126a-3p; mmu-miR-29a-3p; mmu-miR-30e-5p; mmu-miR-451a; mmu-miR-214-3p; mmu-miR-499-5p; mmu-let-7e-5p; mmu-miR-466i-5p; mmu-miR-19b-3p; mmu-miR-101a-3p; mmu-miR-195a-5p; mmu-miR-199a-3p; mmu-miR-15a-5p; mmu-miR-27b-3p; mmu-miR-26a-5p
apoptotic mitochondrial changes	mmu-miR-29c-3p; mmu-miR-34a-5p; mmu-miR-29a-3p; mmu-miR-3070-2-3p; mmu-miR-30e-5p; mmu-miR-214-3p; mmu-miR-499-5p; mmu-miR-466i-5p; mmu-miR-19b-3p; mmu-miR-101a-3p; mmu-miR-195a-5p; mmu-miR-199a-3p; mmu-miR-15a-5p; mmu-miR-26a-5p
cellular response to glucose stimulus	mmu-miR-132-3p; mmu-miR-1927; mmu-miR-29a-3p; mmu-miR-500-3p; mmu-miR-30e-5p; mmu-miR-451a; mmu-miR-499-5p; mmu-miR-466i-5p; mmu-miR-19b-3p; mmu-miR-101a-3p; mmu-miR-30b-5p; mmu-miR-15a-5p; mmu-miR-27b-3p; mmu-miR-26a-5p
positive regulation of blood vessel endothelial cell migration	mmu-miR-29c-3p; mmu-miR-34a-5p; mmu-miR-22-3p; mmu-miR-126a-3p; mmu-miR-29a-3p; mmu-miR-30e-5p; mmu-miR-451a; mmu-miR-214-3p; mmu-miR-499-5p; mmu-let-7e-5p; mmu-miR-466i-5p; mmu-miR-19b-3p; mmu-miR-101a-3p; mmu-miR-195a-5p; mmu-miR-199a-3p; mmu-miR-15a-5p; mmu-miR-26a-5p
positive regulation of cardiac muscle hypertrophy in response to stress	mmu-miR-30e-5p; mmu-miR-451a; mmu-miR-499-5p; mmu-miR-26a-5p
cytochrome-c oxidase activity	mmu-miR-30e-5p; mmu-miR-19b-3p; mmu-miR-101a-3p; mmu-miR-199a-3p; mmu-miR-15a-5p; mmu-miR-26a-5p
nuclear inner membrane	mmu-miR-29c-3p; mmu-miR-34a-5p; mmu-miR-22-3p; mmu-miR-29a-3p; mmu-miR-30e-5p; mmu-miR-19b-3p; mmu-miR-195a-5p; mmu-miR-30b-5p; mmu-miR-199a-3p; mmu-miR-15a-5p; mmu-miR-27b-3p; mmu-miR-26a-5p
AGE-RAGE signaling pathway in diabetic	mmu-miR-29c-3p; mmu-miR-34a-5p; mmu-miR-126a-3p; mmu-miR-29a-3p; mmu-miR-30e-5p; mmu-miR-451a; mmu-miR-214-3p; mmu-miR-499-5p; mmu-let-7e-5p; mmu-miR-466i-5p; mmu-miR-19b-3p; mmu-miR-101a-3p; mmu-miR-195a-5p; mmu-miR-30b-5p;

complications	mmu-miR-199a-3p; mmu-miR-15a-5p; mmu-miR-27b-3p; mmu-let-7i-5p; mmu-miR-26a-5p
AMPK signaling pathway	mmu-miR-29c-3p; mmu-miR-3102-5p; mmu-miR-34a-5p; mmu-miR-132-3p; mmu-miR-1927; mmu-miR-22-3p; mmu-miR-126a-3p; mmu-miR-29a-3p; mmu-miR-30e-5p; mmu-miR-451a; mmu-miR-214-3p; mmu-miR-499-5p; mmu-let-7e-5p; mmu-miR-466i-5p; mmu-miR-19b-3p; mmu-miR-101a-3p; mmu-miR-195a-5p; mmu-miR-199a-3p; mmu-miR-15a-5p; mmu-miR-27b-3p; mmu-miR-26a-5p
Carbohydrate digestion and absorption	mmu-miR-29c-3p; mmu-miR-126a-3p; mmu-miR-30e-5p; mmu-miR-451a; mmu-miR-214-3p; mmu-miR-466i-5p; mmu-miR-19b-3p; mmu-miR-101a-3p; mmu-miR-199a-3p; mmu-miR-15a-5p; mmu-miR-26a-5p
Endometrial cancer	mmu-miR-29c-3p; mmu-miR-34a-5p; mmu-miR-132-3p; mmu-miR-1927; mmu-miR-126a-3p; mmu-miR-30e-5p; mmu-miR-451a; mmu-miR-214-3p; mmu-miR-499-5p; mmu-let-7e-5p; mmu-miR-19b-3p; mmu-miR-101a-3p; mmu-miR-195a-5p; mmu-miR-199a-3p; mmu-miR-15a-5p; mmu-miR-27b-3p; mmu-let-7i-5p; mmu-miR-26a-5p
FoxO signaling pathway	mmu-miR-29c-3p; mmu-miR-34a-5p; mmu-miR-132-3p; mmu-miR-1927; mmu-miR-22-3p; mmu-miR-126a-3p; mmu-miR-29a-3p; mmu-miR-500-3p; mmu-miR-30e-5p; mmu-miR-451a; mmu-miR-214-3p; mmu-miR-499-5p; mmu-let-7e-5p; mmu-miR-466i-5p; mmu-miR-19b-3p; mmu-miR-101a-3p; mmu-miR-195a-5p; mmu-miR-199a-3p; mmu-miR-15a-5p; mmu-miR-27b-3p; mmu-let-7i-5p; mmu-miR-26a-5p
HIF-1 signaling pathway	mmu-miR-29c-3p; mmu-miR-34a-5p; mmu-miR-132-3p; mmu-miR-126a-3p; mmu-miR-29a-3p; mmu-miR-30e-5p; mmu-miR-451a; mmu-miR-214-3p; mmu-miR-499-5p; mmu-let-7e-5p; mmu-miR-466i-5p; mmu-miR-19b-3p; mmu-miR-101a-3p; mmu-miR-195a-5p; mmu-miR-30b-5p; mmu-miR-199a-3p; mmu-miR-15a-5p; mmu-miR-3099-3p; mmu-let-7i-5p; mmu-miR-26a-5p
Longevity regulating pathway	mmu-miR-29c-3p; mmu-miR-3102-5p; mmu-miR-34a-5p; mmu-miR-132-3p; mmu-miR-22-3p; mmu-miR-126a-3p; mmu-miR-29a-3p; mmu-miR-30e-5p; mmu-miR-451a; mmu-miR-214-3p; mmu-miR-466i-5p; mmu-miR-19b-3p; mmu-miR-101a-3p; mmu-miR-195a-5p; mmu-miR-30b-5p; mmu-miR-199a-3p; mmu-miR-15a-5p; mmu-miR-27b-3p; mmu-miR-26a-5p
Longevity regulating pathway - multiple species	mmu-miR-29c-3p; mmu-miR-34a-5p; mmu-miR-132-3p; mmu-miR-22-3p; mmu-miR-126a-3p; mmu-miR-29a-3p; mmu-miR-30e-5p; mmu-miR-451a; mmu-miR-214-3p; mmu-miR-466i-5p; mmu-miR-19b-3p; mmu-miR-101a-3p; mmu-miR-195a-5p; mmu-miR-199a-3p; mmu-miR-15a-5p; mmu-miR-26a-5p
Platelet activation	mmu-miR-29c-3p; mmu-miR-34a-5p; mmu-miR-126a-3p; mmu-miR-3960; mmu-miR-29a-3p; mmu-miR-30e-5p; mmu-miR-451a; mmu-miR-214-3p; mmu-let-7e-5p; mmu-miR-466i-5p; mmu-miR-19b-3p; mmu-miR-101a-3p; mmu-miR-199a-3p; mmu-miR-15a-5p; mmu-let-7i-5p; mmu-miR-26a-5p

Prolactin signaling pathway	mmu-miR-29c-3p; mmu-miR-34a-5p; mmu-miR-132-3p; mmu-miR-1927; mmu-miR-126a-3p; mmu-miR-30e-5p; mmu-miR-451a; mmu-miR-214-3p; mmu-miR-499-5p; mmu-miR-466i-5p; mmu-miR-19b-3p; mmu-miR-101a-3p; mmu-miR-195a-5p; mmu-miR-199a-3p; mmu-miR-15a-5p; mmu-miR-26a-5p
Relaxin signaling pathway	mmu-miR-29c-3p; mmu-miR-34a-5p; mmu-miR-132-3p; mmu-miR-1927; mmu-miR-126a-3p; mmu-miR-29a-3p; mmu-miR-30e-5p; mmu-miR-451a; mmu-miR-214-3p; mmu-miR-499-5p; mmu-let-7e-5p; mmu-miR-466i-5p; mmu-miR-19b-3p; mmu-miR-101a-3p; mmu-miR-195a-5p; mmu-miR-199a-3p; mmu-miR-15a-5p; mmu-let-7i-5p; mmu-miR-26a-5p
Transcriptional misregulation in cancer	mmu-miR-3102-5p; mmu-miR-34a-5p; mmu-miR-132-3p; mmu-miR-1927; mmu-miR-22-3p; mmu-miR-126a-3p; mmu-miR-29a-3p; mmu-miR-500-3p; mmu-miR-30e-5p; mmu-miR-451a; mmu-miR-2861; mmu-miR-466i-5p; mmu-miR-19b-3p; mmu-miR-101a-3p; mmu-miR-195a-5p; mmu-miR-30b-5p; mmu-miR-199a-3p; mmu-miR-15a-5p; mmu-miR-27b-3p; mmu-let-7i-5p; mmu-miR-26a-5p
negative regulation of signalling pathways like negative regulation of autophagy	mmu-miR-29c-3p; mmu-miR-34a-5p; mmu-miR-29a-3p; mmu-miR-30e-5p; mmu-miR-214-3p; mmu-miR-499-5p; mmu-let-7e-5p; mmu-miR-466i-5p; mmu-miR-19b-3p; mmu-miR-101a-3p; mmu-miR-195a-5p; mmu-miR-199a-3p; mmu-miR-15a-5p; mmu-miR-26a-5p.
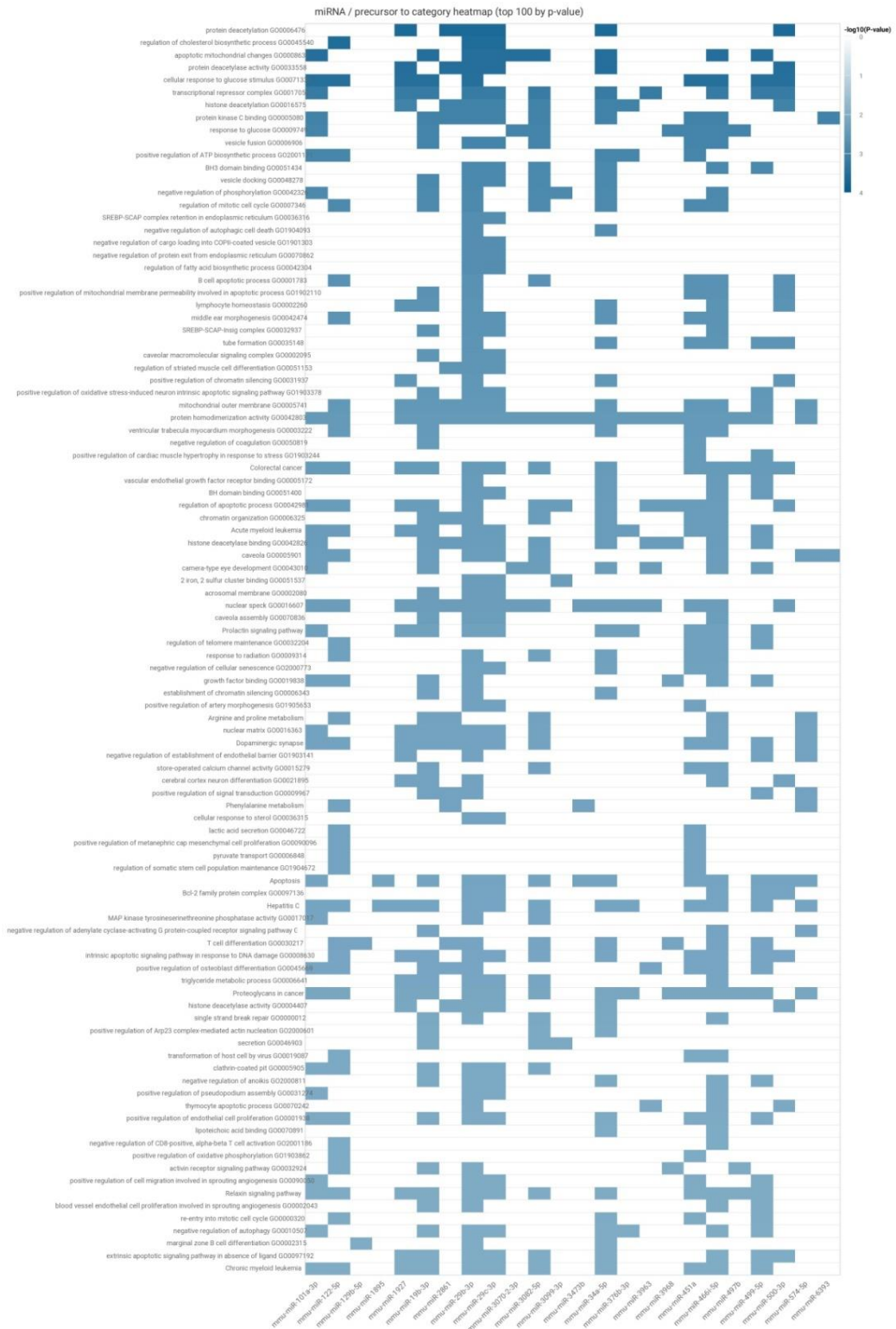
Fig.9. Heat map showing differential enrichment of signalling pathways in wild-type control vs untreated PPAR α⁻/⁻ mice

The top enriched signalling pathways were enlisted in Table 2:

Table 2: Differential enrichment of signalling pathways in wild-type control mice vs. untreated PPAR α$^{-/-}$ mice

Signalling Pathway	miRNA
protein deacetylation	mmu-miR-34a-5p; mmu-miR-29c-3p; mmu-miR-1927; mmu-miR-500-3p; mmu-miR-29b-3p; mmu-miR-2861
regulation of cholesterol biosynthetic process	mmu-miR-29c-3p; mmu-miR-122-5p; mmu-miR-29b-3p
protein deacetylase activity	mmu-miR-34a-5p; mmu-miR-29c-3p; mmu-miR-1927; mmu-miR-500-3p; mmu-miR-29b-3p; mmu-miR-2861
cellular response to glucose stimulus	mmu-miR-466i-5p; mmu-miR-1927; mmu-miR-451a; mmu-miR-122-5p; mmu-miR-500-3p; mmu-miR-19b-3p; mmu-miR-29b-3p; mmu-miR-499-5p; mmu-miR-101a-3p
transcriptional repressor complex	mmu-miR-3963; mmu-miR-34a-5p; mmu-miR-466i-5p; mmu-miR-29c-3p; mmu-miR-1927; mmu-miR-500-3p; mmu-miR-3082-5p; mmu-miR-19b-3p; mmu-miR-29b-3p; mmu-miR-499-5p; mmu-miR-101a-3p
histone deacetylation	mmu-miR-34a-5p; mmu-miR-29c-3p; mmu-miR-1927; mmu-miR-500-3p; mmu-miR-3082-5p; mmu-miR-29b-3p; mmu-miR-2861; mmu-miR-376b-3p
protein kinase C binding	mmu-miR-34a-5p; mmu-miR-466i-5p; mmu-miR-29c-3p; mmu-miR-451a; mmu-miR-3082-5p; mmu-miR-19b-3p; mmu-miR-29b-3p; mmu-miR-2861; mmu-miR-101a-3p; mmu-miR-6393
response to glucose	mmu-miR-466i-5p; mmu-miR-3070-2-3p; mmu-miR-451a; mmu-miR-3082-5p; mmu-miR-19b-3p; mmu-miR-497b; mmu-miR-101a-3p; mmu-miR-3968
vesicle fusion	mmu-miR-466i-5p; mmu-miR-29c-3p; mmu-miR-451a; mmu-miR-3082-5p; mmu-miR-19b-3p; mmu-miR-29b-3p
positive regulation of ATP biosynthetic process	mmu-miR-34a-5p; mmu-miR-451a; mmu-miR-122-5p; mmu-miR-101a-3p; mmu-miR-376b-3p
BH3 domain binding	mmu-miR-34a-5p; mmu-miR-466i-5p; mmu-miR-29c-3p; mmu-miR-3082-5p; mmu-miR-29b-3p; mmu-miR-499-5p
vesicle docking	mmu-miR-34a-5p; mmu-miR-29c-3p; mmu-miR-3082-5p; mmu-miR-19b-3p; mmu-miR-29b-3p
negative regulation of phosphorylation	mmu-miR-34a-5p; mmu-miR-466i-5p; mmu-miR-3082-5p; mmu-miR-19b-3p; mmu-miR-29b-3p; mmu-miR-101a-3p; mmu-miR-3099-3p

|	
regulation of mitotic cell cycle	mmu-miR-34a-5p; mmu-miR-466i-5p; mmu-miR-451a; mmu-miR-122-5p; mmu-miR-3082-5p; mmu-miR-19b-3p; mmu-miR-29b-3p
SREBP-SCAP complex retention in endoplasmic reticulum	mmu-miR-29c-3p; mmu-miR-29b-3p
negative regulation of cargo loading into COPII-coated vesicle	mmu-miR-29c-3p; mmu-miR-29b-3p
negative regulation of protein exit from endoplasmic reticulum	mmu-miR-29c-3p; mmu-miR-29b-3p
regulation of fatty acid biosynthetic process	mmu-miR-29c-3p; mmu-miR-29b-3p
B cell apoptotic process	mmu-miR-466i-5p; mmu-miR-451a; mmu-miR-122-5p; mmu-miR-500-3p; mmu-miR-3082-5p; mmu-miR-29b-3p
lymphocyte homeostasis	mmu-miR-34a-5p; mmu-miR-466i-5p; mmu-miR-1927; mmu-miR-500-3p; mmu-miR-19b-3p; mmu-miR-29b-3p
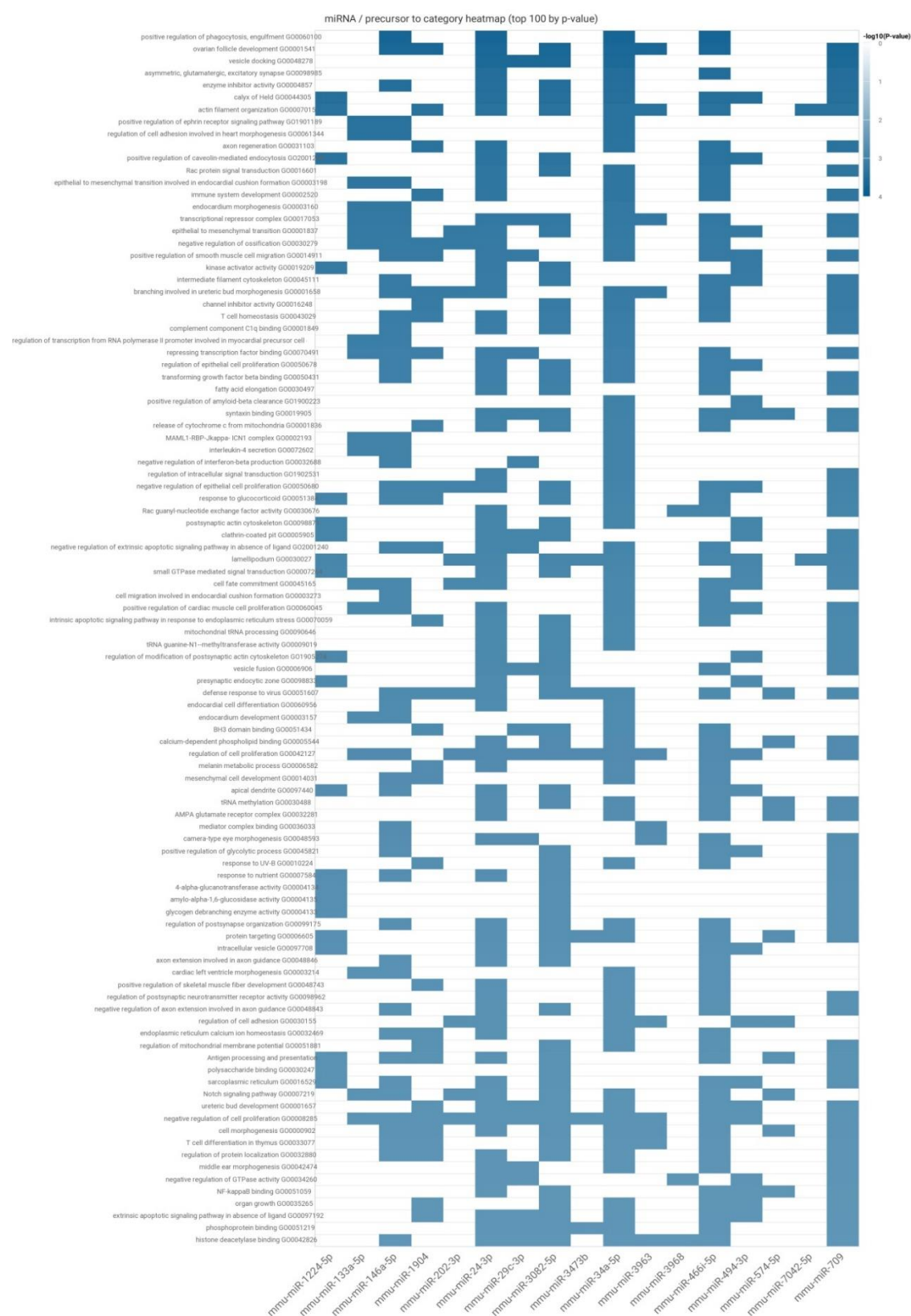
Fig.10. Heat map showing differential enrichment of signalling pathways between wild-type control and ISO-treated PPAR $\alpha^{-/-}$ mice

.The top enriched signalling pathways were enlisted in Table 3:

Table 3: Differential enrichment of signalling pathways in wild-type control vs. ISO-treated PPAR α^{-/-} mice

Table 3: Differential enrichment of signalling pathways in wild-type control vs. ISO-treated PPAR $\alpha^{-/-}$ mice

Signalling Pathway	miRNA
positive regulation of phagocytosis, engulfment	mmu-miR-34a-5p; mmu-miR-466i-5p; mmu-miR-146a-5p; mmu-miR-24-3p
ovarian follicle development	mmu-miR-34a-5p; mmu-miR-3963; mmu-miR-466i-5p; mmu-miR-146a-5p; mmu-miR-1904; mmu-miR-24-3p; mmu-miR-3082-5p; mmu-miR-709
vesicle docking	mmu-miR-34a-5p; mmu-miR-24-3p; mmu-miR-3082-5p; mmu-miR-709; mmu-miR-29c-3p
asymmetric, glutamatergic, excitatory synapse	mmu-miR-34a-5p; mmu-miR-466i-5p; mmu-miR-24-3p; mmu-miR-709
enzyme inhibitor activity	mmu-miR-34a-5p; mmu-miR-146a-5p; mmu-miR-24-3p; mmu-miR-3082-5p; mmu-miR-709
calyx of Held	mmu-miR-34a-5p; mmu-miR-466i-5p; mmu-miR-1224-5p; mmu-miR-494-3p; mmu-miR-24-3p; mmu-miR-3082-5p; mmu-miR-709
actin filament organization	mmu-miR-34a-5p; mmu-miR-3963; mmu-miR-466i-5p; mmu-miR-1224-5p; mmu-miR-1904; mmu-miR-24-3p; mmu-miR-7042-5p; mmu-miR-3082-5p; mmu-miR-709
positive regulation of ephrin receptor signaling pathway	mmu-miR-34a-5p; mmu-miR-146a-5p; mmu-miR-133a-5p
regulation of cell adhesion involved in heart morphogenesis	mmu-miR-34a-5p; mmu-miR-146a-5p; mmu-miR-133a-5p
axon regeneration	mmu-miR-34a-5p; mmu-miR-466i-5p; mmu-miR-1904; mmu-miR-24-3p; mmu-miR-709
positive regulation of caveolin-mediated endocytosis	mmu-miR-466i-5p; mmu-miR-1224-5p; mmu-miR-494-3p; mmu-miR-24-3p; mmu-miR-3082-5p
Rac protein signal transduction	mmu-miR-34a-5p; mmu-miR-466i-5p; mmu-miR-24-3p; mmu-miR-3082-5p; mmu-miR-709
epithelial to mesenchymal transition involved in endocardial cushion formation	mmu-miR-34a-5p; mmu-miR-466i-5p; mmu-miR-146a-5p; mmu-miR-24-3p; mmu-miR-133a-5p
immune system development	mmu-miR-34a-5p; mmu-miR-466i-5p; mmu-miR-1904; mmu-miR-24-3p; mmu-miR-709
endocardium morphogenesis	mmu-miR-34a-5p; mmu-miR-146a-5p; mmu-miR-133a-5p
transcriptional repressor complex	mmu-miR-34a-5p; mmu-miR-3963; mmu-miR-466i-5p; mmu-miR-146a-5p; mmu-miR-24-3p; mmu-miR-133a-5p; mmu-miR-3082-5p; mmu-miR-709; mmu-miR-29c-3p
epithelial to mesenchymal transition	mmu-miR-34a-5p; mmu-miR-466i-5p; mmu-miR-146a-5p; mmu-miR-202-3p; mmu-miR-494-3p; mmu-miR-24-3p; mmu-miR-133a-5p; mmu-miR-3082-5p; mmu-miR-709

| negative regulation of ossification	mmu-miR-34a-5p; mmu-miR-466i-5p; mmu-miR-146a-5p; mmu-miR-202-3p; mmu-miR-1904; mmu-miR-24-3p; mmu-miR-133a-5p
positive regulation of smooth muscle cell migration	mmu-miR-34a-5p; mmu-miR-466i-5p; mmu-miR-146a-5p; mmu-miR-494-3p; mmu-miR-1904; mmu-miR-24-3p; mmu-miR-709; mmu-miR-29c-3p
positive regulation of cardiac muscle cell proliferation	mmu-miR-34a-5p; mmu-miR-466i-5p; mmu-miR-146a-5p; mmu-miR-494-3p; mmu-miR-24-3p; mmu-miR-133a-5p; mmu-miR-709

Fig.11. Heat map showing differential enrichment of signalling pathways in ISO-treated wild type mice with untreated PPAR $\alpha^{-/-}$ mice

The top enriched signalling pathways were:

Table 4: Differential enrichment of signalling pathways in ISO-treated wild-type mice vs. untreated PPAR $\alpha^{-/-}$ mice

Signalling Pathway	miRNA
Intramembranous ossification	mmu-miR-195a-5p; mmu-let-7e-5p; mmu-miR-29a-3p
positive regulation of endothelial cell proliferation	mmu-miR-22-3p; mmu-miR-132-3p; mmu-miR-126a-3p; mmu-miR-195a-5p; mmu-miR-378b; mmu-let-7e-5p; mmu-miR-199a-3p; mmu-miR-29a-3p; mmu-miR-29c-3p; mmu-miR-466i-5p
SUMO transferase activity	mmu-miR-22-3p; mmu-miR-30a-5p; mmu-miR-29a-3p; mmu-miR-29c-3p; mmu-miR-30c-5p; mmu-miR-466i-5p
positive regulation of odontogenesis of dentin-containing tooth	mmu-miR-3102-5p; mmu-miR-30a-5p; mmu-miR-30c-5p; mmu-miR-466i-5p
positive regulation of pri-miRNA transcription by RNA polymerase II	mmu-miR-3102-5p; mmu-miR-126a-3p; mmu-miR-378b; mmu-let-7e-5p; mmu-miR-199a-3p; mmu-miR-30a-5p; mmu-miR-30c-5p; mmu-miR-466i-5p
nuclear inner membrane	mmu-miR-22-3p; mmu-miR-195a-5p; mmu-miR-199a-3p; mmu-miR-30a-5p; mmu-miR-29a-3p; mmu-miR-29c-3p; mmu-miR-30c-5p
negative regulation of DNA damage response, signal transduction by p53 class mediator	mmu-miR-22-3p; mmu-miR-195a-5p; mmu-miR-30a-5p; mmu-miR-30c-5p; mmu-miR-466i-5p
cyclin E1-CDK2 complex	mmu-miR-195a-5p; mmu-miR-30a-5p; mmu-miR-30c-5p
ovulation from ovarian follicle	mmu-miR-22-3p; mmu-miR-132-3p; mmu-miR-195a-5p; mmu-miR-30a-5p; mmu-miR-30c-5p
regulation of cell death	mmu-miR-22-3p; mmu-miR-3102-5p; mmu-miR-30a-5p; mmu-miR-30c-5p; mmu-miR-466i-5p
positive regulation of vascular smooth muscle cell proliferation	mmu-miR-132-3p; mmu-miR-126a-3p; mmu-miR-195a-5p; mmu-miR-30a-5p; mmu-miR-29a-3p; mmu-miR-30c-5p; mmu-miR-466i-5p
negative regulation of	mmu-miR-3102-5p; mmu-miR-30a-5p; mmu-miR-30c-5p; mmu-miR-466i-5p

intrinsic apoptotic signaling pathway by p53 class mediator	
negative regulation of vitamin D biosynthetic process	mmu-miR-30a-5p; mmu-miR-30c-5p; mmu-miR-466i-5p
regulation of actin phosphorylation	mmu-miR-30a-5p; mmu-miR-30c-5p
sequestering of actin monomers	mmu-miR-30a-5p; mmu-miR-30c-5p
amyloid fibril formation	mmu-miR-132-3p; mmu-miR-30a-5p; mmu-miR-29a-3p; mmu-miR-30c-5p; mmu-miR-466i-5p
TGF-beta signaling pathway	mmu-miR-3102-5p; mmu-miR-132-3p; mmu-miR-378a-3p; mmu-miR-378b; mmu-let-7e-5p; mmu-miR-199a-3p; mmu-miR-30a-5p; mmu-miR-29a-3p; mmu-miR-30c-5p; mmu-miR-466i-5p
definitive hemopoiesis	mmu-miR-126a-3p; mmu-miR-378a-3p; mmu-miR-199a-3p; mmu-miR-30a-5p; mmu-miR-30c-5p; mmu-miR-466i-5p
negative regulation of dendritic spine development	mmu-miR-22-3p; mmu-miR-3102-5p; mmu-miR-132-3p; mmu-miR-466i-5p

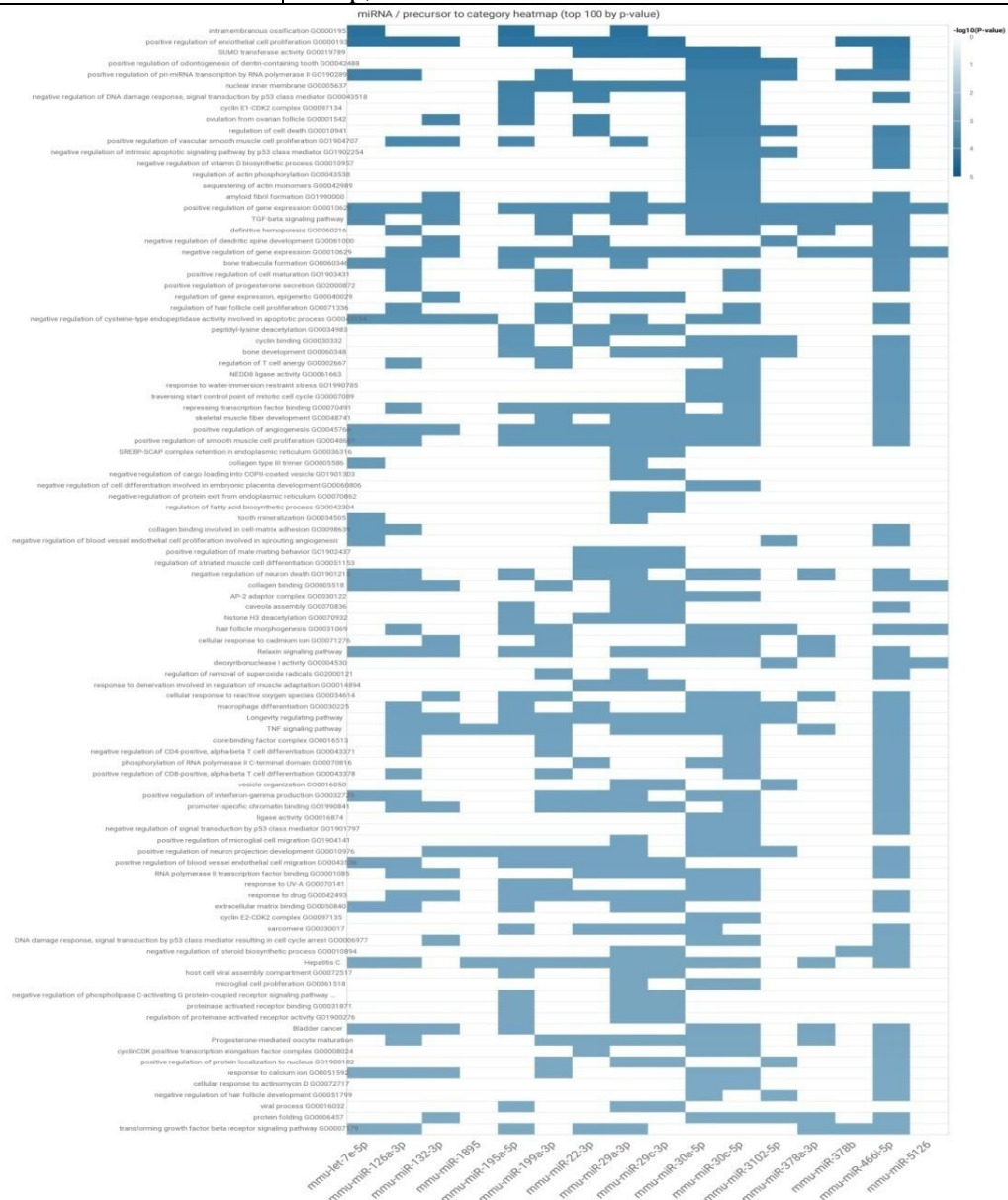Fig.12. Heat-map showing differential enrichment of signalling pathways in ISO-treated wild-type mice vs ISO-treated PPAR α$^{-/-}$ mice

As can be seen from Figure 12, miRNA profile of ISO-treated wild type mice were compared with ISO-treated PPAR α$^{-/-}$ mice. The top enriched signalling pathways were:

Table 5: Differential enrichment of signalling pathways in ISO-treated wild-type mice vs. ISO-treated PPAR $\alpha^{-/-}$ mice

Signalling Pathway	miRNA
positive regulation of smooth muscle cell proliferation	mmu-miR-29c-3p; mmu-miR-22-3p; mmu-miR-126a-3p; mmu-miR-29a-3p; mmu-miR-133a-5p; mmu-miR-30e-5p; mmu-let-7e-5p; mmu-miR-195a-5p; mmu-miR-214-3p; mmu-miR-30a-5p; mmu-miR-494-3p; mmu-miR-1927; mmu-miR-146a-5p; mmu-miR-20a-5p; mmu-miR-709
positive regulation of endothelial cell proliferation	mmu-miR-29c-3p; mmu-miR-22-3p; mmu-miR-126a-3p; mmu-miR-29a-3p; mmu-miR-30e-5p; mmu-miR-132-3p; mmu-let-7e-5p; mmu-miR-195a-5p; mmu-miR-214-3p; mmu-miR-146a-5p; mmu-miR-20a-5p; mmu-miR-378b; mmu-miR-709
circadian rhythm	mmu-miR-22-3p; mmu-miR-3102-5p; mmu-miR-3960; mmu-miR-29a-3p; mmu-miR-30e-5p; mmu-miR-132-3p; mmu-miR-195a-5p; mmu-miR-214-3p; mmu-miR-30a-5p; mmu-miR-494-3p; mmu-miR-146a-5p; mmu-miR-20a-5p; mmu-miR-709
positive regulation of blood vessel endothelial cell migration	mmu-miR-29c-3p; mmu-miR-22-3p; mmu-miR-126a-3p; mmu-miR-29a-3p; mmu-miR-30e-5p; mmu-let-7e-5p; mmu-miR-195a-5p; mmu-miR-214-3p; mmu-miR-494-3p; mmu-miR-146a-5p; mmu-miR-20a-5p; mmu-miR-709
positive regulation of cell growth involved in cardiac muscle cell development	mmu-miR-22-3p; mmu-miR-29a-3p; mmu-miR-30e-5p; mmu-miR-132-3p; mmu-miR-195a-5p; mmu-miR-494-3p; mmu-miR-20a-5p; mmu-miR-709
negative regulation of cysteine-type endopeptidase activity involved in apoptotic process	mmu-miR-126a-3p; mmu-miR-29a-3p; mmu-miR-30e-5p; mmu-miR-132-3p; mmu-let-7e-5p; mmu-miR-214-3p; mmu-miR-30a-5p; mmu-miR-494-3p; mmu-miR-146a-5p; mmu-miR-20a-5p; mmu-miR-709
positive regulation of DNA methylation	mmu-miR-22-3p; mmu-miR-30e-5p; mmu-miR-132-3p; mmu-miR-709
positive regulation of collagen biosynthetic process	mmu-miR-29a-3p; mmu-miR-30e-5p; mmu-miR-132-3p; mmu-miR-214-3p; mmu-miR-30a-5p; mmu-miR-1927; mmu-miR-20a-5p
histone deacetylation	mmu-miR-29c-3p; mmu-miR-22-3p; mmu-miR-3102-5p; mmu-miR-29a-3p; mmu-miR-195a-5p; mmu-miR-1927; mmu-miR-20a-5p; mmu-miR-709
JAK-STAT signaling pathway	mmu-miR-29c-3p; mmu-miR-126a-3p; mmu-miR-29a-3p; mmu-miR-378a-3p; mmu-miR-30e-5p; mmu-miR-132-3p; mmu-let-7e-5p; mmu-miR-195a-5p; mmu-miR-214-3p; mmu-miR-30a-5p; mmu-miR-

	1927; mmu-miR-146a-5p; mmu-miR-20a-5p; mmu-miR-1949; mmu-miR-709
FoxO signaling pathway	mmu-miR-29c-3p; mmu-miR-22-3p; mmu-miR-126a-3p; mmu-miR-29a-3p; mmu-miR-378a-3p; mmu-miR-30e-5p; mmu-miR-132-3p; mmu-let-7e-5p; mmu-miR-195a-5p; mmu-miR-214-3p; mmu-miR-30a-5p; mmu-miR-494-3p; mmu-miR-1927; mmu-miR-146a-5p; mmu-miR-20a-5p; mmu-miR-709
negative regulation of smooth muscle cell apoptotic process	mmu-miR-29a-3p; mmu-miR-133a-5p; mmu-miR-30e-5p; mmu-miR-494-3p; mmu-miR-709
positive regulation of glucose import	mmu-miR-22-3p; mmu-miR-126a-3p; mmu-miR-29a-3p; mmu-miR-30e-5p; mmu-miR-214-3p; mmu-miR-30a-5p; mmu-miR-494-3p; mmu-miR-20a-5p; mmu-miR-709
collagen type III trimer	mmu-miR-29a-3p; mmu-let-7e-5p
negative regulation of cell death	mmu-miR-22-3p; mmu-miR-378a-3p; mmu-miR-30e-5p; mmu-miR-132-3p; mmu-miR-195a-5p; mmu-miR-214-3p; mmu-miR-30a-5p; mmu-miR-146a-5p; mmu-miR-20a-5p; mmu-miR-709
negative regulation of plasma membrane long-chain fatty acid transport	mmu-let-7e-5p; mmu-miR-214-3p; mmu-miR-709
negative regulation of transcription from RNA polymerase II promoter involved in smooth muscle cell differentiation	mmu-miR-22-3p; mmu-miR-30e-5p; mmu-miR-132-3p
positive regulation of cardiac muscle hypertrophy	mmu-miR-22-3p; mmu-miR-29a-3p; mmu-miR-30e-5p; mmu-miR-30a-5p; mmu-miR-494-3p; mmu-miR-146a-5p; mmu-miR-20a-5p
negative regulation of intrinsic apoptotic signaling pathway	mmu-miR-29c-3p; mmu-miR-29a-3p; mmu-miR-30e-5p; mmu-miR-132-3p; mmu-miR-195a-5p; mmu-miR-214-3p; mmu-miR-709
PI3K-Akt signaling pathway	mmu-miR-29c-3p; mmu-miR-22-3p; mmu-miR-3102-5p; mmu-miR-126a-3p; mmu-miR-29a-3p; mmu-miR-378a-3p; mmu-miR-30e-5p; mmu-miR-132-3p; mmu-let-7e-5p; mmu-miR-195a-5p; mmu-miR-214-3p; mmu-miR-30a-5p; mmu-miR-494-3p; mmu-miR-1927; mmu-miR-146a-5p; mmu-miR-20a-5p; mmu-miR-1949; mmu-miR-709

Top pathways that were observed included positive regulation of smooth muscle cell proliferation, positive regulation of cell growth involved in cardiac muscle cell development, negative regulation of cysteine-type endopeptidase activity involved in apoptotic process,

positive regulation of cardiac muscle hypertrophy, negative regulation of intrinsic apoptotic signaling pathway and PI3K-Akt signaling pathway.
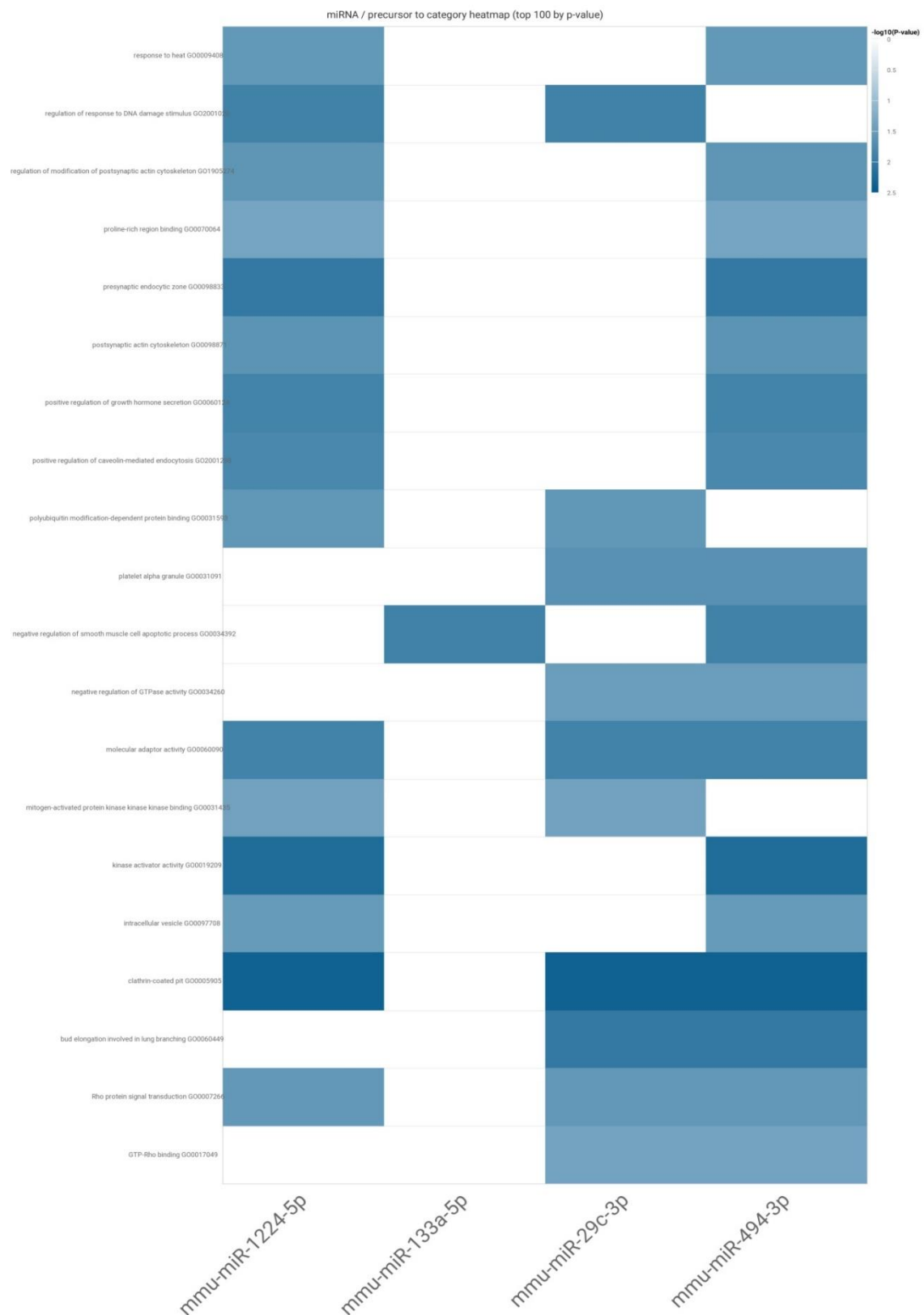
Fig.13. .Heat-map showing differential enrichment of signalling pathways in untreated PPAR $\alpha^{-/-}$ mice vs ISO-treated PPAR $\alpha^{-/-}$ mice

As can be seen from Figure 13, miRNA profile of untreated PPAR $\alpha^{-/-}$ mice were compared with ISO-treated PPAR $\alpha^{-/-}$ mice. The top enriched signalling pathways were:

Table 6: Differential enrichment of signalling pathways in untreated PPAR $\alpha^{-/-}$ mice vs. ISO-treated PPAR $\alpha^{-/-}$ mice

Signalling Pathway	miRNA
Clathrin-coated pit	mmu-miR-29c-3p; mmu-miR-494-3p; mmu-miR-1224-5p
kinase activator activity	mmu-miR-494-3p; mmu-miR-1224-5p
bud elongation involved in lung branching	mmu-miR-29c-3p; mmu-miR-494-3p
presynaptic endocytic zone	mmu-miR-494-3p; mmu-miR-1224-5p
negative regulation of smooth muscle cell apoptotic process	mmu-miR-494-3p; mmu-miR-133a-5p
regulation of response to DNA damage stimulus	mmu-miR-29c-3p; mmu-miR-1224-5p
molecular adaptor activity	mmu-miR-29c-3p; mmu-miR-494-3p; mmu-miR-1224-5p
positive regulation of growth hormone secretion	mmu-miR-494-3p; mmu-miR-1224-5p
positive regulation of caveolin-mediated endocytosis	mmu-miR-494-3p; mmu-miR-1224-5p
platelet alpha granule	mmu-miR-29c-3p; mmu-miR-494-3p
postsynaptic actin cytoskeleton	mmu-miR-494-3p; mmu-miR-1224-5p
regulation of modification of postsynaptic actin cytoskeleton	mmu-miR-494-3p; mmu-miR-1224-5p
polyubiquitin modification-dependent protein binding	mmu-miR-29c-3p; mmu-miR-1224-5p
response to heat	mmu-miR-494-3p; mmu-miR-1224-5p
Rho protein signal transduction	mmu-miR-29c-3p; mmu-miR-494-3p; mmu-miR-1224-5p
intracellular vesicle	mmu-miR-494-3p; mmu-miR-1224-5p
negative regulation of GTPase activity	mmu-miR-29c-3p; mmu-miR-494-3p
mitogen-activated protein kinase kinase kinase binding	mmu-miR-29c-3p; mmu-miR-1224-5p
GTP-Rho binding	mmu-miR-29c-3p; mmu-miR-494-3p
proline-rich region binding	mmu-miR-494-3p; mmu-miR-1224-5p

Identification of mRNA targets of the differentially expressed miRNA

We used the miRNet algorithm to identify experimentally validated mRNA targets of the differentially expressed miRNAs in the control as well as experimental groups and the functional relevance was characterized. In the first comparison that was made, a total of 2136 unique targets for the miRNAs were retrieved.As shown in Fig. 1, analysis of the network interaction graph showed that **mmu-mir-15a-5p, mmu-mir-26a-5p, mmu-mir-466i-5p**, **,mmu-mir-30e-5p and mmu-mir-19b-3p** were the important hubs in the network out of the 32 miRNA and among these **mmu-mir-15a-5p** was the most important hub as it interacted with maximum number of nodes, with the highest node degree and betweenness compared to other nodes, while **mmu-mir-3963** had the lowest node degree.As shown in Table 1, the top mRNA target list was dominated by genes like Ncan, Hdac4 and Avl9 . We further performed canonical pathway analysis (non-disease) to understand the biological relevance of the miRNA targets. Several significant pathways were identified (adjusted $p < 0.05$) that were influenced by the miRNA targets.The top significant pathways were primarily associated with collagen formation, collagen biosynthesis and activation of BAD protein.

Fig.14. Figure depicting the miRNA-target interaction hub of wild-type mice vs ISO-treated wild-type

Table7: Top miRNAs and genes in the network interaction hub

Node	Degree	Betweenness
mmu-mir-15a-5p	516	900592.3
mmu-mir-26a-5p	422	698670.8
mmu-mir-466i-5p	418	769892.8
mmu-mir-30e-5p	382	633262.7
mmu-mir-19b-3p	320	546842.8
mmu-mir-34a-5p	55	86036.55
mmu-mir-451a	48	65341.75
mmu-mir-132-3p	47	96212.75
mmu-mir-3102-5p	47	56721.66
mmu-mir-1927	42	74197.45
mmu-mir-29a-3p	41	56371.4
mmu-mir-30b-5p	38	4862.914
mmu-mir-195a-5p	33	11850.87
mmu-mir-27b-3p	27	38132.43
mmu-mir-101a-3p	26	43452.52
mmu-mir-22-3p	26	43041.5
Ncan	4	32870.91
Zfp329	4	10293.45
Hdac4	4	5430.17
Avl9	4	18908.88
B4galt6	4	28073.08
Bcl2	4	20551.92
Bicd1	4	4253.983
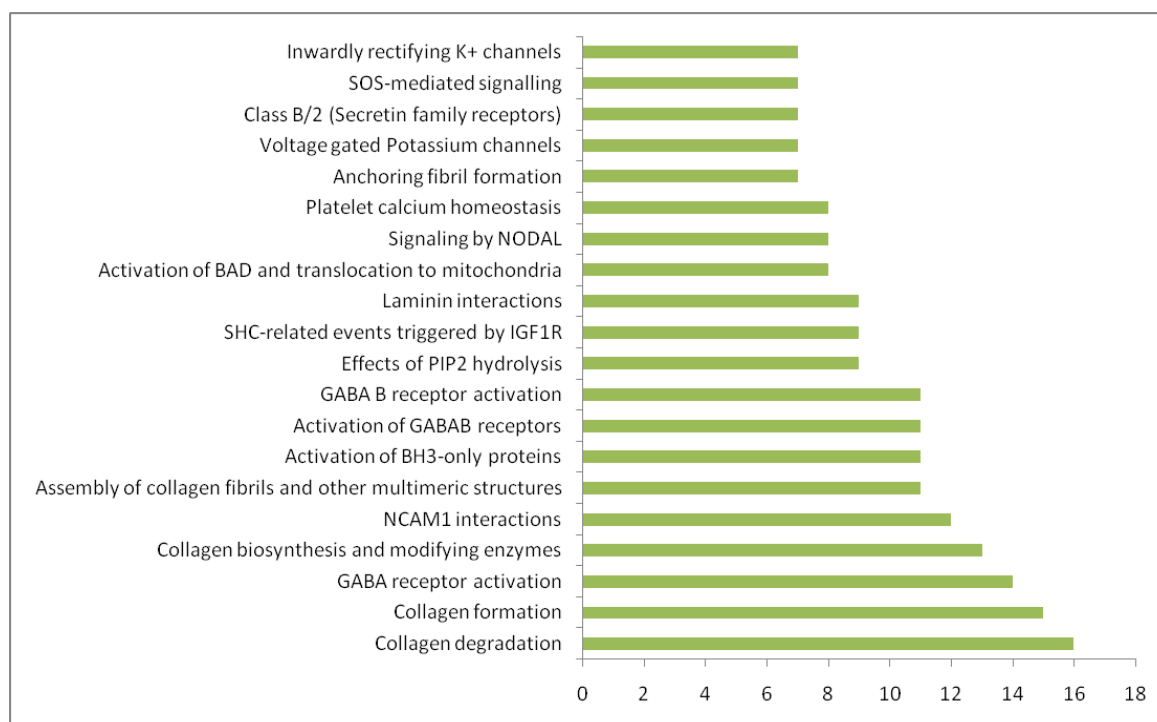
Fig.15. Bar Graph showing top 20 pathways influenced by the validated miRNA targets (p>0.05)

Another comparison was made between wild-type control mice and the untreated PPAR α-/- mice.A total of 1295 unique targets for the miRNAs were retrieved.As shown in Fig. 2, analysis of the network interaction graph showed that **mmu-mir-466i-5p, mmu-mir-19b-3p**,**mmu-mir-3082-5p** and **mmu-mir-122-5p** were the important hubs in the network out of the 21 miRNA and among these **mmu-mir-466i-5p** was the most important hub as it interacted with maximum number of nodes, with the highest node degree and betweenness compared to other nodes, while **mmu-mir-1895** had the lowest node degree.As shown in Table 2, the top mRNA target list was dominated by genes like Zffp113, Iffo2, Gm14137 and Akt3. Canonical pathway analysis (non-disease) was further performed to elucidate the biological relevance of the miRNA targets. Several significant pathways were identified (adjusted p < 0.05) that were influenced by the miRNA targets.The top significant pathways were primarily associated with ECM proteoglycans, collagen formation, collagen biosynthesis ,Activation of BH-3 only proteins, Activation of NODAL and NCAM1 interactions.

Fig.16. Figure depicting the miRNA-target interaction hub of wild-type control mice vs untreated PPAR α-/- mice

Table8: Top miRNAs and genes in the network interaction hub

Node	Degree	Betweenness
mmu-mir-466i-5p	418	558220.2
mmu-mir-19b-3p	320	391835.1
mmu-mir-3082-5p	215	262925.2
mmu-mir-122-5p	86	107476.5
mmu-mir-34a-5p	55	64982.42
mmu-mir-29b-3p	51	57244.31
mmu-mir-451a	48	58575.2
mmu-mir-1927	42	52755.46
mmu-mir-574-5p	30	33492.86
mmu-mir-101a-3p	26	27758.29
mmu-mir-29c-3p	22	11938.91
mmu-mir-3473b	18	16505.88
mmu-mir-499-5p	16	17844.57
mmu-mir-3099-3p	15	15057.47
mmu-mir-500-3p	15	16150.81
mmu-mir-3968	13	14589.1
mmu-mir-376b-3p	11	13095
mmu-mir-2861	11	13095
mmu-mir-3070-2-3p	7	5952.062
mmu-mir-3963	7	6646.452

mmu-mir-1895	4	2812.14
Zfp113	3	17917.52
Iffo2	3	14478.85
Gm14137	3	28981.61
Akt3	3	8865.921
Bcl2l11	3	28903.67
Ccnd1	3	9837.636
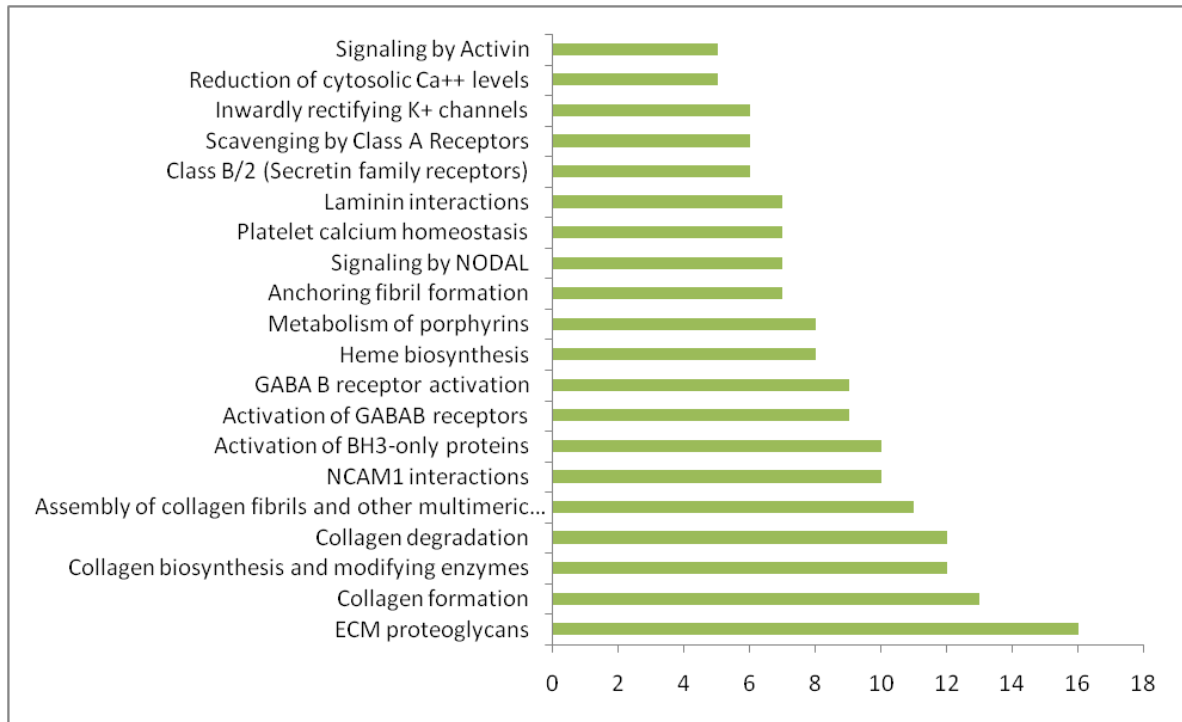
Fig.17. Bar Graph showing top 20 pathways influenced by the validated miRNA targets (p>0.05)

Further, wild-type control mice was compared with ISO-treated PPAR α-/- mice, wherein a total of 1274 unique mRNA targets for the 15 miRNA were retrieved.As shown in Fig. 3. Network interaction graph revealed mmu-mir-466i-5p,mmu-mir-24-3p,mmu-mir-709 and mmu-mir-3082-5p to be the most important hubs out of the 15miRNA and among these mmu-mir-466i-5p turned out to be the most important hub as it interacted with maximum number of nodes,and also had highest node degree as well as betweenness compared to other nodes.However, mmu-mir-3963, exhibited the lowest node degree.As shown in Table, genes that dominated the top mRNA target list were CD93,Itsn1,Trmt10a,Slc35e2 and Cdk7. Several significant pathways were identified (adjusted p < 0.05) that were influenced by the miRNA targets.The top significant pathways were primarily associated with NOD1/2 signalling pathway, Glycosphingolipid metabolism, and CASP 8 activity is inhibited.
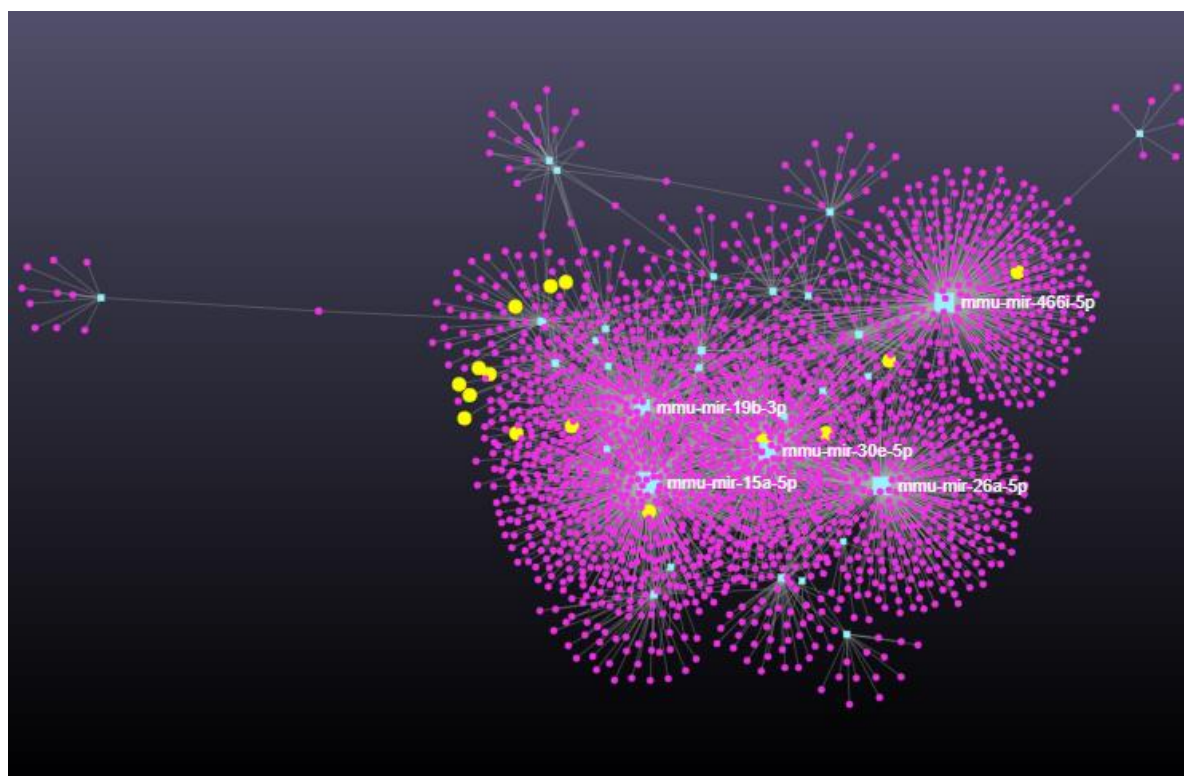
Fig.18. Figure depicting the miRNA-target interaction hub of wild-type control mice vs ISO-treated PPAR α-/- mice

Table 9: Top miRNAs and genes in the network interaction hub

Node	Degree	Betweenness
mmu-mir-466i-5p	418	427084.7
mmu-mir-24-3p	371	387717.6
mmu-mir-709	274	259451.9
mmu-mir-3082-5p	215	185349.3
mmu-mir-34a-5p	55	44893.99
mmu-mir-494-3p	34	35184.68
mmu-mir-574-5p	30	18505.83
mmu-mir-146a-5p	22	18393.84
mmu-mir-29c-3p	22	23182.07
mmu-mir-3473b	18	12329.69
mmu-mir-3968	13	10454.05
mmu-mir-1904	10	9079.624
mmu-mir-1224-5p	10	6723.893
mmu-mir-202-3p	9	10268

|		
mmu-mir-3963	7	6474.824
Cd93	5	17733.8
Itsn1	4	12069.86
Trmt10a	4	10839.68
Slc35e2	4	10839.68
Cdk7	3	15595.84
T2	3	3870.913
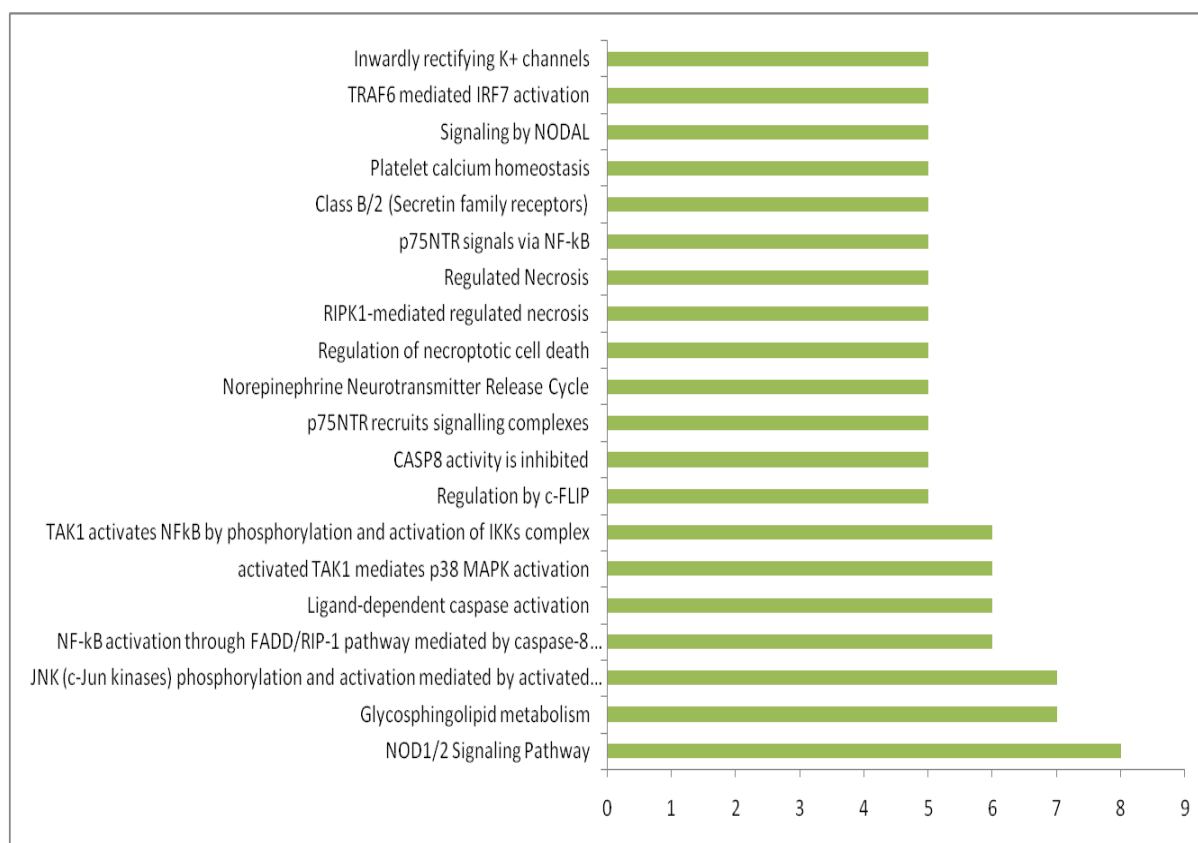
Fig.19. Bar Graph showing top 20 pathways influenced by the validated miRNA targets (p>0.05)

Next, the comparison was made between PPAR α-/- mice as well as ISO-treated PPAR α-/- mice.A total of 65 unique targets for the miRNAs were retrieved.As shown in Fig. , analysis of the network interaction graph showed that **mmu-mir-494-3p** and **mmu-mir-1224-5p** were the important hubs in the network out of the 2 miRNA and among these **mmu-mir-494-3p** was the most important hub as it interacted with maximum number of nodes, with the highest node degree and betweenness compared to other nodes.As shown in Table 2, the top mRNA target list was dominated by genes like Itsn1, Dpm1, Brat1 and Ephx3.Canonical pathway analysis (non-disease) was further performed to elucidate the biological relevance of the miRNA targets. Several significant pathways were identified (adjusted

p < 0.05) that were influenced by the miRNA targets.The top significant pathways were primarily associated with GPCR downstream signalling, metabolism, Metabolism of lipids and lipoprotein and glycogen breakdown.
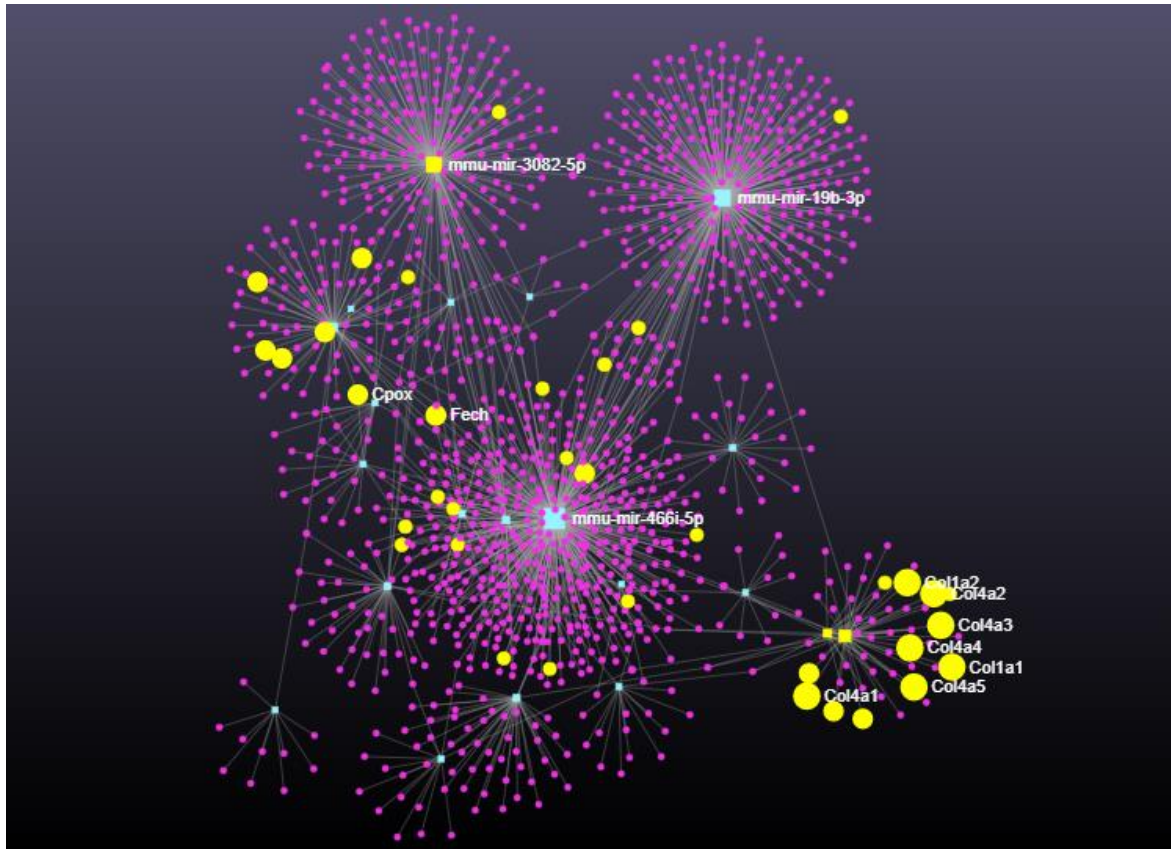

Fig.20. Figure depicting the miRNA- target interaction hub of PPAR α-/- mice vs ISO-treated PPAR α-/- mice

Table10: Top miRNAs and genes in the network interaction hub

Node	Degree	Betweenness
mmu-mir-494-3p	34	891
mmu-mir-1224-5p	10	351
Itsn1	2	340
Dpm1	1	0
Brat1	1	0
Ephx3	1	0
Pex13	1	0
Agl	1	0
Gmip	1	0
Magee2	1	0
Olig3	1	0
Mkrn3	1	0
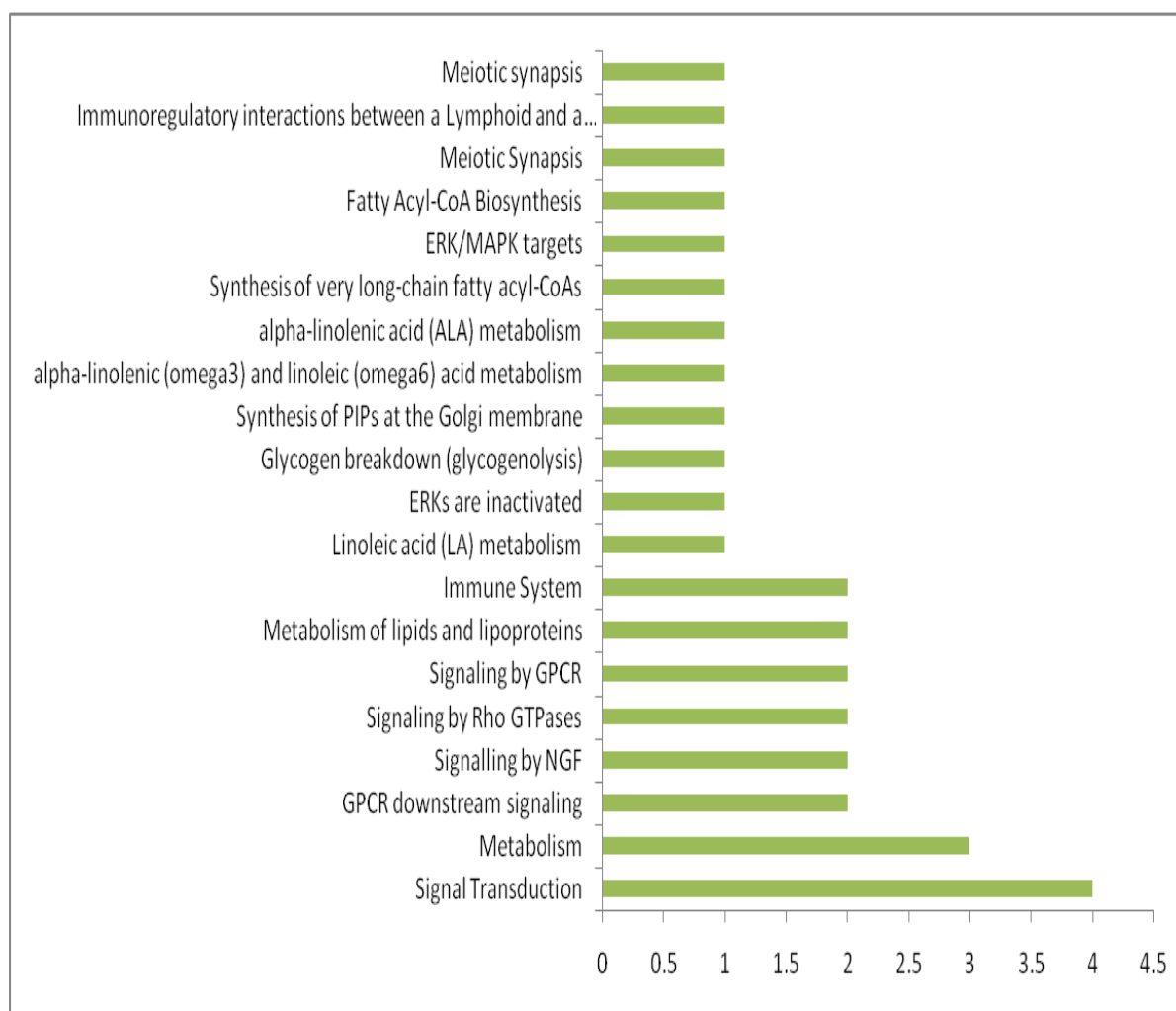
Fig.21.Bar Graph showing top 20 pathways influenced by the validated miRNA targets (p>0.05)

Next, the comparison was made between ISO-treated wild-type mice vs ISO-treated PPAR α-/- mice.A total of 1016 unique targets for the miRNAs were retrieved.As shown in Fig. , analysis of the network interaction graph showed that **mmu-mir-30e-5p, mmu-mir-709,mmu-mir-30a-5p,mmu-mir-132-3p** and **mmu-mir-3102-5p** were the important hubs in the network out of the 21 miRNA and among these **mmu-mir-146a-5p** was the most important hub as it interacted with maximum number of nodes, with the highest node degree and betweenness compared to other nodes.As shown in Table 2, the top mRNA target list was dominated by genes like Hdac4, Zfp26 and Sco1.Canonical pathway analysis (non-disease) was further performed to elucidate the biological relevance of the miRNA targets. Several significant pathways were identified (adjusted p < 0.05) that were influenced by the miRNA targets.The top significant pathways were primarily associated with Degradation of ECM, ECM proteoglycans, Collagen Biosynthesis and NF-kB is activated and signals survival.
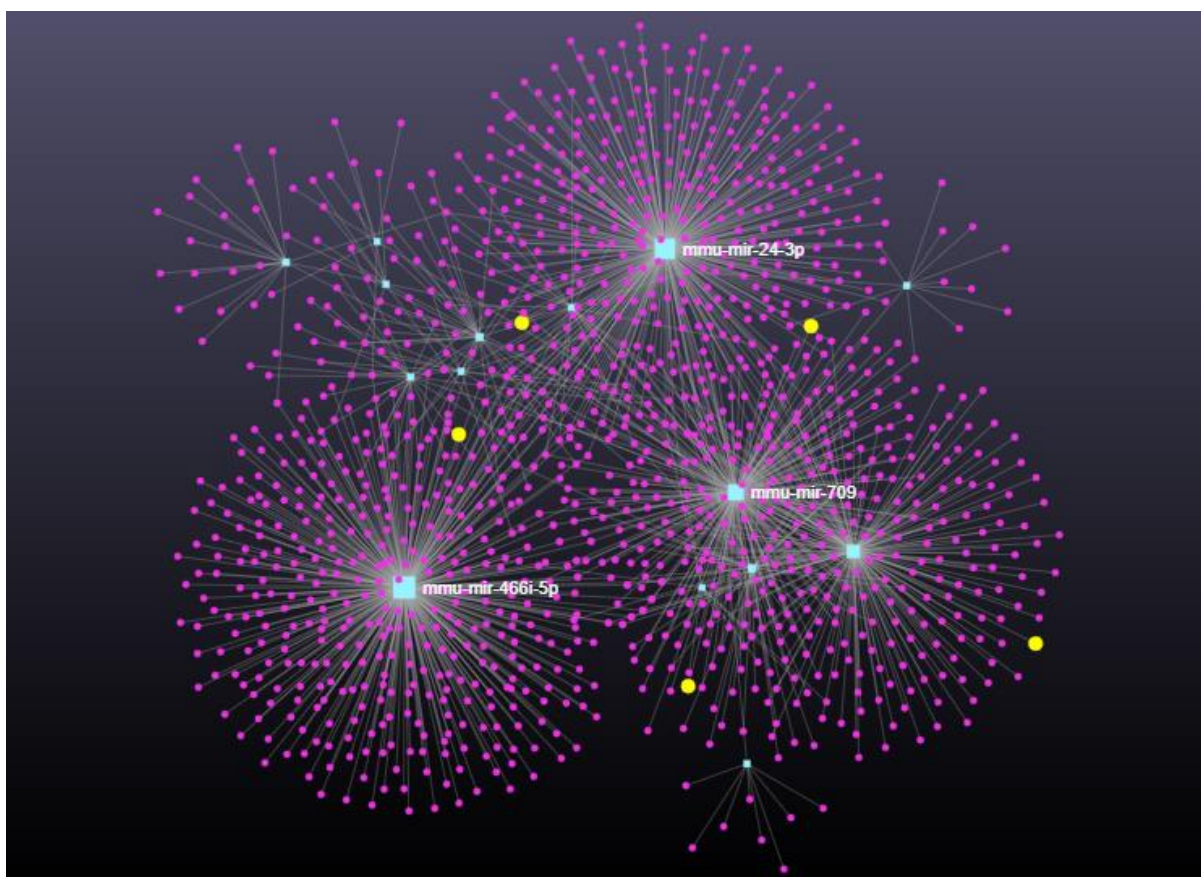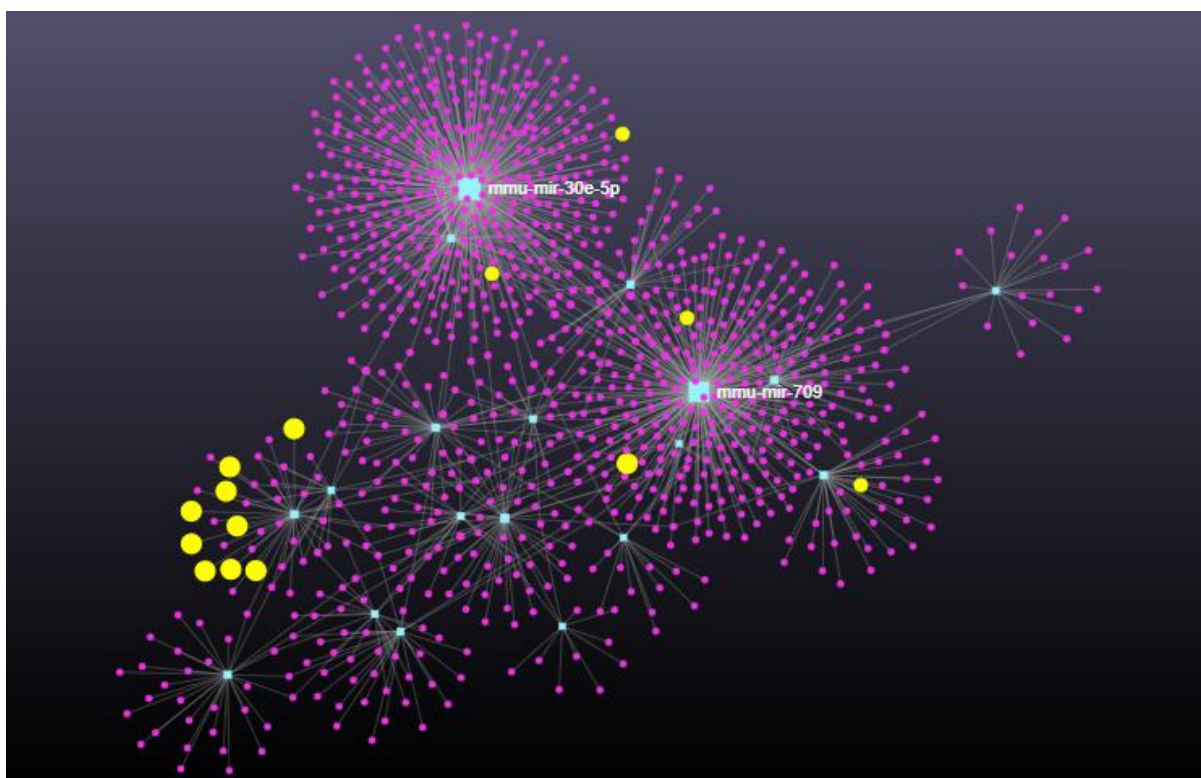
Fig.22. Figure depicting the miRNA- target interaction hub of ISO-treated wild-type mice vs ISO-treated PPAR α-/- mice

Table11: Top miRNAs and genes in the network interaction hub

| Node	Degree	Betweenness
mmu-mir-30e-5p	382	320819.9
mmu-mir-709	274	294862.1
mmu-mir-30a-5p	51	18667.08
mmu-mir-132-3p	47	50322.05
mmu-mir-3102-5p	47	37127.06
mmu-mir-1927	42	35677.35
mmu-mir-29a-3p	41	34983.87
mmu-mir-20a-5p	38	34037.33
mmu-mir-494-3p	34	32416.9
mmu-mir-195a-5p	33	30116.46
mmu-mir-22-3p	26	23205.85
mmu-mir-146a-5p	22	18264
Hdac4	4	4489.581
Zfp26	4	16422.14
Sco1	3	6923.307
Trp53rk	3	17892.05
Dpy19l1	3	17892.05
Wdr89	3	17892.05
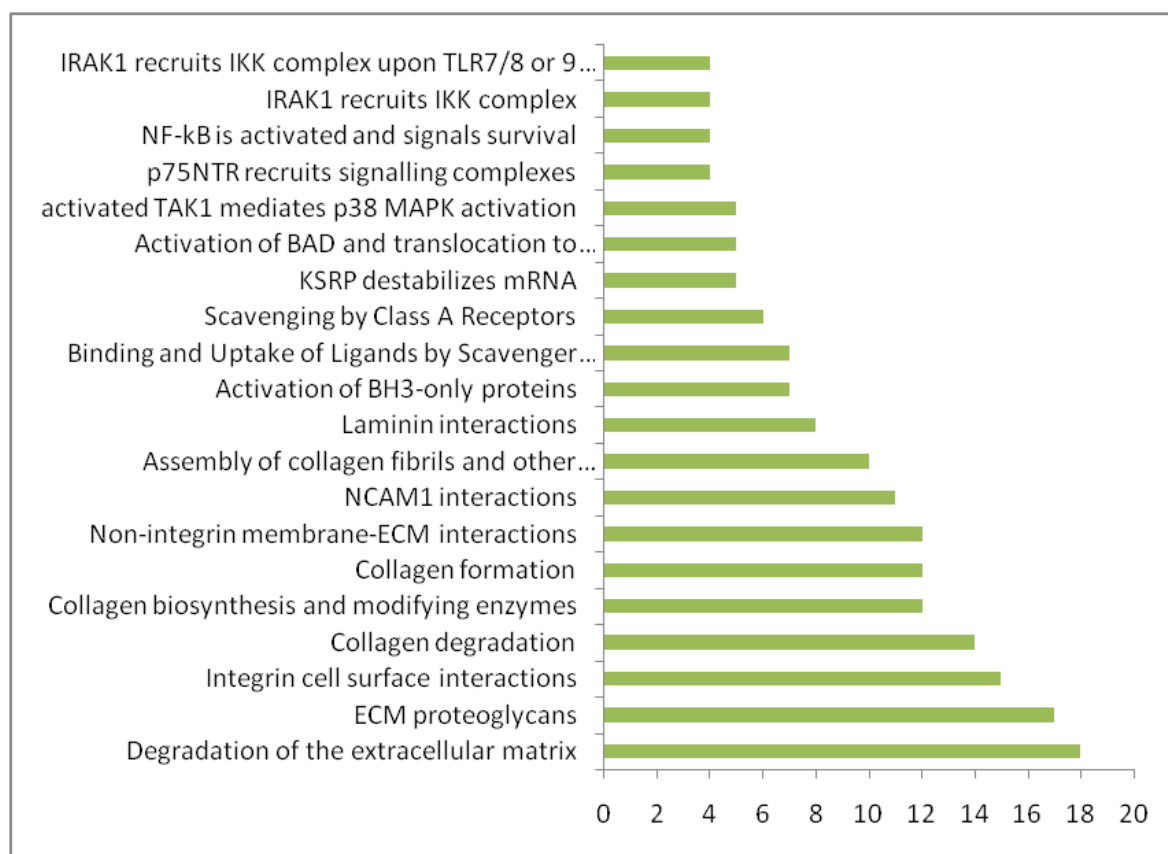
Fig.23.Bar Graph showing top 20 pathways influenced by the validated miRNA targets (p>0.05)

Next, the comparison was made between ISO-treated wild-type mice vs untreated PPAR α-/- mice.A total of 708 unique targets for the miRNAs were retrieved.As shown in Fig. , analysis of the network interaction graph showed that **mmu-mir-466i-5p, mmu-mir-30a-5p,mmu-mir-30a-5p,mmu-mir-30c-5p and mmu-mir-132-3p** were the important hubs in the network out of the 17 miRNA and among these **mmu-mir-126a-3p** was the most important hub as it interacted with maximum number of nodes, with the highest node degree and betweenness compared to other nodes.As shown in Table 2, the top mRNA target list was dominated by genes like Hdac4,Runx1,Six4 and Mdm2.Canonical pathway analysis (non-disease) was further performed to elucidate the biological relevance of the miRNA targets. Several significant pathways were identified (adjusted $p < 0.05$) that were influenced by the miRNA targets.The top significant pathways were primarily associated with ECM proteoglycans, Assembly of collagen fibrils, collagen formation, Laminin interaction and Integrin cell surface interactions.
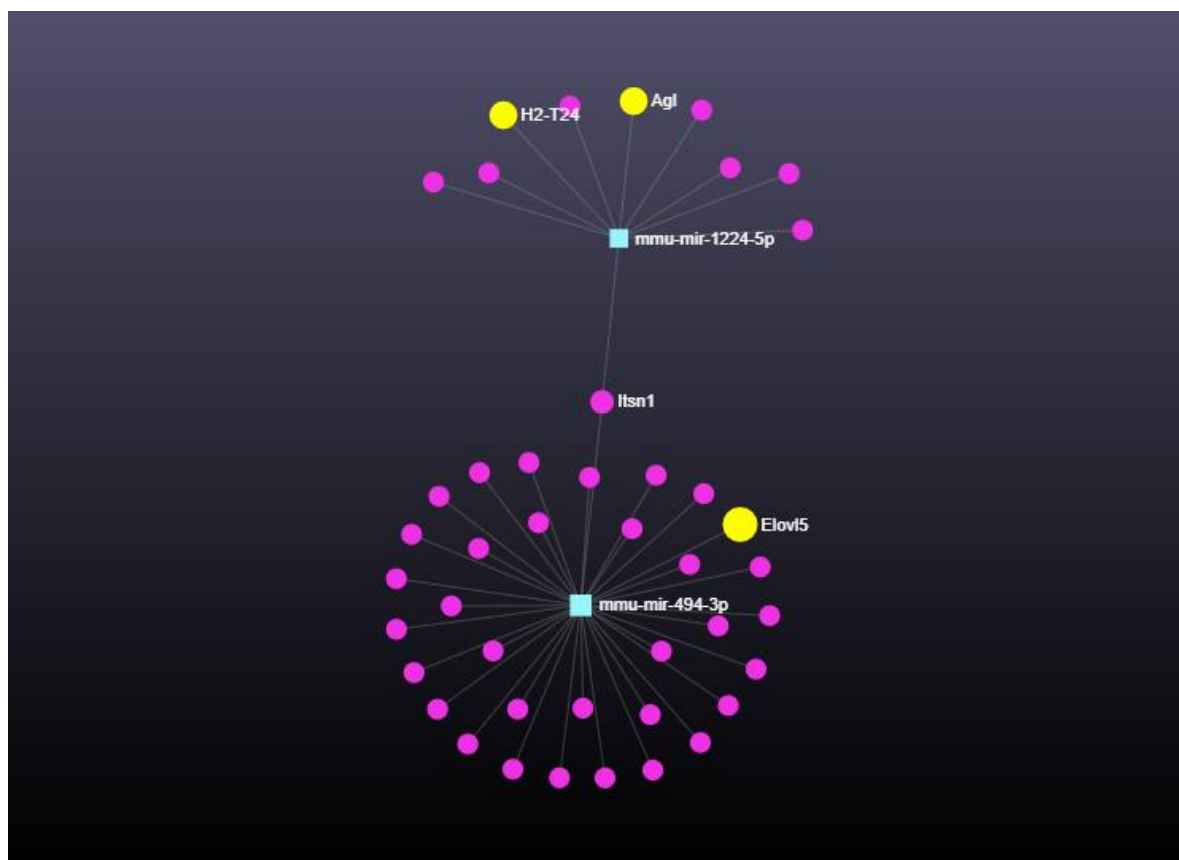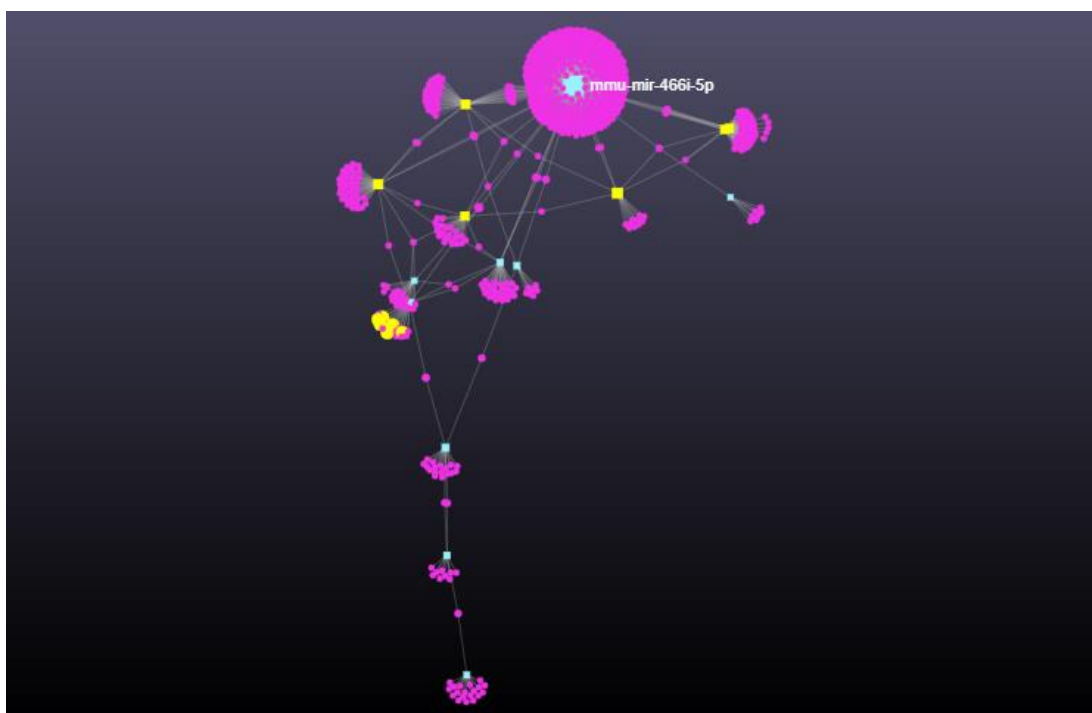
Fig.24. Figure depicting the miRNA- target interaction hub of untreated PPAR α-/- mice vs ISO-treated PPAR α-/- mice

Table12: Top miRNAs and genes in the network interaction hub

Node	Degree	Betweenness
mmu-mir-466i-5p	418	225710.2
mmu-mir-30a-5p	51	16135.3
mmu-mir-30c-5p	47	16208.13
mmu-mir-132-3p	47	29122.06
mmu-mir-3102-5p	47	22958.53
mmu-mir-29a-3p	41	38391.57
mmu-mir-195a-5p	33	19943.37
mmu-mir-22-3p	26	15805.75
mmu-mir-29c-3p	22	7171.818
mmu-let-7e-5p	21	34213.28
mmu-mir-378a-3p	20	13414
mmu-mir-199a-3p	16	8125.633
mmu-mir-378b	12	20805.5
mmu-mir-5126	10	19684.83
mmu-mir-126a-3p	8	4984
Hdac4	4	5460.918
Runx1	4	11122.52
Il18r1	3	6991.639
Six4	3	6991.639
Gm14137	3	33573.07
Mdm2	3	6991.639
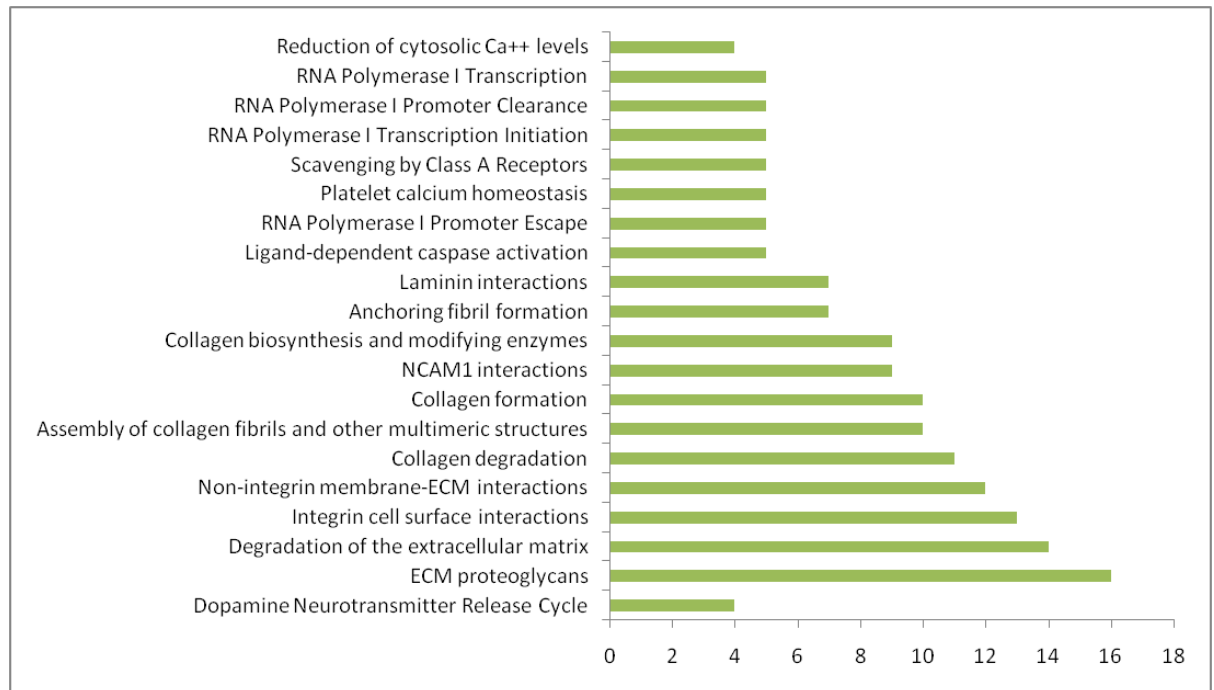
Fig.25.Bar Graph showing top 20 pathways influenced by the validated miRNA targets (p>0.05)

Validation of microarray data by RT-PCR
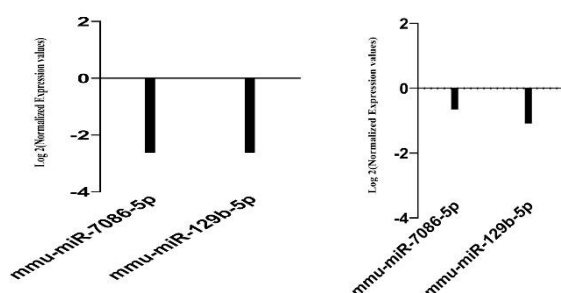
Fig.26. Validation of miRNAs identified in ISO-treated wild-type mice compared to control group using RT-PCR: Custom Panel for miRNA RT-PCR Arrays designed for the samples were used according to the manufacturer's instructions. miRNA quality and quantity were determined and was reverse transcribed using miRCURY LNA-RT kit. The Ct cut-off was set to 37.

RT-PCR was used to validate the data and a subset of miRNAs were validated in the different experimental groups. ISO-treated wild-type mice was compared with untreated wild-type control and miRNA-7086-5p was found to be downregulated (fold) resembling the data obtained using microarray. Similarly, another miRNA-129b-5p was also downregulated in ISO-treated wild-type mice (Fig.26.).

Similar subset of miRNAs was validated in control vs untreated PPAR α-/- mice, where RT-PCR data revealed downregulation of miRNA-7086-5p and miRNA-129b-5p, along with that downregulation of other miRNAs like miRNA-7218-5p, miRNA-6904-5p, miRNA-7028-5p and upregulation of 34a-5p was observed. RT-PCR data resembled the data obtained from microarray (Fig.27.).
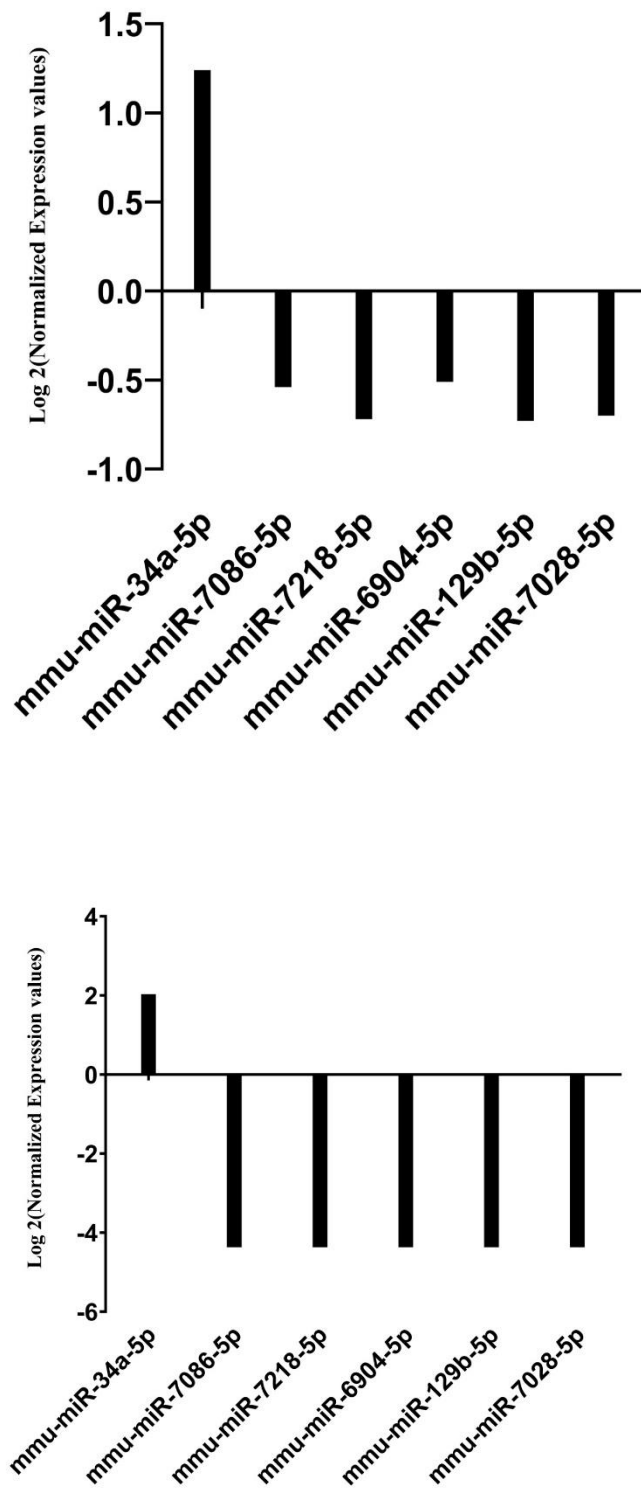
Fig.27. Validation of miRNAs identified in untreated PPAR α⁻/⁻ mice compared to control group: Custom Panel for miRNA RT-PCR Arrays designed for the samples were used according to the manufacturer's instructions. miRNA quality and quantity were determined and was reverse transcribed using miRCURY LNA-RT kit. The Ct cut-off was set to 37.
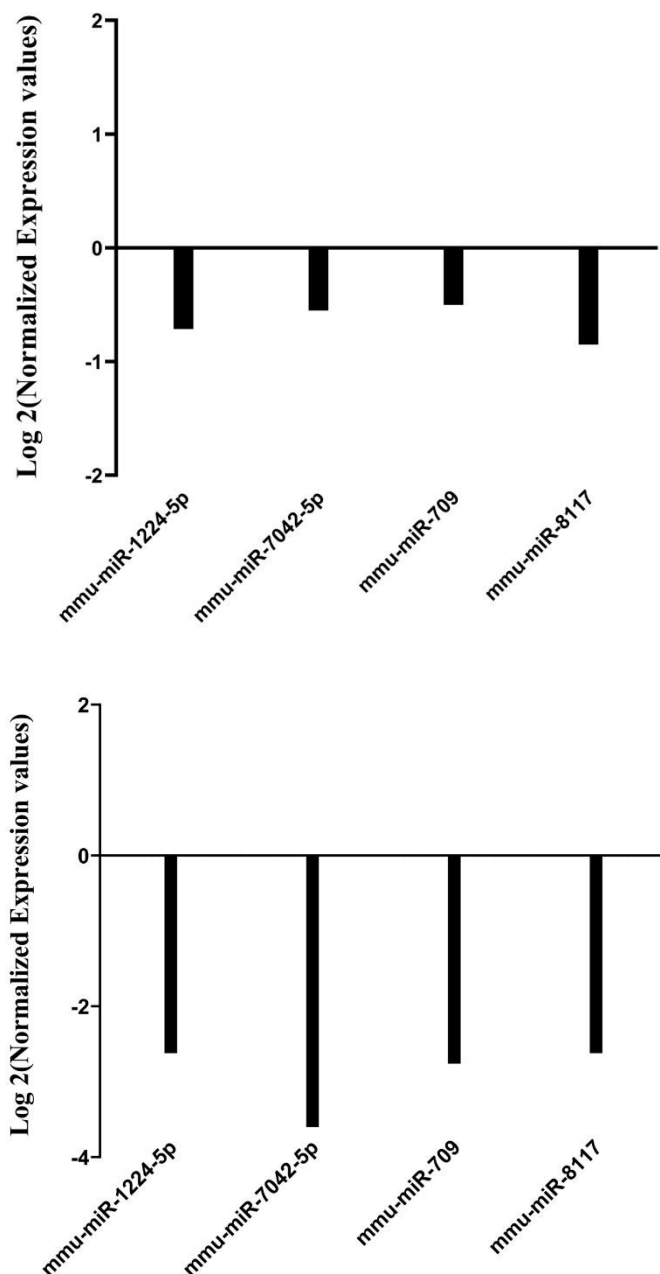
Fig.28. Validation of miRNAs identified in ISO-treated PPAR $\alpha^{-/-}$ mice compared to control group: Custom Panel for miRNA RT-PCR Arrays designed for the samples were used according to the manufacturer's instructions. miRNA quality and quantity were determined and was reverse transcribed using miRCURY LNA-RT kit. The Ct cut-off was set to 37.

Previous subset of miRNAs showed no significant change in ISO-treated PPAR $\alpha^{-/-}$ mice (Fig.28.). A new subset of miRNA showed differential expression in this experimental group when compared to wild-type control. In ISO-treated wild-type mice miRNA-1224-5p, miRNA-7042-5p, miRNA-709 and miRNA-8117 were significantly downregulated and this RT-PCR data clearly resembled the microarray data as similar downregulation of these miRNAs was observed in both the cases.

Conclusion

PPARα plays a critical role in the regulation of genes which are extensively altered in cardiac hypertrophy. The mechanism regarding most of the miRNAs and their functional relevance in Isoproterenol-induced cardiac hypertrophy in context to PPAR-α, remains poorly understood. In this study, we have employed high-throughput miRNA microarray technology to identify differentially expressed miRNAs in isoproterenol-induced cardiac hypertrophy in PPAR $\alpha^{-/-}$ mice when compared to untreated PPAR $\alpha^{-/-}$ mice and to elucidate the functional relevance of their mRNA targets. So far, no previous studies have reported miRNA expression levels in the heart of cardiac hypertrophy induced PPAR $\alpha^{-/-}$mice. Our results revealed expression of several miRNAs that are abundantly expressed in cardiac hypertrophy. Comparisons were made between untreated wild-type mice, isoproterenol-treated wild-type mice, PPAR $\alpha^{-/-}$ mice and isoproterenol-treated PPAR $\alpha^{-/-}$ mice. Around 34 miRNAs were under expressed in Isoproterenol-treated wild-type mice when compared to untreated wild-type mice and around 20 miRNAs were overexpressed. In case of PPAR $\alpha^{-/-}$ mice, around 30 miRNAs were under expressed in comparison to untreated wild-type mice whereas around 15 were overexpressed. In ISO-treated PPAR $\alpha^{-/-}$ mice, around 12 miRNAs were under expressed and 11 miRNAs were over expressed in comparison to untreated wild-type control. Untreated PPAR $\alpha^{-/-}$ mice showed around 12 distinct under expressed miRNAs as well as 10 over expressed miRNAs in comparison to ISO-treated wild-type mice. Further comparison between ISO-treated wild-type mice and ISO-treated PPAR $\alpha^{-/-}$ mice revealed 18 under expressed and 15 over expressed miRNAs whereas comparison between untreated PPAR $\alpha^{-/-}$ mice and ISO-treated PPAR $\alpha^{-/-}$ mice revealed only a small subset of genes getting distinctly expressed (Fig 7). Signalling pathways that were enriched because of distinct expression of these miRNAs in ISO-treated wild-type mice. Sparse literature is available on dysregulated miRNAs in cardiac hypertrophy that have stated around 15 miRNAs that are pro-hypertrophic and around 13 miRNAs that are anti-hypertrophic. Few reports have also addressed the upregulation of around 11miRNAs that are hypertrophic and downregulation of around 5 miRNAs that are mostly anti-hypertrophic as established previously. Consistent with the previous studies, we did find upregulation of various pro-hypertrophic genes in our experimental models like miR-132-3p, miR-199a, and miR-195a-5p in cardiac-hypertrophy induced models. Surprisingly, a set of unreported miRNAs were observed in our study that were differentially expressed. MiRNA Enrichment Analysis Tool (miEAA) revealed pathways that were enriched in different experimental groups. Apoptotic mitochondrial changes were enhanced along with positive regulation of cardiac muscle hypertrophy in response to stress in ISO-treated wild-type mice. Comparison between wild-type control and untreated PPAR $\alpha^{-/-}$ mice revealed enrichment of pathways involved in protein acetylation, histone deacetylation and regulation of cholesterol biosynthetic process. Surprisingly comparison between ISO-treated wild-type mice with untreated PPAR $\alpha^{-/-}$ mice revealed negative regulation of intrinsic apoptotic signalling pathway by p53 class mediator was one of the top 20 enriched signalling pathways. Thus, suggesting a sub set of miRNAs are controlling this pathway resulting in downregulation of apoptosis. Identification of miRNA targets using miRNet algorithm revealed top miRNAs targeting genes involved in collagen biosynthesis. Interestingly, analysis of ISO-treated PPAR $\alpha^{-/-}$ mice revealed mRNA targets like CD93, along with Caspase 8 activity inhibition as one of the top pathways

Downregulation of miRNA-1224-5p, miRNA-7042-5p, miRNA-709 and miRNA-8117 between the wild-type control and ISO-treated PPAR $\alpha^{-/-}$ mice tissue samples and was unique to this group (Fig. 3B). The results were subsequently validated with RT-qPCR and it showed striking resemblance with microarray data (Fig. 4C).

In conclusion, we have identified and unveiled the functional relevance of differentially expressed miRNAs in ISO-treated PPAR $\alpha^{-/-}$ mice. As of now, limited literature was available about miRNA abundance and their altered expression in cardiac hypertrophy models in the absence of PPAR α protein. So for the very first time, using PPAR $\alpha^{-/-}$ mice, we showed that several miRNAs are differentially expressed that have never been reported in context to cardiac hypertrophy. Additionally, pathway analysis, indicated that the dysregulated miRNAs target genes were enriched mostly in signal transduction pathways. Overall, our findings suggest the miRNAs expression profile of miRNAs like mmu-miR-3102-5p; mmu-miR-30a-5p; mmu-miR-30c-5p; mmu-miR-466i-5p is significantly altered in response to cardiac hypertrophy in PPAR$^{-/-}$ mice that eventually impacts the apoptotic pathway in a negative manner.

DISCUSSION

Cardiomyocytes undergo specific adaptive modifications to meet up with the increased energy demand in response to any hypertrophic stimuli (*Vega et al. 2017; Schirone et al. 2017*). Here we show that PPAR α plays a critical role in the adaptive phase of the cardiomyocytes by drifting the cardiomyocytes towards autophagy and preventing apoptosis. We studied this switching mechanism in the cardiac cells for which, isoproterenol was used to induce cardiac hypertrophy in PPAR α$^{-/-}$ mice model.

Intra – peritoneal injection of isoproterenol for duration of 2 weeks led to the development of hypertrophied hearts in the PPAR α$^{-/-}$ mice as was clearly evident from HW/BW ratio and the HW/TL ratio (*George et al. 2010*). Cardiac hypertrophy in ISO-treated wild-type mice as well as ISO-treated PPAR α$^{-/-}$ mice was significantly prominent as compared to the control (untreated wild type). Increased expression of hypertrophic marker genes such as ANP and BNP further validated the development of cardiac hypertrophy in the experimental groups. Histopathological study revealed enhanced collagen deposition thereby suggesting extensive fibrosis in the absence of PPAR α which is one of the major hallmarks of cardiac remodelling.

Consistent with hypertrophic pathophysiology data obtained so far, the PPAR α$^{-/-}$ mice exhibited significant cardiac dysfunction that was more pronounced in the presence of isoproterenol. Significant reduction in Ejection fraction and Fractional shortening was observed in both the isoproterenol-treated groups. Even in the absence of isoproterenol, these cardiac function parameters were compromised in PPAR α$^{-/-}$ mice suggesting that the absence of PPAR α is sufficient to cause cardiac dysfunction (*Ichihara et al. 2006*). Evidently, cardiac output was markedly declined in all the groups when compared to wild-type control further confirming the impaired heart function. Development of cardiac hypertrophy in the mice model was further confirmed by the increase in LV mass.

Protein profiling data obtained from the mass spectrometric analysis of the heart tissue revealed the proteins that, in absence of PPAR α, are closely associated with cardiac stress. Majority of the proteins were involved in mitochondrial dysfunction and impaired fatty acid β-oxidation pathway such as mitochondrial fusion protein like Opa1, fission protein FIS1 that were quite enhanced while critical genes involved in the Fatty acid β-oxidation like FABP7 – a fatty acid binding protein, ACAA1A and ACOX1 exhibited significant reduction, thereby reflecting the impact of absence of PPAR α function in distinct signalling pathways (*Leone et al.1999; Rakhshandehroo et al 2009*).

One of the striking observations was the decrease in apoptotic pathway as ISO-induced cardiac hypertrophy has been related with elevated stress; the results in our study indicated an abrupt decrease in p53-induced apoptotic pathway in the absence of PPAR α.

As stress gets aggravated in the presence of Isoproterenol-treatment, that is likely to trigger apoptosis, we examined genes associated with apoptosis. Proteome profiler Antibody Array that was used to assess multiple genes regulating apoptosis revealed several anti-apoptotic genes like Bcl-x, Bcl-2, HO-1 were either up regulated or showed no change in PPAR α$^{-/-}$ mice and isoproterenol-treated PPAR α$^{-/-}$ mice, that suggests inclination towards cell survival. On the contrary, pro apoptotic genes like Caspase 3, Claspin, Bad, Cytochrome C, FAS/CD95, p53,

Mcl-1, Smac/Diablo, p27/kip1, TRAIL R2/TNFRSF10B, TNFR1/TNFRSF1A exhibited noticeable decline in the PPAR $\alpha^{-/-}$ as well as isoproterenol treated PPAR $\alpha^{-/-}$ mice when compared to normal wild-type mice. However, ISO-treated wild-type mice showed expected upsurge in apoptotic markers as an inclination towards cardiomyocyte cell death is eventually the outcome of induced stress due to cardiac hypertrophy. Therefore, the absence of PPARα can be suggestive of this deviation from apoptotic pathway.

To understand further, another experimental model was used, that is, high-cholesterol diet fed PPAR $\alpha^{-/-}$ mice model to ensure that this phenomenon is solely dependent on PPAR α. Pathological cardiac hypertrophy was implicated in high-cholesterol diet fed PPAR $\alpha^{-/-}$ mice model independent of isoproterenol treatment. Involvement of high cholesterol diet in inducing pathological cardiac hypertrophy has already been reported previously but the study has been mostly limited to wild-type mice and its influence on PPAR $\alpha^{-/-}$ mice has not been explored yet. In our study, High-cholesterol diet fed PPAR $\alpha^{-/-}$ mice developed cardiac hypertrophy as was established by the increase in hypertrophic markers like ANP and BNP apart from these, the Masson Trichome staining revealed significant accumulation of collagen in both PPAR $\alpha^{-/-}$ mice as well as HCD fed PPAR $\alpha^{-/-}$ mice.

Western Blot analysis of apoptotic markers in both the experimental models revealed a significant reduction in cleaved caspase-9 in cardiac hypertrophy-induced PPAR $\alpha^{-/-}$ mice whereas no significant change was observed in c-PARP protein level. Down regulation of cleaved caspase-9 implies possible interference in the basic apoptotic signalling pathway resulting from the absence of PPAR α as both the cardiac hypertrophy models exhibit similar results. Further analysis of the apoptosis mediators using Panther based classifications unleashed a surprising decline in p53 pathway in the absence of PPAR α. The recent development in the study of p53 has established the binding potential of p53 to PPAR α (*Rana et al. 2019*). Surprisingly, both normal and hypertrophied PPAR $\alpha^{-/-}$ mice exhibited noticeable downregulation of p53 in contrast to the up-regulation in WT mice (ISO-treated as well as control). To further confirm a direct association of p53 with PPAR α, expression profile of Dbc1 and Mdm2 was examined as previous studies have already reported the role of Dbc1 in p53 stabilization as well as Mdm2, a negative regulator of p53 stability (*Moll UM, and Petrenko O, 2003; Qin et al. 2015*). Therefore, it can be suggested that p53 downregulation might be an outcome of the decrease in Dbc1 expression and an elevation in Mdm2 expression. As expected, Dbc1 expression was indeed found to be reduced in PPAR $\alpha^{-/-}$ mice along with p53 decrease, in contrast, to an upsurge in Mdm2 expression. Thus, absence of PPAR α protein could be suggested to hinder p53-mediated apoptotic response. Both the cardiac-hypertrophy induced PPAR $\alpha^{-/-}$mice model exhibited similar pattern of down regulation of the apoptotic markers thereby suggesting the involvement of PPAR α.

The role of PPAR α in the down regulation of apoptosis was investigated in the cardiomyocytes by dissecting the PTEN/pAkt/mTOR pathway to further understand the underlying mechanism. Previous reports have suggested the critical role of PTEN in modulating apoptosis, along with that many studies have also addressed the PPAR α dependent transcriptional regulation of PTEN (*Kitagishi Y and Matsuda S, 2013*). Downregulation of PTEN was observed in PPAR α

[^-/-] mice both in response to isoproterenol as well as HCD thereby suggesting an important role of PPAR α in contributing to the down regulation of PTEN.

Surprisingly, autophagy markers like Beclin1 and LC3 A/B exhibited significant up regulation in the absence of PPAR α. Since mTOR negatively regulates autophagy, so mTOR-independent pathway, as may be conceived maintains an increase in the autophagy markers. To further understand the mechanism of mTOR-independent pathway, the protein level of Calpain-1 that is a renowned mTOR independent modulator of autophagy was examined. Western Blot analysis revealed significant reduction in Calpain-1 in the absence of PPAR α that explains the increase in autophagy even when mTOR protein exhibits an upsurge. Both isoproterenol-treated as well as HCD-fed PPAR α [^-/-] mice model showed significant increase in Autophagy genes like Atg3, Atg 5, Atg7 and Atg12.The data therefore explains, although the phenomenon is PPAR α dependent but is exhibited mostly in the presence of a hypertrophic signal.

Further experiments were carried out in H9C2 cell line to validate this downregulation of apoptosis followed by an increase in autophagy in cardiomyocytes in the absence of PPAR α. Western blot analysis of PTEN resembled the same pattern as observed in vitro thereby indicating PPAR α dependent mechanism. Autophagy marker Beclin1 was significantly increased in PE-treated H9C2 cell line in the absence of PPAR α whereas apoptotic marker cPARP showed no noticeable change. Autophagosome assay was performed in H9C2 cell line that further validated the increase in autophagy. Serum starved cardiomyocytes were used as positive control for autophagy and were compared with PE treated as well as GW6471 incubated cell. Autophagosome formation was significantly elevated in the presence of GW6471 when compared to PE treated cells, indicating similar increase in autophagy as observed *in vivo* in the absence of PPAR α. Cholesterol incubated H9C2 cell line in the presence of GW6471 exhibited prominent increase in autophagy when compared to cells incubated with cholesterol alone, thereby suggesting that the absence of PPAR α might function as a pre-requisite to mediate such an unexpected shift in signalling pathway.

Consistent with the observed data of down regulation of apoptosis, it could be suggested that to maintain cardiac homeostasis the autophagic flux might play a compensatory role in stress-induced cardiomyocytes.

In this study although hemodynamics was significantly compromised in hypertrophied mice but at the cellular level the cardiomyocyte pertains to cope with the stimuli by inhibiting apoptosis and surviving through the stress by entering an adaptive stage, where a compensatory phase is maintained and development to heart failure is prevented. Impaired cardiac function in PPAR α [^-/-] also supports the previous reports that the absence of PPAR α results in cardiac dysfunction but its absence is likely to help the cardiomyocytes to prevent programmed cell death and thereby may avoid cardiomyocytes drop.

The absence of PPAR α is known to be associated with various pathophysiological changes that includes cardiac remodelling and hypertrophy, however, in the presence of hypertrophy inducing signal, PPAR α tends to promote apoptosis that ultimately results in cardiomyocyte death, whereas its absence leads to a shift towards autophagy rather than apoptosis even in the

presence of hypertrophic signals. Such an adaptive signalling shift as evident from increase in autophagy markers possibly could explain the importance of the compensatory mechanism that operates in the cardiomyocytes in order to sustain through the myocardial stress.

With the emerging role of miRNA in regulating various gene expression and thereby regulating cardiac gene remodelling, miRNA microarray analysis gave a clearer picture of alteration in various genes regulating signalling pathways in cardiac hypertrophy. Around 54 miRNAs were differentially expressed in ISO-treated wild-type mice when compared to wild-type control most of which comprised of already reported miRNAs like miR-132-3p, miR-22-3p and various unreported novel miRNAs like miR-1927.Differentially expressed miRNA in PPAR $\alpha^{-/-}$ mice mostly constituted of unreported miRNAs like miR-7028,miR-6401,miR-7682-3p.Similarly, miRNAs observed in ISO-treated PPAR $\alpha^{-/-}$ mice comprised of mostly unreported novel miRNAs like miR-8117,miR-3473g. Impact of miRNAs on signalling pathways revealed enhanced apoptotic mitochondrial changes in ISO-treated wild-type mice when compared to wild-type control. MiRNAs like miR-132-3p regulated the cellular response to glucose stimulus. A subset of miRNAs like miR-30e-5p, miR-451a regulated the cardiac muscle hypertrophy in response to stress, therefore indicating that stress-induced cardiomyocytes exhibit an inclination towards hypertrophy as well as metabolic switch towards glycolysis. Comparison between untreated PPAR $\alpha^{-/-}$ mice and wild-type control revealed most of the enriched signalling pathways were comprised of cholesterol biosynthetic process regulation, regulation of fatty acid, protein deacetylation and cellular response to glucose stimulus thereby indicating response to fatty acid accumulation in the absence of PPAR α transcription factor. Similarly, most of the top enriched signalling pathways in ISO-treated PPAR $\alpha^{-/-}$ mice consisted of cell adhesion regulation involved in heart morphogenesis, positive regulation of smooth muscle migration and positive regulation of cardiac muscle cell proliferation. Further comparison between untreated PPAR $\alpha^{-/-}$ mice and ISO-treated wild-type mice revealed enrichment of pathways regulated by miRNAs like negative regulation of intrinsic apoptotic signalling pathway by p53 class mediator. MiRNAs regulating this pathway were mmu-miR-3102-5p; mmu-miR-30a-5p; mmu-miR-30c-5p; mmu-miR-466i-5p and have not been reported in context to PPAR $\alpha^{-/-}$ mice. Similarly, comparison between ISO-treated wild-type mice and ISO-treated PPAR$\alpha^{-/-}$ mice exhibited enrichment of negative regulation of intrinsic apoptotic signalling pathway as well as negative regulation of cell death and negative regulation of smooth muscle cell apoptotic process thereby suggesting a significant decline in apoptotic pathway that resembled the data obtained in Chapter 1 and reported in *Kumari et al*.2022.Comparison between untreated PPAR $\alpha^{-/-}$ mice and ISO-treated PPAR $\alpha^{-/-}$ mice exhibited enrichment of positive regulation of caveolin-mediated endocytosis, post-synaptic actin cytoskeleton and polyubiquitin modification-dependent protein binding.

Identification of mRNA targets regulated by differentially expressed miRNA revealed top targets like Ncan,Hdac4 and Bcl2 that constituted top miRNA-target interaction hub in ISO-treated wild-type mice.Top pathways regulated by these mRNA targets included collagen formation, collagen degradation and collagen biosynthesis as well as modifying enzymes.Similarly, in PPAR $\alpha^{-/-}$ mice top miRNA-target interaction hub comprised of miRNA-466i-5p affecting mostly the mRNA targets like Col1a,Col4a1 and Col4a2.Collagen

biosynthesis was one of the top signalling pathway followed by reduction of cytosolic Ca++ levels and signalling by Nodal. Thereby indicating significant collagen deposition in the absence of PPARα, suggestive of switch towards pathological state resembling hypertrophy-induced cardiomyocyte response. ISO-treated PPAR α$^{-/-}$ mice exhibited 3 major miRNA nodes comprising of miR-466i-5p, miR-24-3p and miR-709 that targeted mRNAs like Slc35e2, Cdk7 and T2. Consistent with the previous results obtained in case of ISO-treated PPAR α$^{-/-}$ mice, top pathways affected form miRNA-target interaction hub included Casp8 activity inhibition, regulation of necroptotic cell death and glycosphingolipid metabolism. Comparison between untreated PPAR α$^{-/-}$ mice and ISO-treated PPAR α$^{-/-}$ mice exhibited 2 major miRNA-target hub comprising of miR-494-3p and miR-1224-5p. Signalling pathways getting influenced mostly included glycogen breakdown pathway showing an inclination towards usage of glucose as an energy source. Comparison of ISO-treated wild-type mice with untreated PPAR α$^{-/-}$ mice and ISO-treated PPAR α$^{-/-}$ mice comprised of most of the miRNA-mRNA target interaction hub affecting the degradation of Extracellular Matrix, ECM proteoglycans and collagen biosynthesis and non-Integrin membrane-ECM interaction.

Validation of a subset of miRNAs based on the differential expression in the experimental groups revealed RT-PCR data resembling the miRNA microarray data. MiRNAs like miR - 7086-5p and miR-129b-5p were significantly downregulated in ISO-treated wild-type mice similar to microarray data. Protective effects of miRNA-129b-5p have recently been reported wherein overexpression of miR-129-5p activates Nrf2 pathway and alleviates the effects of hypertrophy, in ISO-induced cardiac hypertrophy downregulation of miR-129-5p indicates a shift towards pathological state (*Ye H et al. 2021*). On the contrary, miR-7086 has not yet been reported in context to cardiac hypertrophy. Down regulation of miRNAs like miRNA-7218-5p, miRNA-6904-5p, miRNA-7028-5p miRNA-7086-5p as well as miRNA-129b-5p and upregulation of 34a-5p observed in the RT-PCR data of untreated PPAR α$^{-/-}$ mice in comparison to wild-type control. Role of 34a-5p has already been reported in context to cardiac hypertrophy wherein inhibition of miR-34a proves to be promising strategy in order to treat cardiac pathology (*Bernardo BC et al, 2014*). MiR-34a has emerged as one of the molecular markers and its upregulation indicates pathological cardiac remodelling in PPAR α$^{-/-}$ mice (*Zhu L et al., 2019*). Most of the downregulated miRNAs like miRNA-6904-5p, miRNA-7028-5p have not yet been reported in context to cardiac hypertrophy. Validation of miRNA-1224-5p, miRNA-7042-5p, miRNA-709 and miRNA-8117 in ISO-treated PPAR α$^{-/-}$ mice exhibited similar downregulation as observed in miRNA microarray data, out of which only miRNA-1224-5p has been reported in context cardiac hypertrophy whereas miRNA-7042-5p, miRNA-709 and miRNA-8117 have been reported for the first time in ISO-treated PPAR α$^{-/-}$ mice.

As established in Chapter1, absence of PPAR α has been associated with the inhibition of apoptosis as revealed by downregulation of various apoptotic factors including PTEN and increase in autophagy markers (*Kumari et al, 2022*). Cardiomyocytes thereby enters a compensatory phase with sustained baseline autophagy to prevent cell death and heart failure. Microarray profiling of miRNA reveals another regulatory hub that gives insights into the miRNA-mRNA interplay in the absence of PPAR α.Consistent with the proteomics data obtained from the ISO-treated PPARα $^{-/-}$ mice that revealed inhibition of various apoptotic

signalling pathway, miRNA microarray data exhibited negative regulation of apoptotic pathway via various miRNAs like mmu-miR-3102-5p; mmu-miR-30a-5p; mmu-miR-30c-5p; mmu-miR-466i-5p. Detailed exploration of the miRNA network revealed resemblance with the proteomics data. The microarray data along with the previous data that included decline in apoptotic pathway provides new insights into the cardiac remodelling in the absence of PPAR α.

In summary, although PPAR α plays a significant role in the regulation of fatty acid β oxidation genes in cardiomyocytes but its absence results in alteration of transcriptional as well as proteomic profile of the heart that encompasses the apoptotic signalling. Inhibition of apoptosis in the absence of PPAR α is also under the control of several miRNAs identified in our study that negatively regulate apoptosis. Involvement of miRNA thereby reveals the miRNA-mRNA network that persists in this complex regulation. Several miRNAs exhibiting differential expression have been reported for the very first time in our study in hypertrophy-induced PPAR $\alpha^{-/-}$ mice and these miRNAs could be targeted to reverse the diseased hypertrophic state thereby contributing to the development of therapeutic approaches.

REFERENCES

1. Alarcón CR, Lee H, Goodarzi H, Halberg N, Tavazoie SF. N6-methyladenosine marks primary microRNAs for processing. Nature. 2015 Mar 26;519(7544):482-5. doi: 10.1038/nature14281. Epub 2015 Mar 18. PMID: 25799998; PMCID: PMC4475635.

2. Aubert G, Vega RB, Kelly DP. Perturbations in the gene regulatory pathways controlling mitochondrial energy production in the failing heart. Biochim Biophys Acta. 2013 Apr;1833(4):840-7. doi: 10.1016/j.bbamcr.2012.08.015. Epub 2012 Aug 31. PMID: 22964268; PMCID: PMC3570640.

3. Aubert G, Vega RB, Kelly DP. Perturbations in the gene regulatory pathways controlling mitochondrial energy production in the failing heart. Biochim Biophys Acta. 2013 Apr;1833(4):840-7. doi: 10.1016/j.bbamcr.2012.08.015. Epub 2012 Aug 31. PMID: 22964268; PMCID: PMC3570640.

4. Barbosa-da-Silva S, Souza-Mello V, Magliano DC, Marinho Tde S, Aguila MB, Mandarim-de-Lacerda CA. Singular effects of PPAR agonists on nonalcoholic fatty liver disease of diet-induced obese mice. Life Sci. 2015 Apr 15;127:73-81. doi: 10.1016/j.lfs.2015.02.003. Epub 2015 Mar 4. PMID: 25748419.

5. Barger PM, Brandt JM, Leone TC, Weinheimer CJ, Kelly DP. Deactivation of peroxisome proliferator-activated receptor-alpha during cardiac hypertrophic growth. J Clin Invest. 2000 Jun;105(12):1723-30. doi: 10.1172/JCI9056. PMID: 10862787; PMCID: PMC378509.

6. Bernstein E, Kim SY, Carmell MA, Murchison EP, Alcorn H, Li MZ, Mills AA, Elledge SJ, Anderson KV, Hannon GJ. Dicer is essential for mouse development. Nat Genet. 2003 Nov;35(3):215-7. doi: 10.1038/ng1253. Epub 2003 Oct 5. Erratum in: Nat Genet. 2003 Nov;35(3):287. PMID: 14528307.

7. BING RJ, SIEGEL A, UNGAR I, GILBERT M. Metabolism of the human heart. II. Studies on fat, ketone and amino acid metabolism. Am J Med. 1954 Apr;16(4):504-15. doi: 10.1016/0002-9343(54)90365-4. PMID: 13148192.

8. Boon RA, Dimmeler S. MicroRNAs in myocardial infarction. Nat Rev Cardiol. 2015 Mar;12(3):135-42. doi: 10.1038/nrcardio.2014.207. Epub 2014 Dec 16. PMID: 25511085.

9. Bravo-San Pedro JM, Kroemer G, Galluzzi L. Autophagy and Mitophagy in Cardiovascular Disease. Circ Res. 2017 May 26;120(11):1812-1824. doi: 10.1161/CIRCRESAHA.117.311082. PMID: 28546358.

10. Burelle Y, Wambolt RB, Grist M, Parsons HL, Chow JC, Antler C, Bonen A, Keller A, Dunaway GA, Popov KM, Hochachka PW, Allard MF. Regular exercise is associated with a protective metabolic phenotype in the rat heart. Am J Physiol Heart Circ Physiol. 2004 Sep;287(3):H1055-63. doi: 10.1152/ajpheart.00925.2003. Epub 2004 Apr 22. PMID: 15105170.

11. Burkart EM, Sambandam N, Han X, Gross RW, Courtois M, Gierasch CM, Shoghi K, Welch MJ, Kelly DP. Nuclear receptors PPARbeta/delta and PPARalpha direct distinct metabolic regulatory programs in the mouse heart. J Clin Invest. 2007 Dec;117(12):3930-9. doi: 10.1172/JCI32578. PMID: 18037994; PMCID: PMC2082147.

12. Calore M, Lorenzon A, Vitiello L, Poloni G, Khan MAF, Beffagna G, Dazzo E, Sacchetto C, Polishchuk R, Sabatelli P, Doliana R, Carnevale D, Lembo G, Bonaldo P, De Windt L, Braghetta P, Rampazzo A. A novel murine model for arrhythmogenic cardiomyopathy points to a pathogenic role of Wnt signalling and miRNA dysregulation. Cardiovasc Res. 2019 Mar 15;115(4):739-751. doi: 10.1093/cvr/cvy253. PMID: 30304392.

13. Campbell FM, Kozak R, Wagner A, Altarejos JY, Dyck JR, Belke DD, Severson DL, Kelly DP, Lopaschuk GD. A role for peroxisome proliferator-activated receptor alpha (PPARalpha) in the control of cardiac malonyl-CoA levels: reduced fatty acid oxidation rates and increased glucose oxidation rates in the hearts of mice lacking PPARalpha are associated with higher concentrations of malonyl-CoA and reduced expression of malonyl-CoA decarboxylase. J Biol Chem. 2002 Feb 8;277(6):4098-103. doi: 10.1074/jbc.M106054200. Epub 2001 Dec 4. PMID: 11734553.

14. Chen YT, Wang J, Wee AS, Yong QW, Tay EL, Woo CC, Sorokin V, Richards AM, Ling LH. Differential MicroRNA Expression Profile in Myxomatous Mitral Valve Prolapse and Fibroelastic Deficiency Valves. Int J Mol Sci. 2016 May 18;17(5):753. doi: 10.3390/ijms17050753. PMID: 27213335; PMCID: PMC4881574.

15. Cheng L, Ding G, Qin Q, Huang Y, Lewis W, He N, Evans RM, Schneider MD, Brako FA, Xiao Y, Chen YE, Yang Q. Cardiomyocyte-restricted peroxisome proliferator-activated receptor-delta deletion perturbs myocardial fatty acid oxidation and leads to cardiomyopathy. Nat Med. 2004 Nov;10(11):1245-50. doi: 10.1038/nm1116. Epub 2004 Oct 10. PMID: 15475963.

16. Chiong M, Wang ZV, Pedrozo Z, Cao DJ, Troncoso R, Ibacache M, Criollo A, Nemchenko A, Hill JA, Lavandero S. Cardiomyocyte death: mechanisms and translational implications. Cell Death Dis. 2011 Dec 22;2(12):e244. doi: 10.1038/cddis.2011.130. PMID: 22190003; PMCID: PMC3252742.

17. Chiu HC, Kovacs A, Blanton RM, Han X, Courtois M, Weinheimer CJ, Yamada KA, Brunet S, Xu H, Nerbonne JM, Welch MJ, Fettig NM, Sharp TL, Sambandam N, Olson KM, Ory DS, Schaffer JE. Transgenic expression of fatty acid transport protein 1 in the heart causes lipotoxic cardiomyopathy. Circ Res. 2005 Feb 4;96(2):225-33. doi: 10.1161/01.RES.0000154079.20681.B9. Epub 2004 Dec 23. PMID: 15618539.

18. Chiu HC, Kovacs A, Ford DA, Hsu FF, Garcia R, Herrero P, Saffitz JE, Schaffer JE. A novel mouse model of lipotoxic cardiomyopathy. J Clin Invest. 2001 Apr;107(7):813-22. doi: 10.1172/JCI10947. PMID: 11285300; PMCID: PMC199569

19. Creemers EE, van Rooij E. Function and Therapeutic Potential of Noncoding RNAs in Cardiac Fibrosis. Circ Res. 2016 Jan 8;118(1):108-18. doi: 10.1161/CIRCRESAHA.115.305242. Epub 2015 Nov 4. PMID: 26538569.

20. Degenhardt K, Mathew R, Beaudoin B, Bray K, Anderson D, Chen G, Mukherjee C, Shi Y, Gélinas C, Fan Y, Nelson DA, Jin S, White E. Autophagy promotes tumor cell survival and restricts necrosis, inflammation, and tumorigenesis. Cancer Cell. 2006 Jul;10(1):51-64. doi: 10.1016/j.ccr.2006.06.001. PMID: 16843265; PMCID: PMC2857533.

21. Denli AM, Tops BB, Plasterk RH, Ketting RF, Hannon GJ. Processing of primary microRNAs by the Microprocessor complex. Nature. 2004 Nov 11;432(7014):231-5. doi: 10.1038/nature03049. Epub 2004 Nov 7. PMID: 15531879

22. Derda AA, Woo CC, Wongsurawat T, Richards M, Lee CN, Kofidis T, Kuznetsov VA, Sorokin VA. Gene expression profile analysis of aortic vascular smooth muscle cells reveals upregulation of cadherin genes in myocardial infarction patients. Physiol Genomics. 2018 Aug 1;50(8):648-657. doi: 10.1152/physiolgenomics.00042.2017. Epub 2018 May 18. PMID: 29775430.

23. Desvergne B, Michalik L, Wahli W. Transcriptional regulation of metabolism. Physiol Rev. 2006 Apr;86(2):465-514. doi: 10.1152/physrev.00025.2005. PMID: 16601267.

24. Doenst T, Nguyen TD, Abel ED. Cardiac metabolism in heart failure: implications beyond ATP production. Circ Res. 2013 Aug 30;113(6):709-24. doi: 10.1161/CIRCRESAHA.113.300376. PMID: 23989714; PMCID: PMC3896379.

25. Doenst T, Pytel G, Schrepper A, Amorim P, Färber G, Shingu Y, Mohr FW, Schwarzer M. Decreased rates of substrate oxidation ex vivo predict the onset of heart failure and contractile dysfunction in rats with pressure overload. Cardiovasc Res. 2010 Jun 1;86(3):461-70. doi: 10.1093/cvr/cvp414. Epub 2009 Dec 24. PMID: 20035032.

26. Dyck JR, Lopaschuk GD. Malonyl CoA control of fatty acid oxidation in the ischemic heart. J Mol Cell Cardiol. 2002 Sep;34(9):1099-109. doi: 10.1006/jmcc.2002.2060. PMID: 12392882.

27. Finck BN, Kelly DP. Peroxisome proliferator-activated receptor alpha (PPARalpha) signaling in the gene regulatory control of energy metabolism in the normal and diseased heart. J Mol Cell Cardiol. 2002 Oct;34(10):1249-57. doi: 10.1006/jmcc.2002.2061. PMID: 12425323.

28. Finck BN, Kelly DP. Peroxisome proliferator-activated receptor gamma coactivator-1 (PGC-1) regulatory cascade in cardiac physiology and disease. Circulation. 2007 May 15;115(19):2540-8. doi: 10.1161/CIRCULATIONAHA.107.670588. PMID: 17502589.

29. Finck BN, Lehman JJ, Leone TC, Welch MJ, Bennett MJ, Kovacs A, Han X, Gross RW, Kozak R, Lopaschuk GD, Kelly DP. The cardiac phenotype induced by PPARalpha overexpression mimics that caused by diabetes mellitus. J Clin Invest. 2002 Jan;109(1):121-30. doi: 10.1172/JCI14080. PMID: 11781357; PMCID: PMC150824.

30. Finck BN, Lehman JJ, Leone TC, Welch MJ, Bennett MJ, Kovacs A, Han X, Gross RW, Kozak R, Lopaschuk GD, Kelly DP. The cardiac phenotype induced by PPARalpha overexpression mimics that caused by diabetes mellitus. J Clin Invest. 2002 Jan;109(1):121-30. doi: 10.1172/JCI14080. PMID: 11781357; PMCID: PMC150824.

31. Galluzzi L, Bravo-San Pedro JM, Levine B, Green DR, Kroemer G. Pharmacological modulation of autophagy: therapeutic potential and persisting obstacles. Nat Rev Drug Discov. 2017 Jul;16(7):487-511. doi: 10.1038/nrd.2017.22. Epub 2017 May 19. PMID: 28529316; PMCID: PMC5713640.

32. George JC, Liner A, Hoit BD. Isoproterenol-induced myocardial injury: a systematic comparison of subcutaneous versus intraperitoneal delivery in a rat model. Echocardiography. 2010 Jul;27(6):716-21. doi: 10.1111/j.1540-8175.2009.01107.x. Epub 2010 Mar 25. PMID: 20345437.

33. Ha M, Kim VN. Regulation of microRNA biogenesis. Nat Rev Mol Cell Biol. 2014 Aug;15(8):509-24. doi: 10.1038/nrm3838. Epub 2014 Jul 16. PMID: 25027649.

34. Hammond SM. An overview of microRNAs. Adv Drug Deliv Rev. 2015 Jun 29;87:3-14. doi: 10.1016/j.addr.2015.05.001. Epub 2015 May 12. PMID: 25979468; PMCID: PMC4504744.

35. Han J, Lee Y, Yeom KH, Kim YK, Jin H, Kim VN. The Drosha-DGCR8 complex in primary microRNA processing. Genes Dev. 2004 Dec 15;18(24):3016-27. doi: 10.1101/gad.1262504. Epub 2004 Dec 1. PMID: 15574589; PMCID: PMC535913.

36. Harris KS, Zhang Z, McManus MT, Harfe BD, Sun X. Dicer function is essential for lung epithelium morphogenesis. Proc Natl Acad Sci U S A. 2006 Feb 14;103(7):2208-13. doi: 10.1073/pnas.0510839103. Epub 2006 Feb 1. PMID: 16452165; PMCID: PMC1413733.

37. Hill JA, Karimi M, Kutschke W, Davisson RL, Zimmerman K, Wang Z, Kerber RE, Weiss RM. Cardiac hypertrophy is not a required compensatory response to short-term pressure

overload. Circulation. 2000 Jun 20;101(24):2863-9. doi: 10.1161/01.cir.101.24.2863. PMID: 10859294.

38. Horvitz HR, Sulston JE. Isolation and genetic characterization of cell-lineage mutants of the nematode Caenorhabditis elegans. Genetics. 1980 Oct;96(2):435-54. doi: 10.1093/genetics/96.2.435. PMID: 7262539; PMCID: PMC1214309.

39. Huss JM, Kelly DP. Nuclear receptor signaling and cardiac energetics. Circ Res. 2004 Sep 17;95(6):568-78. doi: 10.1161/01.RES.0000141774.29937.e3. PMID: 15375023.

40. Huss JM, Kelly DP. Nuclear receptor signaling and cardiac energetics. Circ Res. 2004 Sep 17;95(6):568-78. doi: 10.1161/01.RES.0000141774.29937.e3. PMID: 15375023.

41. Ichihara S, Obata K, Yamada Y, Nagata K, Noda A, Ichihara G, Yamada A, Kato T, Izawa H, Murohara T, Yokota M. Attenuation of cardiac dysfunction by a PPAR-alpha agonist is associated with down-regulation of redox-regulated transcription factors. J Mol Cell Cardiol. 2006 Aug;41(2):318-29. doi: 10.1016/j.yjmcc.2006.05.013. Epub 2006 Jun 27. PMID: 16806263.

42. Irukayama-Tomobe Y, Miyauchi T, Sakai S, Kasuya Y, Ogata T, Takanashi M, Iemitsu M, Sudo T, Goto K, Yamaguchi I. Endothelin-1-induced cardiac hypertrophy is inhibited by activation of peroxisome proliferator-activated receptor-alpha partly via blockade of c-Jun NH2-terminal kinase pathway. Circulation. 2004 Feb 24;109(7):904-10. doi: 10.1161/01.CIR.0000112596.06954.00. Epub 2004 Feb 16. PMID: 14967736.

43. Jin Y, Zhou TY, Cao JN, Feng QT, Fu YJ, Xu X, Yang CJ. MicroRNA-206 Downregulates Connexin43 in Cardiomyocytes to Induce Cardiac Arrhythmias in a Transgenic Mouse Model. Heart Lung Circ. 2019 Nov;28(11):1755-1761. doi: 10.1016/j.hlc.2018.09.008. Epub 2018 Oct 4. PMID: 30322759.

44. Kang BY, Wang W, Palade P, Sharma SG, Mehta JL. Cardiac hypertrophy during hypercholesterolemia and its amelioration with rosuvastatin and amlodipine. J Cardiovasc Pharmacol. 2009 Oct;54(4):327-34. doi: 10.1097/FJC.0b013e3181b76713. PMID: 19687748.

45. Kang PM, Izumo S. Apoptosis and heart failure: A critical review of the literature. Circ Res. 2000 Jun 9;86(11):1107-13. doi: 10.1161/01.res.86.11.1107. PMID: 10850960.

46. Kanherkar RR, Bhatia-Dey N, Csoka AB. Epigenetics across the human lifespan. Front Cell Dev Biol. 2014 Sep 9;2:49. doi: 10.3389/fcell.2014.00049. PMID: 25364756; PMCID: PMC4207041.

47. Kaushik S, Cuervo AM. Autophagy as a cell-repair mechanism: activation of chaperone-mediated autophagy during oxidative stress. Mol Aspects Med. 2006 Oct-Dec;27(5-6):444-54. doi: 10.1016/j.mam.2006.08.007. Epub 2006 Sep 15. PMID: 16978688; PMCID: PMC1855281.

48. Kehat I, Molkentin JD. Molecular pathways underlying cardiac remodeling during pathophysiological stimulation. Circulation. 2010 Dec 21;122(25):2727-35. doi: 10.1161/CIRCULATIONAHA.110.942268. PMID: 21173361; PMCID: PMC3076218.

49. Khvorova A, Reynolds A, Jayasena SD. Functional siRNAs and miRNAs exhibit strand bias. Cell. 2003 Oct 17;115(2):209-16. doi: 10.1016/s0092-8674(03)00801-8. Erratum in: Cell. 2003 Nov 14;115(4):505. PMID: 14567918.

50. Kitagishi Y, Matsuda S. Diets involved in PPAR and PI3K/AKT/PTEN pathway may contribute to neuroprotection in a traumatic brain injury. *Alzheimers Res Ther*. 2013;5(5):42. Published 2013 Sep 26. doi:10.1186/alzrt208

51. Kumari R, Ray AG, Mukherjee D, Chander V, Kar D, Kumar US, Bharadwaj P V P D, Banerjee SK, Konar A, Bandyopadhyay A. Downregulation of PTEN Promotes Autophagy *via* Concurrent Reduction in Apoptosis in Cardiac Hypertrophy in PPAR $\alpha^{-/-}$ Mice. Front Cardiovasc Med. 2022 Feb 11;9:798639. doi: 10.3389/fcvm.2022.798639. PMID: 35224041; PMCID: PMC8881053.

52. Ladomery MR, Maddocks DG, Wilson ID. MicroRNAs: their discovery, biogenesis, function and potential use as biomarkers in non-invasive prenatal diagnostics. Int J Mol Epidemiol Genet. 2011 Aug 30;2(3):253-60. Epub 2011 Aug 3. PMID: 21915364; PMCID: PMC3166153.

53. Lai L, Leone TC, Keller MP, Martin OJ, Broman AT, Nigro J, Kapoor K, Koves TR, Stevens R, Ilkayeva OR, Vega RB, Attie AD, Muoio DM, Kelly DP. Energy metabolic reprogramming in the hypertrophied and early stage failing heart: a multisystems approach. Circ Heart Fail. 2014 Nov;7(6):1022-31. doi: 10.1161/CIRCHEARTFAILURE.114.001469. Epub 2014 Sep 18. PMID: 25236884; PMCID: PMC4241130.

54. Lee RC, Feinbaum RL, Ambros V. The C. elegans heterochronic gene lin-4 encodes small RNAs with antisense complementarity to lin-14. Cell. 1993 Dec 3;75(5):843-54. doi: 10.1016/0092-8674(93)90529-y. PMID: 8252621.

55. Lee RC, Feinbaum RL, Ambros V. The C. elegans heterochronic gene lin-4 encodes small RNAs with antisense complementarity to lin-14. Cell. 1993 Dec 3;75(5):843-54. doi: 10.1016/0092-8674(93)90529-y. PMID: 8252621.

56. Lee RC, Feinbaum RL, Ambros V. The C. elegans heterochronic gene lin-4 encodes small RNAs with antisense complementarity to lin-14. Cell. 1993 Dec 3;75(5):843-54. doi: 10.1016/0092-8674(93)90529-y. PMID: 8252621.

57. Leone TC, Weinheimer CJ, Kelly DP. A critical role for the peroxisome proliferator-activated receptor α (PPARα) in the cellular fasting response: the PPARα-null mouse as a model of fatty acid oxidation disorders. *Proceedings of the National Academy of Sciences of the United States of America.* 1999;**96**(13):7473–7478.

58. Li R, Zheng W, Pi R, Gao J, Zhang H, Wang P, Le K, Liu P. Activation of peroxisome proliferator-activated receptor-alpha prevents glycogen synthase 3beta phosphorylation and inhibits cardiac hypertrophy. FEBS Lett. 2007 Jul 10;581(17):3311-6. doi: 10.1016/j.febslet.2007.06.017. Epub 2007 Jun 19. PMID: 17597616.

59. Li Y, Liang Y, Zhu Y, Zhang Y, Bei Y. Noncoding RNAs in Cardiac Hypertrophy. J Cardiovasc Transl Res. 2018 Dec;11(6):439-449. doi: 10.1007/s12265-018-9797-x. Epub 2018 Aug 31. PMID: 30171598.

60. Li Z, Wang J, Yang X. Functions of autophagy in pathological cardiac hypertrophy. Int J Biol Sci. 2015 Apr 27;11(6):672-8. doi: 10.7150/ijbs.11883. PMID: 25999790; PMCID: PMC4440257.

61. Liew CW, Xu S, Wang X, McCann M, Whang Kong H, Carley AC, Pang J, Fantuzzi G, O'Donnell JM, Lewandowski ED. Multiphasic Regulation of Systemic and Peripheral Organ Metabolic Responses to Cardiac Hypertrophy. Circ Heart Fail. 2017 Apr;10(4):e003864. doi: 10.1161/CIRCHEARTFAILURE.117.003864. PMID: 28404627; PMCID: PMC5466817.

62. **Lionetti** V, Stanley WC, Recchia FA. Modulating fatty acid oxidation in heart failure. Cardiovasc Res. 2011 May 1;90(2):202-9. doi: 10.1093/cvr/cvr038. Epub 2011 Feb 2. PMID: 21289012; PMCID: PMC3078800.

63. Liu C, Xue R, Wu D, Wu L, Chen C, Tan W, Chen Y, Dong Y. REDD1 attenuates cardiac hypertrophy via enhancing autophagy. Biochem Biophys Res Commun. 2014 Nov 7;454(1):215-20. doi: 10.1016/j.bbrc.2014.10.079. Epub 2014 Oct 22. PMID: 25450383.

64. Lopaschuk GD, Belke DD, Gamble J, Itoi T, Schönekess BO. Regulation of fatty acid oxidation in the mammalian heart in health and disease. Biochim Biophys Acta. 1994 Aug 4;1213(3):263-76. doi: 10.1016/0005-2760(94)00082-4. PMID: 8049240.

65. Lopaschuk GD, Folmes CD, Stanley WC. Cardiac energy metabolism in obesity. Circ Res. 2007 Aug 17;101(4):335-47. doi: 10.1161/CIRCRESAHA.107.150417. PMID: 17702980.

66. Lopaschuk GD, Ussher JR, Folmes CD, Jaswal JS, Stanley WC. Myocardial fatty acid metabolism in health and disease. Physiol Rev. 2010 Jan;90(1):207-58. doi: 10.1152/physrev.00015.2009. PMID: 20086077.

67. Madrazo JA, Kelly DP. The PPAR trio: regulators of myocardial energy metabolism in health and disease. J Mol Cell Cardiol. 2008 Jun;44(6):968-75. doi: 10.1016/j.yjmcc.2008.03.021. Epub 2008 Apr 4. PMID: 18462747.

68. Mohammed SF, Hussain S, Mirzoyev SA, Edwards WD, Maleszewski JJ, Redfield MM. Coronary microvascular rarefaction and myocardial fibrosis in heart failure with preserved ejection fraction. Circulation. 2015 Feb 10;131(6):550-9. doi: 10.1161/CIRCULATIONAHA.114.009625. Epub 2014 Dec 31. PMID: 25552356; PMCID: PMC4324362.

69. Moll UM, Petrenko O. The MDM2-p53 interaction. Mol Cancer Res. 2003 Dec;1(14):1001-8. PMID: 14707283.

70. Muthuramu I, Mishra M, Aboumsallem JP, Postnov A, Gheysens O, De Geest B. Cholesterol lowering attenuates pressure overload-induced heart failure in mice with mild hypercholesterolemia. Aging (Albany NY). 2019 Sep 4;11(17):6872-6891. doi: 10.18632/aging.102218. Epub 2019 Sep 4. PMID: 31484164; PMCID: PMC6756886.

71. Naga Prasad SV, Duan ZH, Gupta MK, Surampudi VS, Volinia S, Calin GA, Liu CG, Kotwal A, Moravec CS, Starling RC, Perez DM, Sen S, Wu Q, Plow EF, Croce CM, Karnik S. Unique microRNA profile in end-stage heart failure indicates alterations in specific cardiovascular signaling networks. J Biol Chem. 2009 Oct 2;284(40):27487-99. doi: 10.1074/jbc.M109.036541. Epub 2009 Jul 29. Retraction in: J Biol Chem. 2016 Jul 15;291(29):14914. PMID: 19641226; PMCID: PMC2785678.

72. Nakamura M, Sadoshima J. Mechanisms of physiological and pathological cardiac hypertrophy. Nat Rev Cardiol. 2018 Jul;15(7):387-407. doi: 10.1038/s41569-018-0007-y. PMID: 29674714.

73. Neely JR, Morgan HE. Relationship between carbohydrate and lipid metabolism and the energy balance of heart muscle. Annu Rev Physiol. 1974;36:413-59. doi: 10.1146/annurev.ph.36.030174.002213. PMID: 19400669.

74. Neubauer S. The failing heart--an engine out of fuel. N Engl J Med. 2007 Mar 15;356(11):1140-51. doi: 10.1056/NEJMra063052. PMID: 17360992.

75. Ogata T, Miyauchi T, Sakai S, Takanashi M, Irukayama-Tomobe Y, Yamaguchi I. Myocardial fibrosis and diastolic dysfunction in deoxycorticosterone acetate-salt hypertensive rats is ameliorated by the peroxisome proliferator-activated receptor-alpha activator fenofibrate, partly by suppressing inflammatory responses associated with the nuclear factor-kappa-B pathway. J Am Coll Cardiol. 2004 Apr 21;43(8):1481-8. doi: 10.1016/j.jacc.2003.11.043. PMID: 15093887.

76. Oka S, Zhai P, Yamamoto T, Ikeda Y, Byun J, Hsu CP, Sadoshima J. Peroxisome Proliferator Activated Receptor-α Association With Silent Information Regulator 1 Suppresses Cardiac Fatty Acid Metabolism in the Failing Heart. Circ Heart Fail. 2015 Nov;8(6):1123-32. doi: 10.1161/CIRCHEARTFAILURE.115.002216. Epub 2015 Oct 6. PMID: 26443578; PMCID: PMC4651813.

77. Okada C, Yamashita E, Lee SJ, Shibata S, Katahira J, Nakagawa A, Yoneda Y, Tsukihara T. A high-resolution structure of the pre-microRNA nuclear export machinery. Science. 2009 Nov 27;326(5957):1275-9. doi: 10.1126/science.1178705. PMID: 19965479.

78. Okada C, Yamashita E, Lee SJ, Shibata S, Katahira J, Nakagawa A, Yoneda Y, Tsukihara T. A high-resolution structure of the pre-microRNA nuclear export machinery. Science. 2009 Nov 27;326(5957):1275-9. doi: 10.1126/science.1178705. PMID: 19965479.

79. Oldfield CJ, Duhamel TA, Dhalla NS. Mechanisms for the transition from physiological to pathological cardiac hypertrophy. Can J Physiol Pharmacol. 2020 Feb;98(2):74-84. doi: 10.1139/cjpp-2019-0566. PMID: 31815523.

80. Opie LH. Metabolism of the heart in health and disease. I. Am Heart J. 1968 Nov;76(5):685-98. doi: 10.1016/0002-8703(68)90168-3. PMID: 4235250.

81. Opie LH. Metabolism of the heart in health and disease. II. Am Heart J. 1969 Jan;77(1):100-22 contd. doi: 10.1016/0002-8703(69)90135-5. PMID: 4882561.

82. Oudit GY, Kassiri Z, Zhou J, Liu QC, Liu PP, Backx PH, Dawood F, Crackower MA, Scholey JW, Penninger JM. Loss of PTEN attenuates the development of pathological hypertrophy and heart failure in response to biomechanical stress. Cardiovasc Res. 2008 Jun 1;78(3):505-14. doi: 10.1093/cvr/cvn041. Epub 2008 Feb 15. PMID: 18281373.

83. Oudit GY, Sun H, Kerfant BG, Crackower MA, Penninger JM, Backx PH. The role of phosphoinositide-3 kinase and PTEN in cardiovascular physiology and disease. J Mol Cell Cardiol. 2004 Aug;37(2):449-71. doi: 10.1016/j.yjmcc.2004.05.015. PMID: 15276015.

84. Park CY, Choi YS, McManus MT. Analysis of microRNA knockouts in mice. Hum Mol Genet. 2010 Oct 15;19(R2):R169-75. doi: 10.1093/hmg/ddq367. Epub 2010 Aug 30. PMID: 20805106; PMCID: PMC2981466.

85. Qin B, Minter-Dykhouse K, Yu J, Zhang J, Liu T, Zhang H, Lee S, Kim J, Wang L, Lou Z. DBC1 functions as a tumor suppressor by regulating p53 stability. Cell Rep. 2015 Mar 3;10(8):1324-34. doi: 10.1016/j.celrep.2015.01.066. Epub 2015 Feb 26. PMID: 25732823; PMCID: PMC4351187.

86. Rakhshandehroo M, Hooiveld G, Müller M, Kersten S. Comparative analysis of gene regulation by the transcription factor PPARα between mouse and human. *PLoS ONE.* 2009;**4**(8)

87. Rakhshandehroo M, Knoch B, Müller M, Kersten S. Peroxisome proliferator-activated receptor alpha target genes. PPAR Res. 2010;2010:612089. doi: 10.1155/2010/612089. Epub 2010 Sep 26. PMID: 20936127; PMCID: PMC2948931.

88. Rana S, Datta R, Chaudhuri RD, Chatterjee E, Chawla-Sarkar M, Sarkar S. Nanotized PPARα Overexpression Targeted to Hypertrophied Myocardium Improves Cardiac Function by Attenuating the p53-GSK3β-Mediated Mitochondrial Death Pathway. Antioxid Redox Signal. 2019 Feb 10;30(5):713-732. doi: 10.1089/ars.2017.7371. Epub 2018 May 9. PMID: 29631413.

89. Rane S, Sayed D, Abdellatif M. MicroRNA with a MacroFunction. Cell Cycle. 2007 Aug 1;6(15):1850-5. doi: 10.4161/cc.6.15.4551. Epub 2007 Jun 6. PMID: 17660716.

90. Raso A, Dirkx E, Philippen LE, Fernandez-Celis A, De Majo F, Sampaio-Pinto V, Sansonetti M, Juni R, El Azzouzi H, Calore M, Bitsch N, Olieslagers S, Oerlemans MIFJ, Huibers MM, de Weger RA, Reckman YJ, Pinto YM, Zentilin L, Zacchigna S, Giacca M, da Costa Martins PA, López-Andrés N, De Windt LJ. Therapeutic Delivery of miR-148a Suppresses Ventricular Dilation in Heart Failure. Mol Ther. 2019 Mar 6;27(3):584-599. doi: 10.1016/j.ymthe.2018.11.011. Epub 2018 Nov 17. PMID: 30559069; PMCID: PMC6403487.

91. Riehle C, Wende AR, Zhu Y, Oliveira KJ, Pereira RO, Jaishy BP, Bevins J, Valdez S, Noh J, Kim BJ, Moreira AB, Weatherford ET, Manivel R, Rawlings TA, Rech M, White MF, Abel ED. Insulin receptor substrates are essential for the bioenergetic and hypertrophic response of the heart to exercise training. Mol Cell Biol. 2014 Sep 15;34(18):3450-60. doi: 10.1128/MCB.00426-14. Epub 2014 Jul 7. PMID: 25002528; PMCID: PMC4135616.

92. Rigano D, Sirignano C, Taglialatela-Scafati O. The potential of natural products for targeting PPARα. Acta Pharm Sin B. 2017 Jul;7(4):427-438. doi: 10.1016/j.apsb.2017.05.005. Epub 2017 Jun 16. PMID: 28752027; PMCID: PMC5518659.

93. Roncarati R, Viviani Anselmi C, Losi MA, Papa L, Cavarretta E, Da Costa Martins P, Contaldi C, Saccani Jotti G, Franzone A, Galastri L, Latronico MV, Imbriaco M, Esposito G, De Windt L, Betocchi S, Condorelli G. Circulating miR-29a, among other up-regulated microRNAs, is the only biomarker for both hypertrophy and fibrosis in patients with hypertrophic cardiomyopathy. J Am Coll Cardiol. 2014 Mar 11;63(9):920-7. doi: 10.1016/j.jacc.2013.09.041. Epub 2013 Oct 23. PMID: 24161319.

94. Ruwhof C, van der Laarse A. Mechanical stress-induced cardiac hypertrophy: mechanisms and signal transduction pathways. Cardiovasc Res. 2000 Jul;47(1):23-37. doi: 10.1016/s0008-6363(00)00076-6. PMID: 10869527.

95. Saraste A, Pulkki K, Kallajoki M, Heikkilä P, Laine P, Mattila S, Nieminen MS, Parvinen M, Voipio-Pulkki LM. Cardiomyocyte apoptosis and progression of heart failure to transplantation. Eur J Clin Invest. 1999 May;29(5):380-6. doi: 10.1046/j.1365-2362.1999.00481.x. PMID: 10354194.

96. Schiattarella GG, Hill JA. Inhibition of hypertrophy is a good therapeutic strategy in ventricular pressure overload. Circulation. 2015 Apr 21;131(16):1435-47. doi: 10.1161/CIRCULATIONAHA.115.013894. PMID: 25901069; PMCID: PMC4408778.

97. Schirone L, Forte M, Palmerio S, Yee D, Nocella C, Angelini F, Pagano F, Schiavon S, Bordin A, Carrizzo A, Vecchione C, Valenti V, Chimenti I, De Falco E, Sciarretta S, Frati G. A Review of the Molecular Mechanisms Underlying the Development and Progression of Cardiac Remodeling. Oxid Med Cell Longev. 2017;2017:3920195. doi: 10.1155/2017/3920195. Epub 2017 Jul 2. PMID: 28751931; PMCID: PMC5511646.

98. Shimizu I, Minamino T. Physiological and pathological cardiac hypertrophy. J Mol Cell Cardiol. 2016 Aug;97:245-62. doi: 10.1016/j.yjmcc.2016.06.001. Epub 2016 Jun 2. PMID: 27262674.

99. Small EM, Frost RJ, Olson EN. MicroRNAs add a new dimension to cardiovascular disease. Circulation. 2010 Mar 2;121(8):1022-32. doi: 10.1161/CIRCULATIONAHA.109.889048. PMID: 20194875; PMCID: PMC2847432.

100. Son NH, Park TS, Yamashita H, Yokoyama M, Huggins LA, Okajima K, Homma S, Szabolcs MJ, Huang LS, Goldberg IJ. Cardiomyocyte expression of PPARgamma leads to cardiac

dysfunction in mice. J Clin Invest. 2007 Oct;117(10):2791-801. doi: 10.1172/JCI30335. PMID: 17823655; PMCID: PMC1964508.

101. Strøm CC, Aplin M, Ploug T, Christoffersen TE, Langfort J, Viese M, Galbo H, Haunsø S, Sheikh SP. Expression profiling reveals differences in metabolic gene expression between exercise-induced cardiac effects and maladaptive cardiac hypertrophy. FEBS J. 2005 Jun;272(11):2684-95. doi: 10.1111/j.1742-4658.2005.04684.x. PMID: 15943803.

102. Tardiff JC. Cardiac hypertrophy: stressing out the heart. J Clin Invest. 2006 Jun;116(6):1467-70. doi: 10.1172/JCI28884. PMID: 16741569; PMCID: PMC1464918.

103. van Empel VP, Bertrand AT, Hofstra L, Crijns HJ, Doevendans PA, De Windt LJ. Myocyte apoptosis in heart failure. Cardiovasc Res. 2005 Jul 1;67(1):21-9. doi: 10.1016/j.cardiores.2005.04.012. PMID: 15896727.

104. van Rooij E, Sutherland LB, Liu N, Williams AH, McAnally J, Gerard RD, Richardson JA, Olson EN. A signature pattern of stress-responsive microRNAs that can evoke cardiac hypertrophy and heart failure. Proc Natl Acad Sci U S A. 2006 Nov 28;103(48):18255-60. doi: 10.1073/pnas.0608791103. Epub 2006 Nov 15. PMID: 17108080; PMCID: PMC1838739.

105. Vega RB, Konhilas JP, Kelly DP, Leinwand LA. Molecular Mechanisms Underlying Cardiac Adaptation to Exercise. *Cell Metab*. 2017;25(5):1012-1026. doi:10.1016/j.cmet.2017.04.025

106. Vega RB, Konhilas JP, Kelly DP, Leinwand LA. Molecular Mechanisms Underlying Cardiac Adaptation to Exercise. Cell Metab. 2017 May 2;25(5):1012-1026. doi: 10.1016/j.cmet.2017.04.025. PMID: 28467921; PMCID: PMC5512429.

107. Vidigal JA, Ventura A. The biological functions of miRNAs: lessons from in vivo studies. Trends Cell Biol. 2015 Mar;25(3):137-47. doi: 10.1016/j.tcb.2014.11.004. Epub 2014 Dec 4. PMID: 25484347; PMCID: PMC4344861.

108. Wang J, Liew OW, Richards AM, Chen YT. Overview of MicroRNAs in Cardiac Hypertrophy, Fibrosis, and Apoptosis. Int J Mol Sci. 2016 May 18;17(5):749. doi: 10.3390/ijms17050749. PMID: 27213331; PMCID: PMC4881570.

109. Wang J, Yang X. The function of miRNA in cardiac hypertrophy. Cell Mol Life Sci. 2012 Nov;69(21):3561-70. doi: 10.1007/s00018-012-1126-y. Epub 2012 Aug 25. PMID: 22926414; PMCID: PMC3474911.

110. Wang Y, Medvid R, Melton C, Jaenisch R, Blelloch R. DGCR8 is essential for microRNA biogenesis and silencing of embryonic stem cell self-renewal. Nat Genet. 2007 Mar;39(3):380-5. doi: 10.1038/ng1969. Epub 2007 Jan 28. PMID: 17259983; PMCID: PMC3008549.

111. Warren JS, Oka SI, Zablocki D, Sadoshima J. Metabolic reprogramming via PPARα signaling in cardiac hypertrophy and failure: From metabolomics to epigenetics. Am J Physiol Heart Circ Physiol. 2017 Sep 1;313(3):H584-H596. doi: 10.1152/ajpheart.00103.2017. Epub 2017 Jun 23. PMID: 28646024; PMCID: PMC6425516.

112. Watanabe K, Fujii H, Takahashi T, Kodama M, Aizawa Y, Ohta Y, Ono T, Hasegawa G, Naito M, Nakajima T, Kamijo Y, Gonzalez FJ, Aoyama T. Constitutive regulation of cardiac fatty acid metabolism through peroxisome proliferator-activated receptor alpha associated with age-dependent cardiac toxicity. J Biol Chem. 2000 Jul 21;275(29):22293-9. doi: 10.1074/jbc.M000248200. PMID: 10801788.

113. Wehbe N, Nasser SA, Pintus G, Badran A, Eid AH, Baydoun E. MicroRNAs in Cardiac Hypertrophy. Int J Mol Sci. 2019 Sep 23;20(19):4714. doi: 10.3390/ijms20194714. PMID: 31547607; PMCID: PMC6801828.

114. Wightman B, Ha I, Ruvkun G. Posttranscriptional regulation of the heterochronic gene lin-14 by lin-4 mediates temporal pattern formation in C. elegans. Cell. 1993 Dec 3;75(5):855-62. doi: 10.1016/0092-8674(93)90530-4. PMID: 8252622.

115. Wisneski JA, Stanley WC, Neese RA, Gertz EW. Effects of acute hyperglycemia on myocardial glycolytic activity in humans. J Clin Invest. 1990 May;85(5):1648-56. doi: 10.1172/JCI114616. PMID: 2185277; PMCID: PMC296617

116. Wojciechowska A, Braniewska A, Kozar-Kamińska K. MicroRNA in cardiovascular biology and disease. Adv Clin Exp Med. 2017 Aug;26(5):865-874. doi: 10.17219/acem/62915. PMID: 29068585.

117. Wongsurawat T, Woo CC, Giannakakis A, Lin XY, Cheow ESH, Lee CN, Richards M, Sze SK, Nookaew I, Kuznetsov VA, Sorokin V. Transcriptome alterations of vascular smooth muscle cells in aortic wall of myocardial infarction patients. Data Brief. 2018 Feb 6;17:1112-1135. doi: 10.1016/j.dib.2018.01.108. PMID: 29876469; PMCID: PMC5988399.

118. Xia P, Liu Y, Cheng Z. Signaling Pathways in Cardiac Myocyte Apoptosis. Biomed Res Int. 2016;2016:9583268. doi: 10.1155/2016/9583268. Epub 2016 Dec 22. PMID: 28101515; PMCID: PMC5215135.

119. Yagyu H, Chen G, Yokoyama M, Hirata K, Augustus A, Kako Y, Seo T, Hu Y, Lutz EP, Merkel M, Bensadoun A, Homma S, Goldberg IJ. Lipoprotein lipase (LpL) on the surface of cardiomyocytes increases lipid uptake and produces a cardiomyopathy. J Clin Invest. 2003 Feb;111(3):419-26. doi: 10.1172/JCI16751. PMID: 12569168; PMCID: PMC151861.

120. Yang Q, Li Y. Roles of PPARs on regulating myocardial energy and lipid homeostasis. J Mol Med (Berl). 2007 Jul;85(7):697-706. doi: 10.1007/s00109-007-0170-9. Epub 2007 Mar 14. PMID: 17356846.

121. Yoda M, Kawamata T, Paroo Z, Ye X, Iwasaki S, Liu Q, Tomari Y. ATP-dependent human RISC assembly pathways. Nat Struct Mol Biol. 2010 Jan;17(1):17-23. doi: 10.1038/nsmb.1733. Epub 2009 Dec 6. PMID: 19966796; PMCID: PMC2915567.

122. Zhang H, Kolb FA, Jaskiewicz L, Westhof E, Filipowicz W. Single processing center models for human Dicer and bacterial RNase III. Cell. 2004 Jul 9;118(1):57-68. doi: 10.1016/j.cell.2004.06.017. PMID: 15242644.

123. Zhang L, Jaswal JS, Ussher JR, Sankaralingam S, Wagg C, Zaugg M, Lopaschuk GD. Cardiac insulin-resistance and decreased mitochondrial energy production precede the development of systolic heart failure after pressure-overload hypertrophy. Circ Heart Fail. 2013 Sep 1;6(5):1039-48. doi: 10.1161/CIRCHEARTFAILURE.112.000228. Epub 2013 Jul 16. PMID: 23861485.

PUBLICATIONS

Downregulation of PTEN Promotes Autophagy *via* Concurrent Reduction in Apoptosis in Cardiac Hypertrophy in PPAR $\alpha^{-/-}$ Mice

Ritu Kumari[1], Aleepta Guha Ray[1], Dibyanti Mukherjee[1], Vivek Chander[1], Dipak Kar[1], Uppulapu Shravan Kumar[2], Deepak Bharadwaj P.V.P.[3], Sanjay K. Banerjee[2], Aditya Konar[1] and Arun Bandyopadhyay[1]*

[1] Cell Biology and Physiology Division, CSIR-Indian Institute of Chemical Biology, Kolkata, India, [2] Department of Biotechnology, National Institute of Pharmaceutical Education and Research, Guwahati, India, [3] Department of Pharmacology and Toxicology, National Institute of Pharmaceutical Education and Research, Guwahati, India

Cardiac hypertrophy is characterized by an increase in the size of the cardiomyocytes which is initially triggered as an adaptive response but ultimately becomes maladaptive with chronic exposure to different hypertrophic stimuli. Prolonged cardiac hypertrophy is often associated with mitochondrial dysfunctions and cardiomyocyte cell death. Peroxisome proliferator activated receptor alpha (PPAR α), which is critical for mitochondrial biogenesis and fatty acid oxidation, is down regulated in hypertrophied cardiomyocytes. Yet, the role of PPAR α in cardiomyocyte death is largely unknown. To assess the role of PPAR α in chronic hypertrophy, isoproterenol, a β-adrenergic receptor agonist was administered in PPAR α knock out (PPAR $\alpha^{-/-}$) mice for 2 weeks and hypertrophy associated changes in cardiac tissues were observed. Echocardiographic analysis ensured the development of cardiac hypertrophy and compromised hemodynamics in PPAR $\alpha^{-/-}$ mice. Proteomic analysis using high resolution mass spectrometer identified about 1,200 proteins enriched in heart tissue. Proteins were classified according to biological pathway and molecular functions. We observed an unexpected down regulation of apoptotic markers, Annexin V and p53 in hypertrophied heart tissue. Further validation revealed a significant down regulation of apoptosis regulator, PTEN, along with other apoptosis markers like p53, Caspase 9 and c-PARP. The autophagy markers Atg3, Atg5, Atg7, p62, Beclin1 and LC3 A/B were up regulated in PPAR $\alpha^{-/-}$ mice indicating an increase in autophagy. Similar observations were made in a high cholesterol diet fed PPAR $\alpha^{-/-}$ mice. The results were further validated *in vitro* using NRVMs and H9C2 cell line by blocking PPAR α that resulted in enhanced autophagosome formation upon hypertrophic stimulation. The results demonstrate that in the absence of PPAR α apoptotic pathway is inhibited while autophagy is enhanced. The data suggest that PPAR α signaling might act as a molecular switch between apoptosis and autophagy thereby playing a critical role in adaptive process in cardiac hypertrophy.

Keywords: cardiac hypertrophy, PPAR α, apoptosis, autophagy, PTEN

INTRODUCTION

Cardiomyocyte tends to execute an adaptive mechanism in order to survive the stress induced by various external stimuli. Cardiac hypertrophy is one such example where adaptive response helps to overcome the increased demands of the failing heart. However, prolonged hypertrophy leads to pathological conditions and eventually heart failure occurs. Cardiac hypertrophy brings about significant changes that mark extensive remodeling both at the cellular and molecular levels (1, 2). Cardiomyocyte size is increased along with extensive fibrosis, marked by reprogramming of the fetal gene expression such as atrial natriuretic peptide (ANP), brain natriuretic peptide (BNP) and reduced expression of the genes for fatty acid oxidation. Available reports demonstrated that inhibition of PPAR α and PGC1 α signaling is a prerequisite for fetal genes re-expression as well as reduced fatty acid oxidation (3, 4).

Prolonged cardiac hypertrophy leads to PPAR α mediated metabolic reprogramming resulting into reduced fatty acid oxidation (5). Pressure overload in heart in response to β-adrenergic receptors induces myocardial hypertrophy and cardiac remodeling, that is accompanied by down regulation of PPAR α leading to energy metabolic disorder (6). Under normal condition, the heart utilizes saturated fats as the primary metabolic fuel. However, in the absence of PPAR α activity, accumulation of excess fat is responsible for the metabolic switch from fatty acid oxidation toward glycolysis (7–10). High-cholesterol diet has also been directly implicated in cardiac hypertrophy since the resulting lipotoxicity stimulates compensatory mechanism as a defense toward chronic pressure overload in heart (11). Severe hypercholesterolemia as well as administration of β adrenergic receptor agonist such as isoproterenol in mice hearts has been associated with significant cardiomyocyte death and development of heart failure (7, 8, 12).

Multiple signaling molecules and pathways regulate cardiomyocyte apoptosis which might lead to heart failure (13). PTEN that is reported to be widely expressed in cardiomyocytes is activated in response to I/R injury or β-adrenergic receptor stimulation and contributes to cardiac apoptosis (14, 15). PTEN functions as a lipid phosphatase that dephosphorylates phosphatidylinositol (3,4,5)-trisphosphate (PIP3) to phosphatidylinositol (4,5)-bisphosphate (PIP2) and negatively regulates PI3K/AKT signaling pathway (16). Deletion of PTEN has been associated with enhanced Akt Phosphorylation and activation of Akt, whereas over expression of PTEN results in Akt inactivation as well as cardiomyocyte death (17). PI3K/Akt pathway mediates anti-apoptotic effects in cardiomyocytes as

established by Akt downregulation following pro-apoptotic insults (17). Stimulation of Akt has been reported to protect against myocardial injury and attenuate apoptosis (18).

Many reports suggest metabolic stress dependent activation of apoptotic pathway that leads to cell death as the cellular mechanism fails to cope with the increased energy demands (19). However, an inclination toward the autophagy pathway helps in sustaining the metabolic stress by promoting cell survival while defects in autophagy could promote cell death and inflammation (19, 20).

Several studies have reported the mTOR mediated regulation of autophagy (21). Autophagy is a dynamic self-degradative process that is essential to maintain cellular homeostasis. Growing evidences have revealed association between cardiac hypertrophy as well as autophagy (22, 23). Baseline autophagy functions by removing damaged organelle aggregates and preventing cardiomyocytes from cytotoxicity (22, 23). Moderate tuning of autophagy has been reported to be beneficial for the cardiac health as it maintains cellular homeostasis and prevents cell death.

Available literatures have demonstrated that PPAR α signaling plays an important role in the transcription of various genes associated with fatty acid oxidation as well as mitochondrial biogenesis and thereby plays a pivotal role in the pathophysiology of cardiac hypertrophy.

To explore the involvement of PPAR α in cardiomyocyte adaptive mechanism, PPAR α-/- mice was used that revealed significant down regulation in apoptosis that was explained by the decrease in PTEN. Several studies have implicated the direct transcriptional regulation of PTEN *via* PPARα but the sustained down regulation of PTEN in the presence of isoproterenol that is a β-adrenergic receptor agonist, was observed in our study. Based on the findings, our aim was to understand how the absence of PPAR α influences apoptosis in hypertrophied cardiomyocytes. This might also reveal how PPAR α mediated signaling influences the adaptive mechanism of the cardiomyocytes in stress-induced hypertrophy.

MATERIALS AND METHODS

Animal Studies

The protocol was approved by the Institutional Ethics Committee (Reference no. IICB/AEC/Meeting/Sep/2019/4) and the animals were handled in accordance with the Committee for the Purpose of Control and Supervision of Experiments on Animals (CPCSEA), Ministry of Social Justice, and Government of India (Registration no. 147/1999/CPCSEA). Male and female mPPAR α−/− mice (F2 homozygotes; hybrids of Sv/129 3 C57BL/6N genetic background 3 months-old were obtained from The Jackson Laboratory (Bar Harbor, Maine, USA) and bred in the Central Animal Facility CSIR-IICB, Kolkata. Genotyping of the PPARα−/− mice was done using primers flanking the region that was knocked out and has been added as **Supplementary Figure 4**. C57BL/6 wild-type mice and PPARα−/− mice were intraperitoneally injected with 30 mg/kg/day dose of isoproterenol for 14-days. 3 months-old PPARα−/− mice were divided into two groups and were fed

---

Abbreviations: PPARα, Peroxisome proliferator-activated receptor alpha; PGC 1 α, PPAR γ (Peroxisome proliferator-activated receptor gamma) coactivator 1 alpha; ACOX1, Acyl-CoA Oxidase 1; Acaa1a, Acetyl-CoA Acyltransferase 1; ACAA2, acetyl-Coenzyme A acyltransferase 2; HSD17B12, 17-beta hydroxysteroid dehydrogenase-12; PRKAG2, Protein Kinase AMP-Activated Non-Catalytic Subunit Gamma 2; EP300, E1A Binding Protein P300; GAPDH, Glyceraldehyde 3-phosphate dehydrogenase; ANP, Atrial Natriuretic peptide; BNP, Brain Natriuretic peptide; LC 3 I/II, Microtubule-associated protein light chain 3;Dbc1, Deleted in bladder cancer protein 1;Mdm2 Mouse double minute 2 homolog;FIS 1, Mitochondrial fission 1 protein;FABP7, Fatty acid binding protein 7;OPA1 Optic Atrophy 1;c-PARP cleaved-Poly (ADP-ribose) polymerase; WT, wild-type.

S. No.	Gene	Forward primer	Reverse primer
1	GAPDH	TGGCCTTCCGTGTTCCTAC	GAGTTGCTGTTGAAGTCGCA
2	Acaa1a	TCTCCAGGACGTGAGGCTAAA	CGCTCAGAAATTGGGCGATG
3	HSD17 B12	GGCTTCCTGTACTGGGTGG	CACGTTTTGCTAACTCTTCTGC
4	ACAA2	CTGCTACGAGGTGTGTTCATC	AGCTCTGCATGACATTGCCC
5	Acox1	TAACTTCCTCACTCGAAGCCA	AGTTCCATGACCCATCTCTGTC
6	PRKA G2	AATGAACACTTTCAAGAGACCCC	CCAACTTGGAACTTGTGGGAAT
7	Ep300	TTCAGCCAAGCGGCCTAAA	CGCCACCATTGGTTAGTCCC

two types of diet, normal chow diet (kcal: protein = 25%; carbohydrate = 58%; fat =17%) and high cholesterol diet (HCD, Research Diets Inc., catalog no. D12336 with 1.25% cholesterol). Mice were maintained on 12-h dark /12-h light cycle and allowed to have easy access to food and water. The number of animals (n) was at least 6 for all the different experimental conditions. At the end of the experimental duration, the animals were anesthetized by an intraperitoneal injection of 100 mg/kg ketamine with 10 mg/kg xylazine hydrochloride and sacrificed *via* cervical dislocation. The heart was collected for histological and biochemical analysis.

Histological Staining

The heart tissues were fixed in 10% formalin, embedded in paraffin and then cut into 5 μm thin sections using microtome. Haematoxylin and Eosin (H&E) staining and Masson Trichome staining were performed to observe increase in cardiomyocyte size (morphological changes) and collagen deposition, respectively. Stained slides were visualized using light microscope.

RNA Extraction and Reverse-Transcription

RNA was isolated using Tri Reagent solution (Sigma) according to manufacturer protocol. RNA concentration and purity (A260/A280 N 1.9) was analyzed using Nanodrop 2000. Real-time PCR was performed using Luna® Universal One-Step RTqPCR Kit (NEB) with 300 ng of RNA per reaction in 96-well optical reaction plates in AB Real Time 7500 Fast system. RT-PCR primers were designed using Primer Bank. The primer sequences are provided in **Table 1.**

Tissue Homogenization

Heart tissue was homogenized using Teflon Homogenizer in RIPA Buffer with protease inhibitor cocktail (ProteoGuard™ EDTA-Free Protease Inhibitor Cocktail, Clonetech) and centrifuged at 16,000 g at 4°C for 20 min.

Western Blot Analysis

Protein concentrations were determined using DC™ Protein Assay Kit (Bio-Rad). Equal amount (30 ug) protein Samples were separated on 1.5 mm 10% sodiumdodecylsulfate polyacrylamide

gels and transferred onto PVDF membranes (Merck-Millipore). Membranes were blocked with 5% skimmed milk or 5% BSA (HiMedia, #TC194) and probed using the following antibodies: Anti-Opa1 (ab42364), Anti-Annexin V (8555S), Anti-c-PARP (sc-56196), Anti-Caspase 9 (9508S), Anti-p53 (2524S), Anti-Mdm2 (sc-965), Anti-Dbc1 (5857S), Anti-mTOR(sc-517464), Anti-pAkt:ser-473(sc-293125), Anti-PTEN(sc-7974), Anti-Bcl-2(sc-7382), Anti-LC3 A/B(ab128025), Anti-p62(ab91526), Anti-Beclin1 (ab55878), Anti-Atg3(3415T), Anti-Atg5(12994T), Anti-Atg7(8558T), Anti-Calpain (sc-271856), Anti-GAPDH (G8795), and anti-β-actin (Sigma A5441) overnight at 4°C. The membranes were washed three times in TBS-T and incubated with alkaline phosphatase conjugated secondary antibodies [Sigma A5153 (Mouse) and Sigma A9919 (Rabbit)] for 2 h at room temperature. Membranes were washed three times with TBST and developed using NBT-BCIP (Fermentes R0841, R821) in alkaline phosphatase buffer. After development of colored product on the membranes, they were washed with water, dried and images acquired using a scanner. Images were quantified using Image J software using β-actin and GAPDH as loading control for mice samples.

Mass- Spectrometry

Heart tissue samples were homogenized using Rapigest SF Surfactant (Waters, #186001861), protein concentration was estimated and 100 ug of protein was used for sample preparation. 100 mM of freshly prepared 1, 4-dithiothreitol (DTT; Sigma #10197777001; final conc.10 mM) was added and incubated at 56°C for 40 min. The tubes were cooled to room temperature and 200 mM of freshly prepared Iodoacetamide (IAA, Sigma #I6125; final conc. 20 mM) was added and incubated for 1 h at room temperature. Excess IAA was quenched by adding DTT and incubated at room temperature for 20 min. Digestion was performed at 37°C overnight with mild agitation using 1 μg Trypsin protease (Pierce Thermo, #90057). The reaction was stopped the next morning using 0.1% Formic Acid (Sigma, #5330020050) and incubated at room temperature for 20 min. The samples were frozen, lyophilized and reconstituted in 0.1% formic acid before mass spectrometry analysis.

Reconstituted samples were subjected to mass spectrometric analysis using Orbitrap mass spectrometer (LTQ-XL, ThermoFisher Scientific) after chromatographic separation and peptide fractionation through a C18 easy spray nano column (3 μm, 100 A) by nano LC (Easy-nLC1000). The injection volume was 2 μl for each sample. Total gradient was set for 145 min with a spray rate of 300 nl/min. Scan range for Orbitrap was from 350 to 2,000 (m/z) with minimum three peaks and a resolution of 60,000. Ionic fragmentation was done by collision induced dissociation (CID) method. Protein identification was performed by Thermo Proteome Discoverer version 1.4.0. MS/MS spectra were matched against MASCOT in assistance with Percolator. Static Modification was set for N-terminal acetylation and Carbamidomethylation of Cysteine. Dynamic modification was set for Methionine (oxidation) and minimum missed cleavage number was set at two. Swissprot was used as reference software for protein identification.

Biological triplicates of the eight groups were compared using label-free relative quantification proteomic software SIEVE (Thermofisher Scientific, Waltham, MA, version.2.1.377). SIEVE directly processed the raw files from Thermo experimental datasets. To identify the statistically significant differences between LC-MS experiment datasets, the software calculated the p-value for the expression ratio of each differential peak. Spectra belonging to the peaks that were found to have statistically significant differential expression were then searched against the protein database MASCOT for peptide and protein identifications. Heat map was generated using graph pad prism software for the dataset.

PANTHER software (http://www.pantherdb.org/) was used for analyzing the significant alterations in the expressions of proteins and genes obtained from Thermo Proteome Discoverer and to identify their percent enrichment in Biological Processes and Molecular Functions.

The mass spectrometry proteomics data have been deposited to the ProteomeXchange Consortium *via* the PRIDE partner repository with the dataset identifier PXD025470.

Reviewer account details:
Username: reviewer_pxd025470@ebi.ac.uk
Password: z0EdUgUV.

Cell Culture and Treatment

H9C2(2-1) cardiomyocytes were acquired from the National Center for Cell Science (Pune, India) and cultured in Dulbecco's modified Eagle medium (DMEM) with high glucose (4.5 g/liter), sodium bicarbonate (3.7 g/liter) and fetal bovine serum (FBS;10%) in an incubator maintained at 37 C, 5% CO_2 and 80% relative humidity (RH). Cells were serum starved for 18–24 h before experimentation. Hypertrophy was induced by treating serum-starved H9C2 (2-1) cells with 100 μM Phenylephrine (PE; Sigma-Aldrich, USA) for 24h. PPAR α antagonist, GW 6471 (TOCRIS, 4618) dissolved in ethanol was used at a working concentration of 10 uM to block the PPAR α signaling.

Autophagy Assay

H9C2 (2-1) cell line was seeded in a 6-well and divided into six groups. I-control, II-PE treated (treatment dose, 100 μM), III-serum starved, IV-GW6471 incubated (treatment dose, 10 μM), V-PE+GW6471, VI-serum starved+GW6471. After 24 h incubation, medium was removed 100 ul of autophagosome detection reagent working solution was added to each well as per manufacturer's instructions (Sigma-Aldrich, MAK138). After 15 min incubation at 37 C, 5% CO_2 and 80% relative humidity (RH), each well was washed three times using PBS. Experiment was repeated along with two more groups I-cholesterol (50 μM), II-cholesterol+GW6471 to resemble the *in vivo* high cholesterol diet induced cardiac hypertrophy. Cells were seeded in a 96-well and same protocol was followed except the reading was taken using a microplate reader (Varioskan, LUX) at 518 nm.

Proteome Profiler™ Antibody Array

Proteome profiler Antibody assay was performed using Proteome Profiler™ Antibody Array kit (R&D SYSTEMS) with 400 μg of

protein per sample and the data obtained was quantified using Image J software.

Echocardiography

The animal cardiac function was measured using the small animal imaging system (Vevo LAZR-X 3100, FUJIFILM Visual Sonics). Animals were anesthetized with 4% isoflurane and maintained anesthesia with 1–2% isoflurane during the Imaging procedure. Post-anesthesia, the animal was placed over the animal imaging platform. Essential parameters like respiration rate, electrocardiogram (ECG), body temperature, and heart rate were recorded throughout the imaging. The MX400 ultrasound transducer was used with a mouse small cardiology application in parasternal long-axis view (PLAX). Cardiac functions like cardiac output, ejection fraction, and fractional shortening were calculated from brightness mode (B-mode), where the heart left ventricular region was focused in a two-dimensional manner. Whereas Left ventricular mass (LV mass), systolic volume, diastolic volume were measured for each animal from the Motion Mode (M-mode) image. The echocardiography images were captured from videotape, and data were collected with the help of digital image analysis cardiac package software (Vevo Lab 3.1.1).

Isolation and Culture of Neonatal Rat Ventricular Myocytes

Neonatal rat ventricular myocytes (NRVM) from 2-day-old Sprague-Dawley rat pups were isolated. Hearts were dissected and rinsed in Ads buffer (116.3 mMNaCl, 19.7 mM HEPES, 9.4 mMNaH2PO4, 5.5 mM glucose, 5.3 mMKCl, 0.83 mMMgSO4 [pH 7.4]). Atria were removed, and ventricles were minced and incubated at 37°C in a solution of enzymes containing 0.2% collagenase type II (381 U/mg) and pancreatin (0.6 mg/ml) in Ads buffer in the presence of 95% O2 and 5% CO2 for four successive digestions of 10 min each. The supernatant of the first tissue digestion was discarded. The supernatants obtained after each digestion were centrifuged for 5 min at 1,000 rpm. The cell pellets obtained in each round of digestion were resuspended in M199 growth medium (supplemented with 10% fetal bovine serum, and 100 U/ml penicillin-streptomycin, pH 7.2). The resuspended cells were pooled and passed through cell strainer, preplated in T25 cm2 flask (BD), and incubated for 1 h in a CO_2 incubator for cardiomyocyte enrichment. The supernatants containing cardiomyocytes were collected by brief centrifugation and resuspended in growth medium. The cells were seeded onto collagen I-coated coverslips (Biocoat; BDLabware, Bedford, USA) in M199 medium supplemented with 10% FBS. Fresh media was replaced after 18 h of cell seeding and cultured for 2 days.

Immunofluorescence and Microscopy

Cells were fixed in 4% paraformaldehyde for 20 min washed in PBS and incubated for 5 min in 0.2% triton X-100 in PBS. Cells were blocked in 1% BSA for 30 min before incubating with anti alpha -sarcomeric antibody (Sigma Aldrich) for overnight. Cells were washed two times in PBS for 5 min each and incubated with anti mouse Allexa flour 594 (molecular

probes) for 1 h washed 3X and mounted on slide and pictured. High resolution image were acquired on 63x oil immersion objective lensNA 1.4,on Zeiss LSM 980 confocal microscope and processed on ZEN Blue. All images were acquired under identical Laser power, detector gain, offset and pinhole aperture window.

Statistical Analysis

Statistical analysis was performed using Graph-Pad Prism Software version 6. Unpaired, 2-tailed Student's t-test or two-way ANOVA followed by *post-hoc* Tukey's Test was used to calculate statistically significant differences between control and experimental groups. Data represents mean ± S.D. of 3 individual experiments. Difference between two groups were analyzed using Student's t-test (control and experimental group), along with that individual experimental groups were also compared using Unpaired, 2-tailed Student's t-test. $p < 0.05$ was set as the threshold for statistical significance between the control and various experimental groups.

RESULTS

Induction of Isoproterenol-Induced Cardiac Hypertrophy in PPAR α $^{-/-}$ Mice

HW/BW ratio which is considered as the index of cardiac hypertrophy was monitored following 14 days treatment of PPAR $\alpha^{-/-}$ mice with β-adrenergic receptor agonist, isoproterenol (**Figure 1A**). The HW/BW ratio in PPAR $\alpha^{-/-}$ mice (4.45 ± 0.29 mg/g) was significantly increased ($p > 0.0001$) compared to that of wild-type mice (3.44 ± 0.13 mg/g, $p > 0.0001$) which was similarly enhanced (4.6 ± 0.29 mg/g, $p > 0.0001$) on isoproterenol treatment (**Figure 1A**). Thus, PPAR $\alpha^{-/-}$ mice developed cardiac hypertrophy (4.45 ± 0.299 mg/g, $p > 0.0001$), even without isoproterenol treatment. As shown in **Figure 1A**, hypertrophy was also induced in normal mice due to isoproterenol treatment (4.00 ± 0.059 mg/g, $p > 0.0001$). To further confirm the development of hypertrophy, the heart weight to tibia length (HW/TL) ratio was calculated in the same experimental animals. As shown in **Figure 1B**, HW/TL ratio was significantly increased due to isoproterenol treatment both in wild-type as well as PPAR $\alpha^{-/-}$ mice compared to the untreated animal.

Fetal Gene Re-expression in Response to Isoproterenol Treatment

Cardiac hypertrophy is associated with cardiac remodeling, which brings about significant alterations in the cardiomyocytes including enhanced size, fibrosis and modification in transcriptional profile. One of such major changes is reverting back to fetal gene expression program. Atrial natriuretic peptide (ANP) and Brain natriuretic peptide (BNP) are specifically expressed in the heart in fetal stage and are switched off in the adult stage. Therefore, ANP and BNP are considered as markers of cardiac hypertrophy. Increased expression of ANP and BNP was observed both in wild type as well as PPAR $\alpha^{-/-}$mice in response to isoproterenol treatment (**Figure 1C**).

Myocardial Fibrosis in Isoproterenol-Treated Wild-Type and PPAR α $^{-/-}$ Mice

As cardiac hypertrophy results into myocardial fibrosis and increase in cardiomyocyte size, histological staining was carried out in heart tissue sections in both wild-type as well as PPAR $\alpha^{-/-}$ mice. Masson Trichome staining (**Figure 1D**) revealed collagen deposition in isoproterenol treated wild-type mice heart tissue sections when compared to untreated wild-type mice. Extensive collagen deposition pertaining to myocardial fibrosis was observed (**Figure 1D**) in isoproterenol-treated PPAR $\alpha^{-/-}$ mice heart tissue sections and similar results were observed in untreated PPAR $\alpha^{-/-}$ mice. Morphological examination using Haematoxylin and Eosin (H&E) staining revealed increased cardiomyocyte size in untreated PPAR $\alpha^{-/-}$ as well as isoproterenol-treated PPAR $\alpha^{-/-}$ mice (**Figure 1E**). The cardiomyocyte cross-section area (μm^2) revealed enhanced cardiomyocyte size in wild-type isoproterenol treated mice heart tissue, along with untreated PPAR $\alpha^{-/-}$ as well as isoproterenol-treated PPAR $\alpha^{-/-}$ mice heart tissue when compared to untreated wild-type mice (**Figure 1E**).

Echocardiographic Measurements Revealed Cardiac Dysfunction in PPAR α $^{-/-}$ Mice

Cardiac function was assessed in wild-type and PPAR $\alpha^{-/-}$ mice by echocardiography following 14 day isoproterenol treatment. Representative echocardiographic images have been displayed in **Figure 2A**, that were obtained in M-Mode from each group. Chronic administration of isoproterenol resulted in significant impact on cardiac function in isoproterenol treated wild-type as well as PPAR $\alpha^{-/-}$ mice. Ejection fraction and fractional shortening were significantly decreased to a similar degree in isoproterenol-treated wild type, untreated PPAR $\alpha^{-/-}$ as well as isoproterenol-treated PPAR $\alpha^{-/-}$ mice. Ejection fraction was decreased by 33.29% in isoproterenol-treated wild type, 39.4% in untreated PPAR $\alpha^{-/-}$ mice and 38.73% in isoproterenol-treated PPAR $\alpha^{-/-}$ mice (**Figure 2B**). Fractional shortening was decreased by 46.7% in isoproterenol-treated wild type mice, 53.5% in untreated PPAR $\alpha^{-/-}$ mice and 51.67% in isoproterenol-treated PPAR $\alpha^{-/-}$ mice (**Figure 2C**). LV mass was enhanced significantly in isoproterenol-treated wild type mice, and was further escalated in untreated PPAR $\alpha^{-/-}$ as well as isoproterenol-treated PPAR $\alpha^{-/-}$ mice when compared to untreated wild-type mice (**Figure 2D**). Cardiac output was decreased by 31% both in isoproterenol-treated wild type and untreated PPAR $\alpha^{-/-}$ mice and 24.57% in isoproterenol-treated PPAR $\alpha^{-/-}$ mice (**Figure 2E**). End-systolic and diastolic volumes were significantly increased in isoproterenol-treated wild type mice (65.24 and 34.86%, respectively), untreated PPAR $\alpha^{-/-}$ mice (105.5 and 71.7%) and isoproterenol-treated PPAR $\alpha^{-/-}$ mice (121.5 and 90.4%) as shown in **Figures 2F,G**.

Differential Protein Expression in Isoproterenol Treated PPAR α $^{-/-}$ Mice Heart

To explore the pathways that are controlled *via* PPAR α in cardiac hypertrophy, we performed protein profiling in heart
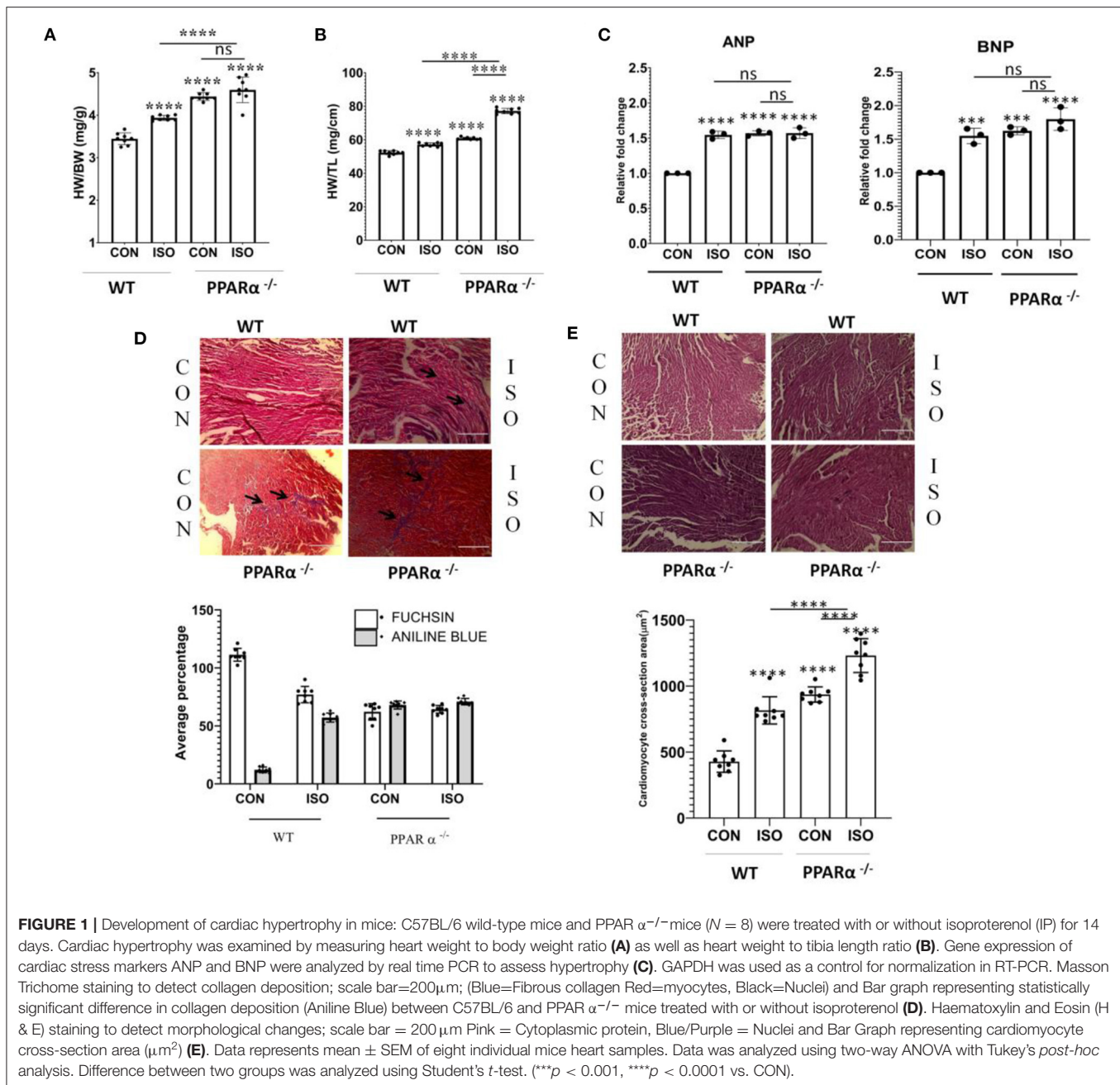
FIGURE 1 | Development of cardiac hypertrophy in mice: C57BL/6 wild-type mice and PPAR α$^{-/-}$ mice ($N = 8$) were treated with or without isoproterenol (IP) for 14 days. Cardiac hypertrophy was examined by measuring heart weight to body weight ratio **(A)** as well as heart weight to tibia length ratio **(B)**. Gene expression of cardiac stress markers ANP and BNP were analyzed by real time PCR to assess hypertrophy **(C)**. GAPDH was used as a control for normalization in RT-PCR. Masson Trichome staining to detect collagen deposition; scale bar=200μm; (Blue=Fibrous collagen Red=myocytes, Black=Nuclei) and Bar graph representing statistically significant difference in collagen deposition (Aniline Blue) between C57BL/6 and PPAR α$^{-/-}$ mice treated with or without isoproterenol **(D)**. Haematoxylin and Eosin (H & E) staining to detect morphological changes; scale bar = 200 μm Pink = Cytoplasmic protein, Blue/Purple = Nuclei and Bar Graph representing cardiomyocyte cross-section area (μm^2) **(E)**. Data represents mean ± SEM of eight individual mice heart samples. Data was analyzed using two-way ANOVA with Tukey's *post-hoc* analysis. Difference between two groups was analyzed using Student's *t*-test. (***$p < 0.001$, ****$p < 0.0001$ vs. CON).

tissues collected from wild type and PPAR α$^{-/-}$ mice by high resolution mass spectrometry. Differential protein expression pattern was observed, marked by an increase in mitochondrial fusion proteins like Opa1, fission protein FIS1 and down regulation of fatty acid binding protein like FABP7 (**Figure 3A**). PPAR α is a nuclear transcription factor which targets the genes involved in fatty acid β-oxidation and drives their transcription. Differential expression of PPAR α target genes as observed by proteomics analysis was also validated using RT-PCR. Fatty acid β-oxidation is a multi-step process and requires forefront play of multiple genes. Therefore, we examined several of its

target genes in the heart tissue of the same mice. As shown in **Figure 3B**, the mRNA levels of Acox1, Acaa1a, Acaa2 and Hsd17B12 were decreased in isoproterenol treated PPAR α$^{-/-}$ mice compared to wild type control. We also examined genes that are not transcriptionally regulated *via* PPAR α, but tend to alter in cardiac hypertrophy (PRKAG2 and EP300). As shown in **Figure 3D**, the expression of PRKAG2 and EP300 showed a significant decline in response to isoproterenol but no such down regulation was observed in the absence of PPAR α. Though PRKAG2 expression was down regulated in presence of isoproterenol, it was increased irrespective of PPAR α, whereas
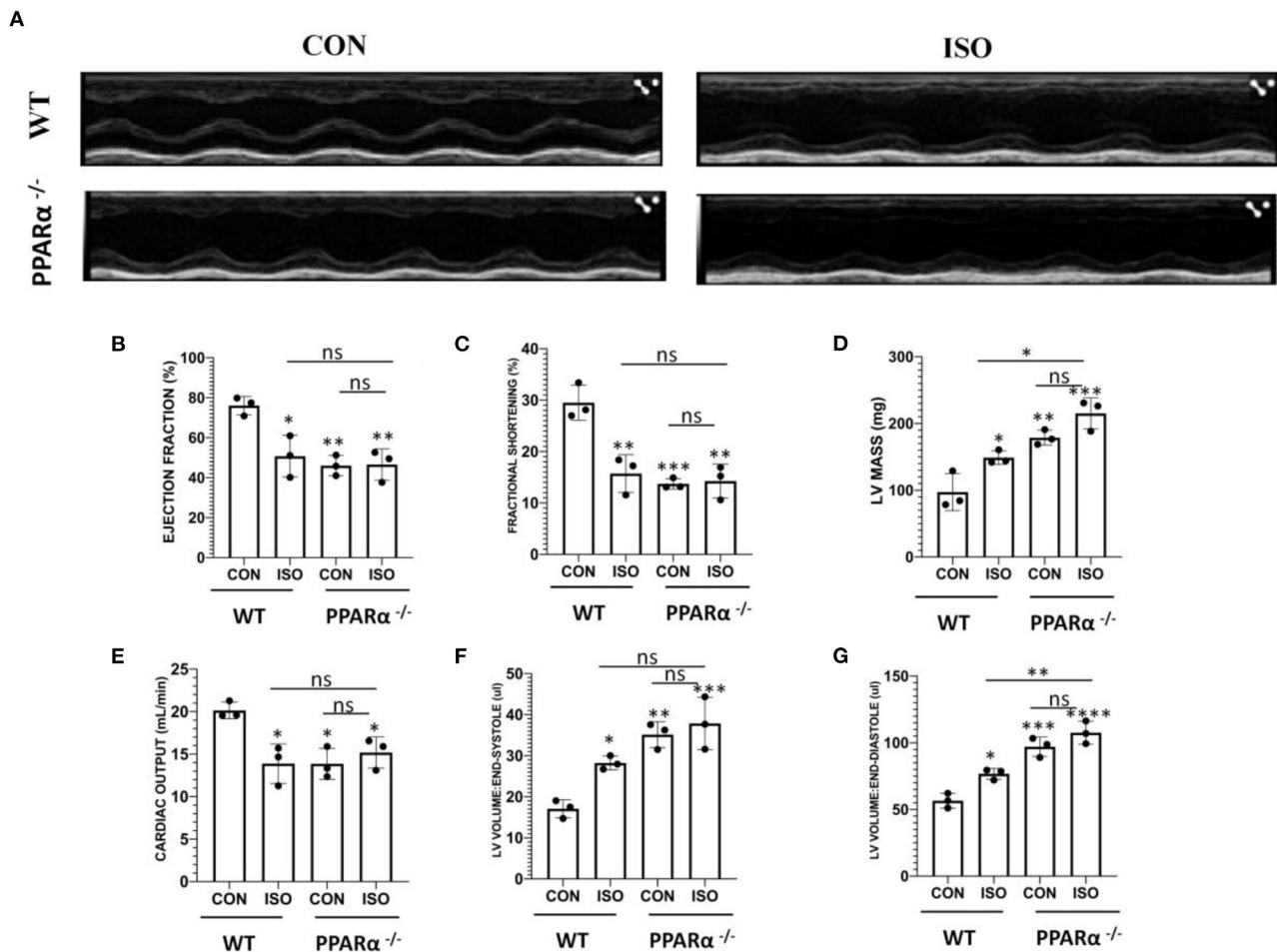
FIGURE 2 | Echocardiography for *in vivo* assesment of cardiac function: Cardiac function was assessed by echocardiography in wild-type and PPAR $\alpha^{-/-}$ mice. Representative images from parasternal short axis view of the heart acquired in M-Mode **(A)**. Bar graphs showing ejection fraction **(B)**, fractional shortening **(C)**, LV mass **(D)**, cardiac output **(E)**, LV volume in end-systole **(F)** LV volume in end-diastole **(G)**. Data was analyzed using two-way ANOVA with Tukey's post-hoc analysis. (*$p < 0.05$, **$p < 0.01$, ***$p < 0.001$, ****$p < 0.0001$ vs. CON).

EP300 remained unaltered. The absence of PPAR α thus marks a reduction in fatty-acid β-oxidation *via* significant reduction in the genes that are essential in the process. As isoproterenol treatment in PPAR $\alpha^{-/-}$ mice exacerbates stress conditions that triggers apoptosis, we also examined some of the apoptotic markers that showed striking alteration in the proteome profile. Interestingly, SIEVE-based relative quantification revealed about 2-fold down regulation of Annexin V in PPAR $\alpha^{-/-}$ mice. In Isoproterenol-treated PPAR $\alpha^{-/-}$ mice, similar down regulation of Annexin V was observed. Panther classification of proteins by pathway analysis showed specific changes in cellular processes (**Figure 3B**). Interestingly, it revealed unexpected decrease in p53 pathway in the absence of PPAR α that is one of the inducers of apoptosis. Annexin V is a Ca^{++} dependent phospholipid binding protein, and actively binds phosphatidylserine, that is expressed on the outer leaflet of plasma membrane during apoptosis. Since most of the studies indicated the involvement of apoptosis in stress conditions, we further validated it *via* western blotting

for AnnexinV, and observed reduced levels in the PPAR $\alpha^{-/-}$ as well as isoproterenol-treated PPAR $\alpha^{-/-}$ mice (**Figure 3C**). Western Blot was also performed for Opa1 to further validate the differential protein expression pattern. Opa1 expression was decreased on isoproterenol treatment in wild-type mice whereas normal level was observed in the absence of PPAR α (**Figure 3C**). Since hypertrophy associated cardiomyocyte apoptosis is a well-established phenomenon and our study revealed the down-regulation of Annexin V in isoproterenol treated PPAR $\alpha^{-/-}$ mice, we further examined other apoptotic markers in the same tissue.

Down Regulation of Major Apoptotic Markers

Hypertrophy associated cardiac stress induces up regulation of critical apoptotic markers and directs the cell toward programmed cell death. In context to the previous results (**Figure 3**), we examined anti-apoptotic markers Bcl-2, Bcl-x,
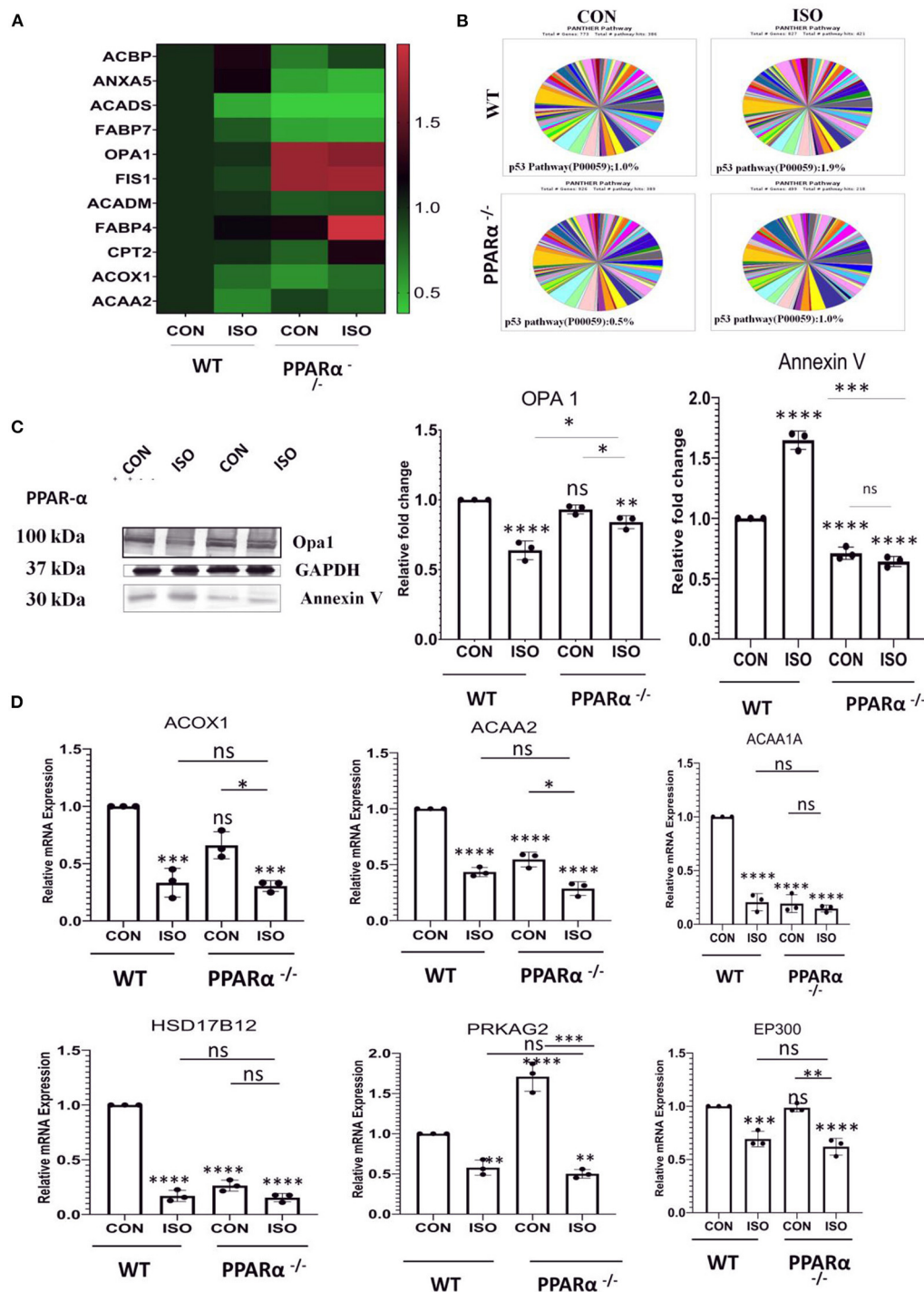
FIGURE 3 | Identification of impaired signaling pathways in PPAR $\alpha^{-/-}$ mice heart by Proteomic analysis: Cardiac tissue proteins were analyzed by Orbitrap LC-MS (*N* = 5) followed by relative quantification of differentially expressed protein by SIEVE **(A)**. The validation of proteomic results for a subset of candidates was performed by RT-PCR using heart tissue obtained from the experiments as mentioned earlier. Expression of PPAR α target genes, such as ACOX1, Acaa1a, ACAA2, HSD17B12 along with genes independent of PPAR α regulation like PRKAG2 and EP300 were examined **(B)**. Enrichment of specific pathways were analyzed using Panther classification **(C)**. The expression of Annexin V and OPA 1 was examined by immunoblotting which was quantitated by densitometric analysis **(D)**. GAPDH was used as the loading control. Data represents mean ± S.D. of 3 separate experiments. Data was analyzed using two-way ANOVA with Tukey's *post-hoc* analysis. Difference between two groups was analyzed using Student's *t*-test. (*$p < 0.05$, **$p < 0.01$, ***$p < 0.001$, ****$p < 0.0001$ vs. CON).

Catalase, HO-1, HO-2, Hsp70, Hsp27 and Hsp60 along with pro-apoptotic markers like Bad, Caspase 3, Claspin, Cytochrome C, FAS/CD95, Mcl-1, p53, p27/kip1, Smac/Diablo, TRAIL R2/TNFRSF10B, TNFR1/TNFRSF1A in wild-type controls as well as PPAR $\alpha^{-/-}$ mice, treated with isoproterenol using the proteome profiler (**Supplementary Figure 2**). Pro-apoptotic markers were down regulated in PPAR $\alpha^{-/-}$ mice whereas up regulation of anti-apoptotic markers was observed except Hsp27 as well as Hsp60, suggesting compensatory role of Hsp70 as all the three Heat shock proteins function to inhibit apoptosis. To elucidate whether this downregulation was limited to isoproterenol induced cardiac hypertrophy in PPAR $\alpha^{-/-}$ mice, we used high cholesterol diet fed PPAR $\alpha^{-/-}$ mice as another experimental model of pathological hypertrophy. Cardiac Hypertrophy in HCD fed PPAR $\alpha^{-/-}$ mice was confirmed *via* HW/BW ratio as well as HW/TL ratio (**Supplementary Figure 1**). Extensive collagen deposition and increased cardiomyocyte size further confirmed the development of cardiac hypertrophy in HCD fed PPAR $\alpha^{-/-}$ mice (**Supplementary Figure 1**). Significant down regulation of p53 and cleaved Caspase 9 was observed *via* immunoblotting analysis in PPAR $\alpha^{-/-}$ mice as well as isoproterenol-treated PPAR $\alpha^{-/-}$ mice when compared to wild-type control as well as isoproterenol-treated wild-type mice. Another apoptotic marker, c-PARP that is enhanced in isoproterenol-treated wild type mice, showed no change in PPAR $\alpha^{-/-}$ mice, but was significantly decreased in isoproterenol-treated PPAR $\alpha^{-/-}$ mice (**Figure 4A**). Similar results were observed for c-PARP as well as p53 protein in HCD fed PPAR $\alpha^{-/-}$ mice suggesting down regulation of apoptosis in the absence of PPAR α when stimulated with hypertrophy inducing factors (**Figure 4B**). Since caspase 9 is a key player in the formation of apoptosome that drives intrinsic apoptotic pathway, down regulation of cleaved caspase-9 suggests hindrance to intrinsic apoptotic pathway in the absence of PPAR α. So, it led us to further analyse the mediators of apoptosis.

Regulation of p53 by PPAR α

It is established that p53 has a critical role in apoptosis and it binds to PPAR α. p53 is also known to be a positive regulator of fatty-acid β-oxidation. Therefore, we analyzed the fate of p53 in the absence of PPAR α. Isoproterenol-treatment of wild-type mice resulted in up regulation of p53, whereas the same treatment in PPAR $\alpha^{-/-}$ mice failed to escalate its levels (**Figure 4A**). Instead, there was a down regulation of p53 in PPAR $\alpha^{-/-}$ mice as well as in isoproterenol-treated PPAR $\alpha^{-/-}$ mice. Normally, p53 is very unstable but upon binding to Dbc1 its stability is improved. Dbc1 competes with Mdm2, a negative regulator, to promote p53 stability. Dbc1 expression was observed in PPAR $\alpha^{-/-}$ mice and it was found to be reduced along with p53 (**Figure 4A**). Thereby, suggesting a direct co-relation to PPAR α. To further understand the mechanism of p53 down regulation, we examined the levels of Mdm2. Mdm2 is known to negatively regulate p53 by preventing its physical binding to DNA as well as targeting it for proteasomal degradation. Mdm2 showed elevated levels in the absence of PPAR α (**Figure 4A**). Enhanced level of Mdm2 thereby explained the down regulation of p53. This data

indicates that the p53-mediated apoptotic response was inhibited due to the absence of PPAR α.

Modulation of PTEN in the Absence of PPARα

PTEN that is an inducer of apoptosis in normal conditions and is transcriptionally activated *via* PPAR α was analyzed using western blot to understand the impact of PPAR α on apoptosis in cardiac hypertrophy. Down regulation of PTEN correlated with the absence of PPARα as observed in **Figure 5A**, whereas wild-type control showed normal PTEN level that was enhanced on isoproterenol treatment. Western Blot analysis of PTEN in PPAR $\alpha^{-/-}$ mice as well as High-Cholesterol Diet fed PPAR $\alpha^{-/-}$ mice showed similar pattern as hypertrophic stimulation in PPAR $\alpha^{-/-}$ mice failed to enhance PTEN levels (**Figure 5B**). Further downstream signaling proteins were analyzed like p-Akt and mTOR as well as pro survival protein Bcl-2, all of which showed upregulation in the absence of PPAR α. This suggested an inclination toward survival upon hypertrophic stimulation as observed by the enhanced protein levels in PPAR $\alpha^{-/-}$ as well as isoproterenol-treated PPAR $\alpha^{-/-}$ mice when compared to wild-type control as well as isoproterenol-treated wild-type mice (**Supplementary Figure 3**). Similar results were obtained in high cholesterol diet fed PPAR $\alpha^{-/-}$ mice wherein enhanced levels of mTOR was observed *via* immunoblotting, although no significant change was observed in pAkt protein levels between normal chow diet fed PPAR $\alpha^{-/-}$ mice and HCD fed PPAR $\alpha^{-/-}$ mice (**Supplementary Figure 3**).

Up Regulation of Autophagy Markers

Autophagy is negatively regulated by mTOR and the down regulation of apoptosis indicated the switching on a compensatory mechanism for managing the stress-induced cardiomyocyte. Autophagy is known to play essential role in quality control through clearance of damaged proteins and organelles. Therefore, we examined the level of autophagy markers. As shown in **Figures 6A,B**, the levels of the autophagy markers such as p62, Beclin1 and LC3 A/B showed a significant increase in heart tissue of PPAR $\alpha^{-/-}$ mice when compared to control ($p < 0.001$). Both PPAR $\alpha^{-/-}$ as well as isoproterenol-treated PPAR $\alpha^{-/-}$ mice showed an upregulation when compared to wild-type control as well as isoproterenol-treated wild-type mice indicating an induction of autophagy and an inclination toward adaptive response that might help in sustaining the cardiac stress (**Figure 6A**). HCD fed PPAR $\alpha^{-/-}$ mice showed similar increased levels of autophagy markers p62, Beclin1 and LC3A/B when compared to normal chow diet fed PPAR $\alpha^{-/-}$ mice indicating an upsurge toward autophagy in PPAR $\alpha^{-/-}$ mice upon hypertrophic stimulation.

Upregulation of Atg 3, 5 and 7 in the Absence of PPAR α

Atg genes that are known to mediate autophagy were analyzed using western Blot. Atg 3, 5 and 7 in PPAR $\alpha^{-/-}$ as well as isoproterenol-treated PPAR $\alpha^{-/-}$ mice were found to be upregulated when compared to wild-type control as well as isoproterenol-treated wild-type mice indicating an enhanced
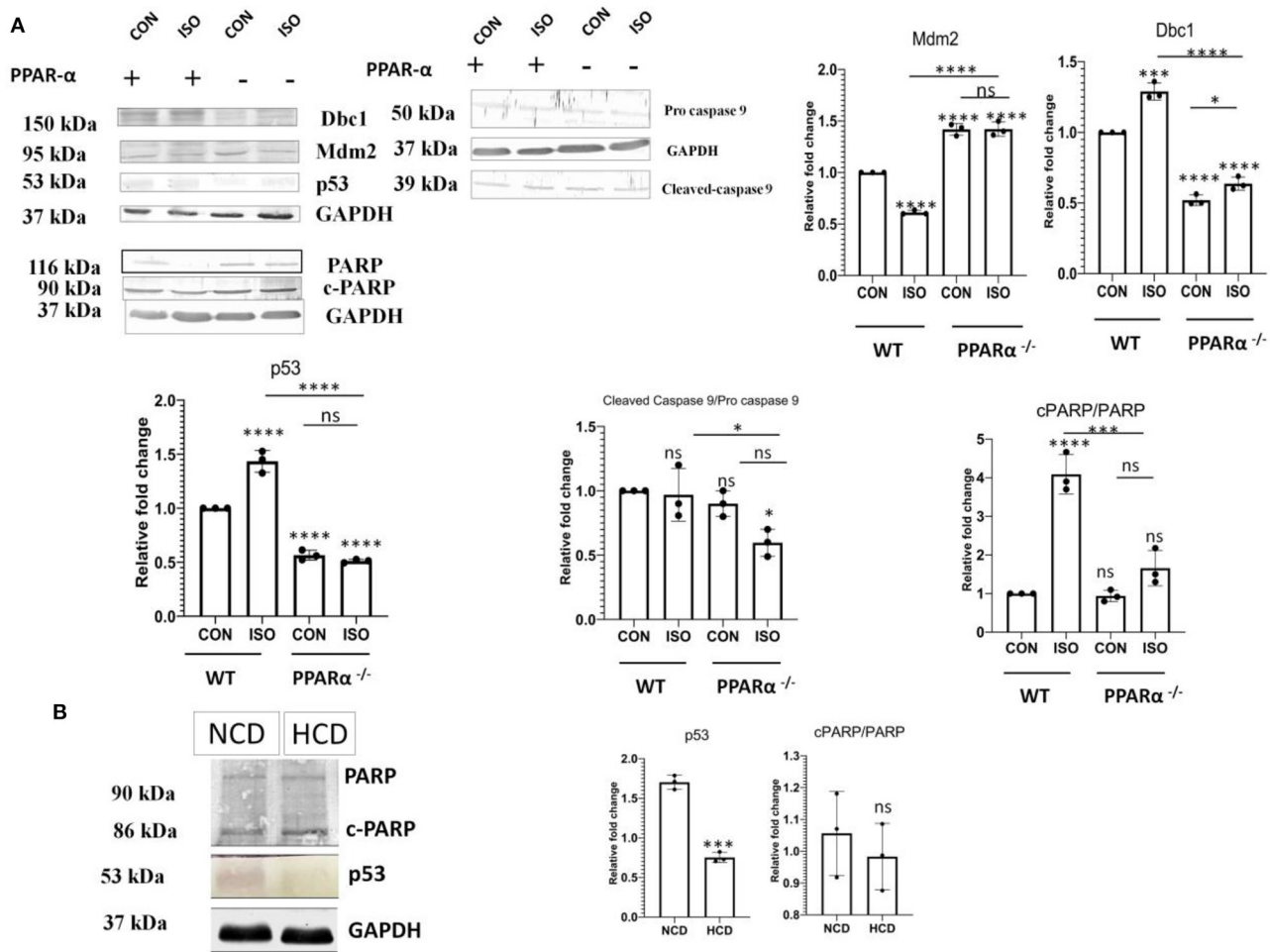
FIGURE 4 | Attenuation of Apoptotic markers. Protein levels of apoptotic markers p53, Dbc1, Mdm2, c-caspase 9 and c-PARP in mice heart tissue obtained from the experiments as mentioned earlier were compared *via* immunoblot **(A)**. Protein levels of apoptotic markers p53 and c-PARP in normal chow diet fed (NCD) PPAR α $^{-/-}$ mice as well as high cholesterol diet fed (HCD) PPAR α $^{-/-}$ mice compared using immunoblot **(B)**. GAPDH was used as a loading control. Data represents mean ± S.D. of three individual experiments. Data was analyzed using two-way ANOVA with Tukey's *post-hoc* analysis. Difference between two groups was analyzed using Student's *t*-test. (*$p < 0.05$, ***$p < 0.001$, ****$p < 0.0001$ vs. CON).

autophagy even in the presence of mTOR (**Figure 7A**). Moreover, HCD fed PPAR α$^{-/-}$ mice resembled this pattern of Atg genes when compared to NCD fed PPAR α$^{-/-}$ mice, thus Atg genes are substantially increased in PPAR α$^{-/-}$ mice specifically when stimulated with hypertrophy inducing factor (**Figure 7B**). To further understand this autophagy induction even in the presence of mTOR, calpain protein levels were analyzed. Calpain is an inhibitor of autophagy and its downregulation mediates mTOR independent autophagy. Significant decrease in the protein levels of calpain in both the experimental models explained the increase in autophagy in a mTOR-independent manner (**Figures 7A,B**).

Downregulation of PTEN and Induction of Autophagy in Cardiomyocytes *in vitro*

Our previous observations demonstrated the downregulation of apoptosis followed by an increase in autophagy in hypertrophy induced in PPAR α$^{-/-}$ mice. Next, we further investigated the

effects of PPAR α absence upon hypertrophic stimulation *in vitro*. Neonatal rat ventricular myocytes (NRVM) were treated with phenylephrine (PE) a β-adrenergic receptor agonist for 48 h and PPAR α was inhibited using GW6471, PPAR α antagonist. Consistent with previous results, autophagy assay revealed enhanced autophagy in GW6471 incubated myocytes, even in the presence of PE when compared to control as was indicated by an elevated number of bright blue dot stained autophagic vacuoles (**Figure 8A**). Confocal microscopy revealed sarcomeric striation pattern through α-actinin staining (pink) along with the autophagic vacuoles (**Figure 8A**). PE alone failed to show such increase in autophagy, suggesting that hypertrophy in the absence of PPAR α antagonist, shows no such inclination toward autophagy as the absence of PPAR α mediates this alteration. Measurement of relative fluorescence performed in H9C2 cardiomyocytes using microplate reader revealed similarly enhanced autophagy when PPAR α was
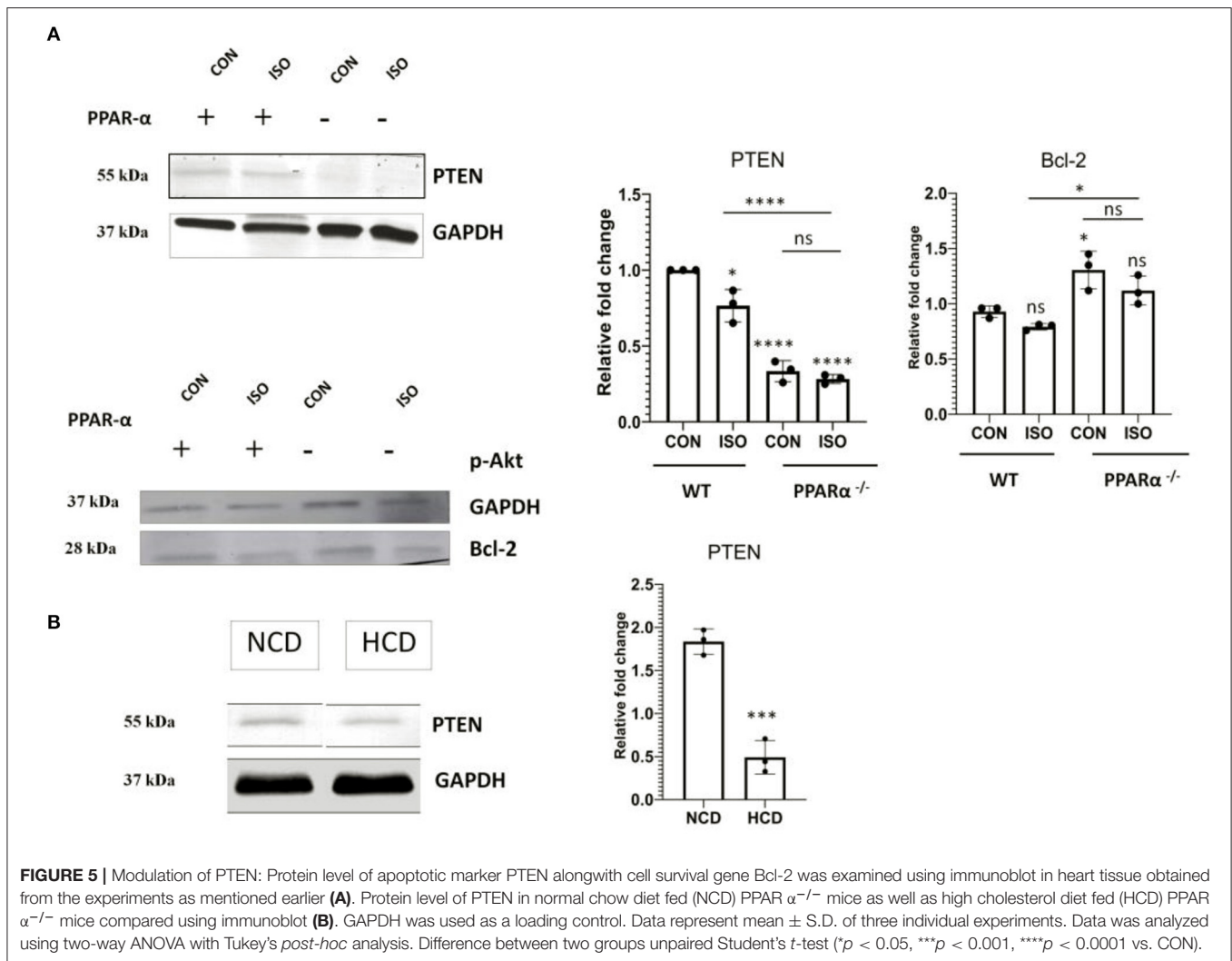
FIGURE 5 | Modulation of PTEN: Protein level of apoptotic marker PTEN alongwith cell survival gene Bcl-2 was examined using immunoblot in heart tissue obtained from the experiments as mentioned earlier **(A)**. Protein level of PTEN in normal chow diet fed (NCD) PPAR α$^{-/-}$ mice as well as high cholesterol diet fed (HCD) PPAR α$^{-/-}$ mice compared using immunoblot **(B)**. GAPDH was used as a loading control. Data represent mean ± S.D. of three individual experiments. Data was analyzed using two-way ANOVA with Tukey's *post-hoc* analysis. Difference between two groups unpaired Student's *t*-test (*$p < 0.05$, ***$p < 0.001$, ****$p < 0.0001$ vs. CON).
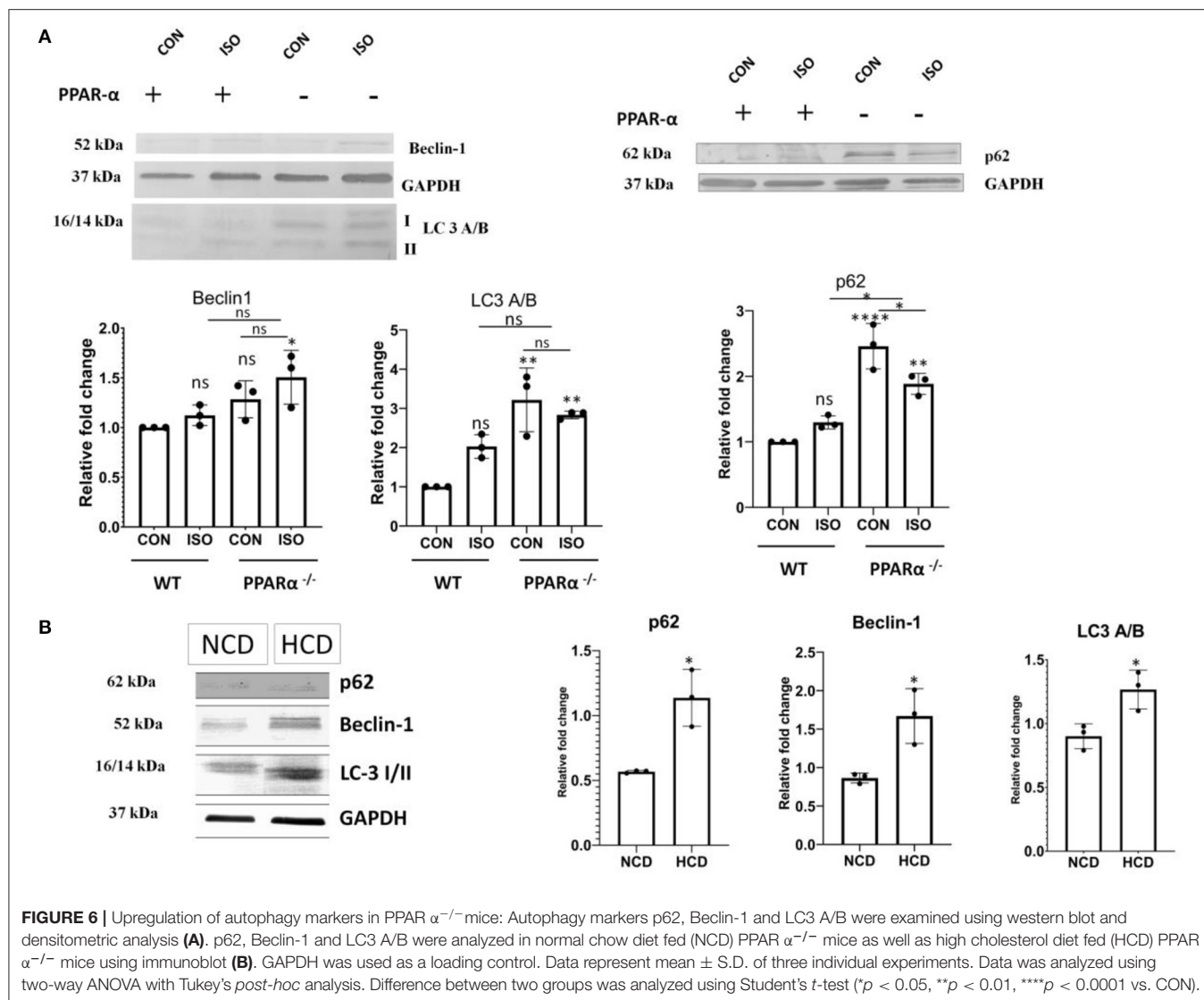
blocked by GW6471. Also, cholesterol incubated cells in the presence of GW6471 showed increase in autophagy when compared to cells treated with cholesterol alone (**Figure 8B**). To elucidate the status of apoptosis *in vitro*, PTEN expression was analyzed in H9C2 cells which was found to be increased in the presence of PE which was significantly down regulated in the presence of GW6471.Autophagy marker Beclin1 was checked *in vitro* and the results somewhat resembled *in vivo* data and showed slight increase in comparison to untreated control cells, whereas apoptosis marker cPARP showed no change between the experimental groups (**Figure 8C**).

DISCUSSION

The myocardium responds to mechanical as well neurohumoral stimuli by adjusting myocytes size accompanied with intracellular molecular switching for maintaining normal functions (24–26). However, persistence of hypertrophic conditions may lead to maladaptation and cardiac failure (27–29). Such maladaptation is partly due to the failure of

the intracellular machineries for coping up to the altered hemodynamics (30). Impaired PGC 1 α – PPAR α signaling, mitochondrial dysfunctions and imbalanced bioenergetics are known to contribute significantly to this maladaptation of hypertrophic myocardium (31–33). It has been observed in previous studies that hypertrophy- induced post–translational modification of PPAR α causes a decline in the ligand sensitivity and expression of PPAR α, thus is directly associated with the impaired fatty acid oxidation (5). This could be suggestive of the fact that cardiomyocytes undergo certain adaptive modifications to meet up with the increase in the energy demand in response to hypertrophic stimuli. Here we show that PPAR α plays a central role in the adaptive phase of the cardiomyocytes by driving toward autophagy and preventing apoptosis. We desired to study these alterations in the cardiac cells for which, we used isoproterenol to develop cardiac hypertrophy in PPAR α$^{-/-}$ mice model.

Intra – peritoneal injection of isoproterenol for duration of 2 weeks resulted in the development of hypertrophied hearts in the PPAR α$^{-/-}$ mice as evident from HW/BW ratio and the HW/TL

FIGURE 6 | Upregulation of autophagy markers in PPAR $\alpha^{-/-}$ mice: Autophagy markers p62, Beclin-1 and LC3 A/B were examined using western blot and densitometric analysis **(A)**. p62, Beclin-1 and LC3 A/B were analyzed in normal chow diet fed (NCD) PPAR $\alpha^{-/-}$ mice as well as high cholesterol diet fed (HCD) PPAR $\alpha^{-/-}$ mice using immunoblot **(B)**. GAPDH was used as a loading control. Data represent mean ± S.D. of three individual experiments. Data was analyzed using two-way ANOVA with Tukey's *post-hoc* analysis. Difference between two groups was analyzed using Student's *t*-test (*$p < 0.05$, **$p < 0.01$, ****$p < 0.0001$ vs. CON).
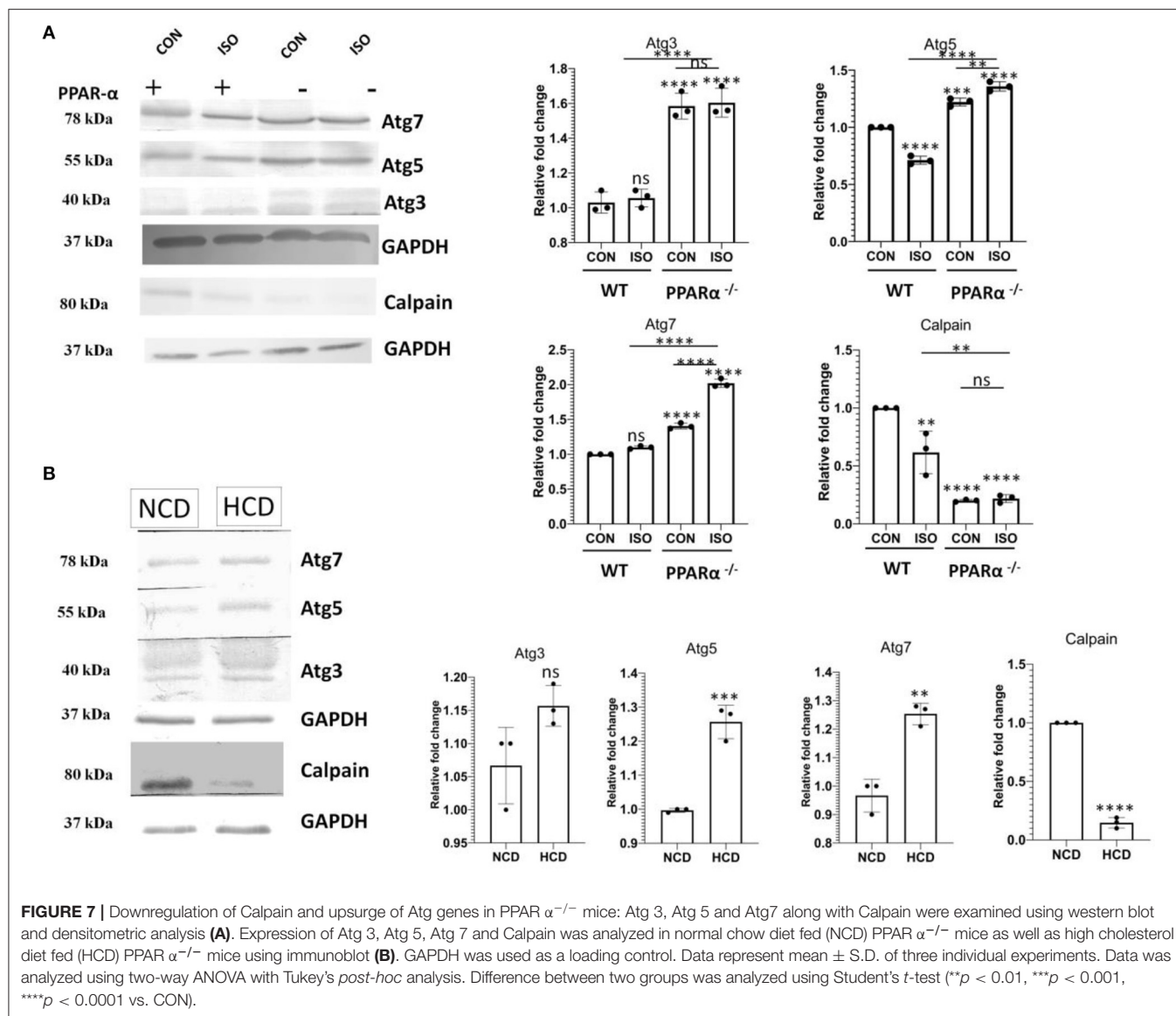
ratio. It is observed that hypertrophy in isoproterenol-treated wild-type mice and isoproterenol-treated PPAR $\alpha^{-/-}$ mice were more pronounced when compared to the control (untreated wild type). Additionally, the development of hypertrophy is validated by increased expression of hypertrophic marker genes such as ANP and BNP. Histopathological study revealed increased collagen deposition indicating extensive fibrosis in the absence of PPAR α which is the hallmark of cardiac remodeling. The absence of PPAR α thereby seems to be associated with myocardial fibrosis that tends to be an outcome of the stress in its absence.

Consistent with hypertrophic pathophysiology, the PPAR $\alpha^{-/-}$ mice show significant alterations in heart functions which are more pronounced due to treatment with isoproterenol. Reduction in Ejection fraction as well as Fractional shortening occurred in both the isoproterenol-treated groups. In the absence of isoproterenol, these parameters are compromised in PPAR $\alpha^{-/-}$ mice suggesting that absence of PPAR α is enough to cause cardiac dysfunctions. Evidently, cardiac output showed marked decline in all the groups when compared to wild-type

control further affirming to the impaired heart functions in hypertrophied heart. Increased LV mass further confirmed the development of cardiac hypertrophy in the mice model.

We used the protein profiling data generated from the mass spectrometric analysis of the heart tissue to examine the proteins that, in deficiency of PPAR α, are closely associated with cardiac stress and are involved, especially, in mitochondrial dysfunction and impaired fatty acid β-oxidation pathway. A marked increase in the mitochondrial fusion protein like Opa1, fission protein FIS1 while a decrease in the levels of FABP7—a fatty acid binding protein, ACAA1A, ACOX1 and several such critical genes involved in the Fatty acid β-oxidation were observed, thereby reflecting the impact of absence of PPAR α in distinct signaling pathways. Validation of the mass spectrometric data through both immunoblot as well as qpcr, revealed a similar expression pattern. One of the striking changes observed was the decline in apoptotic pathway. Surprisingly, SIEVE-based relative quantification, as well as western blot analysis, revealed about a significant down regulation of Annexin V (an apoptotic

FIGURE 7 | Downregulation of Calpain and upsurge of Atg genes in PPAR $\alpha^{-/-}$ mice: Atg 3, Atg 5 and Atg7 along with Calpain were examined using western blot and densitometric analysis **(A)**. Expression of Atg 3, Atg 5, Atg 7 and Calpain was analyzed in normal chow diet fed (NCD) PPAR $\alpha^{-/-}$ mice as well as high cholesterol diet fed (HCD) PPAR $\alpha^{-/-}$ mice using immunoblot **(B)**. GAPDH was used as a loading control. Data represent mean ± S.D. of three individual experiments. Data was analyzed using two-way ANOVA with Tukey's *post-hoc* analysis. Difference between two groups was analyzed using Student's *t*-test (**$p < 0.01$, ***$p < 0.001$, ****$p < 0.0001$ vs. CON).

marker) in both the isoproterenol—treated and untreated PPAR $\alpha^{-/-}$ mice unlike what has been reported in previous studies. Isoproterenol-induced cardiac hypertrophy has been related with increased stress, that exhibits cardiac remodeling whereas in this scenario the results indicated an abrupt change in p53-induced apoptotic pathway in the absence of PPAR α, that was therefore looked further into detail to understand the mechanism.

The earlier studies related the involvement of apoptosis in the pathogenesis of cardiac remodeling (12, 34–36). As treatment of PPAR $\alpha^{-/-}$ mice with isoproterenol aggravates stress conditions, it is likely that apoptosis is triggered under those conditions. So, to confirm the observed data, proteome profiler Antibody Array was used to assess multiple genes regulating apoptosis. Several anti-apoptotic genes like Bcl-2, Bcl-x, HO-1 were observed to be either up regulated or showing no change in PPAR $\alpha^{-/-}$ mice and isoproterenol-treated PPAR $\alpha^{-/-}$ mice, suggesting moderate inclination toward survival while most of the pro apoptotic genes like Bad, Caspase 3, Claspin, Cytochrome C, FAS/CD95,

Mcl-1, p53, p27/kip1, Smac/Diablo, TRAIL R2/TNFRSF10B, TNFR1/TNFRSF1A showed down regulation in the PPAR $\alpha^{-/-}$ as well as isoproterenol treated PPAR $\alpha^{-/-}$ mice when compared to normal wild-type mice. Isoproterenol-treated wild-type mice as expected revealed upsurge in the apoptotic markers exhibiting the impact of isoproterenol-induced cardiac remodeling that initiates stress conditions resulting in cardiomyocyte death. Therefore, the absence of PPAR α leads to perturbation of the genes involved in the apoptotic pathway in the heart as observed from the proteome profiler data, where unlike wild-type isoproterenol treated mice there was no increase in apoptotic markers level. Thus, we wished to validate the same proteome profile data of the apoptotic markers in our test model using western blot.

To further confirm this phenomenon is dependent on PPAR α, another experimental model was used, that is high-cholesterol diet fed PPAR $\alpha^{-/-}$ mice model, wherein the implicated pathological cardiac hypertrophy was independent of
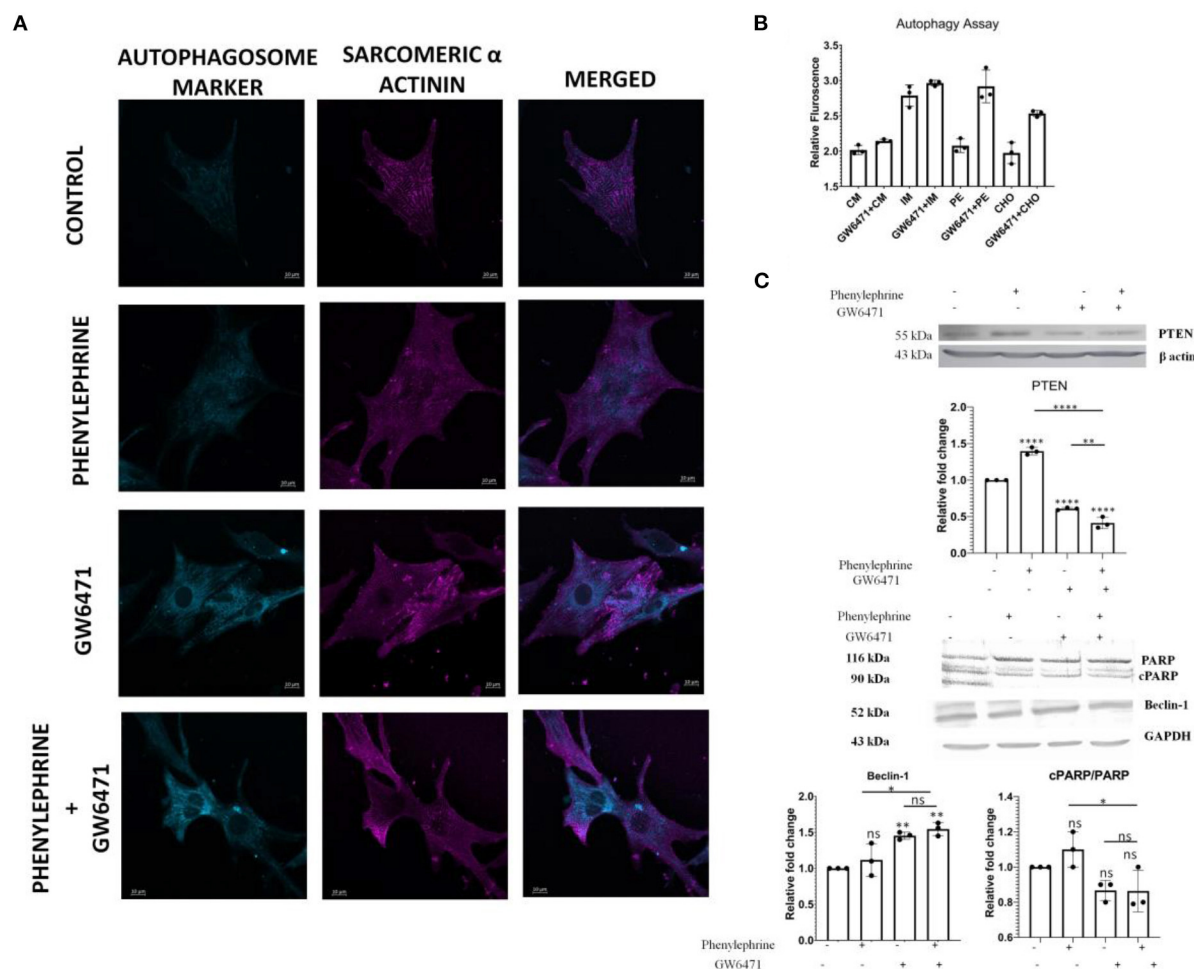
FIGURE 8 | Enhanced Autophagy and alteration of apoptosis and autophagy markers in H9C2 cell line: Representative Confocal images of Autophagy Assay in NRVMs of different treatment groups; scale bar = 10 μm **(A)**. Bar Graph depicting the relative fluorescence in the indicated experiments in H9C2 cell line **(B)**. Western Blot analysis and the quantitative results of PTEN, cPARP/ PARP and Beclin1 **(C)**. Data represent mean ± S.D. of 3 individual experiments. α-actin was used as a loading control. Data was analyzed using two-way ANOVA with Tukey's *post-hoc* analysis. Difference between two groups was analyzed using Student's *t*-test (*$p < 0.05$, **$p < 0.01$, ****$p < 0.0001$ vs. CON).

isoproterenol treatment. Previous reports have already suggested the involvement of high cholesterol diet in inducing pathological cardiac hypertrophy but the study has been mostly limited to wild-type mice and its impact on PPAR α $^{-/-}$ mice is yet to be explored. Therefore, in our study PPAR α $^{-/-}$ mice fed with high-cholesterol diet for 8 weeks were used, wherein the cardiac hypertrophy was established and the hypertrophic markers like ANP and BNP also showed an upsurge as expected, apart from these, the Masson Trichome staining revealed significant accumulation of collagen in both PPAR α$^{-/-}$ mice as well as HCD fed PPAR α$^{-/-}$ mice.

Apoptotic markers were further assessed using immunoblot in both the experimental models. Interestingly, western blot analysis revealed a significant reduction in Caspase-9 in the absence of PPAR α whereas no significant changes were found in c-PARP protein levels. Since Caspase 9 is one of the key components of the intrinsic apoptotic pathway (37, 38), its down regulation implies possible interference in the basic apoptotic

signaling induced by the deficiency of PPAR α as similar results were observed in both the cardiac hypertrophy models. Further analysis of the mediators of apoptosis using Panther based classifications divulged a surprising decrease in p53 pathway in the absence of PPAR α. It is a well-known fact that p53 is an inducer of stress-activated apoptosis (39–41). The recent discovery of the binding potential of p53 to PPAR α and its role as a positive regulator of fatty-acid β-oxidation, led us to analyze the fate of p53 in PPAR α$^{-/-}$ mice (42). A significant downregulation was observed in both normal and hypertrophied PPAR α$^{-/-}$ mice in contrast to the up-regulation in WT mice (treated as well as control). To confirm a direct relationship between p53 and PPAR α, we examined the expression profile of Dbc1 and Mdm2. Previous reports have shown the importance of Dbc1 in p53 stabilization by competing with Mdm2, a negative regulator of p53 stability (43, 44). Therefore, it is likely that p53 downregulation might be a result of the decline in the expression of Dbc1 and an elevation in Mdm2 expression. In support of

our hypothesis Dbc1 expression was found to be reduced in PPAR $\alpha^{-/-}$ mice along with p53, in contrast, to an increase in Mdm2 expression. Thus, PPAR α could be suggested to hinder p53-mediated apoptotic response. Both PPAR $\alpha^{-/-}$ mice as well as isoproterenol-treated PPAR $\alpha^{-/-}$ mice along with the second experimental model i.e. PPAR $\alpha^{-/-}$ mice as well as HCD fed PPAR $\alpha^{-/-}$ mice showed similar pattern of the down regulation of the apoptotic markers thereby suggesting the involvement of PPAR α.

To investigate the role of PPAR α in down regulation of apoptosis in the cardiomyocytes and the underlying mechanism, the PTEN/pAkt/mTOR pathway was dissected. PTEN has emerged as a major regulator of apoptosis and many reports have suggested the critical role of PTEN in modulating apoptosis, apart from the previous studies that have also addressed the PPAR α dependent transcriptional regulation of PTEN (45). Western blot analysis of PTEN revealed down regulation in PPAR $\alpha^{-/-}$, mice both in the response to isoproterenol as well as HCD thereby indicating a causative role of PPAR α with the down regulation of PTEN. Since PTEN/pAkt/mTOR pathway is a conglomeration of different signaling network that involves, cell survival, protein synthesis and regulation of apoptosis, so pAkt as well as mTOR were also analyzed using western blot to reveal the preference of cardiomyocytes toward survival when apoptosis is compromised. There was no significant change in pAkt but the up regulation of mTOR in PPAR $\alpha^{-/-}$ mice could be explained by the nutrient rich condition in the absence of PPAR α due to the accumulation of fatty acids as Fatty acid β-oxidation was significantly affected.

Since many reports have addressed the regulation of autophagy *via* mTOR, so the autophagy pathway was analyzed in PPAR $\alpha^{-/-}$ mice. The significant increase in mTOR suggested a parallel down regulation of autophagy. Surprisingly, various autophagy markers like p62, Beclin1 and LC3 A/B revealed significant up regulation in the absence of PPAR α expression. The increase in p62 could be explained as the role of p62 is subjective to the cell type. The increase in autophagic flux in the heart, results in concurrent upregulation of p62 that plays a protective role in aggresome formation and in the activation of autophagy in stress-induced cardiomyocytes. Since mTOR negatively regulates autophagy, so mTOR-independent pathway supposedly maintains an upsurge in the autophagy markers. To further confirm this, the protein of level of Calpain-1, that is a renowned mTOR independent modulator of autophagy was analyzed, and reduction in Calpain in the absence of PPAR α explains the increase in autophagy that does not correlate with the increase in mTOR (46). Significant increase in Autophagy genes like Atg3, Atg 5, Atg7, and Atg12 were observed in both isoproterenol-treated as well as high cholesterol diet fed PPAR $\alpha^{-/-}$ mice. The data explains although the phenomenon is PPAR α dependent but is exhibited mostly in the presence of a hypertrophic signal.

To further validate the down regulation in apoptosis followed by an upsurge in autophagy in cardiomyocytes in the absence of PPAR α, experiments were also carried out in H9C2 cell line. GW6471 was used to block PPAR α and cardiac hypertrophy was induced using phenylephrine that is a well-known inducer of cardiac hypertrophy (47). Western blot analysis of PTEN resembled the similar pattern as observed *in vitro* thereby indicating PPAR α dependent phenomenon. Increase in autophagy marker Beclin1 was observed in PE-treated H9C2 cell line in the absence of PPAR α whereas apoptotic marker cPARP showed no significant change. To further validate the increase in autophagy, autophagosome assay was performed in H9C2 cell line, wherein serum starved cardiomyocytes that were used as positive control for autophagy were compared with PE treated as well as GW6471 incubated cell. Elevation of autophagosome formation was observed in the presence of GW6471 when compared to PE treated cells, indicating the enhanced autophagy as observed *in vivo* in the absence of PPAR α. Cholesterol treated H9C2 cell line in the presence of GW6471 showed significant increase in autophagy when compared to cells incubated with cholesterol alone, thereby indicating the absence of PPAR α might function as pre-requisite to mediate such change in signaling.
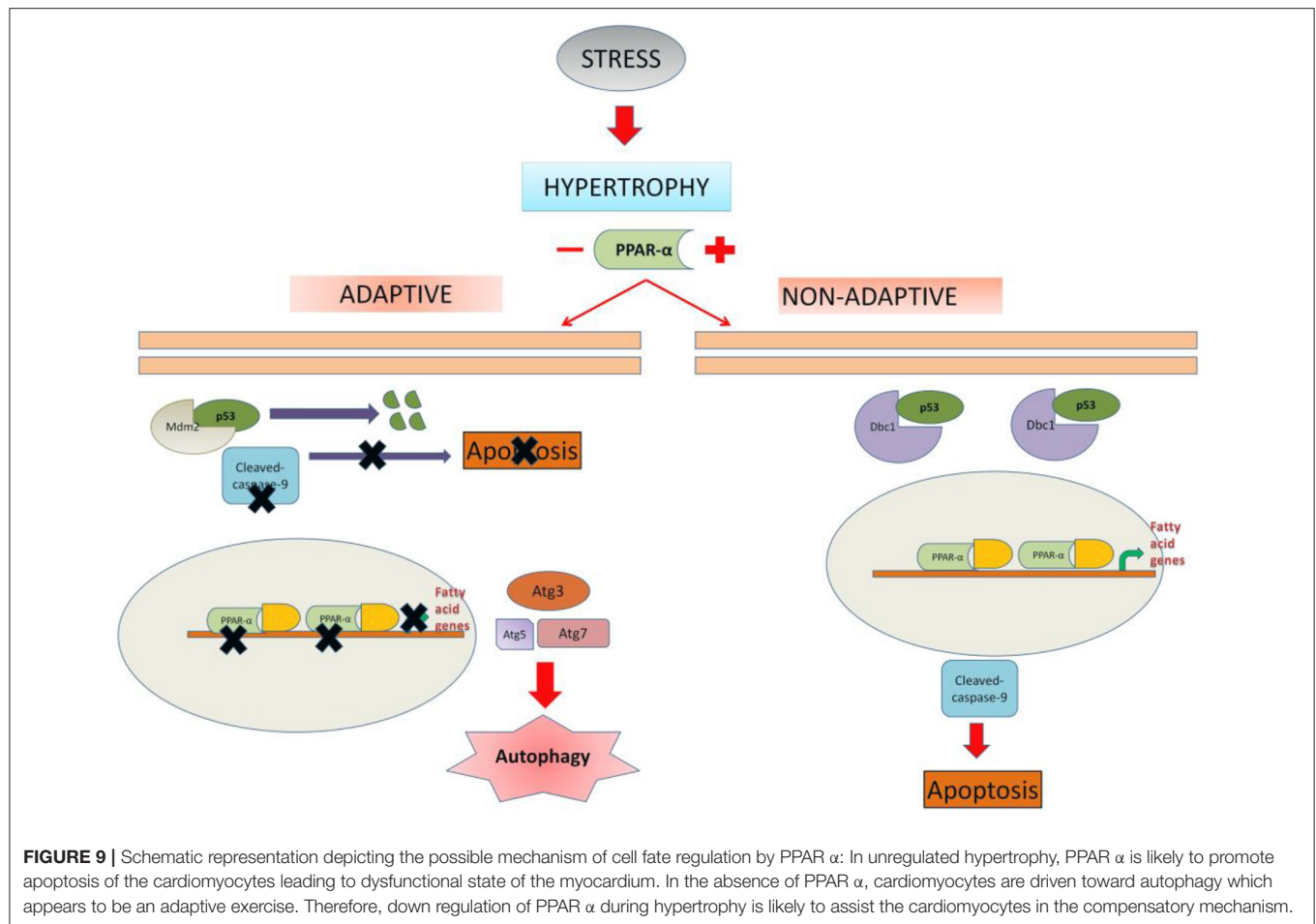
Few pieces of evidence reveal the presence of an association between cardiac hypertrophy and autophagy of the cardiomyocytes (48–50). With the down regulation of apoptosis, it could be suggested that to maintain cardiac homeostasis the autophagic flux might play a compensatory role in stress-induced cardiomyocytes. The increase in autophagic markers like Atg3, Atg5, and Atg 7 in the absence PPAR α expression might drive the cardiomyocytes toward autophagy as compared to apoptosis due to cardiac stress, as an adaptive measure.

The absence of PPAR α is associated with various pathophysiological changes including cardiac remodeling and hypertrophy, however, in the presence of hypertrophy inducing signal, PPAR α tends to promote apoptosis that eventually leads to cardiomyocyte death, whereas its absence causes a shift toward autophagy rather than apoptosis even in the presence of hypertrophic signals. Such adaptive shift as evident from increase in autophagy markers possibly explains the importance of the compensatory mechanism that operates in the cardiomyocytes in order to survive the myocardial stress through baseline autophagy.

In summary, although PPAR α is known to be downregulated in cardiac hypertrophy, this study unveiled a new mechanistic significance of it in the adaptation of the cardiomyocytes which is especially important in the compensatory phase. In normal situation PPAR α drives toward apoptosis whereas, in the absence of PPAR α, hypertrophic cardiomyocytes are driven toward autophagy. It is likely that hypertrophic cardiomyocytes are protected by switching autophagy which might act as a protective mechanism in the early adaptive phase of myocyte hypertrophy (**Figure 9**).

DATA AVAILABILITY STATEMENT

The datasets presented in this study can be found in online repositories. The names of the repository/repositories and accession number(s) can be found below: http://www.proteomexchange.org/, PXD025470. Raw Data for western Blot has been added as **Supplementary Figure 5**.

FIGURE 9 | Schematic representation depicting the possible mechanism of cell fate regulation by PPAR α: In unregulated hypertrophy, PPAR α is likely to promote apoptosis of the cardiomyocytes leading to dysfunctional state of the myocardium. In the absence of PPAR α, cardiomyocytes are driven toward autophagy which appears to be an adaptive exercise. Therefore, down regulation of PPAR α during hypertrophy is likely to assist the cardiomyocytes in the compensatory mechanism.

ETHICS STATEMENT

The protocol was approved by the CSIR-IICB Animal Ethics Committee (Reference no. IICB/AEC/Meeting/Sep/2019/4) and the animals were handled in accordance with the Committee for the Purpose of Control and Supervision of Experiments on Animals (CPCSEA), Ministry of Social Justice, and Government of India (Registration no. 147/1999/CPCSEA).

AUTHOR CONTRIBUTIONS

RK and AR designed and performed the experiments, analyzed results, and drafted the manuscript. DM, VC, UK, DB, SB, DK, and AK conducted experiments. AB analyzed the data, arranged resources, and edited the manuscript. All authors contributed to the article and approved the submitted version.

FUNDING

ACKNOWLEDGMENTS

SUPPLEMENTARY MATERIAL

The Supplementary Material for this article can be found online at: https://www.frontiersin.org/articles/10.3389/fcvm.2022.798639/full#supplementary-material

Supplementary Figure 1 | Development of cardiac hypertrophy in High-cholesterol diet fed PPAR α-/-mice.

Supplementary Figure 2 | Proteome profiler Antibody assay in PPAR α-/-mice.

Supplementary Figure 3 | Upregulation of survival markers in PPAR α-/-mice.

Supplementary Figure 4 | Genotyping of PPAR α-/-mice.

Supplementary Figure 5 | Raw images of western Blot.

REFERENCES

1. Tardiff JC. Cardiac hypertrophy: stressing out the heart. *J Clin Invest.* (2006) 116:1467–70. doi: 10.1172/JCI28884

2. Kehat I, Molkentin JD. Molecular pathways underlying cardiac remodelling during pathophysiological stimulation. *Circulation.* (2010) 122:2727–35. doi: 10.1161/CIRCULATIONAHA.110.942268

3. Vega RB, Konhilas JP, Kelly DP, Leinwand LA. Molecular Mechanisms Underlying Cardiac Adaptation to Exercise. *Cell Metab.* (2017) 25:1012–26. doi: 10.1016/j.cmet.2017.04.025

4. Aubert G, Vega RB, Kelly DP. Perturbations in the gene regulatory pathways controlling mitochondrial energy production in the failing heart. *Biochim Biophys Acta.* (2013) 1833:840–7. doi: 10.1016/j.bbamcr.2012.08.015

5. Warren JS, Oka SI, Zablocki D, Sadoshima J. Metabolic reprograming *via* PPARα signaling in cardiac hypertrophy and failure: From metabolomics to epigenetics. *Am J Physiol Heart Circ Physiol.* (2017) 313:H584–96. doi: 10.1152/ajpheart.00103.2017

6. Benjamin IJ, Jalil JE, Tan LB, Cho K, Weber KT, Clark WA. Isoproterenol-induced myocardial fibrosis in relation to myocyte necrosis. *Circ Res.* (1989) 65:657–70. doi: 10.1161/01.RES.65.3.657

7. Thangaiyan R, Arjunan S, Govindasamy K, Khan HA. Alhomida, AS, et al. Galangin attenuates isoproterenol-induced inflammation and fibrosis in the cardiac tissue of albino wistar rats. *Front Pharmacol.* (2020) 11:585163. doi: 10.3389/fphar.2020.585163

8. Li P, Luo S, Pan C, Cheng X. Modulation of fatty acid metabolism is involved in the alleviation of isoproterenol-induced rat heart failure by fenofibrate. *Mol Med Rep.* (2015) 12:7899–906. doi: 10.3892/mmr.2015.4466

9. Li H, Ma Z, Zhai Y, Lv C, Yuan P, Zhu F, et al. Trimetazidine ameliorates myocardial metabolic remodeling in isoproterenol-induced rats through regulating ketone body metabolism *via* activating AMPK and PPAR α. *Front Pharmacol.* (2020) 11:1255. doi: 10.3389/fphar.2020.01255

10. Tran DH, Wang ZV. Glucose metabolism in cardiac hypertrophy and heart failure. *J Am Heart Assoc.* (2019) 8:e012673. doi: 10.1161/JAHA.119.012673

11. Kang BY, Wang W, Palade P. Sharma, SG., Mehta, et al. Cardiac hypertrophy during hypercholesterolemia and its amelioration with rosuvastatin and amlodipine. *J Cardiovasc Pharmacol.* (2009) 54:327–34. doi: 10.1097/FJC.0b013e3181b76713

12. Muthuramu I, Mishra M. Aboumsallem, JP., Postnov A, Gheysens O, et al. Cholesterol lowering attenuates pressure overload-induced heart failure in mice with mild hypercholesterolemia. *Aging (Albany NY).* (2019) 11:6872–91. doi: 10.18632/aging.102218

13. Xia P, Liu Y, Cheng Z. Signaling pathways in cardiac myocyte apoptosis. *Biomed Res Int.* (2016) 2016:9583268. doi: 10.1155/2016/9583268

14. Ruan H, Li J, Ren S, Gao J, Li G, Kim R, et al. Inducible and cardiac specific PTEN inactivation protects ischemia/reperfusion injury. *J Mol Cell Cardiol.* (2009) 46:193–200. doi: 10.1016/j.yjmcc.2008.10.021

15. Seqqat R, Guo X, Rafiq K, Kolpakov MA, Guo J, Koch WJ, et al. Beta1-adrenergic receptors promote focal adhesion signaling downregulation and myocyte apoptosis in acute volume overload. *J Mol Cell Cardiol.* (2012) 53:240–9. doi: 10.1016/j.yjmcc.2012.05.004

16. Wozniak DJ, Kajdacsy-Balla A, Macias V, Ball-Kell S, Zenner ML, et al. (2017)PTEN is a protein phosphatase that targets active PTK6 and inhibits PTK6 oncogenic signaling in prostate cancer. *Nat Commun 8(1):.* (1508). doi: 10.1038/s41467-017-01574-5

17. Worby CA. Dixon, JE. PTEN. *Annu Rev Biochem.* (2014) 83:641–69. doi: 10.1146/annurev-biochem-082411-113907

18. Sussman MA, Völkers M, Fischer K, Bailey B, Cottage CT, Din S, et al. Myocardial AKT: the omnipresent nexus. *Physiol Rev.* (2011) 91:1023–70. doi: 10.1152/physrev.00024.2010

19. White E. Role of the metabolic stress responses of apoptosis and autophagy in tumor suppression. *Ernst Schering Found Symp Proc.* (2007) (4):23–34. doi: 10.1007/2789_2008_087

20. Degenhardt K, Mathew R, Beaudoin B, Bray K, Anderson D, Chen G, et al. Autophagy promotes tumor cell survival and restricts necrosis, inflammation, and tumorigenesis. *Cancer Cell.* (2006) 10:51–64. doi: 10.1016/j.ccr.2006.06.001

21. Li Z, Wang J, Yang X. Functions of autophagy in pathological cardiac hypertrophy. *Int J Biol Sci.* (2015) 11:672–8. doi: 10.7150/ijbs.11883

22. Galluzzi L, Bravo-San Pedro JM, Levine B, Green DR, Kroemer G. Pharmacological modulation of autophagy: therapeutic potential and persisting obstacles. *Nat Rev Drug Discov.* (2017) 16:487–511. doi: 10.1038/nrd.2017.22

23. Bravo-San Pedro JM, Kroemer G, Galluzzi L. Autophagy and mitophagy in cardiovascular disease. *Circ Res.* (2017) 120:1812–24. doi: 10.1161/CIRCRESAHA.117.311082

24. Schirone L, Forte M, Palmerio S, Yee D, Nocella C, Angelini F, et al. A review of the molecular mechanisms underlying the development and progression of cardiac remodeling. *Oxid Med Cell Longev.* (2017) 2017:3920195. doi: 10.1155/2017/3920195

25. Bayeva M, Sawicki KT, Butler J, Gheorghiade M, Ardehali Molecular H. and cellular basis of viable dysfunctional myocardium. *Circulation Heart Failure.* (2014) 7:680–91. doi: 10.1161/CIRCHEARTFAILURE.113.000912

26. Nakamura M, Sadoshima J. Mechanisms of physiological and pathological cardiac hypertrophy. *Nat Rev Cardiol.* (2018) 15:387–407. doi: 10.1038/s41569-018-0007-y

27. Frey N, Katus HA, Olson EN, Hill, JA. Hypertrophy of the heart: a new therapeutic target? *Circulation.* (2004) 109:1580–9. doi: 10.1161/01.CIR.0000120390.68287.BB

28. Marshall KD, Muller, BN., Krenz M, Hanft LM, McDonald KS, et al. Heart failure with preserved ejection fraction: chronic low-intensity interval exercise training preserves myocardial O2 balance and diastolic function. *J Appl Physiol.* (1985). (2013) 114:13147. doi: 10.1152/japplphysiol.0105 9.2012

29. Schiattarella GG, Hill JA. Inhibition of hypertrophy is a good therapeutic strategy in ventricular pressure overload. *Circulation.* (2015) 131:1435–47. doi: 10.1161/CIRCULATIONAHA.115.013894

30. Ballo P, Bocelli A, Mondillo Adaptive S. and maladaptive cardiac hypertrophy: what is the effective role of heat shock transcription factor 1? *Circ Res.* (2007) 100:e45–6. doi: 10.1161/01.RES.0000259102.33446.65

31. Duncan JG, Finck BN. The PPARalpha-PGC-1alpha axis controls cardiac energy metabolism in healthy and diseased myocardium. *PPAR Res.* (2008) 2008:253817. doi: 10.1155/2008/253817

32. Pisano A, Cerbelli B, Perli E, Pelullo M, Bargelli V, Preziuso C, et al. Impaired mitochondrial biogenesis is a common feature to myocardial hypertrophy and end-stage ischemic heart failure. *Cardiovasc Pathol.* (2016) 25:103–112. doi: 10.1016/j.carpath.2015.09.009

33. Oka S, Alcendor R, Zhai P, Park JY, Shao D, Cho J, et al. PPARα-Sirt1 complex mediates cardiac hypertrophy and failure through suppression of the ERR transcriptional pathway. *Cell Metab.* (2011) 14:598–611. doi: 10.1016/j.cmet.2011.10.001

34. Hilfiker-Kleiner D, Landmesser, Ulf., Drexler H. Molecular Mechanisms in Heart Failure: Focus on Cardiac Hypertrophy, Inflammation, Angiogenesis, and Apoptosis. *J Am Coll Cardiol.* (2006) 48:A56–A66. doi: 10.1016/j.jacc.2006.07.007

35. Adams JW, Sakata Y, Davis MG, Sah VP, Wang Y, Liggett SB, et al. Enhanced Galphaq signaling: a common pathway mediates cardiac hypertrophy apoptotic heart failure. *Proc Natl Acad Sci U S A.* (1998) 95:10140–10145. doi: 10.1073/pnas.95.17.10140

36. Kang PM, Izumo Apoptosis S. and heart failure: A critical review of the literature. *Circ Res.* (2000) 86:1107–13. doi: 10.1161/01.RES.86.11.1107

37. Li P, Zhou L, Zhao T, Liu X, Zhang P, Liu Y, et al. Caspase-9: structure, mechanisms and clinical application. *Oncotarget.* (2017) 8:23996–4008. doi: 10.18632/oncotarget.15098

38. Loreto C, La Rocca G, Anzalone R, Caltabiano R, Vespasiani G, Castorina S, et al. The role of intrinsic pathway in apoptosis activation and progression in Peyronie's disease. *Biomed Res Int.* (2014) 2014:616149. doi: 10.1155/2014/616149

39. Fridman JS, Lowe SW. Control of apoptosis by p53. *Oncogene.* (2003) 22:9030–40. doi: 10.1038/sj.onc.1207116

40. Aubrey BJ. Kelly, GL., Janic A, Herold, MJ, et al. How does p53 induce apoptosis and how does this relate to p53-mediated tumour suppression? *Cell Death Differ.* (2018) 25:104–13. doi: 10.1038/cdd.20 17.169

41. Schuler M, Bossy-Wetzel E, Goldstein JC, Fitzgerald P. Green, DR. p53 induces apoptosis by caspase activation through mitochondrial cytochrome c release. *J Biol Chem.* (2000) 275:7337–42. doi: 10.1074/jbc.275.10.7337

42. Rana S, Datta R, Chaudhuri RD, Chatterjee E, Chawla-Sarkar M, Sarkar S. Nanotized PPARα overexpression targeted to hypertrophied myocardium improves cardiac function by attenuating the p53-GSK3β-mediated mitochondrial death pathway. *Antioxid Redox Signal.* (2019) 30:713–32. doi: 10.1089/ars.2017.7371

43. Akande OE, Damle PK, Pop M, Sherman NE, Litovchick LV, et al. DBC1 regulates p53 stability *via* Inhibition of CBP-dependent p53 polyubiquitination. *Cell Rep.* (2019) 26:3323–35.e4. doi: 10.1016/j.celrep.2019.02.076

44. Nag S, Qin J, Srivenugopal KS, Wang M, Zhang R. The MDM2-p53 pathway revisited. *J Biomed Res.* (2013) 27:254–71. doi: 10.7555/JBR.27.201 30030

45. Kitagishi Y, Matsuda S. Diets involved in PPAR and PI3K/AKT/PTEN pathway may contribute to neuroprotection in a traumatic brain injury. *Alzheimers Res Ther.* (2013) 5:42. doi: 10.1186/alzrt208

46. Sarkar S, Ravikumar B, Floto RA, Rubinsztein DC. Rapamycin and mTOR-independent autophagy inducers ameliorate toxicity of polyglutamine-expanded huntingtin and related proteinopathies. *Cell Death Differ.* (2009) 16:46–56. doi: 10.1038/cdd.2008.110

47. Siddiqui RA, Shaikh SR. Kovacs R, Stillwell W, et al. Inhibition of phenylephrine-induced cardiac hypertrophy by docosahexaenoic acid. *J Cell Biochem.* (2004) 92:1141–59. doi: 10.1002/jcb.20135

48. Li L, Xu J, He L, Peng L, Zhong Q, Chen L, et al. The role of autophagy in cardiac hypertrophy. *Acta Biochim Biophys Sin (Shanghai).* (2016) 48:491–500. doi: 10.1093/abbs/gmw025

49. Cao DJ, Gillette TG, Hill JA. Cardiomyocyte autophagy: remodeling, repairing, and reconstructing the heart. *Curr Hypertens Rep.* (2009) 11:406–11. doi: 10.1007/s11906-009-0070-1

50. Xu M, Wan CX, Huang SH, Wang HB, Fan D, Wu HM, et al. Oridonin protects against cardiac hypertrophy by promoting P21-related autophagy. *Cell Death Dis.* (2019) 10:403. doi: 10.1038/s41419-019-1617-y